STRUCTURAL STABILITY
RESEARCH COUNCIL

SSRC

PROCEEDINGS

1995 Theme Conference

STABILITY PROBLEMS RELATED TO AGING, DAMAGED, & DETERIORATED STRUCTURES

Structural Stability Research Council

Proceedings

1995 Theme Conference

Stability Problems Related to Aging, Damaged & Deteriorated Structures

28-29 March 1995
Kansas City, Missouri

PROCEEDINGS COMPILED BY:
Diana Walsh, Secretarial Assistant

ISBN 1-879749-61-0

THE OPINIONS, FINDINGS, CONCLUSIONS AND RECOMMENDATIONS EXPRESSED HEREIN ARE THOSE OF THE AUTHORS AND DO NOT NECESSARILY REFLECT THE VIEWS OF THE STRUCTURAL STABILITY RESEARCH COUNCIL.

STRUCTURAL STABILITY RESEARCH COUNCIL
Lehigh University
Fritz Engineering Laboratory
13 E. Packer Avenue
Bethlehem, PA 18015-3191 USA
Phone (610)758-3522
FAX (610)758-4522

Printed in the United States of America

FOREWORD

The Structural Stability Research Council organized a day and a half conference concerned with various stability problems in existing metal structures which was held in Kansas City, Missouri on March 28 & 29. This conference followed the 1993 Milwaukee format as an expansion of the half day theme session that had been a traditional part of the annual meeting of the Structural Stability Research Council. The goal of the conference was to present information on the types of problems encountered, methods of assessment and types of rehabilitation that has been successful. In this respect the conference was a great success as shown by the quality of paper appearing in these Proceedings. There were about 70 persons who attended the conference, representing several different countries.

The twenty two papers in these Proceedings were presented in six sessions: one on occurrence & cause, three on evaluation, one repair & strengthening and one devoted specifically to seismic problems. Special recognition is deserving to the keynote speakers for these sessions: Don Sherman, David Wisch, Jim Malley, Fred Moses, Pete Birkemoe and Avanti Schroff. Recognition and thanks is also due to the other contributing authors and coauthors for their efforts in preparing papers and making presentations at the conference.

At noon on Wednesday there was conference luncheon. The speaker at the luncheon was Dr. Urs Meier from the Swiss Federal Laboratories, who shared very interesting information on using advance composite materials to repair deteriorated metal structures. Thanks to Dr. Meier for his time and effort.

A special note of thanks is due to the sponsors who contributed financially to support the conference.

American Institute of Steel Construction
Exxon Production Research Company
Federal Highway Administration
National Center for Earthquake Engineering Research
Unocal Corporation

There were many people involved behind the scenes both before and during the conference to make it a successful event. I thank the active participants of the Scientific Committee for their suggestions regarding topics and speakers: Clarence Miller who chaired the Planning Committee, Kathy Almand, Lynn Beedle, Reidar Bjorhovde, Pete Birkemoe, Jackson Durkee, John Fisher, Ted Galambos, Jerry Haaijer (who is no longer with us), Jim Ricles, Charles Smith, Nick Zettlemoyer and Abdul Zureick. The SSRC staff put forth considerable extra effort in planning and arranging for this conference, in addition to the requirements for the preceding SSRC meeting. For this we recognize: Jim Ricles, Director; Lesleigh Federinic, Administrative Secretary and Diana Walsh, Secretarial Assistant. Also thanks to the students from the University of Kansas for their assistance during the conference.

Hopefully these Proceedings will become an important part of structural engineering literature. They contain some excellent information on overall stability problems in the existing infrastructure and methods of addressing them. Careful reading will also reveal alternate ways of considering the topic and some areas of controversy or question. These will undoubtedly become future topics of consideration by the Structural Stability Research Council.

D. R. Sherman

Donald R. Sherman
Chairman

Milwaukee, Wisconsin
June 1995

CONTENTS

SESSION 6 - REPAIR & STRENGTHENING

STABILITY RELATED DETERIORATION OF STRUCTURES

Donald R. Sherman
University of Wisconsin-Milwaukee

ABSTRACT

The definition of structural deterioration can be expanded to include any problems that occur in existing structures as opposed to new designs. With this definition, deterioration related to stability includes not only the common conception of physical damage and corrosion, but also problems resulting from code changes and even errors in design or construction. The causes of damage and environmental deterioration can be divided into categories of everyday usage and catastrophic events that impact to various degrees, buildings, bridges, offshore structures and lifeline structures. Methodologies for assessment are in developmental stages and considerably more research is still required for evolving reliable methods for assessment and rehabilitation.

As an example of research directed toward understanding the details of deterioration, the significant role that local buckling or dents play in causing catastrophic fracture under cyclic loads is illustrated by the results of a pilot test program using rectangular tubes subject to axial loads. Although axial displacement range, mean displacement and load rate may all have an influence on the number of cycles to fracture, the single factor that separates members that have hundreds of cycles to fracture from those that fracture in fewer than 40 cycles is the presence of a local buckle. The formation of local buckles requires higher axial displacement for tubes with lower width/thickness ratios. Therefore, recent code changes that specify more restrictive width/thickness ratios for braces in seismic design will enhance the performance of tubular members.

INTRODUCTION

Numerous articles have appeared in public and technical literature describing the magnitude of the nation's deteriorating infrastructure problem. The most common problems mentioned are the high percentage of bridge structures with critical or moderate need for rehabilitation and buildings that have sustained damage during an earthquake or are no longer in compliance with modern seismic criteria. Structural engineers are aware of many more specific examples of different types of structures in need of rehabilitation for a wide variety of reasons.

During the 50th Anniversary Conference of the Structural Stability Research Council in 1994, there was a workshop on Deteriorated Structures. Participants from various parts of the world discussed a broad range of problems associated with deterioration. The first part of this paper that deals with the broad aspects of deterioration is based on ideas presented in the workshop. The second part of the paper presents the conclusions of a pilot test program to determine the cause of fractures found in hollow structural section (HSS) braces in the Northridge Earthquake and the factors that may influence the behavior of HSS braces.

TYPES AND CAUSES OF DETERIORATION

In the workshop discussion concerning the types of deterioration that can occur in structures, it was concluded that more than just physical damage should be considered. The topic should be broadened in scope to include the consideration of any stability problems that can occur in

existing structures as opposed to new designs. With this extended definition, the following types of deterioration that influence stability can be identified.

DAMAGE - Local denting or out-of-straightness that produces a condition that members or the structure are no longer within original construction tolerances.

ENVIRONMENTAL - Conditions that lead to loss of cross section in members or alterations of joint characteristics that change the boundary conditions of members.

LEGAL - Changes in applicable codes or in the function of the structure that produce different loads or design criteria.

ERRORS - Either design or construction errors that are not detected until after the structure is built.

Several causes of damage or environmental types of deterioration can be identified. These are divided into categories of everyday usage and catastrophic events.

EVERYDAY USAGE

REPETITIVE LOADS - This includes cyclic loads from equipment, random load variations or other repetitive loads that can produce fatigue conditions. The resulting cracks may influence the section or boundary properties to the extent that stability is degraded in a member or in a structure as a whole.

CORROSION - Environmental conditions can lead to loss of section or deterioration of joints.

LACK OF MAINTENANCE - This could lead to corrosion, build up of material in joints or structural misalignments due to use of equipment (e.g. cranes)

CATASTROPHIC

IMPACT - Impact damage occurs from moving vehicles or falling objects that locally dent and/or permanently bend a member.

SINGLE OVERLOAD - Hurricanes, tornados or unusual vehicle or equipment loads that produce permanent local or general member buckling.

SEISMIC EVENT - Severe horizontal cyclic loads on the structure that produce buckling or fracture in members.

FIRE - Twisting or bending of members beyond construction tolerances but not to the degree where replacement is obviously required.

BLAST - Explosions that occur either from industrial accidents or intentional bombing that produce permanent distortions in the structure.

Deterioration in various forms could occur in many types of steel structures. However, the frequency of types or causes of damage is more prevalent in different structure categories.

BUILDINGS - Exposed columns in industrial buildings and parking structures are frequently subject to vehicle impact and are potentially subject to environmental deterioration. Industrial buildings are also subject to maintenance, overload or cyclic load problems. Any type of building can experience fire, blast or seismic damage. Seismic damage is the most prevalent and most commonly affects braces and joints in steel buildings.

BRIDGES - Vehicle impact frequently occurs in members of bridges. Corrosion and maintenance problems are also frequently encountered. Other source of damage often affect bridge supports and foundations, but these are not within the scope of stability of metal structures.

OFFSHORE STRUCTURES - Work platforms are subject to any of the types or causes of damage that have been identified.

LIFELINE STRUCTURES - Seismic events can damage pipelines and towers. Pipelines are also subject to corrosion or accidental impact from moving equipment. As exposed structures, towers are subject to environmental damage.

Any type of steel structure could require evaluation due to errors or changes in loadings and applicable codes. This is a particular problem with older bridge structures and buildings in seismic regions.

Bridges were commonly designed for 30 to 50 year lives. Bridge loadings have increased considerably over this period and many existing bridges are over 50 years old. As in the case of buildings, many of these older structures have survived and continue to function with loadings well beyond their original design loads because of very conservative design practices.

Starting 50 years ago, offshore structures were originally designed for a 30 year life and to withstand a 25 year wave. Now there is an interest in extending the life of older platforms and the design criteria is a 100 year wave. With modern analysis methods and refined criteria, older structures can frequently be shown to still be adequate.

ASSESSMENT

Once it has been determined that a member or structure is in a deteriorated condition, a decision must be made on selecting one of three options:

1. Leave it as is since it can perform its function in a satisfactory manner.

2. Rehabilitate to improve its condition so it will perform satisfactorily.

3. Replace the member, subassemblage or entire structure.

Although analysis for re-rating bridges has been common practice for many years, general methodologies for assessment are still in formative stages. A draft of a section of API RP2A (Offshore Platforms) has been prepared that presents a general strategy. Similar studies for cracks in bridge structures are also underway. Essentially the strategy consists of a sequence of classifications of the severity of deterioration and its consequences. Each stage increases in complexity. If the results are satisfactory in any stage, the deterioration is dismissed. If not, proceed to the next stage. The stages are:

1. Gather data to document the severity of deterioration.

2. Screen the information and make an experience judgement as to whether the deterioration might be severe enough to limit the function of the structure.

3. Consider the effects at working stress levels.

4. Perform an ultimate strength analysis. Simple and conservative analyses are used first and increasingly complex analyses are used if necessary to demonstrate a margin against failure; e.g.

    a) Elastic analysis without safety factors and using mean yield strengths.

    b) Detailed local analysis if few members are involved.

    c) Global analysis (eg. pushover in the case of offshore platforms)

5. Design the required rehabilitation or replacement.

At any stage the economics of proceeding must be considered. It may be less expensive to rehabilitate or replace than to proceed with the assessment.

Parameters to be considered in the evaluation and assessment are the location of the deterioration in a member and in the structure, severity, structural type (e.g. degree of redundancy), consequences of failure. Included in the latter are considerations of whether the structure is occupied, possible evacuation of personnel with adequate storm warnings, potential environmental pollution and economic importance of the structure.

Although knowledge of the reserve strength of an individual member is important, primary consideration must be given to its effect on the total structure. Therefore, information on its altered stiffness must be known for an elastic analysis and nonlinear characteristics are required for an ultimate strength analysis. If there are many sources of out-of-tolerance in the structure, they can add up to potentially dangerous situation. In an ultimate strength analysis, there is the possibility of a complex analysis to determine a beta or reliability factor for the structure. Although this is an option for engineering decisions, reference to reliability or probability of survival should be avoided when dealing with the public; the public wants a clear statement that the unrepaired or rehabilitated structure is reliable.

Inspection is an important part of the assessment process especially when deterioration is caused by everyday events. In any assessment, it is important to determine the root cause of deterioration so that simple repair does not lead to a recurring problem. As an example not directly related to stability, a crack caused by overload during installation can be rewelded, but fatigue cracks should not be simply rewelded.

REHABILITATION

Tubular members have been rehabilitated with internal grouting and external sleeves or clamps to encase the damaged section with grout. Fiber-reinforced concrete and shotcrete have been used to encase buckled web members in open-web joists to obtain stable hysteresis loops. The objective of grouting is to stabilize local buckles or dents so they do not grow under subsequent static or cyclic loads. However, research has shown that there is a limiting dent depth and out-of-straightness beyond which the original strength of the member cannot be regained. Grout has also been used to reinforce connections.

In bridges, rehabilitation frequently involves increasing capacities and widths in addition to repair of physical deterioration. Several strategies to eliminate stability problems from both bridge and offshore experiences can be mentioned. These include schemes to increase strength or reduce loads.

Replace members with higher strength steel
Add additional braces to compression members
Post-tensioning schemes
Internal or external grout
Insert piles in tubular members with grouted annular space
Intentionally flood submerged tubular members to reduce external pressure
Reduce loads by removing unnecessary appendages that catch drag forces

NEEDED RESEARCH

The whole area of dealing with deteriorated structures is still in the early stages of development, and considerable research is needed for economical and efficient assessment and rehabilitation.

EXPERIMENTAL - Tests are required to determine the behavior and reserve capacity of various types of deterioration for different types of members. These tests are needed to provide a baseline for analytical predictors. Tests are also required to provide information on innovative methods for repairing deterioration.

ANALYTICAL - Further research is needed to develop reliable, efficient and economical analytical methods to determine reserve capacities and behavior of damaged members of various cross sections. The complete nonlinear behavior of members, including the descending branch, must be known in order to conduct collapse analyses of the entire structure.

PRACTICE - Information is needed to classify which dents (severity and location) or other types of deterioration can be accepted. General methodologies must be developed for assessing older structures. A good exchange of information is required so that

successful methods of assessment and rehabilitation are widely known.

HSS BRACE UNDER CYCLIC AXIAL LOAD

As an example of research directed toward determining the causes of catastrophic damage, the results of a pilot tests program on rectangular hollow structural sections (HSS) are presented. This test program was motivated by the observation of a fracture in a 10"x10"x3/8" HSS bracing member with a flat width to thickness ratio (b/t) of 23 in the Northridge Earthquake of January 1994. The test program consisted of testing two thicknesses of 5"x2" HSS under axial displacement with ends pinned for column buckling about the weak axis. The properties of the test specimens are summarized in Table 1.

TABLE 1 - HSS TEST SPECIMEN PROPERTIES

SIZE	b/t	KL/r	F_y ksi	P_y kips	P_{stub} kips
5x2x1/8"	36	83.5	46.1	71.0	77.7
5x2x3/16"	23	86.4	57.0	127.2	161

The size, b/t and column slenderness (KL/r) are based on nominal dimensions. The yield stress (F_y) and the measured stub column strength (P_{stub}) were obtained in static tests while the yield load (P_y) is calculated from the static yield stress and the actual HSS dimensions. The fact that the stub column tests are higher than the yield load reflects enhanced yield properties in the corners of the HSS and indicate that local buckling occurred in the strain hardening range.

The AISC Specification defines a thin-walled HSS under uniform compression as having a b/t that exceed $238/\sqrt{F_y}$, or in this case 35 for the thin HSS. The recent AISC Seismic Provisions limit b/t to $110/\sqrt{F_y}$ or about 15 for both of the two sizes. Therefore, the thicker of the test specimens is similar to the HSS observed after the earthquake and would have been acceptable under the older code provisions, but neither HSS would be acceptable under the newer provisions.

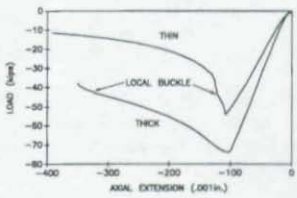

FIG. 1 - AXIAL LOAD-DISPLACEMENT

Both tube sizes were initially tested as columns under very slow monotonic axial loading. The resulting load vs. axial displacement

curves are shown in Fig. 1. Since the column slenderness is almost identical for the two sizes, overall column buckling occurs at essentially the same axial displacement. Subsequent local buckles, however, develop at less displacement in the thinner HSS. In the cyclic test program, axial displacement limits were at 0.200" where only the thin HSS formed a local buckle and at 0.400" where both HSS had local buckling.

The variables in the cyclic test program were the axial displacement range, the mean axial displacement and the rate of loading as determined in the period for a cycle. A similar pattern of behavior was observed in most of the cyclic tests. Column buckling is followed by a local buckle which leaves "horns" at the corners. After several cycles with tension excursions, cracks initiate at the HSS corners on both horns and propagate through the thickness and away from the corners in subsequent cycles. As section is lost at the cracks resulting in an eccentric load, the lateral deflection reverses during the tension part of the cycle but return to the original direction during compression, producing a snap-through behavior. Eventually the crack pops across the local buckle, resulting in increased lateral deflection that creates a large enough eccentricity to reverse the direction of column buckling in the subsequent compression. Table 2 presents the displacement range, the test identification number, the cycle period and the number of cycles for a full fracture across the width of the section.

The most significant conclusion from the tests is that Test #4, which buckled as a column but did not form a local buckle, sustained over 500 cycles of loading without developing a crack. All other tests where local buckling did occur failed in 41 or fewer cycles.

TABLE 2 - CYCLES TO FRACTURE

DISPLACEMENT (in.)	THICK			THIN		
	TEST	PERIOD (s)	CYCLES	TEST	PERIOD (s)	CYCLES
-.200, +.200				7	480	**32**
	4	16	**500+**	8	16	**32**
-.300, +.300				10	2	**27**
-.400, +.200	2	40	**31**			
	5	5	**34**			
	4a	5	**41**		PRELOAD	
	3	2	**40**	9	2	**18**

Although the influence of local buckling is the most significant conclusion in these tests, several secondary conclusion may be made by comparing various tests. Some of these are intuitive, but they have been quantified in these tests.

Tests #3 & 9 - high b/t leads to lower fracture life for the same displacement range and

period.

Tests #7,8 & 9 - higher displacement range leads to lower life.

Test #10 & 9 - mean displacement may have an effect. However, Test #10 was an exception to the general behavior in that a reversal in buckling direction occurred after the cracks initiated but before the pop across the face. A local buckle then formed on the other side, followed by crack initiation, pop and another direction reversal. Cycling on both faces may account for the longer life than Test #9, which had the same range. Test #10 was the only test with full tension yield.

Tests #4a & 5 - precycling may be beneficial. Test #4a was a continuation of Test #4, but with higher displacement range that corresponded to Test # 5 in both displacement range and period.

Tests #7 & 8 - variations in loading rates at periods greater than 16 seconds have no influence on fracture life.

Tests #2,5 & 3 - low periods have a beneficial influence on fracture life.

These pilot tests demonstrate that the only important parameter in determining whether HSS braces will survive a seismic event is the formation of local buckles. The column tests can serve as benchmarks for analytical studies to determine the axial displacements at which local buckles form as a function of b/t, KL/r and the yield strength.

CONCLUSIONS

Several conclusions can be made from the overall discussion in this paper.

1. With an extended definition to include stability considerations in existing structures, "deterioration" can take many forms in addition to damage and corrosion.

2. There are a variety of everyday and catastrophic causes of deterioration that affect different types of structures to a greater or lesser extent.

3. Assessment procedures are in various stages of development in industries concerned with different types of structures.

4. Rehabilitation methods require ingenuity and research.

5. Detailed research on behavior is required to develop guidelines to deterioration causes, assessment procedures and rehabilitation schemes.

6. There is a critical need for dissemination of information by practitioners who have had success in assessment and rehabilitation methods.

RESIDUAL STRENGTH AND REPAIR OF DAMAGED AND DETERIORATED OFFSHORE PLATFORM TUBULARS

J. M. Ricles, W. M. Bruin, T. K. Sooi, M. F. Hebor, and P.C. Schönwetter
Department of Civil and Environmental Engineering, Lehigh University

ABSTRACT

The results of several current research programs related to the behavior of dented and corrosion-damaged tubular brace members and their repair is presented. Investigations were conducted involving large-scale testing and analytical studies. The analytical studies involved assessing the ability of several different methods of analysis, including simple engineering calculations and more sophisticated nonlinear finite element analysis, to predict damaged and repaired member behavior. The results of the test programs indicated that a significant amount in member deterioration could occur due to either dent or corrosion damage. The extent of the ability of a repair to reinstate a damaged member to its original design strength was found to depend on the extent of the damage. The accuracy and reliability of the analytical methods to predict damaged member behavior are illustrated.

INTRODUCTION

Presently, there are over 3500 major offshore fixed platforms located in U.S. waters. These structures exist in a hazardous environment, being constantly susceptible to collision with marine vessels and dropped objects which can cause damage consisting of dent damage of depth d_d and out-of-straightness δ_p (see Fig. 1). Surveys have reported[1] that a significant number of fixed offshore platforms in the U.S. have dent damage.

The marine environment also exposes these platforms to corrosion, requiring the use of counteractive corrosion measures, such as cathodic protection systems and protective coatings. Despite these measures, there are numerous cases reported of platform members which have suffered corrosion damage[1,2]. Shown in Fig. 2 is a schematic of a corroded brace member which had been removed from a Gulf of Mexico platform. A survey of this member by Ostapenko et al.[3] indicated that the member had significant corrosion, consisting of some uniform, but mostly patch-type corrosion. The latter type of corrosion causes a non-uniform reduction of the cross-section's wall thickness. Testing of this, as well as another similar member, resulted in a capacity reduction of 35% and 50%, respectively, compared to a corresponding non-corroded tubular. The loss in capacity is attributed to a premature local buckle which formed in the most severely corroded area of the two specimens.

Improvements in oil recovery methods and economical justifications have resulted in many offshore platforms remaining in service beyond their original design lives. The effects of corrosion and dent damage on the safety of these as well as newer structures has become a growing concern. Knowledge of the residual strength and repairability of dent-damaged and corroded members is highly relevant to the safety, as well as the repairability and requalification of all platforms.

The strength of members with dents, both with and without out-of-straightness, has been a subject of extensive research since the late 1970's[4-11]. Most of the previous experimental work has involved small-scale specimens, where the diameter D is less than 76 mm and the dent-depth d_d less than 0.2D. Even fewer studies have been conducted on the behavior of repaired bracing members with dent damage[12-15]. Virtually no prior research, except for that by Ostapenko et al.[3] has been conducted on the subject of the affect of corrosion on structural performance.

The need to acquire more knowledge about the residual strength and repair of dent damaged and corroded offshore tubular members led to the research report herein. The objectives of these studies[17, 18, 19] were to investigate the behavior of dented and corroded tubular bracing members in order to assess residual strength, and to evaluate their repair by either internal grouting or grouted sleeves. These studies involved both experimental and analytical investigations, where the former utilized large-scale test specimens. The analytical investigations included performing parametric studies to assess the effects of various geometrical and material properties on member behavior.

RESIDUAL STRENGTH AND REPAIR OF DENTED BRACING

Experimental Program

The experimental study associated with the residual strength and repair of dent-damaged bracing involved testing the 27 large-scale specimens summarized in Table 1. The range in nominal dent-depth d_d was from 0% (no dent damage) to 30% of the specimen's diameter D and the out-of-straightness δ_p varied from about 0.001L to 0.01L (where L is the specimen's total length). Non-damaged, dent-damaged, and grout repaired dent-damaged specimens having nominal diameter-to-thickness ratios of D/t = 34.5, 46, and 64 were tested. In some cases specimens with a D/t = 69 were tested in lieu of those with D/t = 64. The repaired specimens were either grouted internally or externally, the latter involving the placement of grout between the member and a steel sleeve which was positioned around the member in the dent-damaged region. All specimens had a nominal diameter D of 219 mm, and an overall length L that ranged from 4542 mm to 4585 mm in order to maintain a slenderness ratio kL/r of approximately 60. Measured values for d_d/D, D, t, and δ_p for each specimen are given in Table 1. The testing of the specimens in the test matrix enabled a direct comparison to be made between the strengths of: (1) grout repaired and non-repaired dented members; and in some cases (2) non-damaged and non-repaired dented members; as well as (3) non-damaged and grout repaired members.

The dented specimens were damaged under controlled conditions using a blunt headed steel wedge and a overhead test machine, where the former was slowly displaced into the side of the tube at midspan to obtain the target depth of the induced dent-damage. In order to minimize the development of global out-of-straightness during the denting process, the member was continuously supported with a bed of hydrostone placed along a length of 609 mm on both sides of midspan. The out-of-straightness δ_p following denting was less than 0.01L for the most severely dented specimens (d_d = 0.3D). The material properties for each specimen, consisting of steel tensile yield strength σ_y and grout compressive strength f'_g (for repaired specimens) were measured by standard methods[20, 21, 22] and are reported in Table 1. All specimens were fabricated from A53 Type B tubular steel, which were annealed to obtain representative prototype yield strengths. Following denting, each specimen was then tested in the self-reacting 2224 kN test frame shown in Fig. 3. Compressive loading was applied to a specimen using a pair of hydraulic hollow-core jacks, each tensioning a rod that reacted against a load beam at one end of the specimen. The test frame featured frictionless spherical bearings at each end, which held a specimen in place and provided pin-ended specimen boundary conditions. Each specimen was fully instrumented to measure axial load, strains, growth in dent-depth, axial shortening, and out-of-plane global displacements during the test. Each test was initially conducted under load control up to peak specimen capacity, after which displacement control was used to capture the post-ultimate behavior of the specimen. Specimens were tested under monotonically applied axial load with an end eccentricity of either e = 0.2D or e = 0.0D (concentric axial load).

The normalized axial load-axial shortening response of specimens having D/t = 64 and an eccentrically applied axial load is shown in Fig. 4. It is seen in this figure that a dent-depth of 0.1D (Specimen C2) can reduce the member's ultimate capacity to approximately 71% of the strength of a corresponding non-damaged specimen (Specimen C5). A further comparison of non-repaired specimen

residual strength P_{sR} to the non-damaged capacity P_0 is summarized in Table 2 and shown in Fig. 5. The results from Specimen C1 are excluded from all of the discussion herein since its test data is suspect. The more deeply dented specimens are shown in Fig. 5 to suffer a loss of capacity to as much as 26% (Specimen C8, D/t = 69, d_d = 0.3D) of the non-damaged member's strength $P_{0'}$. The non-damaged capacity P_0 was based on the Structural Stability Research Council's[20] Column Curve 1 for those comparisons in which a non-damaged member was not tested.

Both the internally grout repair (Specimen C3) and grouted sleeve repair (Specimen C4) are shown in Fig. 4 to have reinstated the strength of a damaged member having a dent-depth of 0.1D to beyond the capacity of a non-damaged member. A comparison of the repaired strength P_R with the non-repaired residual strength P_{sR}, as well as with the undamaged strength $P_{0'}$, for all corresponding specimens of the test matrix is given in Table 3. The relationship between normalized dent-depth d_d/D and the repaired capacity-design strength ratio $P_R/P_{0'}$ for the test specimens is shown in Fig. 6. Fig. 6 and Table 3 both indicate that the grout repair of members with dent-depth of 0.1D and having a different D/t ratio, which include Specimens C3 and C4 as well as Specimens A3 and B3, resulted in an increase in their strength above the non-repaired strength P_{sR}. The repair reinstated each of these specimens to a strength greater than their full non-damaged capacity $P_{0'}$. The non-repaired specimens were observed to develop a significant inward dent growth, which was accompanied by an ovalization of the dented cross-section. Both the internal grout and a grouted sleeve repair inhibited a growth in the dent-depth, the former by obstructing the dent from growing inward and the latter by restraining the dented cross-section from ovalizing.

Internal grouting alone, however, is evidently unsuccessful in reinstating a member with a more severe dent-damage (d_d = 0.3D and δ_p = 0.006L to 0.01L) to its full non-damaged capacity $P_{0'}$, as shown in Fig. 6. This figure implies that internal grouting is successful if the original dent-depth d_d is less than or equal to approximately 0.15D to 0.2D. For a deeper dent-depth, a greater reduction in the cross-section's moment of inertia as well as a larger amount of out-of-straightness δ_0/L occurs, thus making it more susceptible to an overall column-type compression failure. For the values of out-of-straightness of the specimens tested, there appears to be a d_d/D ratio between 15% and 30% beyond which internal grouting is not a viable repair method to restore the member's strength. Further studies of internal grout repair of members having d_d/D in the range 0.15 to 0.30 are currently being conducted to refine the limit of repairability by internal grouting.

Analytical Program

Several different methods of analysis were used to predict the capacity of the non-repaired and internal grout repaired specimens having dent damage. These methods included: (1) beam-column analysis; (2) moment-thrust-curvature (M-P-ϕ) based integration analysis; and, (3) the non-linear finite element method (FEM). Measured material properties, out-of-straightness, and geometric dimensions of each specimen were used in each method of analysis.

For the non-repaired specimens, the beam-column analyses involved two formulations, namely: (1) UC-DENT, and (2) unity check equations. The UC-DENT approach[17,18] uses beam-column theory to obtain the quadratic expression shown below from which the ultimate axial load P_{ud} of a dent-damaged tubular brace can be obtained:

$$P_{ud}^2\left[\frac{1}{A_d}+\frac{e+e_d}{S_d}-\frac{L_1 L_d e\,(1+C_d)}{EI_d\beta S_d}P_{Ed}\right]\frac{1}{P_{Ed}}-P_{ud}\left[\frac{e+e_d}{S_d}+\left(\delta_0-\frac{L_1 L_d M_e}{EI_d\beta}\right)\frac{(1+C_d)}{S_d}\right.$$
$$\left.+\frac{F_{pd}e^*}{P_{Ed}S_d}+\frac{1}{A_d}+\frac{F_{pd}}{A_d P_{Ed}}+\frac{\sigma_y}{P_{Ed}}\right]+\sigma_y+\frac{F_{pd}}{A_d}\left(1+\frac{A_d e^*}{S_d}\right)=0 \qquad (1)$$

The analysis accounts for end eccentricity, e, and initial out-of-straightness, δ_o. Failure of the dent-damaged member is assumed to occur when the stress in the dent saddle of the member reaches its yield stress σ_y, not considering any increase in member strength beyond first yield. Eqn. (1) is therefore considered to provide a conservative estimate for a dented member's residual strength. More details about this analysis method can be found in Ricles et al.[17, 18]. The unity check equations[8] consist of moment-axial load interaction expressions which are based on strength and stability limit states, respectfully, where for strength:

$$\frac{P}{P_{ud}} + \left(\frac{M}{M_{ud}}\right)^{0.5\gamma} = UC \tag{2a}$$

and for stability:

$$\frac{P}{P_{crd}} + \left(\frac{C_m M}{\left(1 - \frac{P}{P_{Ed}}\right) M_{ud}}\right)^{0.5\gamma} = UC \tag{2b}$$

Eqns. (2a) and 2(b) provide an estimate of a dented member's residual strength by setting each interaction equation to 1.0 (e.g. UC=1.0), and solving for the ultimate axial load P. Eqns. (2a) and (2b) were each calibrated from analysis of members whose dent-depths d_d were generally less than 20% of the member diameter, and out-of-straightness δ_o less than 0.01L of the total member length. More details of the use of Eqns. (2a) and (2b) can be found in Loh[8].

For the beam-column analysis of the repaired specimens, the formulation of Parsanejad[13] was used to predict the capacity P_{ud} of a repaired specimen, where:

$$P_{ud} = A_{tr}\sigma_{ud} \tag{3a}$$

and

$$\frac{1}{\sigma_{e,tr}}\sigma_{ud}^2 - \left[1 + \frac{A_{tr}e_1}{S_{tr}} + \frac{\sigma_y A_{tr}}{\sigma_{e,tr}A_{tr}^*}\right]\sigma_{ud} + \sigma_y\frac{A_{tr}}{A_{tr}^*} = 0 \tag{3b}$$

Eqn. (3b) is based on beam-column theory, with transformed section properties for the undented cross-section (A_{tr}), dented cross-section (A_{tr}^*), elastic section modulus (S_{tr}), and which accounts for member initial out-of-straightness effects. More details can be found in Parsanejad[13].

In the moment-thrust curvature based (M-P-ϕ) approach, the member was discretized into segments, as illustrated in Fig. 7. For the analysis of non-repaired members, empirical M-P-ϕ relationships for dented[4] and undented segments[23, 24] were used in conjunction with numerical integration[25] to account for second order effects, and to determine the member's axial load-deformation relationship. The M-P-ϕ relationship for a dented, non-repaired segment is shown in Fig. 8, which is that by Duan et al.[4]. Note that this relationship can be used to predict the loading and unloading branch of the load-deformation behavior of a dent-damaged member. Duan's M-P-ϕ relationship is based on an assessment and regression analysis of data from over 150 experimental tests of dent-damaged specimens, and represents an empirical expression for a dented tubular's moment-curvature response under a given axial load P. The dent-depth and out-of-straightness values of the test specimens in the database were in the range of up to 0.2D and 0.01L, respectively. A few tests had d_d = 0.23D and δ_o between 0.01L and 0.03L, respectively. Duan's

empirical expression for the M-P-ϕ relationship is very convenient, for during the integration analysis the curvature ϕ can be obtained directly based on the current moment M and axial load P.

In the analysis of the repaired specimens the member is also discritized into segments, however, the M-P-ϕ relationship of a grouted tube segment has to be computed by separate analyses of its cross-section. The computation involves generating data points corresponding to the moment-curvature (M-ϕ) response of the dented and undented sections of the grouted member for a specified axial force P. The cross-section of the grouted tube is first discritized into fibers, each fiber representing either steel or grout, based on the fiber's location. The material properties are defined for steel and grout fibers corresponding to their stress-strain curves. A data point corresponding to the M-P-ϕ relationship is established by iteration, involving the locating of the position of the neutral axis within the cross-section for a specific curvature ϕ and axial load P. Assumptions in the analysis include plane sections remaining plane and full bond (i.e., compatibility) between the steel and grout. An example of the M-P-ϕ relationship for a dented, grouted cross-section is shown in Fig. 9. Further details of the moment-thrust-curvature M-P-ϕ based integration method of analysis for non-repaired and internal grout repaired members can found in Fan[16] and Mathew et al.[26].

The non-linear finite element method (FEM) is considered the most advanced approach. For this purpose, the commercially available finite element program ABAQUS[27] was used. The finite element analysis was based on an updated Lagrangian formulation to capture the effects of large displacements, and Green's strain and second Piola-Kirchoff stress to model the moderate strain levels and the corresponding stress conjugate. The von Mises yield criterion with isotropic strain hardening was used in conjunction with eight node shell elements to model the steel tube in both the non-repaired and repaired specimen analysis. A typical mesh for the finite element model of a non-repaired specimen is shown in Fig. 10(a). Taking advantage of symmetry in boundary conditions, the finite element model for the non-repaired specimens consisted of 422 eight-node shell elements, 1831 nodes, and approximately 10400 degrees of freedom.

The non-linear finite element mesh used for analyzing internally grout repaired members is shown in Fig. 10(b), where also one-quarter of the member was modeled by taking advantage of symmetry. A combination of eight node shell elements and eight node and six node solid elements were used to model a section of the damaged member from the dent to a longitudinal distance of three diameters away. The remaining part of the member was modeled using beam-column elements. The solid elements were used to model the internal grout, whereas the shell elements were used to model the steel tube. Full bond transfer was assumed between the shell and the solid elements. The beam-column elements were assigned section properties related to those of a composite grout filled beam-column. Constraint equations were used to ensure compatibility between the beam-column and the shell elements at their interface. The grout was modeled using the confined concrete with tension stiffening option available in the ABAQUS library for material models. Taking advantage of symmetry, the FEM model consisted of a total of about 500 elements and approximately 8300 degrees of freedom.

The finite element analysis of a dented, non-repaired member involved four stages, similar to those of the experiments, namely: (1) supporting the member to prevent imposing excessive global out-of-straightness damage, and the loading of a knife edge indentor to create the dent-damage; (2) unloading of the indentor; (3) removal of the indentor and associated support from the model, as well as specifying the pin-ended boundary conditions; and (4) applying the axial load and utilizing the modified RIKS[28] solution scheme to solve for the non-linear force-deformation response of the member. The internal grout repaired specimens involved an intermediate stage of analysis between stages (3) and (4), in order to incorporate the solid brick grout elements into the model following denting, and thereby simulate a grout repair of a damaged member.

A comparison of the experimental residual strength P_{EXP} with that predicted by analysis, P_{PRED}, for the non-repaired specimens is shown in Fig. 11 and listed in Table 4. In Fig. 11, the comparison of the

effectiveness of the various analytical methods is made by plotting the normalized dent-depth d_j/D against the P_{EXP}/P_{PRED} ratio. Wherever possible, additional specimens tested by others[3, 5, 8, 9, 10] were analyzed and included in order to expand the available database. It is seen in Fig. 11(b) that the UC-DENT formulation provides a lower bound prediction to the experimental capacities, where the mean and coefficient of variation (COV) for the ratio of P_{EXP}/P_{PRED} is 1.553 and 0.178, respectively. For a deeper dent-depth a greater degree of conservatism exists in estimating member strength, as evident in Fig. 11(b). On the average, the unity check results provide a good prediction but larger scatter is seen in Fig. 11(d) when the d_j/D ratio exceeds 15%. The mean and COV for the ratio of P_{EXP}/P_{PRED}, when P_{PRED} is based on Loh's unity check, is 1.081 and 0.123, respectively. The FEM is shown in Fig. 11(a) to provide the best correlation between experimental and predicted capacities for all ranges of d_j/D ratios where the P_{EXP}/P_{PRED} has a mean of 1.018 and COV of 0.088. The M-P-ϕ approach also provides a reasonable prediction of member capacity where the mean and COV for the P_{EXP}/P_{PRED} ratio is 1.027 and 0.120, respectively. However, a data point associated with a member diameter-to-thickness ratio of D/t = 69 and d_j = 0.3D (Specimen C8) has a P_{EXP}/P_{PRED} ratio equal to 1.56, whereas a specimen of similar dent-depth but with D/t = 34.5 (Specimen A8) has a P_{EXP}/P_{PRED} ratio equal to 1.02. The reliability of Duan's M-P-ϕ empirical expression to predict dented member capacity for cases with deeper dent-depths and large D/t ratios (D/t > 46) deserves further study.

The comparison between the experimental capacities and predicted capacities using Parsanejad's method, M-P-ϕ based integration, and FEM, respectively, for internal grout repaired specimens is shown in Fig. 12 as a function of normalized dent-depth d_j/D, and is also listed in Table 5. Additional analysis of specimens tested by others[12, 13, 15] is also included in Fig. 12(a) and (b). The mean for the ratio of P_{EXP}/P_{PRED} for Parsanejad's approach and the M-P-ϕ based method is 1.186 and 1.075, respectively. The comparison shown in Fig. 12 indicates that in general, Parsanejad's approach is conservative and that the M-P-ϕ approach provides a better prediction of the repaired member capacity. A slightly larger scatter between the predicted and experimental capacities is seen in both of the approaches compared to the UC-DENT and M-P-ϕ integration analysis methods for non-repaired specimens, where the COV is 0.22 and 0.16 for Parsanejad's and the M-P-ϕ based analysis, respectively. Table 5 indicates that the M-P-ϕ analysis of the repaired specimens of deeper dent-depth (d_j = 0.15D and 0.30D) and D/t = 69 significantly over predicts member capacity. This over prediction is also seen in Parsanejad's method, and is attributed to the Poisson effect where the tube's diameter increases under an axial compressive load, causing the tube's wall to separate from the grout. The consequence of this separation is a reduction of the member's stiffness with respect to out-of-plane movement due to second order effects. This phenomena is not accounted for in the formulation for Parsanejad's and M-P-ϕ based analysis methods, and was observed in the experimental testing to be more prominent in the specimens with a higher D/t ratio. The finite element studies were able to more accurately predict the repaired capacity of specimens with D/t=69, and had the overall best agreement between predicted (P_{PRED}) and experimental (P_{EXP}) specimen capacity, as reflected in Fig. 12(c). For the finite element analysis results, the mean and COV for the ratio of P_{EXP}/P_{PRED} was 0.97 and 0.09, respectively.

Analytical Parametric Study

The M-P-ϕ approach is computationally efficient compared to the FEM, and has been shown above to provide a good prediction for a member's capacity, particularly when the D/t ratio is less than 46. The M-P-ϕ approach was therefore used to conduct a parametric study in order to investigate the interaction of global out-of-straightness δ_j/L and dent-depth d_j/D on a member's residual and repaired capacity, respectively. The results for the study having D/t = 34 are shown in Fig. 13(a) which represents a plot relating the variables δ_j/L and d_j/D to member ultimate capacity $P_{u,inc}$. In Fig. 13(a) the shaded surface is associated with non-repaired residual strength and the unshaded surface the repaired strength with internal grouting. It is seen in this figure that a greater reduction in capacity, both damaged and repaired, takes place

when the two effects of out-of-straightness and dent-depth are both considered simultaneously. Similar results were found for analysis using other values of D/t.

The repaired strength surface and the value for the undamaged strength of a member with D/t = 34 (the latter plotted as a flat surface) are shown superimposed in Fig. 13(b). The non-damaged member had an out-of-straightness of δ_o = 0.001L, based on the API-RP2A limit for out-of-straightness[29]. The line corresponding to the intersection between the repaired strength and non-damaged capacity surfaces indicates the effect of global out-of-straightness and dent-depth on repairability, and establishes a bound beyond which the full undamaged strength cannot be obtained by internal grout repair. For D/t = 34 this bound can be closely approximated by

$$\frac{\delta_p}{L} \le 0.01\left[1 - 0.8\frac{d_d}{D} - 6.4\left(\frac{d_d}{D}\right)^2\right] \quad \text{, where } \frac{d_d}{D} \le 0.33 \tag{4a}$$

For members with D/t = 46,

$$\frac{\delta_p}{L} \le 0.013\left[1 - \frac{d_d}{D} - 4.8\left(\frac{d_d}{D}\right)^2\right] \quad \text{, where } \frac{d_d}{D} \le 0.36 \tag{4b}$$

and, for members with D/t = 64,

$$\frac{\delta_p}{L} \le 0.017\left[1 - 1.3\frac{d_d}{D} - 3\left(\frac{d_d}{D}\right)^2\right] \quad \text{, where } \frac{d_d}{D} \le 0.40 \tag{4c}$$

For a given d_d/D and D/t ratio, internal grout repair is a viable repair technique to restore a member's capacity to its undamaged strength, if the δ_p/L and d_d/D ratios satisfy the above inequalities. As implied by Eqn. (4a), a member with D/t = 34 having a dent-depth which exceeds 0.33D cannot have its full non-damaged strength reinstated by internal grout repair, regardless of how small its out-of-straightness may be. The same is true if d_d exceeds 0.36 and 0.40 for members with a D/t of 46 and 64, respectively.

RESIDUAL STRENGTH AND REPAIR OF CORRODED TUBULARS

Experimental Program

The experimental study associated with assessing the residual strength and repair of corroded tubulars focused on the local buckling strength. A complete description of both the experimental and analytical program is found in Hebor and Ricles[19]. As noted previously, in the study by Ostapenko et al.[3] it was found that the patch with the most severe corrosion controls the local buckling of a tubular member. The study by the authors which is presented herein involved an investigation into the affects the geometry of a single patch of corrosion had on the local buckling strength, where the patch was idealized as an ellipse. *Cases of multiple patches of corrosion in a cross-section are to evaluated in future studies. Unlike uniform* corrosion, patch type corrosion causes the centroid of the cross-section to shift in a direction away from the patch, resulting in larger compressive stress to develop at the reduced wall thickness due to the combined effects of compressive axial force and flexure acting on the cross section.

As shown in Fig. 14, the parameters needed to describe the geometry of a corrosion patch include: (1) the length of the major c and minor h axes of the ellipse (where c=0.5DΘ, in which Θ and D are equal to the angle around the circumference which is subtended by the patch, and the outside

diameter of the cross-section, respectively, and h is equal to the height of the corrosion, as measured along the longitudinal axis of the tubular); (2) reduced-to-original wall thickness ratio (t_r/t); and, (3) member diameter-to-thickness ratio D/t. There are numerous profiles of the wall thickness within the corrosion patch that could be described by the parameters c and t_r/t, as shown in Fig. 15. Measuring accurately the thickness profile of a corrosion patch is difficult in the field due to inspection limitations and adverse environmental conditions. Consequently, the experimental test program involved testing 10 specimens having different sets of values for D/t, t_r/t, and Θ, with a thickness profile in the patch that was similar to that shown in Fig. 15(b), which will be referred to as the "experimental" profile. The affect of thickness profile on a member's local buckling strength was assessed analytically by examining a "step" and "cosine" thickness profile shown in Fig. 15(a) and (c), which would represent two extremes. The results from this parametric study will be discussed later. A parametric study was also conducted which determined that the member's local buckling strength was independent of the height h of the patch, as long as h was equal to or greater than 0.5D. In all test specimens a value of 0.5D was used for the height of the corrosion patch.

The matrix of 10 test specimens is shown in Table 6, where D/t ratios of 34, 46, and 64 were investigated. The nomenclature used to identify each specimen in the test program consisted of the D/t ratio, t_r/t ratio, and Θ, as shown in column 1 of Table 6. Hence, Specimen 34-33-58 was a tubular member having D/t=34, t_r/t = 0.33, and Θ = 58 degrees. Specimens 34-100-0, 46-100-0, and 64-100-0 were non-corroded tubulars which were used as control specimens. Specimen 46-00-95 had an elliptical shaped hole, simulating a case of corrosion which had progressed completely through the wall thickness. All specimens, except for the non-corroded ones, had a length of L=1409.7 mm and a slenderness ratio of L/r = 18.5. The non-corroded specimens were actually stub columns having a length equal to 3.5 times their diameter. All specimens were fabricated from ERW A53 Type B steel tubulars. Each specimen of a particular D/t ratio was cut from the same tubular. In order to obtain material properties representative of in-situ offshore tubulars, the steel tubulars with D/t = 34 and 46 were annealed. The average static yield stress σ_y and ultimate stress σ_u are reported in Table 6, and were determined by conducting standard ASTM[21] tensile coupon tests. The results for σ_y coincided closely with that determined from stub-column tests. The stub-column tests were done in accordance with standard procedures[20]. Stub-column stress-strain curves indicated that the annealed tubulars had virtually no residual stresses. The specimens fabricated from the tubulars of D/t=64 were found to have a linear stress-strain curve up to at least 90 percent of the compressive yield stress, indicating that there were no significant residual stresses present in these specimens. Hence, the experimental results reported herein do not include the effects of fabrication residual stresses, however, an analytical study of residual stresses[19] showed that they had little effect and in some cases actually increased the residual strength of patch corroded tubular members. The maximum difference in member capacity when accounting for residual stresses was found to be 2%.

Corrosion damage to the specimens was simulated by reducing the wall thickness by mechanically removing material with the use of a hand-held electric powered grinder. This simulation method was determined to be adequate, since corrosion is known not to cause any material property changes to tubulars having a yield strength less than 690 MPa. As noted previously, the contour of each specimen with corrosion had an idealized profile, consisting of zero slope at the most reduced area and at the edges of the corrosion patch (e.g. at the center and the edges of the ellipse of corrosion.). This contour was selected on the basis of idealized contours from measurements of actual corroded specimens[3]. During the grinding process, measurements were performed to ensure that the correct reduced wall thickness was obtained. These measurements of the corroded area were performed using a template of the corrosion profile and also with ultrasonic methods. Ultrasonic thickness measurements for Specimens 34-33-58 and 34-33-95 are shown in Fig. 16 as an unfolded surface over a longitudinal length of 0.5D. Thickness reduction values t_r for each specimen are given in Table 6, where they have been normalized by the original measured wall thickness t. The diameter, D, and wall thickness, t, of

each specimen were also measured, with averaged values included also in Table 6. As noted above, the height h of each corrosion patch was equal to 0.5 D (110 mm).

Each specimen was tested in a 2670 kN Satec overhead testing machine, as shown schematically Fig. 17. The instrumentation plan is also shown in Fig. 17, and consisted of a load cell to measure the applied axial load; transducers to monitor specimen axial shortening, radial movement of the corrosion patch due to local buckling; with longitudinal strain measured using strain gages. Each specimen was also white washed in order to observe the development of yield line patterns.

The testing of each specimen commenced with load applied under displacement control at a rate of 0.25 mm/minute. The loading was stopped and the head displacement held constant at significant events, such as the onset of local buckling and maximum load, in order to obtain static load measurements. The test was terminated when either the specimen capacity had degraded to 80 percent of the peak axial load, or the specimen's axial shortening reached approximately 13 mm in the post-ultimate load range.

Typical response of a corroded specimen began with linear elastic behavior, and uniform longitudinal strain throughout the specimen. As the axial shortening was increased, the axial load also increased and the longitudinal strains in the corroded cross section became non-uniform, while the strains in the cross-section at 0.5 D away from the corroded cross section remained uniform. Yielding was observed to first occur in the corrosion patch with a subsequent pronounced local buckle forming at the center of the corroded patch. The ultimate load of the specimen was attained three to five percent above the load at which the local buckle first formed. For all specimens, except Specimen 34-33-58, the local buckle mode was an outward movement and resembled an "elephant-foot" mode, initiating at the center of the corroded area and propagating around the circumference. The local buckling in Specimen 34-33-58 caused an inward movement. The inward or outward mode of buckling was dependent on the aspect ratio (c/h) of the patch of corrosion. The corrosion patch for Specimen 34-33-58 had an aspect ratio very close to 1.0, resulting in the inward local buckle becoming the critical mode. All other specimens had a corrosion patch with an aspect ratio ranging from 1.67 to 5.47, resulting in the outward local buckling mode. Both modes of local buckling are shown in Fig. 18.

As the axial deformation was continued, the buckling became more pronounced as it propagated around the circumference of the cross section. In addition, yielding became more extensive in the corroded cross section and also propagated around the circumference. The consequence of the yielding and local buckling was a loss of capacity, as shown in the axial load-deformation response of Specimen 46-33-95 given in Fig. 19.

A summary of the experimental axial load capacity $P_{u,exp}$ of each specimen is given in Table 7, where they have been normalized by the full axial yield capacity P_y. The experimental capacity of the non-corroded specimens (34-100-0, 46-100-0, 64-100-0) were all equal to 1.0 P_y. The axial load-deformation response of Specimen 46-100-0 is compared with that of Specimen 46-33-95 in Fig. 19, where it is evident that local buckling caused a significant loss of capacity in the corroded specimen. A comparison of the ratio of $P_{u,exp}/P_y$ of the corroded and corresponding non-corroded specimens in column 3 of Table 7 indicates that the loss of strength in corroded specimens with D/t=34 ranged from 8 percent to 32 percent, where a greater loss occurred for specimens with deeper corrosion (e.g. smaller t_c/t values) and wider corrosion patches (e.g. larger Θ values). An examination of corroded specimens having D/t=46 and Θ=95 degrees shows a reduction in capacity of 8 percent to over 21 percent compared to their corresponding non-corroded capacity. Specimen 46-33-95 is shown to have suffered a 19 percent reduction in strength due to corrosion. A comparison with Specimen 34-33-95, which has a lower D/t ratio but with the same extent of corrosion and a 17.5 percent capacity reduction, indicates that corroded specimens with larger D/t ratios have a slightly larger capacity reduction due to the corrosion patch. The

influence of the above parameters on the capacity of a corroded member will be discussed more under the results of the analytical parametric study.

The experimental program to study the repair of patch corroded members also included the testing of two repaired specimens. The two repaired specimens were inflicted with the same corrosion as Specimen 46-00-95 so that a direct comparison of repaired and non-repaired specimen capacities could be made. With respect to each other, the two repaired specimens were identical except for the grout used to fill the annulus between the sleeve and the damaged tubular. One of the repaired specimens used a cement-based grout (Specimen 46-00-95-C), while the other used an epoxy-based grout (Specimen 46-00-95-E). The two repaired specimens and non-repaired Specimen 46-00-95 are shown in Fig. 20. Because the purpose of testing was to investigate a concept rather than a specific repair, the sleeve was not designed as it would be in practice, for the sleeve was not split into two halves nor were there any clamping brackets. The steel sleeve used for the repair had an inside diameter of 257 mm, a wall thickness of 9.5 mm, and a length of 267 mm. These sleeve and tubular dimensions produced an annulus between the tubular and the sleeve of 19 mm. To prepare the wall surface of the tubular for the repair sleeve, as well as provide a consistent, uniform surface roughness, the grout contact surfaces of the tubular and the sleeve were sandblasted to a consistent roughness of approximately 3 mils. Based on material tests[19], it was determined that the epoxy-based grout had a bond strength and compressive strength approximately 7.6 and 1.8 times greater, respectively, than that of the cement-based grout.

The test setup, and instrumentation were the same as that for the non-repaired specimens, as shown previously in Fig. 17, with the addition of eight longitudinal strain gages around the circumference of the outside surface of the repair sleeve at mid-height, and eight more longitudinal strain gages along the length of the sleeve on the 0 and 180 degree sides.

The non-repaired specimen (Specimen 46-00-95) had a static residual strength of $0.783P_y$, representing a capacity reduction of 21.7 percent compared to an undamaged tubular. The normalized axial load-shortening response of this specimen is plotted in Fig. 21, where it is compared to that of the repaired, as well as the non-corroded (46-100-00) tests. It is apparent from the normalized load-deformation plots in Fig. 21 that both repaired specimens, 46-00-95-C (Cement-based grout) and 46-00-95-E (Epoxy-based grout), were successful in reinstating the capacity to that of the undamaged member. For both of the repaired specimens the sleeve was stiff enough to provide proper hoop restraint to confine the cross section from buckling outward. Both repaired specimens failed by gross yielding of their cross section outside the sleeve repair.

While the ultimate load was not affected, there is a definite influence of grout bond strength on the behavior of the repair. The lower strength cement-based grout resulted in a more non-uniform strain distribution, yielding, and an eventual inward local buckling of the corroded cross section, as well as an overall excessive lateral deflection of the specimen. These undesirable effects were caused by the lower bond (1.1 MPa) strength of the cement-based grout which could not preserve full compatibility between the tubular and the sleeve. These effects also account for the "softening" and nonlinearity of the load-deformation plot just prior to the ultimate load (see Fig. 21(a)). The damaged cross section still possessed an internal eccentricity and reduced gross section, leading to a reduced resistance to local buckling; however, the effects of these problems was minimized by the confinement of the sleeve. In contrast, the epoxy-based grout had a bond capacity (8.38 MPa) high enough to preserve the compatibility between the tubular and the sleeve, which prevented yielding and local buckling of the corroded cross section. The normalized load-deformation plot in Fig. 21(b) is linear up to the ultimate load. It was found that the strain distribution was more uniform throughout the epoxy-based repair and lateral deflections were reduced by over 80%.

Other positive aspects about the use of epoxy-based grout include the curing time and the inertness of the epoxy. The epoxy-based grout reached 80 to 90 percent of full strength in twenty-four

hours (epoxy-based grout cubes exceeded a compressive strength of 55.2 MPa in 24 hours), and reached full strength in seven days. In contrast, cement-based grout attains only minimal strength after twenty-four hours and needs 21 to 28 days to reach full strength. Furthermore, the epoxy-based grout is not influenced by contact with water, and can be used to displace water without detrimental effects. In contrast, the strength of the cement-based grout is highly dependent on the water to cement ratio. Therefore, the quality of the cement-based grout can be more affected by forcing it to displace water during a repair.

Analytical Program

The commercial finite element program ABAQUS[27] was used to perform a finite element analysis of each of the non-repaired corrosion specimens. Material properties from the tensile tests and nominal dimensions of each specimen were used in the finite element models. The same eight node shell element, the material modeling for the steel tube, and the solution scheme that was used for the analysis of the dent-damaged specimens was utilized in the analysis of the corroded specimens.

Taking advantage of symmetry about mid-height and the cross section, and by using the appropriate boundary conditions, only one quarter of each specimen had to be modeled (as shown in Fig. 22). The finite element mesh was refined in the area where corrosion existed (e.g. near mid-height of the specimens). A typical mesh had 350 shell elements, and 7000 degrees of freedom. The reduction of the wall thickness due to the corrosion was modeled, as shown in Fig. 23, by assigning each element Ω_i in the corroded area with an associated reduced thickness t_i and an associated mid-surface offset. The mid-surface offset was created by assigning coordinates to the element nodes corresponding to the appropriate offset. Modeling the corrosion in this manner attempted to align the inside face of each element while staggering the outside face, in order to simulate a thickness reduction occurring from the outside wall surface.

Several initial analyses were conducted to assess the sensitivity of the capacity of the tubular member to the element mesh, particularly in the corrosion patch area. It was found that good agreement with experimental results was obtained when considering the thickness reduction to occur over a rectangular area of height h in the specimen's longitudinal direction which was equal to or greater than a critical value h_{crit} of approximately 0.5D. The distance h_{crit} is associated with the minimum corroded distance for which the local buckle wave can form in the longitudinal direction of the specimen. This greatly simplified the analysis, for only the elements within the rectangular area of width $c=0.5D\Theta$ and height h_{crit} needed to have a reduced thickness. As noted previously, the experimental study concentrated on corrosion patches with height h greater than or equal to h_{crit}, and therefore, the height of the corrosion patch was not considered as a parameter. For patch corroded tubular members with h less than h_{crit}, the assumption of h equal to h_{crit} would produce a conservative estimate of the residual strength.

A comparison of the predicted specimen capacity $P_{u,FEM}$ by the finite element analyses with the experimental result $P_{u,exp}$ is presented in column 4 of Table 7. The agreement is shown to be good, with the ratio of $P_{u,FEM}/P_{u,exp}$ ranging from 0.922 to 1.0, with a mean of 0.980 and a coefficient of variation (COV) of 0.024. The results for the finite element analysis and experimental study are also plotted in Fig. 24(a) where good agreement between the two is also evident.

A simplified elastic analysis for predicting the capacity of each non-repaired specimen was also performed. The centroid shift, e, the section modulus, S_g, and the area, A_g, of the corrosion-damaged cross section was calculated by discretizing it into 100 segments and summing the first and second moments for each segment about the geometric center of the cross section. The stresses from direct axial loads, flexure due to the centroidal shift, and fixed end moments, M_{FEM}, were then superimposed and equated to the yield stress of the specimen as follows:

$$\frac{P_u}{A_d} + \frac{P_u e}{S_d} - \frac{M_{FEM}}{S_d} = \sigma_y \tag{5}$$

The load, P_u, to cause the stress at the center of the corrosion patch to reach yield was then determined. This load was used as the estimate, $P_{u,est}$, of the capacity of the specimen. The fixed end moments, M_{FEM}, were determined from analysis, and found to cause no more than a 3 percent increase in the predicted load, $P_{u,est}$. The yield stress σ_y was used in Eqn. (5) in lieu of a theoretical local buckling stress σ_u, because all the specimens were observed to develop yielding in the center of the corrosion patch prior to when local buckling in the patch had occurred. This simplified elastic analysis produced reasonable results, which are listed in column 5 of Table 7 and shown in a correlation scatter plot with the experimental results in Fig. 24(b). The agreement between the predicted capacities and the experimental results is good, with values of the ratio $P_{u,est}/P_{u,exp}$ ranging from 0.849 to 1.04 (see Table 7), and having a mean of 0.977 and COV of 0.051.

Parametric Study

Several parametric analytical studies were performed in order to assess the affects of the geometrical parameters which describe the corrosion patch and tube, namely: t_r/t, Θ, and D/t. Also included in these studies was the affect of the profile within the corrosion patch. Three profiles were studied, which had been referred to earlier (see Fig. 15), namely: (a) "step"; (b) "experimental"; and, (c) "cosine". The "cosine" and "step" profiles represent the upper and lower bound, respectively, associated with the member's local buckling strength for a given set of values for the parameters θ and t_r/t. The purpose of investigating profile effects was to assess the difference between these two bounds, since in practice it is likely that the thickness profile cannot be measured accurately in the field, and consequently it may be desirable to use the "step" profile if it is not overly conservative.

Shown in Fig. 25 are selected results associated with the "experimental" profile and where h=0.5D. Each set of results presented in Fig. 25(a), (b), and (c) represents a series of analysis where two of the three parameters t_r/t, Θ, and D/t were held constant, and the third varied. The ensuing relationships between the normalized member capacity P_u/P_y and the independent parameter that was varied, either t_r/t, θ, or D/t, are each known as coordinate functions. Fig. 25 indicates that each of these coordinate functions is linear. Furthermore, the member local buckling capacity P_u/P_y is shown to be significantly sensitive to the parameter Θ (see Fig. 25(a)) and t_r/t (see Fig. 25(b)), whereas it is not as sensitive to the member's D/t ratio (see Fig. 25(c)).

A data base was developed by conducting 29 analyses, in which the parameters t_r/t, Θ, and D/t were systematically varied in the analysis models. Included in these analyses were models of the experimental test specimens. The linear coordinate functions were subsequently combined using a multi-variable regression analysis to obtain a closed form expression for P_u/P_y as a function of the parameters t_r/t, Θ, and D/t, where:

$$P_u/P_y = 1.0 - 0.001\left(\frac{D}{t}\right) + 0.052\left(\frac{t_r}{t}\right) - 0.0026(\Theta) - 0.0028\left(\frac{t_r}{t}\right)(\Theta) \tag{6a}$$

in which

$$34 \le \frac{D}{t} \le 100; \quad 0 \le \frac{t_r}{t} \le 1.0; \quad 58^\circ \le \Theta \le 311^\circ \tag{6b}$$

A comparison of the experimental specimen capacity $P_{u,exp}$ and the predicted value $P_{u,eq}$ by Eqn. (6a) has the ratio of $P_{u,eq}/P_{u,exp}$ ranging from 0.894 to 1.02, see Table 7, with a mean of 0.977 and COV of 0.044,

indicating that good agreement exists between the predicted and experimental capacities. A comparison between the experimental and regression analysis capacity predictions is shown in Fig. 24(a). The comparison between the finite element analysis results for member capacity $P_{u,FEM}$ and $P_{u,reg}$, in which the former was used to create the database for the regression analysis, is given in Fig. 24(c). The agreement between $P_{u,FEM}$ and $P_{u,reg}$ for the 29 analysis cases is generally good, where the ratio $P_{u,reg}/P_{u,FEM}$ varies from 0.925 to 1.115, and has a mean of 1.001 and COV of 0.034.

The affect of the thickness profile within the corrosion patch on member local buckling strength P_c/P_y is shown in Fig. 26, where the coordinate functions are plotted for member strength with θ, t_c/t, and D/t as the independent variables, respectively, for the "step" and "cosine" profiles. Fig. 26(d) shows the affect of the normalized patch height h/D on P_c/P_y, where the experimental data has been superimposed. The results in Fig. 26(d) indicate that for both the "step" and "cosine" profiles that the decrease in strength P_c/P_y is constant for a patch height h greater than or equal to 0.5D. The maximum discrepancy in P_c/P_y is 14% between the results based on the upper and lower bounds computed using the "step" and "cosine" profile. The experimental data is within 7% of the two bounds. The remaining coordinate functions (Figs. 24(a), (b), and (c)) are shown to vary linearly for both profiles, with the difference between the two becoming larger as the corrosion patch width (θ) and depth (t_c/t) increase (see Fig. 26(a) and (b)).

The discrepancy in the prediction for P_c/P_y using the "cosine" and "step" profiles is 10% and 14% for $\theta=60^0$ and 100^0, respectively, and increases to 45% for $\theta=320^0$ (see Fig. 26(a)). The latter case, where $\theta=320^0$ and $t_c/t=0.33$, is considered to be a significantly corroded case. The discrepancy is much less when varying t_c/t , where the predicted strength P_c/P_y based on the "step" and "cosine" profiles is within 7% and 12% of each other when t_c/t is equal to 0.66 and 0.33, respectively (see Fig. 26(b)). The discrepancy in the predicted value for P_c/P_y using the two "step" and "cosine" profiles remains fairly constant as the D/t ratio increases, being about 13% (see Fig. 26(c)). In all cases, the experimental data is bounded by the 'step" and "cosine" profiles, and is within 7% of these bounds.

Although there is some difference in the predicted strengths using the "cosine" and "step" profiles, actual corrosion patch profiles will fall in between these profiles and the predicted strengths from them will bound the actual capacity. An assessment of the results presented in Fig. 26 indicates that the difference in the results for P_c/P_y based on the two bounds is at most 14% when θ is less than 120^0, where the patch width c is one-third the member circumference (e.g., c=0.33D), and anticipated to be 26% when $\theta=180^0$ (corresponding to c=0.5D). Considering the uncertainties associated with the analysis of an offshore structure, including wave load estimation as well as structural modeling of members and the foundation, and the difficulty in accurately measuring a corrosion profile, it appears to be practical to conservatively use the "step" profile in assessing the local buckling strength.

SUMMARY AND CONCLUSIONS

The results of an experimental and analytical study show a significant decrease in the ultimate axial load capacities of tubular members having dent-damage. The non-linear finite element and moment-thrust-curvature based analysis methods are both able to predict reasonably well the behavior of the non-repaired specimens with dents. The M-P-ϕ approach is able to also reasonably and efficiently predict the behavior of repaired specimens having D/t ratios of 46 or less. Parametric studies indicate that the interaction of dent-depth and out-of-straightness can have a significant effect on a member's ultimate capacity. An internal grout repair was shown experimentally to be able to reinstate a member to its original strength if the out-of-straightness and dent-depth were less than approximately 0.002L and 0.15D, respectively. Analytically it was found that internal grouting is unsuccessful in restoring the capacity of members with D/t=34 and

having a dent-depth of 0.33D or greater and no out-of-straightness. Similar results have been found for members having D/t = 46 , 64, and 69.

The results of an experimental and analytical study on the residual strength of short steel tubulars with idealized patch corrosion subjected to concentric axial load indicated that a significant reduction in capacity occurs due to the initiation of local buckling in the corrosion patch. This local buckling is attributed to the effect of a reduced wall thickness, combined with an amplification of stress at the corroded area due to a shift in the centroid of the cross section. Nonlinear finite element analysis showed the corroded specimen capacity to have linear coordinate functions with respect to the corrosion parameters t_c/t, Θ, and D/t. The shape of the wall thickness profile within the corrosion patch has an affect on the local buckling strength, but was found not to be as significant as the need to use accurate values for the parameters Θ and t_c/t. The local buckling strength in the corrosion patch is independent of the height of the patch h, provided that the corrosion height is equal to or greater than 0.5D. A multi-variable regression analysis resulted in a semi-empirical expression for predicting the axial load capacity of short, patch-corroded steel tubulars. The use of a simplified elastic analysis also provided reasonable approximations of the residual strength. The exterior grouted sleeve repair was found to successfully reinstate the full capacity of a corrosion damaged tubular member. Confinement of the corroded cross-section is the primary mechanism for a successful repair, and low bond strength grouts may be used for sleeve type repairs. However, epoxy-based grouts are more capable of preventing yielding and buckling of the damaged cross section because of their high bond strength. High bond strength grout should be used, particularly when the possibility of inward buckling of the corrosion patch exists.

ACKNOWLEDGMENTS

Financial support for the research reported herein was provided by National Science Foundation (Grant No. MSS 91-57959 PYI and MSS 93-96120 PYI), ATLSS Engineering Research Center Liaison Program at Lehigh University, Chevron Oil Field Research Company, Union Oil Company of California (UNOCAL 76), California State Lands Commission, Pittsburgh Supercomputing Center (Grant No. CTS930012P and MSS940021P), National Sea Grant College Program, National Oceanic and Atmospheric Administration (NOAA), United States Department of Commerce through the California Sea Grant College, and California State Resources Agency. The support of all the sponsors is gratefully appreciated. The opinions expressed herein are those of the authors, and do not necessary reflect the views of any of the sponsors.

REFERENCES

1. Dunn, F. P. (1983), "Offshore Platform Inspection", Proceedings, *International Symposium on the Role of Design, Inspection and Redundancy in Marine Structural Reliability*, Marine Board, National Research Council, National Academic Press.

2. Cole, M.W., Marucci, T.F. and Taft, D.G., (1987) "MODU Marine Safety: Structural Inspection and Readiness Surveys," *Journal of Petroleum Technology*, Society of Petroleum Engineers, November 1987.

3. Ostapenko, A., Wood, B., Chowdhury, A. and Hebor, M. (1993), "Residual Strength of Damaged and Deteriorated Tubular Members in Offshore Structures", *ATLSS Report No. 93-03*, Lehigh University, Bethlehem, Pennsylvania.

4. Duan, L., Chen, W. F. and Loh, J. T. (1993), "Moment Curvature Relationships for Dented Tubular Sections", *Journal of Structural Engineering*, ASCE, Vol. 119, No. 3.

5. Landet, E. and Lotsburg, I. (1992), "Laboratory Testing of Ultimate Capacity of Dented Tubular Members", *Journal of Structural Engineering*, ASCE, Vol. 118, No. 4.

6. Loh, J. T. (1993), "Ultimate Strength of Dented Tubular Steel Members", *Proceedings of the Third International Offshore and Polar Engineering Conference*, Singapore.

7. MacIntyre, J. (1991), "An Analytical Study of Damaged Tubular Member Behaviour", Ph.D. Thesis, University of Toronto, Toronto, Canada.

8. Smith, C. S., Kirkwood, W., and Swan, J. W. (1979), "Buckling Strength and Post-Collapse Behavior of Tubular Bracing Members Including Damage Effects," *BOSS '79*, Imperial College, London, England.

9. Smith, C. S., Somerville, J. W., and Swan, J. W. (1981), "Residual Strength and Stiffness of Damaged Steel Bracing Members", *Proceedings of the Offshore Technology Conf.*, OTC Paper 3981, Houston, Texas.

10. Taby, J. (1986), "Residual Strength of Damaged Tubulars. Final Report," NTNF Programme for Marine Structures, *SINTEF Report No. 6.10*, Trondheim, Norway.

11. Padula, J.A. and Ostapenko, A., (1989) "Axial Behavior of Damaged Tubular Columns," *Fritz Engineering Laboratory Report No. 508.11*.

12. Boswell, L. F. and D'Mello, C. A. (1988), "Residual and Fatigue Strength of Grout-Filled Damaged Tubular Members", *OTH 89 314*, Offshore Technology Report, U.K. Dept. of Energy.

13. Parsanejad, S. (1987), "Strength of Grout-Filled Damaged Tubular Members", *Journal of Structural Engineering*, ASCE, Vol. 113, No. 3.

14. Parsanejad, S., Gusheh, P. (1992) "Behavior of Partially Grout Filled Damaged Tubular Members." *Journal of Structural Engineering*, ASCE, Vol 118, No. 11, PP. 3055-3066.

15. Billington, C.J., Harwood, R.G., and Tebbett, I.E., "Grouted Repairs to Steel Offshore Structures" *OTH 84 202*, Offshore Technology Report, Wimpey Laboratories Limited, London, United Kingdom, 1984.

16. Fan, C.H. (1994), "Assessment and Prediction of the Behavior of Dent-Damaged and Internally Grout Repaired Tubular Steel Bracing Using Moment Curvature-Based Integration Methods", M.S. Thesis, Department of Civil Engineering, Lehigh University, Bethlehem, Pennsylvania.

17. Bruin, W.M. (1994), "Residual Strength and Repair of Significantly Dented Offshore Platform Bracing", M.S. Thesis, Lehigh University, Department of Civil Engineering, Bethlehem, Pennsylvania (in preparation)

18. Ricles, J., Gillum, T. and Lamport, W. (1994), "Grout Repair of Dented Offshore Tubular Bracing - Experimental Behavior", *Journal of Structural Engineering*, ASCE, Vol. 120, No. 7.

19. Hebor, M., and Ricles, J. (1994) "Residual Strength and Repair of Corroded Marine Steel Tubulars," *ATLSS Report No. 94-10*, ATLSS Eng. Research Center, Lehigh University, Bethlehem, Pennsylvania.

20. Galambos, T. V. (1988), *Guide to Stability Design Criteria for Metal Structures*, Fourth Edition, Wiley-Interscience Publication, New York, New York.

21. "Test Methods for Tensile Coupon Testing" (1991), *ASTM Special Technical Publication E8-91*, ASTM, Philadelphia, Pennsylvania.

22. "Test Methods for Compressive Strength of Hydraulic Cement Mortars" (1992), *ASTM Special Technical Publication C109-02*, ASTM, Philadelphia, Pennsylvania.

23. Chen, W. F. and Han, D. J. (1985), *Tubular Members of Offshore Structures*, Pitman, London, England.

24. Sohal, I. S., and Chen, W. F. (1988), "Local and Post-Buckling Behavior of Tubular Beam-Columns", *Journal of Struc. Engineering*, ASCE, Vol. 114, No. 5.

25. Newmark, N. M. (1942), "Numerical Procedure For Computing Deflections, Moments and Buckling Loads", *Transaction*, ASCE, May.

26. Mathew, J., Ricles, J., Bruin, W. and Sooi, T. K. (1993), "Moment-Curvature Analysis of Dented Tubular Beam Columns", NSF Research Experience for Undergraduates (REU) Report (unpublished), ATLSS Engineering Research Center, Lehigh University, Bethlehem, Pennsylvania.

27. *ABAQUS User's Manual (Version 5.3)* (1993), Copyright Hibbitt, Karlsson and Sorensen, Inc., 100 Medway Street, Providence, Rhode Island, 02906.

28. Riks, E. (1979) "An Incremental Approach to the Solution of Snapping & Buckling Problems," *Inter. Journal for Solids and Structures*, Vol 15.

29. American Petroleum Institute (1993), "Recommended Practice for Planning, Designing and Constr. Fixed Offshore Platforms - Load Resistance and Factor Design", *RP2A-LRFD*, 20th Edition.

Table 1. Dented Specimen Experimental Test Matrix

Spec.	D/t	d/D	e/D	D [mm]	t [mm]	δ/L	σ_y [MPa]	f'_c [MPa]	Test Description
A1	34.5	0.101	0	219	6.3	0.0007	240	-	Non-repaired
B1	46	0.099	0	219	4.7	0.0009	230	-	Non-repaired
C1	64	0.100	0	220	3.4	0.0012	272	-	Non-repaired
C1-a	64	0.097	0	219	3.4	0.0026	303	-	Non-repaired
A2	34.5	0.098	0.2	219	6.3	0.0006	240	-	Non-repaired
B2	46	0.100	0.2	219	4.7	0.0026	230	-	Non-repaired
C2	64	0.100	0.2	220	3.5	0.0007	272	-	Non-repaired
A3	34.5	0.099	0.2	219	6.3	0.0006	240	30.2	Internal Grout Repair
B3	46	0.100	0.2	219	4.7	0.0011	230	26.8	Internal Grout Repair
C3	64	0.100	0.2	220	3.4	0.0009	272	47.3	Internal Grout Repair
C4	64	0.100	0.2	220	3.5	0.0012	272	42.1	Grouted Sleeve Repair
A5	34.5	0	0.2	219	6.3	0.0002	351	-	Non-damaged
B5	46	0	0.2	219	4.7	0.0001	335	-	Non-damaged
C5	64	0	0.2	220	3.5	0.0009	272	-	Non-damaged
A6	34.5	0.145	0	219	6.4	0.0019	262	-	Non-repaired
B6	*46*	*0.151*	*0*	*219*	*4.8*	*0.0015*	*262*	-	*Non-repaired*
C6	69	0.149	0	218	3.2	0.0018	290	-	Non-repaired
A7	34.5	0.151	0	220	6.4	0.0019	262	38.2	Internal Grout Repair
B7	46	0.149	0	219	4.8	0.0019	283	38.9	Internal Grout Repair
B7 - a	46	0.150	0	219	4.8	0.0021	283	41.2	Reduced Internal Bond

Table 1 (cont'd). Dented Specimen Experimental Test Matrix

B7 - b	46	0.149	0	219	4.8	0.0022	283	17.3	Reduced Grout Strength
C7	69	0.147	0	218	3.2	0.0019	290	44.1	Internal Grout Repair
B17	46	0.198	0	219	4.8	0.0032	283	-	Non-repaired
A8	34.5	0.299	0	219	6.4	0.0099	241	-	Non-repaired
C8	69	0.296	0	219	3.2	0.0060	290	-	Non-repaired
A9	34.5	0.297	0	219	6.4	0.0094	269	37.1	Internal Grout Repair
C9	69	0.300	0	218	3.2	0.0059	290	41.4	Internal Grout Repair

Nominal D/t ratios are reported

Table 2 Comparison of Non-repaired Residual Strength with Non-damaged Specimen Capacity.

Specimen	$P_{NR,EXP}$ [kN]	P_{NR}/P_0
A1	627	0.68
B1	440	0.65
C1-a	378	0.61
A2	405	0.59
B2	231	0.50
C2	205	0.71
A6	623	0.61
B6	400	0.49
C6	276	0.50
B17	374	0.46
A8	276	0.27
C8	147	0.26

Table 3 Comparison of Repaired with Non-repaired and Non-damaged Specimen Capacity.

Specimen	$P_{R,EXP}$ [kN]	P_R/P_{NR}	P_R/P_0
A3	850	2.10	1.23
B3	520	2.25	1.13
C3	543	2.65	1.88
C4	329	1.61	1.14
A7	1081	1.74	1.08
B7	939	2.33	1.15
B7 - a	903	2.25	1.11
B7 - b	814	2.03	1.00
C7	494	1.79	0.90
A9	618	2.24	0.59
C9	356	2.42	0.64

Table 4 Comparison Between Experimental and Predicted Capacity for Non-Repaired Specimens.

Spec.	$P_{NR,EXP}$ [kN]	$P_{NR,EXP}/P_{PRED}$			
		FEM	Numerical Integration	UC-DENT	Unity Check Eq's
A1	627	1.01	0.96	1.46	0.97
B1	440	0.92	1.02	1.53	1.02
C1-a	378	0.96	1.06	1.58	1.23
A2	405	1.04	0.96	1.41	1.20
B2	231	0.90	0.84	1.19	1.13
C2	205	0.92	0.99	1.28	1.24
A6	623	1.08	0.97	1.54	1.05
B6	400	1.02	0.97	1.32	0.95
C6	276	1.04	1.20	1.45	1.27
B17	374	1.08	1.09	1.86	1.15
A8	276	1.01	1.02	2.13	0.97
C8	147	1.05	1.56	1.88	0.84

Table 5 Comparison Between Experimental and Predicted Capacity for Internal Grout Repaired Specimens.

Spec.	$P_{R,EXP}$ [kN]	$P_{R,EXP}/P_{PRED}$		
		FEM	Numerical Integration	Parsanejad
A3	850	1.12	1.08	1.17
B3	520	0.82	0.92	0.96
C3	543	0.96	0.94	0.91
A7	1081	0.92	0.97	0.89
B7	939	0.90	0.94	0.85
B7-a	903	0.97	0.86	0.83
B7-b	814	1.02	0.90	0.86
C7	494	1.06	0.54	0.54
A9	618	0.93	1.07	0.96
C9	356	1.01	0.73	0.67

Table 6 Corroded Specimen Experimental Test Matrix.

Spec.	D [mm]	t [mm]	t/t	Θ [deg]	c [mm]	h [mm]	σ_y [MPa]	σ_u [MPa]
34-100-0	218.5	6.4	1.0	0	0	109.5	255.1	400.0
34-33-58	218.4	6.5	0.33	58.4	111.2	109.5	255.1	400.0
34-33-95	218.7	6.5	0.33	95.7	182.6	109.5	255.1	400.0
34-50-311	218.4	6.4	0.51	311	592.8	109.5	255.1	400.0
46-100-0	218.1	4.8	1.0	0	0	109.5	265.5	413.7
46-00-95	218.2	4.8	0.0	95.7	182.1	109.5	265.5	413.7
46-33-95	218.2	4.8	0.36	95.7	182.1	109.5	265.5	413.7
46-67-95	217.9		0.67	95.7	181.9	109.5	265.5	413.7
64-100-0	218.9	3.4	1.0	0	0	109.5	268.9	420.6
64-60-95	218.9	3.4	0.59	95.7	182.8	109.5	268.9	420.6

Table 7 Corroded Specimen Axial Load Capacity and Comparison with Analytical Results.

Spec.	P_y [kN]	$\frac{P_{u,exp}}{P_y}$	$\frac{P_{u,FEM}}{P_{u,exp}}$	$\frac{P_{u,sim}}{P_{u,exp}}$	$\frac{P_{u,reg}}{P_{u,exp}}$
34-100-0	1065	1.0	1.0	0.997	1.017
34-33-58	1071	0.916	0.969	0.978	0.968
34-33-95	1072	0.825	0.974	0.991	0.994
34-50-311	1054	0.684	0.966	0.849	0.894
46-100-0	859	1.0	1.0	0.997	1.005
46-00-95	858	0.783	0.922	0.928	0.899
46-33-95	858	0.809	0.973	1.01	0.999
46-67-95	861	0.924	0.988	0.984	0.992
64-100-0	614	1.0	1.0	0.997	0.982
64-60-95	614	0.856	1.0	1.04	1.02

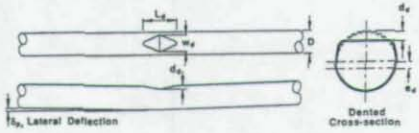

Fig. 1 Dent-Damaged Tubular Member

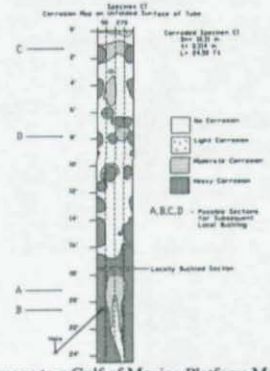

Fig. 2 Corrosion Damage to a Gulf of Mexico Platform Member [Ostapenko et al. 1993]

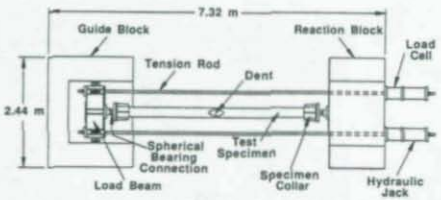

Fig. 3 Experimental Test Setup for Dent-Damaged Specimens

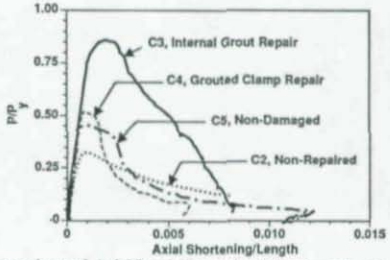

Fig. 4 Experimental Axial Load-Shortening Behavior, D/t =64

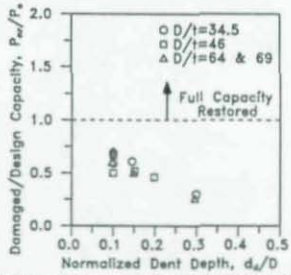

Fig. 5 Effect of Dent Damage on Member Capacity

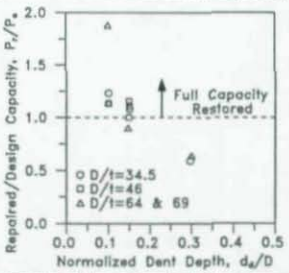

Fig. 6 Effectiveness of Grout Repair of Dent-Damaged Bracing

Fig. 7 Segments for M-P-Φ Numerical Integration Analysis

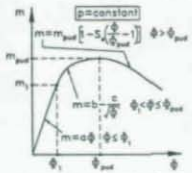

Fig. 8 M-P-Φ Relationship for Dented Tubulars Sections after Duan et al. [1993]

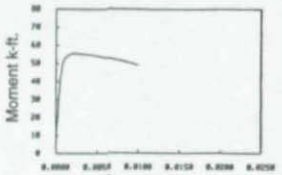

Fig. 9 Numerically Generated M-P-ϕ Relationship for Grout Filled Tubular Section

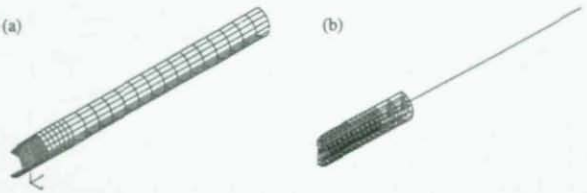

Fig. 10 Typical Finite Element Mesh for (a) Non-repaired, and (b) Internal Grout Repaired Dented Tubular

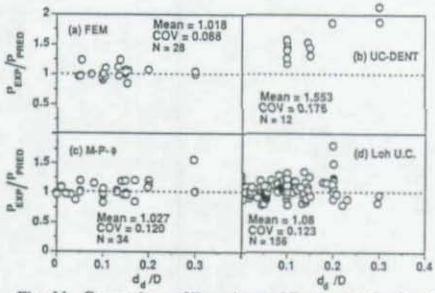

Fig. 11 Comparison of Experimental P_{EXP} with Predicted P_{PRED} Capacity, Non-repaired Dented Tubulars

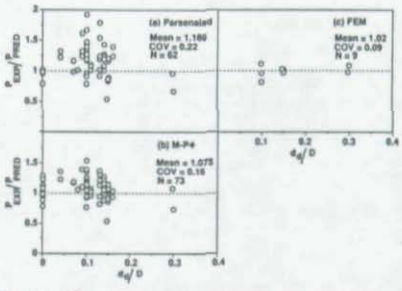

Fig. 12 Comparison of Experimental P_{EXP} with Predicted P_{PRED} Capacity, Internal Grout Repaired Dented Tubulars

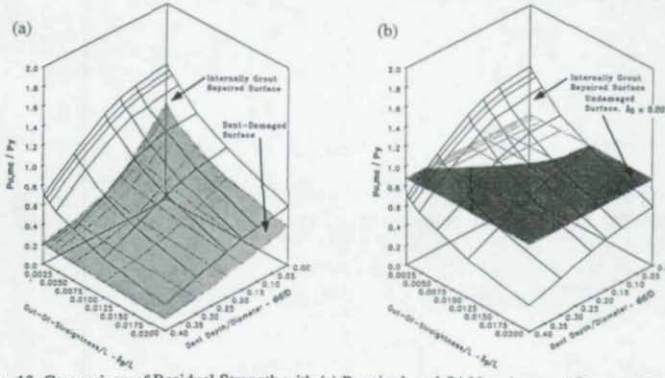

Fig. 13 Comparison of Residual Strength with (a) Repaired, and (b) Non-damaged Strength, D/t=34.5

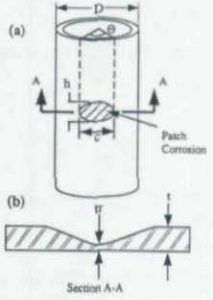

Fig. 14 Geometric Parameters of Tubular Corrosion Patch

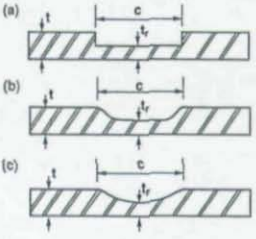

Fig. 15 Corrosion Patch Thickness Profiles Selected for Study: (a) Step, (b) Experimental, and (c) Cosine

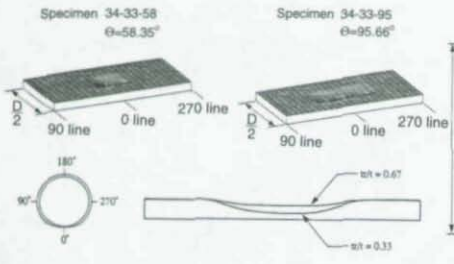

Fig. 16 Measured Wall Thickness Surface Plots and Cross-Sectional Corrosion Profile for Selected Specimens

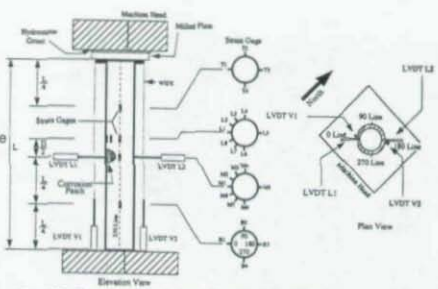

Fig. 17 Experimental Test Setup for Corrosion Specimens

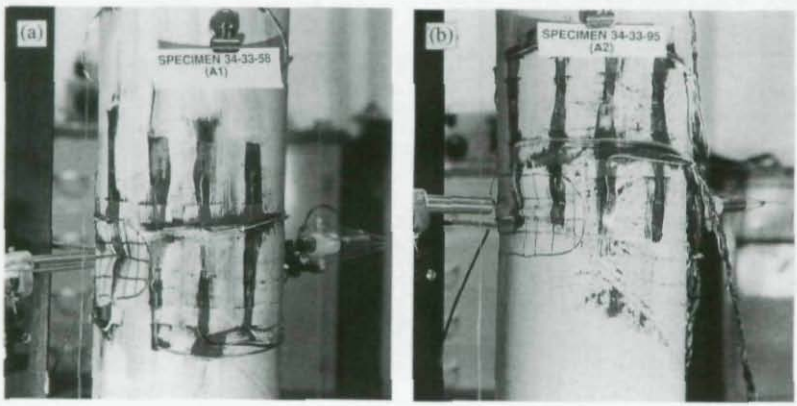

Fig. 18 (a) Inward, and (b) Outward Local Buckling Mode in Corrosion Patch of Selected Specimens

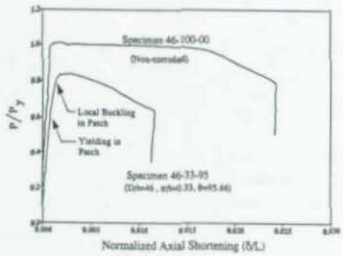

Fig. 19 Axial Load-Shortening Response of Selected Corroded and Non-corroded Specimens

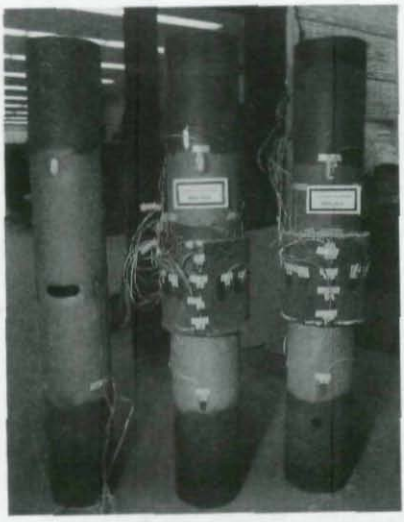

Fig. 20 Corrosion-Damaged Specimen 46-00-95, and Repaired Specimens 46-00-95-C and 46-00-95-E

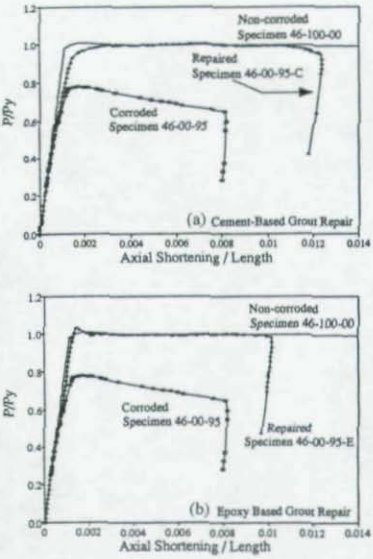

Fig. 21 Axial Load-Shortening Response for (a) Repaired Specimen 46-00-95-C, and (b) Specimen 46-00-95-E

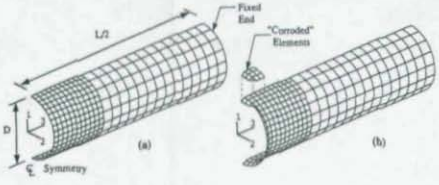

Fig. 22 Finite Element Model of Corroded Specimen: (a) Undeformed Model; and (b) Model with Local Buckling

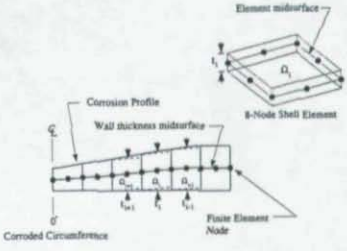

Fig. 23 Placement of Nodes and Plate Element Wall Thickness for Modeling Corrosion Profile

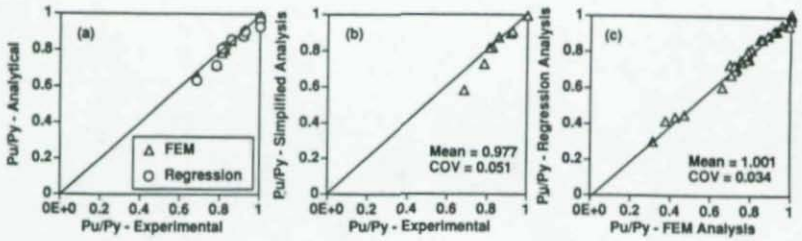

Fig. 24 Comparison of Experimental Capacity with (a) FEM and Regression Analysis, and (b) Simplified Analysis; Comparison of (c) FEM Results with Regression Analysis

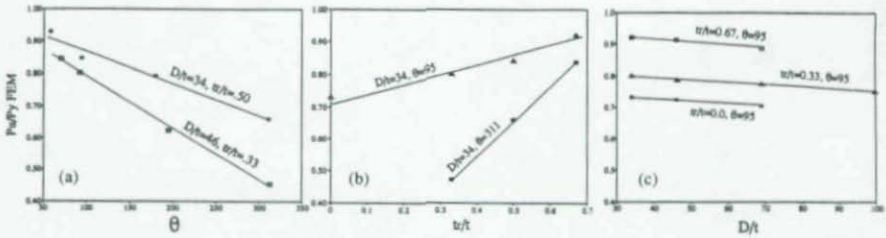

Fig. 25 Variation of Capacity as a Function of Corrosion Parameters (FEM), Experimental Corrosion Profile

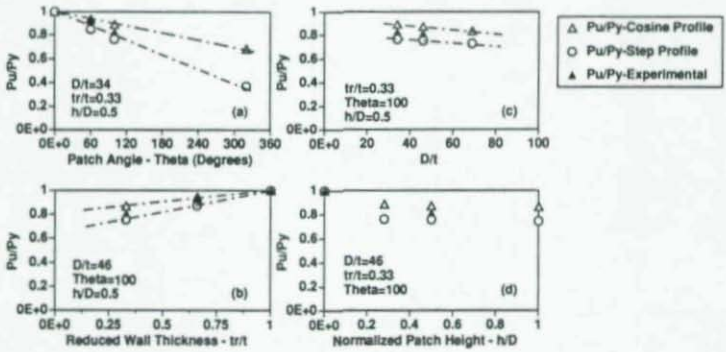

Fig. 26 Variation of Capacity as a Function of Corrosion Parameters and Profile (FEM)

OFFSHORE STRUCTURES - APPROACH TO GENERAL ASSESSMENT

David J. Wisch
Central Offshore Engineering - Texaco Group, Inc.

Abstract

The assessment of existing offshore structures for adequacy is essentially a global stability determination. A multi-level criteria evaluation process has been developed for Gulf of Mexico oil platforms. The impact of engineering preference, variation in load developments, sensitivity of load variance and resistance variance and relationship of component to system resistance variance are reviewed. The overall stability, and hence reliability, of these highly redundant space frame structures typical of offshore platforms is shown to be most sensitive to the load side of the issue, both load generation and inherent variability, rather than the local and component stability issues.

Introduction

The offshore oil industry is nearing its golden anniversary before the end of the century. During the first twenty years, facilities were designed, constructed and operated in a new frontier with each facility being a unique undertaking with rapid advancements in the practice. Hurricanes Hilda and Betsy in the early 1960's provided an impetus for the industry to collectively review lessons learned and develop the first offshore design standard, the 1st edition of API RP 2A issued in 1967. The ensuing twenty years focused on the refinement of design practice in the Gulf of Mexico with thousands of platforms being installed. By the late 1980s, over 3,500 platforms had been installed in the Gulf of Mexico.

Other offshore oil and gas producing areas around the world were also developing during the 1970s and 1980s. By the late 1980s, with over 7,000 platforms worldwide, many had surpassed their original design life estimates and many more were approaching. As with other civil structures, there was a need to retain many of these aging structures in service for additional periods of time.

For nearly 50 years, the industry had focused on information and techniques for designing new facilities. Now the time had arrived to take a more detailed view of the adequacy of existing structures and the methods to assess the adequacy.

The challenge continues to be understanding the performance objectives and then balancing the details to satisfy the objectives. Offshore structures are generally highly redundant space frames but simplistically function as a cantilevered beam-column. Use of historical observation and engineering data must be evaluated routinely to avoid letting bias creep into the system that distorts the economic and technical viability.

Process Development

An industry effort was started to develop guidance for assessment of existing structures similar to the effort some 25 years earlier to develop design guidance. The process has been developed for Gulf of Mexico practice, however the process was developed in a generic context and is now being broadened to address the international community needs.

The assessment process was developed using a top down approach. Top down in the context that fundamental questions were first asked and then processes and quantitative values developed. The key questions first addressed were:

1. What was the process expected to yield?

2. What are the constraints to the process?

Once answers were derived, the following second level objectives were developed:

- Use of consequence based criteria would be utilized
- Multi-level criteria based on consequence would be utilized. From historical perspectives, three major classes (with reference to life safety) of facilities could be observed
  - Manned during the design conditions
  - Normally manned, but unmanned during design conditions (manned during normal operations, but demanned prior to hurricanes - the design condition)
  - Unmanned

  Protection of the environment was also addressed, but in somewhat different manner by requirements of downhole safety valves, limitation of hydrocarbon release potentials, etc.
- The focus would be life safety consequences.
- The process and acceptance criteria would be consistent with present societal practice.
- Economics would be primarily the owner's responsibility, not one of the standard developer. The structural standard would not utilize economics as a key factor, though it is an important issue for an operator managing assets.
- Mitigation of consequences would be an acceptable process to move a facility to a lower criteria category.

An additional directive, capturing both the business reality and the industry capability, was put forth:

The process should utilize the minimum amount of resources to assure adequacy.

This directive was driven from the view that with over 3,800 platforms in the Gulf of Mexico, there is insufficient engineering capacity to perform detailed ultimate capacity checks on each structure. Independent of the industry capacity, historical information did not support such a requirement. Therefore, a three level analysis/assessment process was developed and is depicted in Figure. The triangle on the left side illustrates the amount of engineering and field inspection effort (cost) while the right triangle illustrates the degree of conservatism inherent in the process. When utilizing the ultimate strength check, the intent is to eliminate inherent bias in both the load and resistance to determine the "true" collapse behavior of the facility.

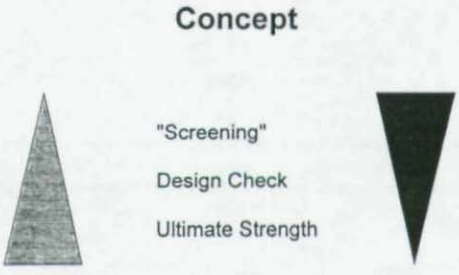

In utilizing a concept of this nature, one of the necessary validations is to assure that a structure passing a "less rigorous" check would always pass the "more rigorous" checks. The task group spent considerable time validating this requirement via historical review and trials.

Within the past several years, considerable work has been underway within the offshore industry in developing both data on damaged components as well as methods to assess the strength of existing structures. A number of joint industry projects have been focusing on determining strength of damaged tubulars, primarily in the bent or corroded condition. Additional work has also been performed on the strength of tubular joints and the foundation capacity. Most of the work has been focused on the resistance values of components, but very recently more attention is being paid to the systems and loads issues.

In the offshore environment, the loads issues have always attracted considerable attention. However, the component resistances have seemed to attract the most attention. This is possibly due to the nature of components lending to being defined, tested and relative easy to quantify compared to wave loads. Components can be modeled numerically as well as tested and then the numerical models calibrated. Performing load testing and calibration to the same level of confidence is orders of magnitude more complex and costly. Hence, there has always been more of an acceptance of the loads side than the resistance in many analysts/designers views. It is possibly a by product that most analysts and designers are structural engineers and not hydrodynamicists, thereby being more accepting of the loads side.

The above can be easily illustrated by looking at the coefficient of variation (COV) used in the recent LRFD code calibration. Component COVs were routinely 15-20% while the load COV was 35% and greater.

With the 1992 Hurricane Andrew experience and the better understanding of systems reliability, a number of studies have recently illustrated the impact of the loading and systems on reliability. While the industry has channeled much money and effort into component resistances, the primary impacts come from load and systems models.

Characteristics

Offshore structures have a very simple structural objective as shown. They can be viewed as relatively "squat" cantilever beam-columns with the majority of the bending loads applied near the end (the zone of the wave activity near the sea surface) and the axial load due to the drilling and production equipment. Many of the jacket structures are tapered "beam-columns" with length-to-depth (water depth to leg spacing) ratios in the range of 3-5 to 1.

While the purpose and essential behavior can be viewed in terms of a cantilever, the structures themselves are highly redundant tubular space frames. They typical have Reserve Strength Ratios (RSRs) of 2-4 with RSR being defined as the ratio of load causing collapse to the design load. While the structures have a myriad of sub-assemblies and details (e.g., tubular joints, high capacity axially loaded piles, wave shielding, etc.), the process must be developed to balance the information required to the level of sophistication desired to determine the simplistic adequacy structural system acting as a simple beam-column.

Designer's Prerogative

As noted earlier, many designers assume the validity of the loads while focusing on fine tuning the resistances. In one sense, the offshore industry was fortunate to have much information available from the performance of structures during Hurricane Andrew when it was developing the process and criteria for determining adequacy of existing facilities.

Following the issuance of the draft guidelines for assessment, one of the joint industry projects involved a benchmark study. Interested parties were provided with the guidelines and the engineering details of a given structure. The parties were provided structural drawings, basic material specifications and the draft guidelines. To provide a consistent benchmark, all parties received copies of questions and subsequent clarifications. There were 13 parties performing benchmark analyses.

Each party was asked to provide design level load, wave height selected according to the guidelines, ultimate capacity of the structure, load level when the first tubular member enters into the non-linear region and the determination as to whether the structure was fit for purpose.

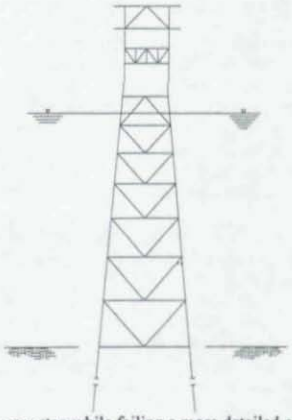

An elevation view of the structure is shown at right. The structure was an actual four leg/pile facility with K-bracing on all faces. It was located in 157 feet of water with all dimensions, locations, elevations, etc. defined. It could be considered a well defined structure with a well defined set of loading conditions. This level of definition could be considered analogous to telling a designer to design a given facility to local building codes.

The objectives of the benchmark were multiple:

1. Determine the variation in assessment practices centered on the analysis component,
2. Validate the premise that a structure would not pass a coarser step while failing a more detailed or refined step,
3. Utilize feedback to develop the process with more clarity.

The objectives were definitely met, but at the same time, one somewhat unanticipated finding became clear.

> The largest impacts on the engineering assessments are in the definition of the loading model and designer prerogatives, not in the determination of component resistances.

The technical area that the most effort has been spent in the past several years, that being the definition of member resistance, was dwarfed by other parameters when reviewing the results.. The results from 13 participants illustrate the wide variation in the process. Some discussion of results should be made. Values illustrated are for two cycles of reporting. The gray plus black bars represent the original range of results for 13 respondents. The black bars represent the values after corrections by several participants. The vertical "ticks" represent the mean value reported in the original cycle. The corrections resulted from incorrect transfer of values to reporting forms, adjustments to values used in wave height selection due to this-interpretation and several other factors.

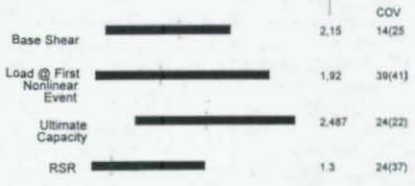

The mean values are reported as are the COVs for both the first and second cycles. It is somewhat disconcerting to note the 14% COV on determination of base shear after interpretation adjustments and

errors were addressed by the respondents. A COV of 7-8% would generally be expected to account for designer interpretations.

The COVs for the load at the first non-linear member event and the ultimate capacity would be expected to be higher than the base shear as was the situation. Again, however, the magnitude is a cause for concern.

The variation in ultimate capacity of the structure as reported by six of the respondents is illustrated. Only six are shown here for clarity with the other seven respondents falling inside the extremes. It may be noted that software variation alone does not account for the differences. Some eight different software packages were utilized and some significant variations were observed between some respondents using the same software package.

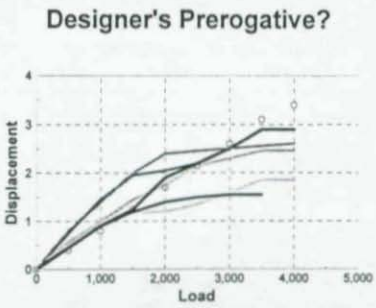

Several observations can be made with the results.

1. The initial stiffness patterns indicated are likely due to the differences in foundation treatment. Some software requires the user to utilize an equivalent linear spring foundation while other software allows for explicit non-linear behavior patterns. Nevertheless, there is cross-over in the ultimate strength determination.
2. There is no clear correlation between the load at first member non-linearity and ultimate strength.
3. While the software packages have varying levels of sophistication, the largest variability is due to the users ability and interpretations.

A review of these select results presents the following question that need to be addressed:

"Should more time and effort be spent on identifying procedures for the designer to use when developing loads and computer models?"

No formal follow-up has been attempted to ascertain the exact reasons for the variation. Informal discussion has led to a number of reasoned hypotheses that are believed to be somewhat interdependent. These include:

- Attention is not necessarily paid to the details of a process as designers/analysts routinely rely on past experience even if it is not recommended in a process. This appears to be especially true in the generation of the environmental loads.
- Engineers by training are conservative and regularly take a conservative approach leading to a ripple effect.
- Widely varying assumptions are made in the computer modeling. This may be representative of personal preference and practice over the years without benchmarking against others.
- Processes that are somewhat vague or leave considerable leeway to interpretation will yield widely varying results.
- New processes will yield higher variability than mature processes. The wave loading recipe is still being adopted by many even though it was released two years ago. The assessment process, as noted, is being finalized.

Systems & Components Example

The second example illustrates the importance of systems understanding in both original design and in evaluation of existing facilities. The draft assessment process was developed with less inherent conservatism as the degrees of sophistication increases as illustrated earlier.

Offshore inspections can be very expensive when using divers and cleaning members and joints to determine the "as-is" condition if necessary for the ultimate strength analysis. It is often necessary to clean the tubular joints of marine growth and perform visual and NDT testing to determine any adverse conditions of the joint that would effect the strength. Understanding the system behavior can have a large impact on the amount and types of inspections necessary to have confidence in the final computed answers. Detailed measurements of dents, bent members, corroded sections, etc. also increase inspection costs dramatically. In addition to the systems behavior, a thorough understanding of the sensitivity to the software and analysis assumptions will help bring value to the process. Without this knowledge, it is difficult or impossible to devise a cost effective inspection program that provides adequate "as-is" condition of structure compatible with the analysis to be employed.

An elevation view of a structure installed in 1976 is provided immediately at right. The critical loading direction for this structure is waves approaching from the right to the left placing all the diagonal bracing in compression. This bracing concept is very typical of structures built in the 1970's. The far right figure is an elevation view of the same structure after rearranging the bracing in a pattern more representative of a common practice in the 1990's. The framing on the left was analyzed for determination of adequacy and an ultimate strength analysis was performed. For illustration purposes an ultimate strength assessment was performed for the structure illustrated on the right, even though it is not a real structure. The reframed structure was investigated to illustrate the impact on framing and inherent sensitivity of components. The sensitivity of components translates directly to level of effort and expense for inspection.

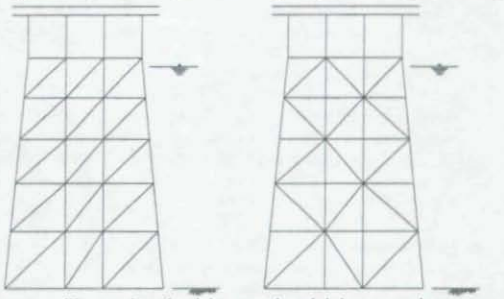

It should be noted that no redesign was performed. Member sizes were retained as is, just reoriented to yield the given framing pattern.

The capacity/displacement behavior is shown at right. Initial non-linear behavior occurs at the same load level as would be expected. However, the behavior deviates from this point. In the compression only bracing, the structures immediately starts to unzip, whereas the other structure exhibits additional strength due to redistribution. Both structures were assumed to have no signficant damage that would effect capacity.

Understanding Impact/Behavior

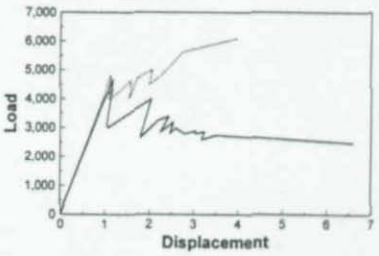

The key issues illustrated here are not the difference in ultimate strength, one having only the elastic level strength while the other has significant reserve, but the issues relating to inspection costs and understanding of the complete process:

1. For the compression only structure, the buckling strength of the members is critical to the capacity of the structure. In this case, extra expenditure on determining the condition of the members is warranted due to the immediate unzipping once the lowest capacity member fails.
2. For the X-braced structure, increased inspection costs are not justified since redistribution is present. Sufficient capacity can be maintained even if an isolated member or two has somewhat degraded capacity provided the degradation is not global in nature.
3. Mean strength of the compression members is the key factor. As noted earlier, the loading COV still dominates the reliability measures of the systems relative to the resistance COV.

Conclusions

1. The recently developed multi-level API process for determining adequacy of existing structures provides a consistent and rational approach.
2. The inherent variability in the load model dominates the uncertainty.
3. While additional work needs to continue on assessing the strength of damaged or deteriorated members, the level should be balanced with the uncertainties in the system, i.e., the loads and designer uncertainties.
4. The dominant uncertainty in the whole process is the engineer, not the load or resistance elements.
5. It is critical to understand the objectives and then tailor the process and the details to meet the objectives. Otherwise, inconsistent results will be obtained and the cost efficiencies necessary will not be obtained.

Acknowledgments

The assistance of Dan Dolan and Stuart Pawsey of PMB Engineering in performing the capacity analyses on the structure illustrated is greatly appreciated.

STRENGTH OF DAMAGED CYLINDRICAL MEMBERS UNDER COMBINED AXIAL LOAD AND BENDING

W. F. Chen
Professor of Structural Engineering
School of Civil Engineering
Purdue University
West Lafayette, IN 47907

ABSTRACT

Cylindrical tubular members are used widely in offshore structures. For members in the wave zone, they are often experienced localized damage caused mainly by supply workboat collisions or dropped object impacts. The assessment of the residual strength of these dented members is necessary for repairing aged offshore platforms. This paper describes a practical method for the analysis and design of dented cylindrical tubular beam-columns as used in offshore structures. To this end, a computer program, BCDENT, was developed, whose capability includes analysis of single- or multi-dent tubular members subjected to axial compression, end moments, and distributed or concentrated lateral loads. The validity and accuracy of the computer model was verified by comparing analytical predictions with the available 151 test results. Against the background of this information, design interaction equations are derived and developed. The proposed method is practical and is therefore recommended for general use.

INTRODUCTION

In the last two decades, experimental and analytical research on structural tubes has made significant progress in establishing refined criteria for the design of undamaged cylindrical tubular members in offshore platforms (Marshall, 1970; Sherman, 1976; Chen and Ross, 1977; Toma and Chen, 1979; Sherman, 1982; Chen and Han, 1985; Loh, 1990). However, available design specifications (API-RP-2A, 1989; API-RP-2A-LRFD, 1989; AISC-LRFD, 1993, AISC-LRFD, 1989) give no specific information on how localized damage affects the behavior and strength of dented cylindrical members under field service conditions. To assess the fitness of these offshore structures in service, technical information is needed for these dented members in terms of both their behavior and ultimate strength.

Damaged cylindrical tubular members were first studied experimentally by Smith, Kirkwood and Sway (1979). During the 80's, a considerable amount of experimental and theoretical research about the effects of damage on the strength and behavior of these members has been conducted (Smith and Dow, 1981; Smith, Somerville and Swan, 1981; Ellinas, 1984; Ueda and Rashed, 1985; Richards and Andronieous, 1985; Yao, Taby and Moan, 1986; Taby and Moan, 1985 and 1987). Recent, MacIntyre and Birkemoe (1989) used a nonlinear finite element shell analysis (ABAQUS) to investigate the denting and subsequent axial compression of dented tubular members. This is the most rigorous procedure among all existing analysis, but it requires a considerable computing effort.

Research reported in the open literature has, in the past, focussed particular attention on

dented cylindrical members subjected to axial compression combined with negative bending (compression at the dent, Fig. 1). In actual offshore structures, however, local damages may occur in any orientations relative to applied end moments (Fig. 2). Dent locations vary along the member, and lateral loading can often accompany axial compression. Little attention has been paid to dented members subjected to loads of different directions with respect to the dents. It was the purpose of a recent study at Purdue University to develop a computer model for the analysis of dented cylindrical beam-column subjected to biaxial bending with respect to the dents (Duan, 1990).

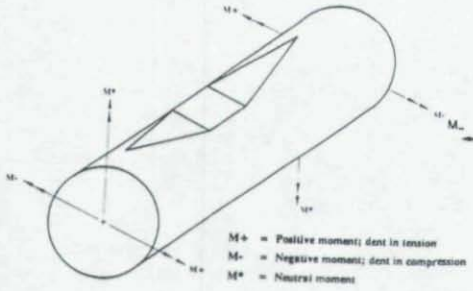

Figure 1. Dented Tubular Segment

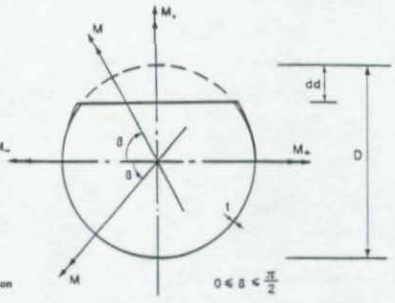

Figure 2. Dented Tubular Section with Different Bending Moments

Based on the moment-curvature (M-P-Φ) relationships developed previously by Duan, Loh and Chen (1993), an analytical procedure and computer program BCDENT were developed to calculate the general behavior of a dented (single or multiple dents) tubular beam-column subjected to loads of different directions and combinations. In general, good agreement was obtained, confirming the validity of the M-P-Φ approach in dented member analysis. The program listing of the BCDENT and typical input/output details are given in a recent book by Chen and Toma (1995).

GENERAL DESCRIPTION OF THE BCDENT PROGRAM

The cylindrical tubular beam-column under BCDENT consideration is treated as an individual member. The initial geometrical imperfections, w_i (out-of-straightness) is considered, and its boundary conditions are pinned. The dents can be multiple in arbitrary orientations and can be located anywhere along the member length. The loading cases include:

1. Constant end axial loads, increasing end bending moments.

2. Constant end axial loads, increasing lateral loads (either linearly distributed or two concentrated loads).

3. Constant end bending moments and/or lateral loads, increasing end axial loads.

The following assumptions were made:

1. Deformations are small. That is, small displacement beam theory was used in the formulation.

2. Shear and torsional deformations were neglected.

3. Strain reversal does not occur in the member, i.e., the member deformations are always monotonically increasing.

4. The member is divided into a number of segments. The properties of these segments are described by their corresponding moment-curvature (M-P-Φ) and moment-axial strain (M-P-ϵ_o) expressions.

5. For an undented section (dd/t < 1.0), the nonlinear M-P-Φ relation is represented by equations reported previously by Duan, Loh and Chen (1993). The M-P-Φ expressions (Fig. 3) include both ascending and descending branches due to local buckling for undented tubular sections with 1% out-of-roundness and with or without residual stresses.

6. For a dented section (dd/t ≥ 1.0), the three-regime M-P-Φ expressions, developed previously by Duan, Loh and Chen (1993) are used (Fig. 4).

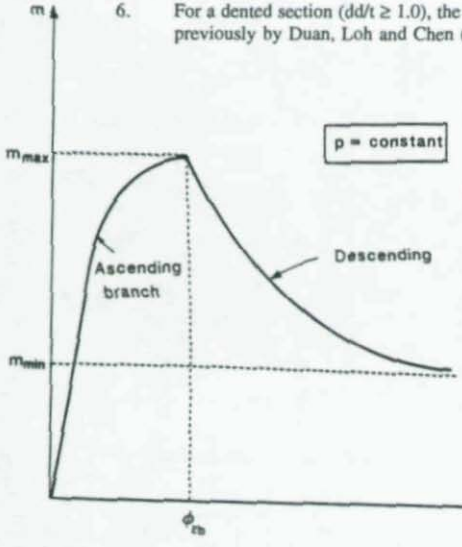

Figure 3. Moment-Thrust-Curvature Curve for Undented Tubular Sections with Local Buckling

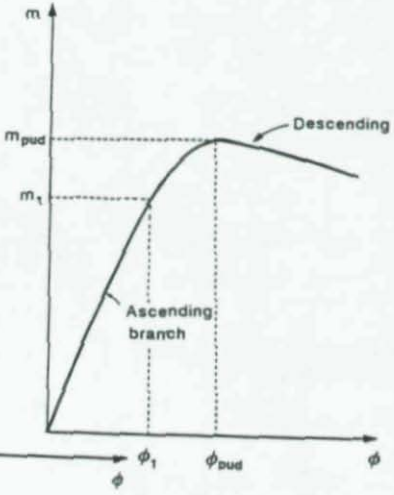

Figure 4. Moment-Thrust-Curvature Curve for Dented Tubular Section

7. A single set of M-P-ε_0 expressions reported by Duan, Loh and Chen (1993), are used for both dented and undented sections with or without residual stresses, and with or without local buckling.

The coordinate system for a biaxially loaded, dented tubular beam-column is shown in Fig. 5. The right-hand rule is used for the sign convention in the analysis (Fig. 2). Figure 6 shows a typical beam-column with several segments subjected to biaxial loadings.

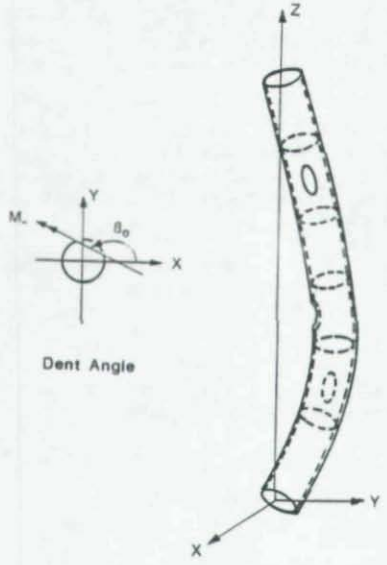

Figure 5. Coordinate System for Biaxially Loaded Dented Tubular Beam-Column

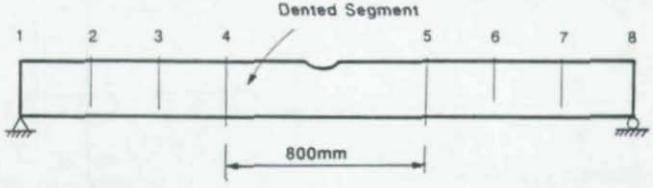

Figure 6. Divided Segment and Stations for Analysis of Landet and Johnson's Tests (1987)

NUMERICAL PROCEDURE

The analytical procedure used in the computer program BCDENT is based on the incremental deflection method. The deflected shape of the member with a specific deflection at a control station is first assumed. The increment of the loads corresponding to this deflection is then computed, followed by computation of the bending moments, taking into account the axial load and the lateral loads. The new deflections are calculated by integrating the curvatures obtained from the known M-P-Φ expressions along the length of the member. Comparisons of the computed new deflections with the assumed deflections are then made to check whether convergence has been achieved. Using the updated deflected shape and repeating this procedure for successive deflection increments at the control station eventually lead to the desired full load-deflection relationship for the dented member.

DENTED CYLINDRICAL MEMBERS

The accuracy and the validity of the M-P-Φ approach are examined by comparing BCDENT predictions to some test results reported by Landet and Johnsen (1987).

Pin-Ended Dented Column Tests

In the present numerical analysis of the Landet's test results (1987), the member is divided into seven segments with eight stations. Since the adopted M-P-Φ expressions for dented tubular sections are based on an average moment and curvature along an 800 mm segment, the length of the dented segment is taken here as 800 mm. The dented M-P-Φ curves are adopted at the two end stations of the dented segment as shown in Fig. 6. The axial load-shortening curves computed by BCDENT are compared with these results for dent depth ratios (dd/D) of 0.1 (D1-35) in Fig. 7. It is seen that the predicted maximum strength is quite close to the test result, but analytical curves generally lower than the tested curves. There are several factors that contribute to this difference. In the analytical studies, the ends of members are assumed to be perfectly pin-ended. In the experiments, some end restraints always exist. Other contributing factors are that the M-P-Φ curves used in the BCDENT are developed on the basis of constant axial load tests, and that the idealized M-P-Φ curves are the pre-maximum region are softer than those tested (Duan, Loh and Chen, 1993).

Dented Beam-Column Tests

The load-deflection curves computed by BCDENT are compared with Landet's beam-column test result (Landent and Johnsen, 1987) in Fig. 8. This test had two lateral concentrated loads coupled with a constant axial compression. Figure 8 is for negative bending case. On the analytical curves, crosses denote the location of maximum lateral concentrated loads Q_{max}; and circles represent the maximum bending moments for the critical dent section M_{max}. It can be seen that the M_{max} point occurs after the Q_{max} point.

In Fig. 8, the dashed line is the analytical result based on the general curve-fit M-P-Φ expressions, implemented in BCDENT, while the dot-dashed line is based on the actual measured M-P-Φ behavior for the particular individual specimen. From Fig. 8, it may be concluded that the M-P-Φ approach can predict adequately the behavior of dented tubular members. The accuracy of the predictions depends mainly on the accuracy of the M-P-Φ expressions used in

the analysis.

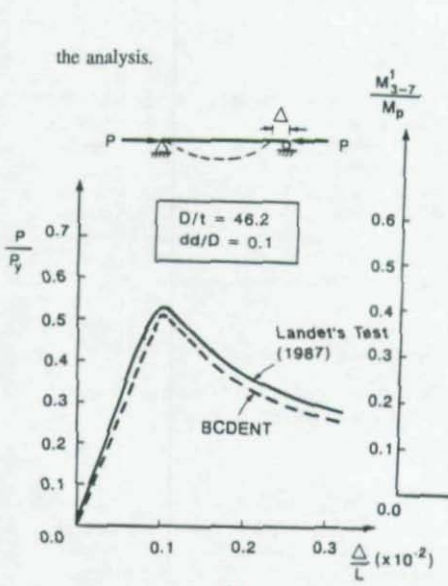

Figure 7. Axial Load-Shortening Curves for Dented Member Test D1-35

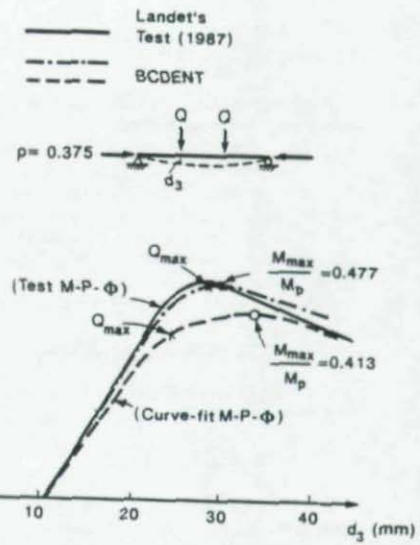

Figure 8. Moment-Deflection Curves for Dented Beam-Column Test D2-37 (Negative Bending)

Ultimate Strength of Dented Members

To further calibrate BCDENT, this section briefly summarizes a comprehensive study of comparisons of BCDENT ultimate strength predictions to all of the available 151 test data in the open literature. Details of comparisons and test data are given in a EPR report by Loh (1991). The available test data are made up of 130 tests with D/t < 80 and 21 tests with D/t = 88 -- 122; member length L = 0.5 mm -- 7.75 m; dent depth to diameter ratio dd/D = 0 -- 0.23; and dent depth to thickness ratio dd/t = 0 -- 25. 107 test specimens are axial and eccentric load cases, and 44 test specimens are combined axial load and moment cases.

A distribution of 130 ratios for dented members with D/t < 80, representing all load types, is shown in Fig. 9. The mean value of measured ultimate strength / strength predicted by BCDENT is 1.01, and the standard deviation is 0.12. A total of 151 ratios is plotted in Fig. 10 for comparisons, including 21 cases with high D/t ratios (D/t = 88 -- 122) for which BCDENT is not valid. The mean value of measured ultimate strength/strength predicted by BCDENT is 1.02, and the standard deviation is 0.13. These comparisons indicate the BCDENT gives a good mean prediction of ultimate strength with a small deviation.

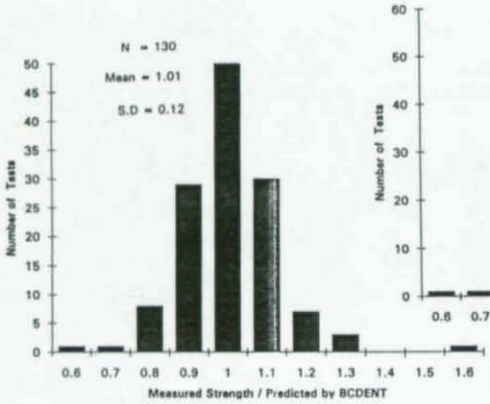

Figure 9. Comparison of Ultimate Strength Prediction by BCDENT to Test Data (D/t<80).

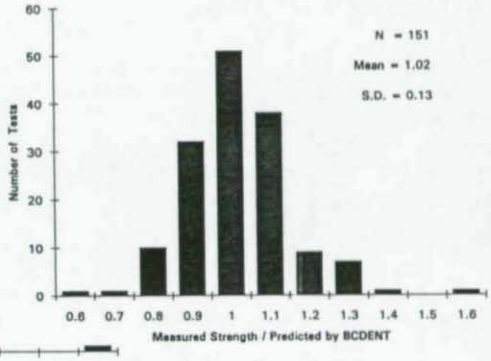

Figure 10. Comparison of Ulitmate Strength Prediction by BCDENT to Test Data

DESIGN INTERACTION EQUATIONS

Although the behavior and strength of damaged members may be carried out by the BCDENT program described previously, simple guidelines and provisions for evaluating dented cylindrical members are needed. It is more convenient and practical to use simple interaction equations.

Figure 2 shows an idealized dented cylindrical section with different bending moments. Figure 1 presents a dented cylindrical segment. In these figures, dd is dent depth; β, dent directional angle; M_+, positive bending moment (dent in tension side); M_-, negative moment (dent in compression side) and M_n, neutral bending moment. The definitions as given in Figs. 1 and 2 will be used in what follows. The axial load and bending moment are always referred to the centroid of the original undamaged circular section.

Duan-Loh-Chen Equations - Sectional Strength

For dented cylindrical beam-column sections, the following design interaction equation was proposed by Duan, Loh and Chen (1993) for analyzing general behavior of dented tubular members

$$\left(\frac{P}{P_{ud}}\right)^{\alpha} + \frac{M}{M_{ud}} = 1.0 \qquad (1)$$

$$\alpha = 1.75 - 0.1 \frac{dd}{t} (1 - \frac{2\beta}{\pi}) \geq 1.0 \tag{2}$$

where P_{ud} is axial compressive strength and M_{ud} is bending moment capacity of a dented section. They can be determined by the following empirical formulas (Duan, Loh and Chen 1993).

$$P_{ud} = \exp (-0.08 \frac{dd}{t}) P_u \tag{3}$$

$$M_{ud} = \exp (-0.06 \frac{dd}{t} \cos\beta) M_u \tag{4}$$

in which cos $\beta \geq 0$; P_u and M_u are mean compression yield strength, and mean maximum moment capacity of a undented tubular section including the effect load buckling, respectively.

They are provided by the API-ASD (1989) formulas:

$$\frac{P_u}{P_y} = \begin{cases} P_y & \text{for } D/t \leq 100 \\ [1.95 - 0.3 (D/t)^{0.25}]P_y & \text{for } D/t > 100 \end{cases} \tag{5}$$

$$M_u = \begin{cases} M_p & \text{for } 0 < \frac{F_y D}{t} \leq 17{,}240 \\ [1.13 - 1.54 \frac{F_y D}{Et}] M_p & \text{for } 17{,}240 < \frac{F_{yD}}{t} \leq 44{,}820 \\ [0.96 - 0.77 \frac{F_y D}{Et}] M_p & \text{for } 44{,}280 < \frac{F_y D}{t} \leq 137{,}900 \end{cases} \tag{6}$$

Loh Equations

Using BCDENT software, a series of comprehensive sensitivity study of the effects of (1) dent locations, (2) member out-of-straightness and (3) moment orientations on ultimate strength has been conducted by the Exxon research team (Loh, Kahlich and Boekers 1992). Against the background of this information, a new set of interaction equations for damaged tubes was developed by Loh (1993).

Section Strength:

Axial Compression, Negative Bending, and Neutral Bending:

$$\frac{P}{P_{nd}} + \sqrt{\left(\frac{M_-}{M_{nd}}\right)^{\alpha} + \left(\frac{M_+}{M_n}\right)^2} \leq 1.0 \tag{7}$$

Axial Compression, Positive Bending, and Neutral Bending:

$$\frac{P}{P_{nd}} + \sqrt{\left(\frac{M_+}{M_n}\right)^2 + \left(\frac{M_+}{M_n}\right)^2} \leq 1.0 \tag{8}$$

Member Stability:

Axial Compression, Negative Bending, and Neutral Bending:

$$\frac{P}{P_{crd}} + \sqrt{\left(\frac{M_-}{[1 - \frac{P}{P_{Ed}}]M_{nd}}\right)^{\alpha} + \left(\frac{M_+}{[1 - \frac{P}{P_E}]M_n}\right)^2} \leq 1.0 \tag{9}$$

Axial Compression, Positive Bending, and Neutral Bending:

$$\frac{P}{P_{crd}} + \sqrt{\left(\frac{M_+}{[1 - \frac{P}{P_E}]M_{nd}}\right)^2 + \left(\frac{M_+}{[1 - \frac{P}{P_E}]M_n}\right)^2} \leq 1.0 \tag{10}$$

where α is exponent = 2 - 3(dd/D); P_{crd}, axial compression capacity of dented members including the effects of out-of-straightness larger than 0.001L; P_{Ed}, the Euler buckling load of damaged members (using properties of damaged section); P_E, the Euler buckling load of undamaged member; M_{nd} and M_n, ultimate bending capacity for dented section under negative bending and undamaged section, respectively. They are determined by the following expressions:

$$\frac{P_{crd}}{P_{crdo}} + \frac{P_{crd}\,[\Delta Y - \Delta Y_o]}{[1 - \frac{P_{crd}}{P_{Ed}}]\,M_{nd}} = 1.0 \tag{11}$$

$$P_{crdo} = \begin{cases} [1 - 0.25\lambda_d^2]P_{nd} & \text{for } \lambda_d < \sqrt{2} \\ P_{Ed} & \text{for } \lambda_d \geq \sqrt{2} \end{cases} \tag{12}$$

$$\lambda_d = \sqrt{\frac{P_{ud}}{P_{Ed}}} \geq \sqrt{\frac{P_{ud}}{P_E}} \tag{13}$$

$$P_{ud} = \exp\left[-0.08\,\frac{dd}{t}\right] P_u \geq 0.45P_u \tag{14}$$

$$P_u = \begin{cases} P_y & \text{for } D/t \leq 60 \\ [1.64 - 0.23\,(D/t)^{0.25}]P_y & \text{for } D/t > 60 \end{cases} \tag{15}$$

$$M_{ud} = \exp\left[-0.06\,\frac{dd}{t}\right] M_u \geq 0.55M_u \tag{16}$$

$$M_u = \begin{cases} M_p & \text{for } 0 < \dfrac{F_y D}{t} \leq 10{,}343 \\ \left[1.13 - 2.58\,\dfrac{F_y D}{Et}\right]M_p & \text{for } 10{,}343 < \dfrac{F_y D}{t} \leq 20{,}685 \\ \left[0.94 - 0.76\,\dfrac{F_y D}{Et}\right]M_p & \text{for } 20{,}685 < \dfrac{F_y D}{t} \leq 300F_y \end{cases} \tag{17}$$

where ΔY is primary out-of-straightness for a dented member; $\Delta Y_o = 0.001L$.

Discussion

Figure 11 shows a comparison of Eq. (1) with 17 dented beam-column test results reported by Landet and Johnsen (1987). Equation (1) has a mean unity check value of 1.04 with a standard deviation of 0.107 (Duan, Loh and Chen 1993). When the dent depth equals to zero, Eq. (1) can be reduced to

$$\left(\frac{P}{P_u}\right)^{1.75} + \frac{M}{M_u} = 1.0 \tag{18}$$

Equation (18) gives a rather accurate estimation of the sectional strength of undamaged tubular members (Duan and Chen 1990).

Loh Equations (7) to (10) are the first complete set of interaction equations for damaged tubular members subjected to combined axial compression and bending. They have been

compared with 128 test data and have a mean value (measured/predicted) of 1.08 with a standard deviation of 1.03 (Fig. 12, Loh 1993). In the limit as the dent depth approaches zero, Loh equations are identical to those for undamaged members in API specifications (1993).

CONCLUDING REMARKS

Computer program BCDENT was developed to assess the strength and behavior of cylindrical steel members under combined axial load and biaxial bending. Loh (1993) proposed a set of equations for evaluating residual strength of these damaged cylindrical members using the computer model developed. Extensive comparisons were also made with the results of tests on actual dented columns, providing final confirmation of the validity of these equations. Since these equations are simple to use and realistic to represent the actual strength, they are recommended for general use.

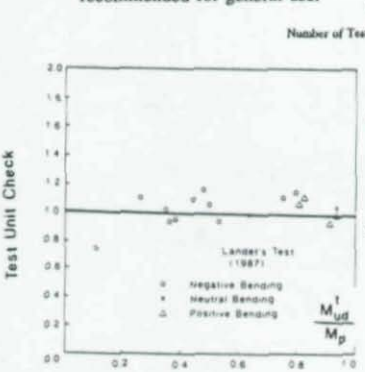

Figure 11. Ultimate Cross-Sectional Strength Check of Dented Tubular Members (Duan and Chen 1993)

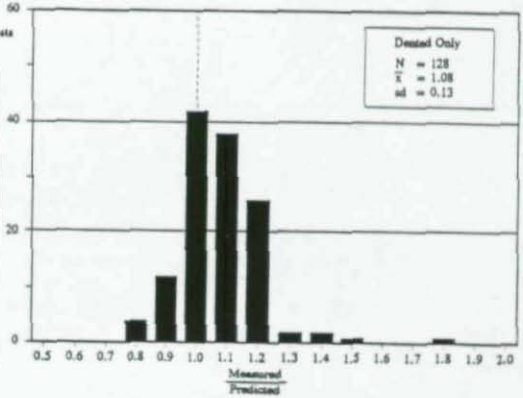

Figure 12. Comparison of Loh Equations with Dented Member Tests (Loh 1993)

REFERENCES

AISC, (1989). *Specification for Structural Steel Buildings -- Allowable Stress and Plastic Design*, American Institute of Steel Construction, Chicago, IL.

AISC, (1993). *Load and Resistance Factor Design Specification for Structural Steel Buildings*, 2nd Ed., American Institute of Steel Construction, Chicago, IL.

API, (1989). *Recommended Practice for Planning, Designing and Constructing Fixed Offshore Platform*, 18th Ed., API-RP-2A, American Petroleum Institute, Washington, D.C.

API, (1989). *Draft Recommended Practice for Planning, Designing and Constructing Fixed Offshore Platforms - Load and Resistance Factor Design*, 1st Ed., API-RP-2A-LRFD, American Petroleum Institute, Washington, DC.

API, (1993). *Recommended Practice for Planning, Designing and Constructing Fixed Offshore Platform--Working Stress Design*, 20th Ed., API-RP-2A, American Petroleum Institute, Washington, D.C.

API, (1993). *Recommended Practice for Planning, Designing and Constructing Fixed Offshore Platforms - Load and Resistance Factor Design*, 1st Ed., API-RP-2A-LRFD, American Petroleum Institute, Washington, D.C.

Chen, W.F. and Ross, D.A., (1977). "Test of Fabricated Tubular Columns," *Journal of Structural Division*, ASCE, Vol. 103, No. ST3, pp. 619-634.

Chen, W.F. and Han, D.J., (1985). *Tubular Members in Offshore Structures*, Pitman, London.

Chen, W.F. and Toma, S., (1995). *Analysis and Software of Tubular Members*, CRC Press, Boca Raton, FL.

Duan, L., (1990). Stability Analysis and Design of Steel Structures, Ph.D. Thesis, School of Civil Engineering, Purdue University, West Lafayette, IN.

Duan, L. and Chen, W.F., (1990). "Design Interaction Equation for Cylindrical Tubular Beam-Column." *Journal of Structural Engineering*, ASCE, 116(7), 1794-1812.

Duan, L., Loh, J.T., and Chen, W.F., (1993). "Moment-Thrust-Curvature Relationships for Dented Tubular Sections," *Journal of Structural Engineering*, ASCE, Vol. 119, No. 3, pp. 809-830.

Duan, L., Chen, W.F., and Loh, J.T., (1993). "Analysis of Dented Tubular Members Using Moment Curvature Approach." *Thin-Walled Structures*, 15(1), 15-41.

Ellinas, C.P., (1984). "Ultimate Strength of Damaged Tubular Bracing Members," *Journal of Structural Engineering*, ASCE, Vol. 110, No. 2, pp. 245-259.

Gu, Y.N., and Li, R.P., (1992). "On the Assessment of Strength of Platform with Damaged Members." *Proceedings of the Second International Offshore and Polar Engineering Conference*, ISOPE, San Francisco, CA. June 14-19, IV, 408-414.

Landet, E. and Johnsen, R.H., (1987). Investigation on Ultimate Strength of Dented Pipes, *Technical Report* No. 87-3278, VERITEC, May 20.

Loh, J.T., (1990). "A Unified Design Procedure for Tubular Members," *Proceedings, 22th Annual Offshore Technology Conference*, OTC 6310, Houston, TX, May 7-10, 365-379.

Loh, J.T., (1991). *Comparison of Dented Member Strength Predictions to Test Data*, Exxon Production Research Company, Houston, TX.

Loh, J.T., Kahlich, J.T., and Broekers, D.L., (1992). *Dented Tubular Steel Members*, Exxon Production Research Co., Houston, TX.

Loh, J.T., (1993). "Ultimate Strength of Dented Tubular Members." *Proceedings of the Second International Offshore and Polar Engineering Conference*, ISOPE, Singapore, June, IV.

MacIntyre, J. and Birkemoe, P.C., (1989). *Damage of Steel Tubular Members in Offshore Structures: A Nonlinear Finite Element Analysis*, Department of Civil Engineering, University of Toronto, Toronto, Ontario, Canada, M5S 1A4.

Marshall, P.W., (1970). "Stability Problems in Offshore Structures," *Proceedings, Annual Technical Sessions, Column Research Council*, St. Louis, MO.

Padula, J.A., and Ostapenko, A., (1989). *Axial Behavior of Damaged Tubular Columns*, Fritz Engineering Laboratory Report No. 508.11, Lehigh University, Bethlehem, PA.

Richards, D.M. and Andronicou, A., (1985). "Residual Strength of Dented Tubulars: Impact Energy Correlation," *Proceedings, Fourth International Offshore Mechanics and Arctic Engineering Symposium*, Dallas, Texas, February 17-21, pp. 522-527.

Sherman, D.R., (1976). "Tests of Circular Steel Tubes in Bending," *Journal of Structural Division*, ASCE, Vol. 102, No. ST11, pp. 2181-2195.

Sherman, D.R., (1982). "Research in North America on the Stability of Circular Tubes," *Proceedings, Annual Technical Sessions*, Structural Stability Research Council, New Orleans, Louisiana.

Smith, C.S., Kirkwood, W. and Swan, J.W., (1979). "Buckling Strength and Post-Collapse Behavior of Tubular Bracing Members Including Damage Effects," *Proceedings, Second International Conference on Behavior of Offshore Structures (BOSS'79)*, Imperial College, London, England, August 28-31, pp. 303-326.

Smith, C.S. and Dow, R.S., (1981). "Residual Strength of Damaged Steel Ships and Offshore Structures," *Journal of Constructional Steel Research*," Vol. 1, No. 4, pp. 2-15.

Smith, C.S., Somerville, J.W. and Swan, J.W. (1981). "Residual Strength and Stiffness of Damaged Steel Bracing Members," *Proceedings, 13th Annual Offshore Technology Conference*, Houston, TX, May 4-7, pp. 273-291.

Taby, J. and Moan, T., (1985). "Collapse and Residual Strength of Damaged Tubular Members," *Proceedings, Fourth International Conference on Behavior of Offshore Structures*, Delft, The Netherlands, July 1-5, pp. 395-408.

Taby, J. and Moan, T., (1987). "Ultimate Behavior of Circular Tubular Members with Large Initial Imperfections," *Proceedings Annual Technical Sessions*, Structural Stability Research Council, Houston, TX, March 24-25, pp. 79-104.

Toma, S. and Chen, W.F., (1979). "Analysis of Fabricated Tubular Columns, *Journal of*

Structural Division, ASCE, Vol. 105, No. ST11, pp. 2343-2366.

Ueda, Y. and Rashed, S.M.H., (1985). "Behavior of Damaged Tubular Structural Members," *Proceedings, Fourth International Offshore Mechanics and Arctic Engineering Symposium*, ASME, Dallas, TX, February 17-21, pp. 528-536.

Yao, T., Taby, J. and Moan, T., (1986). "Ultimate Strength and Post-Ultimate Strength Behavior of Damaged Tubular Members in Offshore Structures," *Proceedings, Fifth International Offshore Mechanics and Artic Engineering Symposium*, III, ASME, pp. 301-308.

SEISMIC DAMAGE ASSESSMENT OF STEEL MEMBERS AND JOINTS

Carlo A. Castiglioni
Associate Professor
Structural Engineering Dept., Politecnico di Milano, Italy

Abstract

A method is presented trying to unify both design and damage assessment methods for high and low cycle fatigue, based on the results of an extensive experimental research programme. Interpreting the stress range $\Delta\sigma$ in a structural component as the one associated to the real strain range $\Delta\varepsilon$ in an ideal perfectly elastic material, high and low cycle fatigue test data can be fitted by the same Wöhler (S-N) lines usually given in Recommendation for (high cycle) fatigue design of steel structures. Local buckling can be regarded as a notch effect, intrinsic to the various shapes, and related to their geometrical properties (c/t_f and d/t_w slenderness ratios of the flanges and the web). A linear damage accumulation rule together with the previously defined S-N curves can lead to a reliable collapse criterion also for members under seismic loading.

1. Introduction

Eurocode-3 [1] defines fatigue as "damage in a structural part, through gradual crack propagation caused by repeated stress fluctuations". Depending on a number of factors, these load excursions may be introduced either under stress or strain controlled conditions. Depending on the number of cycles sustainable to failure, and on their amplitude, we can distinguish failure for high or low cycle fatigue.

Failure by high cycle fatigue is characterised by a large number of withstandable cycles with a nominal stress range $\Delta\sigma$ in the elastic range. This is a well known effect [2] although only a limited number of typologies of connections and of structural details can be considered at present thoroughly investigated, and the general aspects of this problem, as well as the basic methodologies for assessment and design, can be considered well established.

Low cycle fatigue is characterised by a small number of cycles to failure, with large plastic deformations. In general, low cycle fatigue problems in civil engineering structures arise either under seismic loading or in pressure vessels or under severe thermal cycling. Cycles with large amplitudes in the plastic range are usually connected with local buckling in structural members. At present, knowledge of low cycle fatigue behavior of civil engineering connections is not jet as well established as the high cycle fatigue one; in particular, there is no generally recognised design or damage assessment method for low cycle fatigue, and a clear definition of a collapse criterion is lacking.

In this paper a procedure is described, trying to unify design and damage assessment methods for structural details under high and low cycle fatigue. After discussing the proposed approach, its experimental validation based on constant and variable amplitude cyclic test results will be presented. By transforming the nominal strain range $\Delta\varepsilon$ in an equivalent stress range $\Delta\sigma^*=\Delta\varepsilon E$ computed by considering the material as an indefinitely linear elastic one, the experimental test data obtained under cycles with a constant amplitude in the plastic range can be interpolated by the same Stress range-Number of cycles to failure (S-N) lines usually given in

recommendations for the (fatigue) design of steel structures (e.g. [1]). Furthermore, a linear damage accumulation model (Miner's rule [16]), together with the rainflow cycle counting method, can be adopted for the damage assessment under variable amplitude loading.

2. The proposed approach

The proposed approach to unify the design and procedures for steel structures under low and/or high cycle fatigue, originally presented by Ballio & Castiglioni [3], is based on the two following assumptions:

1. To know, for a given structural detail (cycled under strain controlled conditions), the relationships between the number of cycles to failure N_f and the cycle amplitude Δs, expressed in terms of generalised displacement components (i.e. of displacements Δv or of rotation $\Delta\phi$ or of deformation $\Delta\varepsilon$). These relationships have the same meaning in high and in low cycle fatigue with the following difference:
   - in high cycle fatigue the component is subjected to cycles in the elastic range;
   - in low cycle fatigue the component is subjected to cycles in the plastic range
2. Damage accumulation in a structural detail is a linear function of the number of cycles sustained by the component itself. This means to assume that Miner's rule [16] (usually applied in high cycle fatigue damage assessment) can be applied also in low cycle fatigue.

Consequence of the second assumption is the definition of a unified failure criterion for both high and low cycle fatigue: a structural component fails when Miner's damage index reaches unity. Of course, appropriate S-N curves corresponding to the desired safety level should be identified.
Consequence of the first assumption is the possibility to interpret low cycle fatigue with the same laws commonly accepted for high cycle fatigue.
In fact, in high cycle fatigue (under stress controlled conditions):

- a structural component is subjected to load cycles having a constant amplitude $\Delta F<F_y$ (the yield strength of the material, that may be theoretically computed or experimentally evaluated);
- the nominal stress range $\Delta\sigma=\Delta\sigma(\Delta F)$ induced by the external load fluctuations ΔF may computed either theoretically or with conventional methods, and is finally correlated to the number of cycles to failure N_f, independently from the yield strength of the material.

In order to generalise this approach, under the assumption of indefinitely linear elastic material, it can be written:

$$\Delta\sigma = \frac{\Delta F}{F_y}\sigma(F_y) \qquad (1)$$

In low cycle fatigue (under strain controlled conditions):

- a structural component is subjected to displacement cycles having a constant amplitude $\Delta s>s_y$ (associated with the attainment of the yield stress in the material, that may be theoretically computed or experimentally evaluated);

- if the material can be regarded as an elastic perfectly plastic one (as in the case of steel), and the hypothesis of concentrated plastic hinge can be considered realistic (as shown by Ballio & Castiglioni [4] for steel members under seismic loading), it can conventionally be assumed that strains are proportional to the generalised displacement component s, and it can be stated that:

$$\frac{\Delta\varepsilon}{\varepsilon_y} = \frac{\Delta s}{s_y} \qquad (2)$$

This equation defines the nominal strain range in a particular way, as discussed in detail in Ref. [3], taking into account the local reduction of stiffness at plastic hinge location by an equivalent uniform reduction of stiffness along the total beam length, and can be re-written as follows:

$$\Delta\sigma^* = E\Delta\varepsilon = E\frac{\Delta s}{s_y}\varepsilon_y = \frac{\Delta s}{s_y}\sigma(F_y) \qquad (3)$$

- Equation (3) is similar to equation (1), that is valid for high cycle fatigue. The difference consists in having considered cyclic displacements instead of cyclic forces.

3. Experimental validation

3.1 Re-processing the test data

For reprocessing test data according to equation (3), the following parameters must be defined: the number of cycles to failure N_f, the values of the generalised displacement component (s_y) and of the stress level ($\sigma(F_y)$) corresponding at first yield.
Of course, various operative choices are available for the definition of these parameters; in order to clearly identify the consequences of these operative choices, the following considerations should be taken into account.

- To define the number of cycles to failure N_f, a collapse criterion must be adopted, either assumed conventionally a-priori, or identified test by test corresponding to failure. In the first case, for example, failure might be associated with the reduction of the load carrying capacity as proposed in [4], or of the absorbed energy [9].
- The generalised displacement component can be assumed either as a displacement v or as a rotation ϕ. Accordingly, the value corresponding to first yield (the yield displacement v_y or the yield rotation ϕ_y), can be theoretically computed or conventionally defined reprocessing test data, for example adopting the ECCS Recommended procedures [6].
- The nominal stress level ($\sigma(F_y)$) associated to an external load (F_y) causing first yield in the material can be determined experimentally, by means of tensile tests, or theoretically, by applying conventional methods of structural mechanics. In the first case, $\sigma(F_y) = f_y$. In order to apply the second procedure, both the yield strength (F_y) should be determined (e.g. according to ECCS Recommended procedures) and, for flexural members, the dimension of the plastic hinge.

Once determined the number of cycles to failure N_f, test data can be re-processed to plot in a log-log scale N_f vs. $\Delta\sigma^*$ given by eq. (3). The domain $log\ (\Delta\sigma^*=E\Delta\varepsilon)$ *vs.* $log\ N$ is the usual domain for the Wöhler (S-N) curves adopted by various International Codes and Standards for (high cycle) fatigue design of steel structures.
In order to verify the assumption of equivalence of $E\Delta\varepsilon$ - N_f curves for high and low cycle fatigue, hereafter it is tried to interpret the experimental test data of low cycle fatigue tests performed on structural members and joints, by means of the *S-N* curves proposed by Eurocode-3, whose validity is extrapolated in the low cycle fatigue range by means of eq. (3).

3.2 Members

In order to experimentally validate the proposed approach, tests were performed [4,7,8] at the Structural Engineering Department of Politecnico di Milano, on full scale cantilever members of the commercial shapes HE120A, HE140A, HE220A, HE220B and IPE300 (tab.1), using an equipment [5] capable of applying horizontal cyclic actions in a quasi-static way. Presently, the testing programme is continuing, in order to enlarge the data-base; tests are carried out also considering the presence of an axial load [19].

Shape	Area	Flange			Web			
	(cm^2)	b=2c	t_f	c/t_f	h	d	t_w	d/t_w
		(mm)			(mm)			
HE 220A	64.3	220	11.0	10.0	210	152.0	7.0	21.7
HE 220B	*91.0*	*220*	*16.0*	*6.9*	*220*	*152.0*	*9.5*	*16.0*
IPE 300	53.8	150	10.7	7.0	300	248.6	7.1	35.1
HE 120A	25.3	120	8.0	7.5	114	74.0	5.0	14.8
HE 140A	31.4	140	8.5	8.2	133	92.0	5.5	16.7

Table 1- Geometrical properties of specimen shapes

3.2.1 Constant amplitude tests

To date, 40 tests were performed (11 on HE220A shapes, 12 on HE220B and 11 on IPE300, 3 on HE120A, 3 on HE140A) imposing to the specimens displacement cycles with a constant amplitude. Furthermore, 3 tests were performed on HE120A, with an axial load $P/P_y = 0.05$, 1 test on IPE300 with $P/P_y=0.10$ and 8 tests on HE220A specimens, considering three values of the axial load: $P/P_y = 0.05$, 0.10 and 0.125, (where $P_y = f_y A$ is the plastic strength of the cross section).

In high cycle fatigue, strength categories implicitly account for different notch effects, i.e. for different local stress concentrations due to geometry of the detail and/or defects caused by fabrication procedures. It is supposed that the same consideration holds also in the case of low cycle fatigue: local buckling can in fact be regarded as a notch effect, because it induces local stress concentrations in the buckled area (at plastic hinge location). In fact, as already discussed, and in good agreement with previous results by Yamada [10-12], the different geometries of the cross sections make the specimens more or less vulnerable by local buckling effects. This means that each shape, as a function of its geometrical properties, can be considered as

belonging to a definite fatigue strength category, because intrinsically affected by a more or less pronounced notch effect.

It must then be expected that the different shapes considered in this study belong to different fatigue strength categories; furthermore, as the tested specimens evidenced two different failure modes (by cracking in the base material at the plastic hinge locations, or by cracking at the welding of the reinforcement plates to the specimens), it must also be expected that different fatigue strength curves apply to the different failure modes.

Fig. 1 Fatigue strength of beams failed at plastic hinge

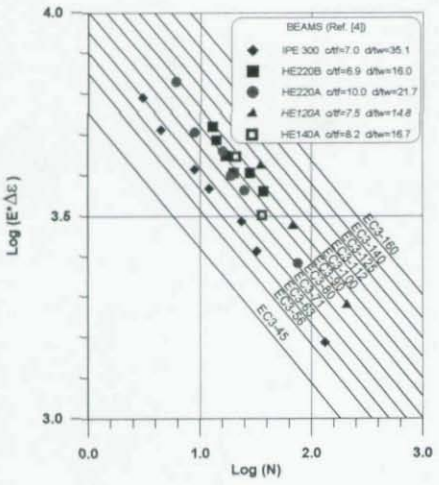

Figure 1 shows the test data for beam specimens [4] failed by cracking in the base material at plastic hinge locations, fitted by the S-N lines of Eurocode-3. The parameter which seems to govern the fatigue behavior of beams is the d/t_w ratio. In fact, it can be noticed that test data for HE120A specimens (having lowest d/t_w) can be fitted by line for category 90, those for HE220B and HE140A (having similar d/t_w) can be fitted by EC-3 line for category 80, those for HE220A by category 71, while those for IPE300 (having largest d/t_w) by category 63.

Figure 2 refers to test data for specimens failed at weldings; HE220A and HE220B specimens can be fitted by category 63 line, while IPE300specimens, despite the same welded detail was adopted for all shapes, are fitted by line 56 and show a lower fatigue strength. This is probably caused by the formation of the plastic hinge nearer to the base (i.e. nearer to the weldment) in IPE specimens rather than in HE ones. This fact seems again to confirm the hypothesis that local buckling can be considered as a notch effect reducing the fatigue strength of the profile.

However, independently on the category of fatigue resistance pertinent to each shape, it is important to notice that the slope of the line fitting (in a log-log plot) the low cycle fatigue test data, reprocessed according to eq. (3), is nearly -3. This is in good agreement with the results of research on high cycle fatigue.

Fig. 2 Fatigue strength of beams failed at weldings

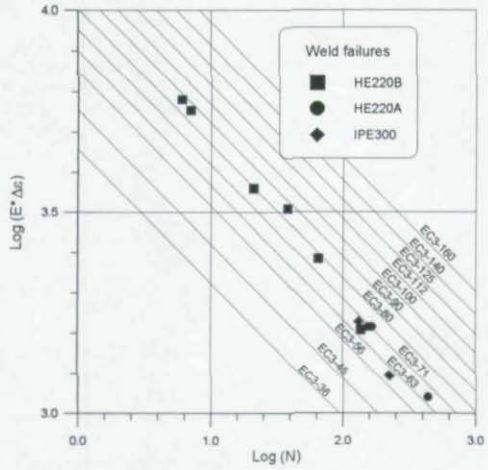

Fig. 3 Effect of axial load on HE220A specimens

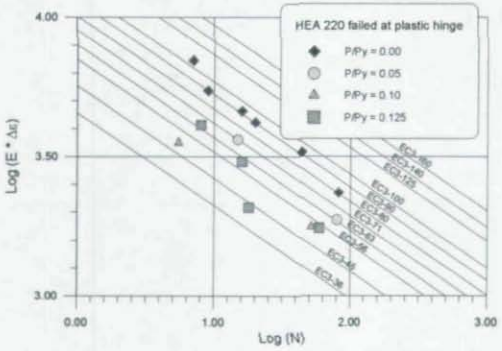

Fig. 3 shows the effect of an axial load applied on top of HE220A specimens. Increasing the applied axial load results in a reduction of the fatigue strength of the member, but also in a scattering of the results, although the average slope of the fitting line remains nearly -3.

It can however be noticed that the line fitting test data for P/P_y=0.10 and 0.125 nearly coincide. The test data available at present are too few to allow definitive conclusions to be drawn; it seems however that, beyond a certain level, the detrimental effect of the axial load on the fatigue strength is reduced, probably because it reduces the tensile strains due to bending, hence "retarding" fatigue crack opening and propagation.
The effects of the operative choices in the definition of the various parameters when re-processing test data, previously discussed, are highlighted in the following figs. 4 and 5.
Fig. 4 shows, for HE220A specimens, the effect of the assumed failure condition, comparing results obtained defining N_f:

- based on experimental evidence, as the one corresponding to the final sudden increase in the deterioration rate (leading to failure)
- based on a condition defined a-priori, associated to a reduction of the load carrying capacity to a given percentage of the yield strength F_y.

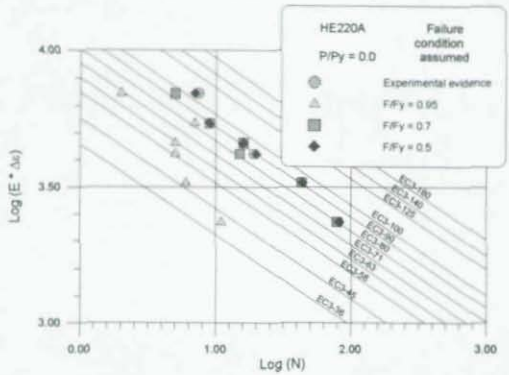

fig. 4 Effect of assumed failure condition on damage assessment

It can be noticed that assuming F/F_y=0.95 leads to conservative assessments of the fatigue strength, as well as to scattering of results, while assuming as failure condition a reduction of strength to $0.50F_y$ leads to assessments similar to those based on test evidence.

Fig. 5 shows the effects of the definition of the stress range $\Delta\sigma^*$ (i.e. of the definition of the yield stress f_y and of the assumed generalised displacement component s) on the assessment of the fatigue strength of HE220A specimens, in the case of a failure condition assumed a-priori corresponding to a reduction of the specimen strength F to $0.50F_y$. It can be noticed that scattering in the results is connected to the definition of the yield strength, while smaller is the influence of the assumed displacement component; in fact, if top displacements v or rotations at plastic hinge location ϕ are assumed as generalised displacement component s in eq. 3, a small

Fig. 5 Effects of definition of the stress range $\Delta\sigma^{*}=E^{*}\Delta\varepsilon$

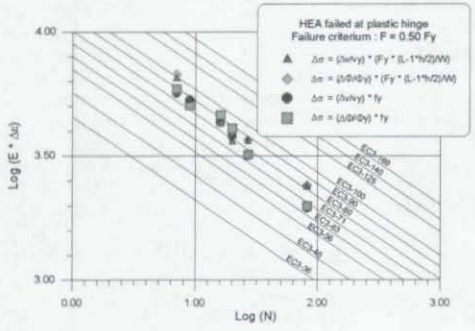

fig. 5.1 ξ=1.0

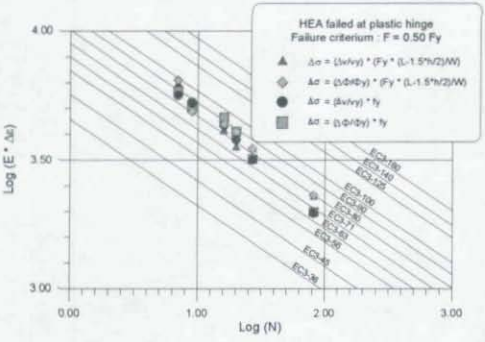

fig. 5.2 ξ=1.5

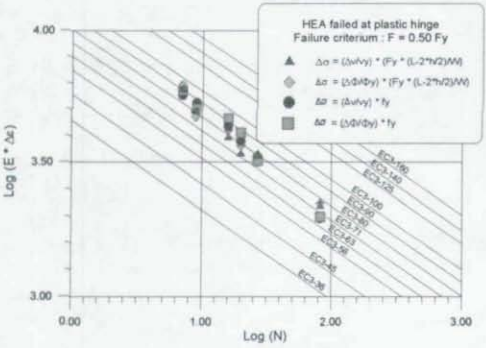

fig. 5.3 ξ= 2.0

scattering can be noticed in the results. On the contrary, if the stress level corresponding at yield ($\sigma(F_y)$) is defined through a tensile test (i.e. coincident with f_y) or by means of structural mechanics (i.e. as F_yL'/W, where W is the section modulus and $L'= L-(\xi h/2)$ the cantilever member length minus half the dimension ξh of the plastic hinge, h being the height of the profile, as from tab. 1), due to the uncertainties connected with the latter definitions of both L' and F_y, a larger scatter in the results can be noticed. Fig. 5.1, 5.2 and 5.3 respectively refer to different values of parameter ξ (respectively assumed equal 1.0, 1.5 and 2.0). It can be noticed how scattering of the results is strongly influenced by this parameter.
Hence, in order to avoid biased results from re-processing test data, extreme accuracy and consistency must be adopted when defining the various parameters. In particular, when possible, the yield strength should be determined by tensile tests.

3.2.2 Variable amplitude tests

Some random displacement histories were numerically obtained by means of a dynamic numerical simulation code, adopting artificial accelerograms obtained on the basis of EC-8 [20] recommended spectra. The oscillograms obtained were adopted as displacement histories and imposed in a quasi-static way to the specimens under testing.

TEST	EC-3 90	EC-3 80	EC-3 71	EC-3 63	Failure
HEA1	0.542	0.772	1.104	1.580	P.H.
HEA9	0.854	1.202	1.740	2.489	P.H.
HEA10	0.599	0.853	1.220	1.746	P.H.
HEA11	0.773	1.040	1.490	2.135	P.H.
HEB1	1.420	2.030	2.900	4.152	P.H.
HEB12	0.717	1.020	1.460	2.090	W
HEB13	0.523	0.744	1.060	1.524	W
IPE9	0.461	0.657	0.939	1.340	P.H.
IPE10	0.385	0.547	0.783	1.120	P.H.
IPE11	0.460	0.660	0.940	1.346	P.H.
IPE15	0.478	0.680	0.973	1.394	P.H.

Table 2 - Damage indexes corresponding tospecimen collapse in variable amplitude tests

At present, a total of 11 variable amplitude tests have been performed at Politecnico di Milano [4] (4 on HE220A shapes, 4 on IPE300 and 3 on HE220B). The experimental results were re-processed by means of the rainflow cycle counting method and Miner's damage index [16] associated with collapse of each specimen was computed, based on the transformation given by equation (3) and on the EC-3 fatigue strength lines previously identified for the various profiles. The obtained results are summarised in table 2 where the failure mode (P.H.= at plastic hinge, W= at welding) and the damage index corresponding to the EC-3 lines are given. It can be noticed that Miner's rule [16] gives damage index values with scatters similar to those commonly accepted in high cycle fatigue, and correctly allows prediction of failure in association with EC-3 line 71 for HE220A specimens and with line 63 for IPE300 specimens. For HEB specimens,

depending on the failure mode, a correct prediction of failure is achieved respectively in association with EC-3 fatigue strength lines 80 and 63. These fatigue strength categories lead to damage assessments on the safe side, increasing the fatigue strength of HE220B specimens by one category results in damage index values nearer to unity.

3.3 Connections

3.3.1 Welded joints

An experimental research was carried out at Politecnico di Milano on welded details commonly adopted in structural steelwork. Different types of connections were considerded: fillet welded coverplates (long and short ones), fillet welds and full penetration groove welds in cruciform joints and butt welded joints. Small specimens (400 mm long) were manufactured and tested imposing axial strain cycles with a constant amplitude. Various tests were performed under different strain ranges. Fig. 6 shows some of these test results (together with results for unwelded specimens obtained during the same study), reprocessed according to eq. (3). The base material plots between EC-3 lines 100-125, 100mm ("long") coverplates between EC-3 lines 56-63, 50mm ("short") coverplates between EC-3 lines 45-63, fillet welds in cruciform joints between EC-3 lines 45-56 full penetration groove welds in cruciform joints plot between EC3-lines 100-125 and butt welded joint between lines 100-112. These results are in good agreement with the classification of the various details by EC-3, where base material is assigned a fatigue strength category ranging between 125 and 160, coverplates to categories ranging between 45 and 63, fillet welds in cruciform joints to category 36 (40-63 by the Italian C.N.R. 10011/86 Code), butt welds to 125 only when 100 % NDT are performed. Of course, the small number of test data presently available did not allow for any regression analysis. This fact, in addition to the absence of residual stresses (due to the small dimension of the specimens), account for eventual small differences between code classification and the results of the present study.

Fig. 6 Fatigue strength of welded joints

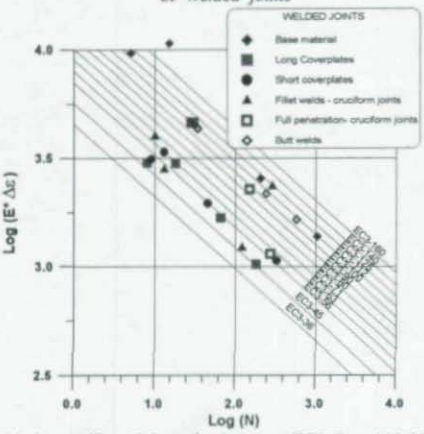

3.3.2 Beam to column connections

It has been tried to apply the same procedure for defining the fatigue strength of beam to column connections[13-15], consisting of welded connections, end plate connections and double seat angle connections. As all these tests were performed under variable amplitude loading according to [6], in order to define the fatigue strength category of each connection re-analysis of test data was carried out adopting Miner's rule, and defining the pertinent EC-3 line a-posteriori, as the one giving, at collapse, a damage index approximately equal to 1.0.

Fig.7 Fatigue strength of beam to column connections

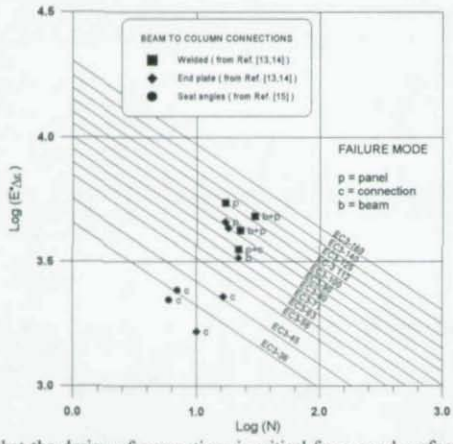

It can be noticed that test data are grouped, depending on the failure mode. The end plate joints from Ref. [13,14] that failed in the connection show a low fatigue strength, similar to that of seat angle connections from Ref. [15]. The other connections (both welded and end plated) show a higher fatigue strength, although the failure mode seems to influence their fatigue behavior. Presently it is tried to enlarge the data base also by collecting and re-analysing test data presented in the literature. Even from these previous results it can however be concluded that the design of connections is critical for a good performance of structures under low cycle fatigue and that, in order to avoid brittle fracture, it should be tried to induce the formation of a plastic hinge in the members, away from the connections. This is of course in good agreement with other results presented in the literature (e.g. [18]).

4. Conclusions

If an equivalent stress range $\Delta\sigma^{*}=E\Delta\varepsilon$ is considered, associated with the actual strain range $\Delta\varepsilon$ in an ideal indefinitely elastic behavior of the material, the S-N lines given by Codes for high cycle fatigue can be adopted for interpreting the low cycle fatigue behavior of beams, welded joints and beam to column connections.

Miner's rule can be adopted, together with the previously defined S-N curves and with a cycle counting method (e.g. Rainflow) to define a unified collapse criterion, valid for both high and low cycle fatigue.

The application of these results and of the proposed method for damage assessment to steel structures under seismic loading may lead to an overcoming of seismic design methods based on the behavior factor as shown in [17].

5. References

1. EUROCODE-3: Design of Steel Structures-Part 1-1: General rules and rules for buildings, ENV1993-1-1
2. WöHLER A., Zeitschrift für Bauwesen, vol.10, 1860.
3. BALLIO G., CASTIGLIONI C.A. A unified approach for the design of steel structures under low and/or high cycle fatigue, Journal of Constructional Steel Research, n.34, May 1995.
4. BALLIO G., CASTIGLIONI C.A., Seismic behavior of steel sections, Journal of Constructional Steel Research, n.29,1994, pp. 21-54
5. BALLIO G., ZANDONINI R., An experimental equipment to test steel structural members and subassemblages subject to cyclic loads, Ingegneria sismica, 2,1985, pp. 25-44.
6. ECCS, T.C.1, T.W.G. 1.3, Recommended testing procedure for assessing the behavior of structural steel elements under cyclic loads, Rept. n. 45, 1986.
7. CASTIGLIONI C.A. Effects of local buckling on cyclic behavior of steel members, SSRC, Proc. Annual Technical Session, Bethlehem, PA, june 1994, pp. 381-195
8. BALLIO G., CASTIGLIONI C.A., Damage assessment in steel members under seismic loading, Proc. of Int. Workshop and Seminar on Behavior of Steel Structures in Seismic Areas,Timisoara, 26-6/1-7, 1994
9. CALADO L., AZEVEDO J., A model for predicting failure of structural steel elements, I.C.S.R., n.14,1989, pp.41-64
10. YAMADA M., Low cycle fatigue fracture limits of various kinds of structural members subjected to alternately repeated plastic bending under axial compression as an evaluation basis or design criteria for aseismic capacity, IV W.C.E.E., Santiago, Chile, Vol.1, B-2, Jan. 1969, pp. 137-151.
11. YAMADA M., et al., Fracture ductility of structural elements and of structures, IX W.C.E.E.,Tokyo, 1988, pp. IV219-IV224.
12. YAMADA M. SHIRAKAWA H, Elasto-plastic bending deformation of wide-flange steel beam-columns subjected to axial load, Part I -II, Stahlbau, vol. 40, n.3 pp. 65-74, vol.5, pp. 143-151, 1971
13. BALLIO G., CHEN Y., An experimental research on beam to column joints: exterior connections, Proc. C.T.A., Viareggio, 1993, pp. 110-120
14. BALLIO G., CHEN Y., An experimental research on beam to column joints: interior connections, Proc. C.T.A., Viareggio, 1993, pp. 121-132
15. CALADO L., FERREIRA J., Cyclic behavior of steel beam to column connections: an experimental research, Proc. Int. Workshop on Behavior of Steel Str. in Seismic Areas, Timisoara, 26-6/1-7, 1994
16. MINER M.A., Cumulative damage in fatigue, J. of Applied Mechanics, Sept. 1945
17. BALLIO G., CASTIGLIONI C.A. "An approach to the seismic design of steel structures based on cumulative damage criteria", Earthquake Engineering & Structural Dynamics, Vol. 23, n.9, 1994, pp. 969-986.
18. BERTERO V., ANDERSON J., KRAWINKLER H., Performance of steel buildings structures during the Northridge earthquake, University of California Berkeley, Rept. n. UCB/EERC-94/09, August 1994
19. CASTIGLIONI C.A., "Seismic behavior of steel Beam-column members", SSRC Proc. ATS&M, Kansas City, March 1995
20. Eurocode-8, Design of structures in seismic regions, Part 1:General rules for buildings.

6. Aknowledgement

This research was sponsored by the Italian Ministry for University and Research MURST (40%)

THE SAC JOINT VENTURE

REDUCING EARTHQUAKE HAZARDS

IN STEEL MOMENT FRAME STRUCTURES

Presented by

James O. Malley
Degenkolb Engineers
and
SAC Project Director for Topical Investigations

INTRODUCTION

Following the January 17, 1994 Northridge earthquake, more than 100 steel buildings with welded moment-resisting frames were found to have experienced beam-to-column connection fractures. The damaged structures cover a wide range of heights ranging from one story to 26 stories; and a wide range of ages spanning from buildings as old as 30 years of age to structures just being erected at the time of the earthquake. The damaged structures are spread over a large geographical area with the highest concentration of reported damage near the epicentral region. Discovery of these extensive connection fractures, often with little associated architectural damage to the buildings, has been very alarming. The discovery has also caused some concern that similar, but undiscovered damage may have occurred in other buildings affected by past earthquakes. Indeed, there have been isolated reports of similar damage having been found in buildings following both the 1971 San Fernando and 1989 Loma Prieta earthquakes.

Welded steel moment frame construction is used commonly throughout the United States and the world, particularly for mid- and high-rise construction. Prior to the Northridge earthquake, this type of construction was considered one of the most seismic-resistant structural systems, due to the fact severe damage to such structures had rarely been reported in past earthquakes, and that only notable collapse of such a structure, the Pino Suarez failure in the 1985 Mexico City earthquake, had ever occurred. That collapse was attributed by investigators to large axial column demands, induced by overly strong bracing in this dual system structure. Subsequent editions of U.S. building codes adopted provisions specifically intended to prevent such failures, and it was presumed by many that buildings designed to these later provisions would be largely collapse resistant. However, the widespread severe structural damage which occurred to such structures calls for re-examination of this premise.

Steel moment frame buildings are designed to resist earthquake ground shaking, based on the assumption that they are capable of extensive yielding and inelastic deformation, without loss of strength. The intended inelastic deformation consists of plastic rotations developing within the beams, at their connections to the columns, and is theoretically capable of resulting in benign dissipation of the earthquake energy delivered to the building. Damage is expected to consist of moderate yielding and localized warping of the steel elements, not fractures. This design approach has developed based on historical precedent, the observation of steel building performance in past earthquakes and limited research that has included laboratory testing of beam-column models and nonlinear analytical studies. Most other types of construction are presumed incapable of the same capacity for energy dissipation and inelastic response, and are designed for proportionately larger lateral forces.

Observation of damaged buildings indicates that contrary to the intended behavior, in many cases fractures initiated within the connections at very limited levels of inelastic behavior. Typically, but not always, fractures initiated at, or near, the complete joint penetration (CJP) weld between the beam bottom flange and column flange (Figure 1). Investigators have suggested a number of factors which may have contributed to this including: notch effects created by the backing bar which is commonly left in place following joint completion; substandard welding that included excessive porosity and slag inclusions as well as incomplete fusion; and potentially, pre-earthquake fractures resulting from initial shrinkage of the weld during cool-down. Such problems could be minimized in future construction, with the application of appropriate welding procedures and more careful exercise of quality control during the construction process.

Once fractures initiated, they progressed in a number of different ways. In many cases, the fractures initiated but did not grow, and could not be detected by visual observation. In other cases, the fracture progressed completely through the thickness of the weld, and if fireproofing was removed, the fractures were evident as a crack through exposed faces of the weld, or the metal just behind the weld. Once such a fracture formed, the beam-column connection has experienced a significant loss of flexural rigidity and capacity. Residual flexural strength and rigidity is developed through a couple consisting of forces transmitted through the remaining top flange connection and the web bolts.

Other fracture patterns also developed. In some cases, the fracture developed into a through-thickness failure of the column flange material behind the weld. In these cases, a portion of the column flange remained bonded to the beam flange, but pulled free from the remainder of the column. This fracture pattern has sometimes been termed a "divot" or "nugget" failure. Such fractures result in a similar degradation in the connection strength as that described above, but also resulted in a local degradation in the axial and flexural strength of the column.

A number of fractures progressed completely through the column flange, along a near horizontal plane that aligns approximately with the beam lower flange. In some cases, these fractures extended into the column web and progressed across the panel zone. Investigators have reported some instances where columns sheared entirely across the section. It is clear that in such cases, the structural integrity of the columns is greatly reduced.

Despite the obvious local strength impairment resulting from these fractures, many damaged buildings did not display overt signs of structural damage, such as permanent drifts, or extreme damage to architectural elements. Until news of the discovery of connection fractures in some buildings began to spread through the engineering community, it was relatively common for engineers to perform cursory post-earthquake evaluations of these buildings and declare that they were undamaged. In order to reliably determine if a building has sustained connection damage, it is necessary to remove architectural finishes and fireproofing and perform nondestructive examination including visual observation and ultrasonic testing. Even if no damage is found, this is a costly process. Repair of damaged connections is even more costly. A few such buildings have sustained so much connection damage that it has been deemed more practical to demolish the structures rather than to repair them.

GOALS AND OBJECTIVES

The Structural Engineers Association of California (SEAOC), the Applied Technology Council (ATC) and California Universities for Research in Earthquake Engineering (CUREe) have combined their considerable resources to address and resolve questions relating to the repair, design and retrofit of steel moment frame structures. Their goal for the SAC Steel Program: Reducing Earthquake Hazards in Steel Moment Frame Structures is to:

> *Develop professional practices and recommend standards for the repair, design and retrofit of steel moment frame buildings so that they provide reliable, cost-effective seismic performance in future earthquakes.*

Three objectives must be met to achieve this goal:

1. Characterize and understand what has happened to steel moment frame buildings in the Northridge earthquake.

2. Prepare interim procedures for professional practices and standards:

   - Identify buildings that may have been damaged and require further investigation.
   - Characterize the safety condition of inspected buildings.
   - Rehabilitate damage buildings to provide life-safety.

3. Prepare recommendations for the repair, design and retrofit of buildings based on a rational understanding of seismic behavior.

The SAC Steel Program has been specifically designed to achieve this goal in a time frame consistent with the urgency of the problem. Accomplishing these objectives will require marshaling both what is known about the design and seismic performance of steel structures, and what can be learned through directed investigations and analyses to augment existing knowledge. The technical challenges to be overcome are complex and difficult.

The five thousand SEAOC members, the eight major earthquake engineering research universities of CUREe, and the national technical resources of the Applied Technology Council (ATC) are committed to mobilizing all available national and international resources to rapidly and systematically achieve these objectives. Each of these organizations has a history of distinguished achievement. Together they provide a formidable resource for solving this important problem.

THE PROBLEM

The Northridge earthquake has effectively invalidated the building code and professional practices used before the earthquake for the design and evaluation of steel moment frame structures. It is not clear at this time how to repair damaged, retrofit undamaged, or design new steel moment frame structures. This leaves owners and structural designers in a precarious situation.

- Should a damaged building be repaired now, using expensive and possibly ineffectual techniques, or wait for better techniques to arrive, but risk more serious, potentially catastrophic, behavior in future earthquakes and aftershocks before it is repaired?
- Should an owner inspects the connections of a building that shows very little visible damage?
- Should a perspective owner buy or should a lender finance an existing steel building?
- Should owners with steel frame buildings awaiting construction continue on schedule, or should they change their designs to correct the apparent deficiencies uncovered by the Northridge earthquake?
- Should designers choose other structural systems until definitive answers to performance questions are known?
- How do we identify buildings that are damaged and pose increased life-safety risks in earthquakes, including aftershocks?
- How do we repair damaged buildings so that they provide life-safety?
- How do we design new buildings and retrofits for existing buildings so that they perform acceptably?

These questions are especially worrisome because we do not currently have the knowledge and experience needed to confidently guide us to good, cost-effective, reliable answers. Until new knowledge is generated, any action in repair, design or retrofit is fraught with the possibility of being deficient in both safety and economy. The implications of this situation are substantial for the design profession, the construction and steel industries, building officials, owners, occupants, lenders, and insurers - not only in the Los Angeles area, but throughout the U.S., and the world.

Among the many issues discussed as the source of the observed poor performance of special moment frame steel connections, there are six main problems most often put forth:

1. Inadequately executed welds.
2. Pre-existing cracks in the weldments.
3. Residual stresses in the joint resulting from the welding and construction process.
4. Use of inappropriate weld material, preparation, process and heat treatment.
5. Through-thickness tension failure of the column flanges.
6. Fundamental problems with the joint configuration.

The repair approaches being implemented by engineers range from a minimum of rebuilding the damaged connections to a maximum of rebuilding and modifying every connection in the structure. While there are many professional opinions expressed on how to resolve these problems for individual buildings, none are backed by experimental or analytical verification indicating that they will yield reliable, cost-effective solutions.

The limited amount of available test data is also being reinterpreted. However, the usefulness of this test data is limited, due to: 1) the small pool of information available; 2) concerns, expressed by engineers and researchers alike, regarding the reduced scale and simplifications introduced in most laboratory specimens; 3) the slow rate at which loads are usually applied during laboratory testing relative to the rapid cycling that occurs during earthquakes; and 4) numerous details found in the field that remain untested today.

In addition, several of the modes of failure observed following the Northridge earthquake have not been observed in any previous laboratory test. Few structural test programs to date have directly addressed issues related to the welding process and its quality assurance. It seems that no simple, quick answer to these problems is likely due to the complexity and number of interrelated technical issues involved and the limited amount of knowledge and experience currently available.

APPROACH

The number and complexity of the technical problems involved, and the importance of the economic and public policy issues raised, suggest that an ad hoc, quick-fix solution is inappropriate and likely to be ineffectual. Indeed, several attempts to date to reach rapid consensus by practicing engineers and researchers have failed - the problems are just too difficult for resolution within the current state of knowledge. A more fundamental investigative approach is needed, one that addresses the full range of associated technical issues and involves the best technical talent and resources available, not only from California, but from throughout U.S.

Restoration of public and professional confidence in the safety and performance of new steel frame buildings and in our ability to evaluate and rehabilitate existing ones requires development and synthesis of knowledge necessary to answer the following simple questions:

- What happened to steel buildings during the Northridge earthquake?
- Why did it happen and can it be predicted?
- How dangerous are damaged structures?
- How can we identify seismically vulnerable structures?
- How can we fix damaged or vulnerable buildings?
- Can this type of damage be avoided in the future?

The SAC Steel Program addresses these questions and will provide answers in the form of recommended standards of practice and draft guidelines. The urgency of these questions and the need for prudent expenditure of funds dictates a short-term program of centrally managed and coordinated investigations.

Achieving the goal and objectives of the project will require a wide array of coordinated individual investigations. These are divided into four basic categories, or tasks:

Task 1: Immediate investigations to characterize and understand what happened to steel moment frame buildings in the Northridge earthquake.

Task 2: Other short-term investigations and efforts to develop and peer review interim guidelines for professional practices and standards for identification, evaluation and rehabilitation.

Task 3: Near-term investigations and analyses to improve understanding of the important factors contributing tot he structural performance of steel moment frames and identification of effective and economical methods of evaluation, analysis, design and rehabilitation.

Task 4: Investigations focusing on the refinement, confirmation and assessment practices and standards for evaluation, rehabilitation and design of steel moment frame structures that are identified in Task 2 as reliable and cost-effective.

Phase 1 of the program which is currently in progress, is specifically addressing Tasks 1 and 2. Tasks 3 and 4 will be the focus of the second phase of the project which will commence later this year. SAC is presently attempting to obtain funding for Phase 2.

TOPICAL INVESTIGATION AND PRODUCT DEVELOPMENT TEAMS

This project requires the participation of experts from a wide variety of fields and disciplines. To foster communications between various individual investigations, and to make specialized technical resources and expertise available to all investigations, Topical Investigation and Product Development Teams have been established.

These groups are also coordinating issues related to uniformity in testing and analysis procedures, instrumentation, data acquisition, inspection, materials testing, and other related technical topics so that the results of various individual investigations can be readily and meaningfully compared and evaluated. For instance, investigators of a particular type of connection detail can call upon the assistance of experts in a second area (e.g., nondestructive evaluation); that state of the art procedures can be used for both investigations, and the results obtained can be compared - for instance, to assess the weld processes used in all joint tests because uniform test procedures were utilized. These coordination efforts are useful between different investigations, e.g., joint and system performance; experiments and analyses; welding and structural component tests, etc. This coordination will produce considerably better and more useful information, and at a lower cost, than if each investigation was independently conducted.

WORK PLAN

The initially formulated Work Plan includes a large number of actions. The following highlights of the draft Work Plan are given to convey the comprehensive set of actions and investigations that were initially perceived as important to achieving the stated goal:

1. The immediate focus of the work effort is on near-term needs related to inspection, evaluation and repair of steel frame buildings in Los Angeles and includes:

    - Workshop(s) to refine investigation plans and identify experts and resources interested in participating in program.
    - Detailed field surveys of steel frame buildings in the heavily shaken area.
    - Study of ground motion characteristics and influences on response.
    - Synthesis and assessment of current worldwide states of knowledge and practice.
    - Development and evaluation of interim guidelines for inspection, evaluation and repair.

2. Longer range tasks focus on professional practices and recommendation of standards for the repair, design and retrofit of steel moment frame buildings so that they provide reliable, cost-effective seismic performance. These tasks include:

   - *Systematically investigate the various technical factors contributing to* seismic performance of steel moment-resisting frames, including metallurgy, welding, structural and fracture mechanics, joint design and behavior, structural system behavior, nondestructive evaluation and inspection techniques.

   - Identify effective inspection procedures and nondestructive evaluation tools.

   - Develop effective and practical modeling and analysis tools for evaluation of existing steel frames and for the design of new structures.

   - Develop, evaluate and document professional practices and recommendations for design guidelines related to repair, evaluation and retrofit, and new construction.

   - Assess the cost-effectiveness, performance expectations and practicability of resulting guidelines and practices through detailed case studies of public buildings damaged by the Northridge earthquake.

   - Laboratory and field experiments, including large scale component, assemblage and structure tests, will be conducted to gather needed information on performance.

3. Implementation of the developed guidelines and standards of practice will be encouraged through frequent workshops and technical bulletins, training materials, instructional programs, and development of electronic data bases.

Professional design issues are also a major aspect of the program.

Effective information dissemination and training programs are crucial to implementation of the findings. These activities are described in part in the subsection below.

Because of the complexity of the technical problems involved and the need to involve experts from many fields, the SAC Joint Venture has established a special management structure. The strong, but responsive centralized management structure will ensure accountability and on-time delivery of project deliverables.

The intellectual resources to solve these problems are being drawn not only from the tremendous base of engineering and technical expertise and analytical and experimental capabilities available through the partners in the SAC Steel Program, but every attempt is being made to engage the best technical talent from throughout the U.S. interested in participating in this program.

Liaison is also being maintained with other on-going investigations and research programs, and relevant information from these sources will be incorporated into the plan and work products of this project.

COMMITMENT TO ENHANCING UTILIZATION OF PROJECT RESULTS

The success of the SAC Steel Program will be measured in terms of both the technical merit of its recommendations and the effectiveness of their communication to the engineering and construction industry.

SAC will develop a Utilization Plan to ensure that end use of its products is paramount in task planning and execution. The Utilization Plan will describe how the project will provide information to potential users and how it will identify the information that is needed by these users. The Utilization Plan will clearly state its commitment to improving utilization of results and will detail the actions planned to facilitate implementation and utilization of results and recommendations. Each project activity will develop a specific Utilization Plan crafted to meet the requirements of that activity, consistent with the format of the overall Utilization Plan. Plans for each project activity will concisely outline the intended beneficiaries of the effort and describe what actions should be taken to enhance the use of the products of the activity. The Utilization Plan will be treated by the Project Management Team as a critical element of the investigation planning and management system - just as important as the investigation objective, plan, personnel, schedule and budget. Utilization Plans for individual activities will be incorporated into the overall project efforts.

Improving the availability of information to the practicing engineer and tailoring that information to respond to his or her practice needs entails many different types of activities. Seven basic steps have been identified:

1. Formulate Utilization Plans to provide the basis for project actions directed towards producing information that is both useful to, and used by, those who have a need for it.

2. Involve practicing professionals directly in advisory and technical review functions as an integral part of project management.

3. Distribute newsletters to make information sources and results known - in addition to wide dissemination of technical reports and publication of technical papers.

4. Prepare bulletins to synthesize and interpret findings on topics of general interest and present them in a form usable by engineers, regulators, contractors, craftspeople, and so on.

5. Develop standards for recording, documenting, storing and distributing analyses and experimental data.

6. Establish an electronic data base for distribution of project schedules, activities and results.

7. Conduct seminars, workshops and training courses on project topics for engineers, regulators, contractors, craftspeople and others.

The goal of requiring Utilization Plans is to focus attention on what is required to make the investigation not only technically successful, but also one that produces information that is both useful to, and used by, those who have a need for it. The Utilization Plan for each activity will include at least the following:

1. Intended beneficiaries of the knowledge or information developed (termed "users" below). Intended users are distinguished from one another by their characteristics. Each activity may have several potential user constituencies.

2. Methods by which the results of the project are to be recorded and presented.

3. The extent to which users will be involved in the formulation of the objectives and Work Plan for the investigation.

4. The specific actions to be taken by the research team to make information available to intended users.

5. Sources of information used to develop the Utilization Plan.

The Project Management Team will regularly review Utilization Plans for each activity, as well as for the project as a whole. Progress toward targets will be measured. Adjustments and new approaches will be tried, if necessary to meet stated goals.

SEISMIC BEHAVIOR OF STEEL BEAM-COLUMN MEMBERS

Carlo A. Castiglioni
Associate Professor
Structural Engineering Dept., Politecnico di Milano, Italy

Abstract

In this paper, the experimental results obtained during an extensive testing program on the cyclic behavior of steel members under bending and/or compression and bending, carried out at the Structural Engineering Department of Politecnico di Milano are presented and discussed.

1. Introduction

The response of a structure under cyclic loading largely depends on its ductility, that is on its ability to dissipate energy and sustain large plastic strains without showing brittle failure mechanisms. Of course, the ductility of a structure is strictly related to that of its members, which is a function of the ductility of the material and is influenced, for the steel, by local effects like fatigue and fracture, as well as by global and local buckling.The importance of structural ductility is clearly evidenced by the great number of research works [1-13] both experimental and analytical, that have been performed all over the world on this topic in the last three decades. Standard testing procedures were also proposed [8,10] with the aim of unifying the experimental approach and obtaining comparable results from different research projects.

As a consequence for these and other researches carried out in different countries, most of the recent codes dealing with the design of structures in seismic regions [14-17] consider the possibility of reducing the horizontal forces obtained through a linear analysis, in order to account for post elastic behavior and ductility.

For a correct statement of the global ductility of a structure, both the ductility demand connected with seismic actions and its global inelastic resources, which depend for example on structural typology, second order effects and eventual brittle fracture mechanisms, must be taken into account.

Extensive research were recently performed in many countries on the dynamic behavior of steel structures. Of course, it is not feasible to perform exclusively dynamic testing programs on full scale structures, because of the costs connected with this kind of approach. A valid alternative is however represented by quasi-static cyclic tests performed on structural elements (or structural systems) combined with numerical simulation of their dynamic behavior.

For an adequate simulation of the behavior of steel members under seismic loading it is however necessary on one side to adopt a constitutive law for the material able to reproduce with sufficient accuracy its inelastic behavior under various loading histories, on the other side to set up numerical models able to simulate the progressive damage of the structural element due to local buckling and low cycle fatigue.

In this paper, the experimental results obtained during an extensive testing program on the cyclic behavior of steel members carried out at the Structural Engineering Department of Politecnico di Milano are presented and discussed. Based on these results, a numerical simulation model was developed and calibrated [11], as well as a simple cumulative damage

model [21,22], based on Miner's rule [19]. Some possible failure criteria for steel members under seismic loading, calibrated against the experimental test results will also be presented and discussed.

2. Experimental research

Research in the field of seismic and cyclic behavior of steel structures has been widely performed, both experimentally and numerically, by the Steel Construction Group of the Structural Engineering Department of Politecnico di Milano [18].
In particular two experimental studies were carried out, the first one dealing with welded box and I shapes [7], the second one dealing with rolled I shapes of the commercial series HEA, HEB and IPE [12]. In both these studies it was tried to adopt shapes with comparable values of the ratio c/t_f (of the half flange width c to the flange thickness t_f), in order to highlight the influence of the restraint offered by the web to the buckling of the flange. The obtained results, as well as the number of discrepancies found in the approaches adopted by the various Codes with regard to the influence of the d/t_w ratio of the web on the behavior of I shapes under cyclic loading, indicated the need for further studies in this field.
Most of these previous experimental research works were carried out following the ECCS Recommended Testing Procedures [8]. According to these Recommendations, groups of three displacement cycles are imposed to the specimen, each group having an increased cycle amplitude. These loading procedures, although allowing a correct assessment of the global behavior of the specimen under testing, are not suitable for the assessment of the single aspects governing such behavior. In fact, by varying the amplitude of the displacement cycles, strain hardening effects are superimposed to reductions in load carrying capacity due to local buckling and low cycle fatigue crack propagation. For this reason, a research program was undertaken at the Structural Engineering Department of Politecnico di Milano [13], focusing on constant amplitude testing, as other authors [10] previously suggested.
The experimental testing program encompasses cyclic quasi-static tests to be performed on full scale laminated steel beams of the commercial series HEA, HEB and IPE.
Two different testing procedures are followed:

1. quasi-static tests with imposed displacement cycles of constant amplitude v;
2. quasi-static tests with imposed displacements following a "random" path, previously obtained by dynamic numerical simulation of the seismic response of similar elements by means of the numerical models set up during earlier research projects [11,18].

Shape	Area	Flange			Web			
	(cm^2)	b=2c	t_f	c/t_f	h	d	t_w	d/t_w
		(mm)			(mm)			
HE 220A	64.3	220	11.0	10.0	210	152.0	7.0	21.7
HE 220B	91.0	220	16.0	6.9	220	152.0	9.5	16.0
IPE 300	53.8	150	10.7	7.0	300	248.6	7.1	35.1
HE 120A	25.3	120	8.0	7.5	114	74.0	5.0	14.8
HE 140A	31.4	140	8.5	8.2	133	92.0	5.5	16.7

Table 1- Geometrical properties of specimen shapes

Within this research program, tests were performed at the Structural Engineering Department of Politecnico di Milano [13] on full scale cantilever members 1.6 m long (fig.1), of the commercial shapes HE120A, HE140A, HE220A, HE220B and IPE300 (whose geometrical propreties are given in tab.1), using an equipment [9] capable of applying horizontal cyclic

actions in a quasi-static way. Presently, the testing programme is continuing, in order to enlarge the data-base, and tests are carried out also considering the presence of an axial load.

3. Beams

To date, 40 tests were performed (11 on HE220A shapes, 12 on HE220B, 11 on IPE300, 3 on HE120A and 3 on HE140A) imposing to the specimens displacement cycles with a constant amplitude.

In addition to the usual hysteresis loops in terms of force applied on the top vs. top displacements, for each specimen experimental measurements were obtained by means of a set of LVDTs positioned as shown in fig. 1, and processed following the ECCS Recommended procedures [8] in order to obtain informations regarding resistance ratio, rigidity ratio, cumulative energy ratio and buckle size which were plotted vs. the number of applied cycles.

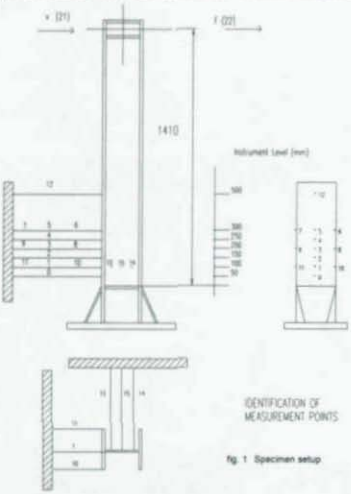

fig. 1 Specimen setup

Before any comment, it is important to remember that, according to the definitions given in EC-3 (see tab. 1), HE220A profile has a c/t_f ratio of the flanges (10.0) larger than that of HE220B (6.9), of IPE300 (7.0), of HE120A (7.5) and of HE140A (8.2), while its width to thickness ratio for the web (d/t_w= 21.7) is intermediate between those of HE120A (14.8) and of IPE300 (d/t_w =35.1), and a little larger than those of HE220B (d/t_w =16.0) and of HE140A (d/t_w =16.7) which are similar to each other.

In order to highlight the different effect of the geometrical properties of the cross section on the behaviour of beams under cyclic loading, some typical results are here presented and discussed with particular reference to specimens which were tested under cycle amplitudes resulting in similar values of the ductility ratio $\Delta v/v_y$.

Figures 2, 3, 4 and 5 respectively show, plotted vs. the number of cycles withstanded by the specimen:

- the resistance ratio (F/F_y), of the load carrying capacity of the specimen at each positive reversal normalised on the yield strength determined according to ECCS Recommended procedures [8];
- the rigidity ratio (k/k_y) of the stiffness, conventionally determined according to Ref. [8] as the tangent modulus corresponding to the change of the sign of the applied load, normalised on the elastic initial one;

- the cumulative energy ratio (E/E_y) of the absorbed cumulative energy (defined as the sum of the areas of all the cycles withstanded by the specimen) normalised on the energy absorbable, under the same cycles, by an ideal specimen made of an elastic perfectly plastic material;
- the buckle size of the flange edges (i.e. the maximum out of plane deflection of the flange due to buckling).

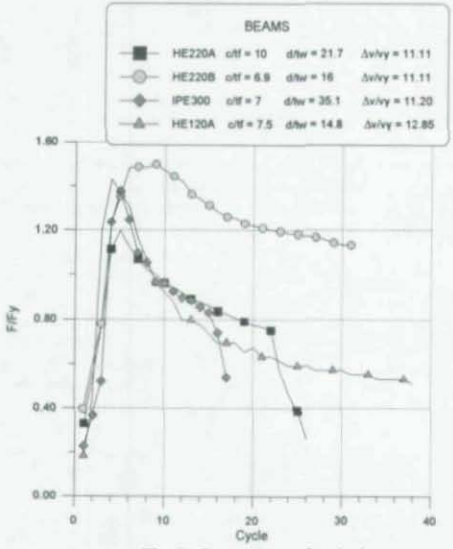

Fig. 2 Comparison of typical strength degradation trends

The following fig. 6 plots for all the HE220A, HE220B and IPE300 specimens tested under constant amplitude loading, the cumulative energy ratio vs. the number of imposed cycles times the cyclic excursion in the plastic range (computed as Δv-$2v_y$) divided by v_y. The term on abscissa can be regarded as the total cumulative excursion in the plastic range withstanded by the specimen.

By examining these figures, the following considerations can be drawn, having a general validity, for the shapes examined in this study:

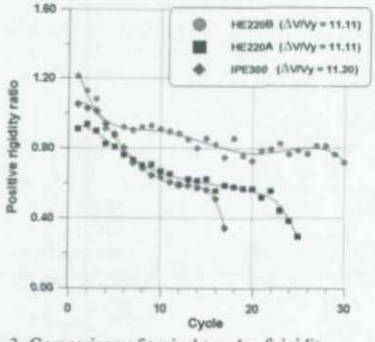

fig. 3 Comparison of typical trends of rigidity ratio for HE220A, HE220B and IPE300 shapes

1. Deterioration effects, causing a reduction in load carrying capacity, stiffness and hysteresis loops area begin earlier in specimens having larger c/t_f ratio (e.g. HE220A), but beams characterised by larger d/t_W ratios (e.g. IPE300), although initially following an intermediate behavior experience much faster degradation;

2. A major role in governing local buckling effects is played by the web slenderness ratio d/t_w.
3. Buckling develops completely within a few cycles, whose number seems to depend on the d/t_w ratio, then stabilisation of the buckles size occurs.

For all types of profile, once local buckling takes place and buckle size stabilisation occurs, also the hysteresis loops stabilise, and the rate of reduction in load carrying capacity decreases with increasing the number of cycles imposed to the specimen, until a final stage is reached, when the deterioration rate suddenly increases again and the specimen collapses after a few cycles. Specimens having lower values of d/t_w show a more gradual transition from the (longer) phase of cycle stabilisation to that leading to collapse.

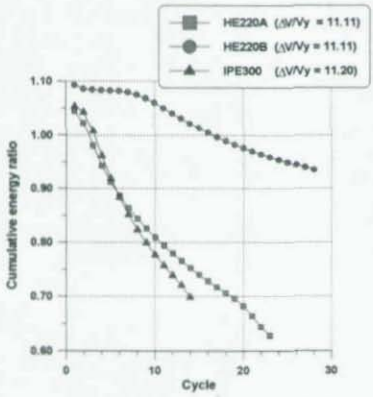

fig. 4 Comparison of typical trends of adsorbed energy ratio for HE220A, HE220B and IPE300 shapes

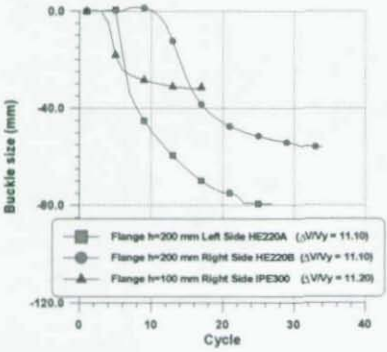

fig. 5 Comparison of typical trends of buckle size for HE220A, HE220B and IPE300 shapes

4. The differences in behavior at the final stage, between HEB specimens, HEA and IPE ones are associated with a difference in their failure modes. HEA and IPE beams generally collapse by steady crack propagation due to low-cycle fatigue effects; the HEB specimens, on the contrary, evidence some kind of brittle fracture of both the flange and the web, either at the specimen-to-base welds or at the plastic hinge where, due to large localised distortions, surface cracks usually develop a few cycles after local buckling of the flange plates.

fig. 6 Cumulative energy ratio vs. total cumulative excursion in the plastic range withstanded by the specimen, for all beam tested under constant amplitude cycles

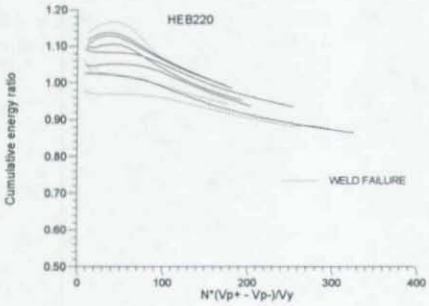

fig. 6.1 HE220B

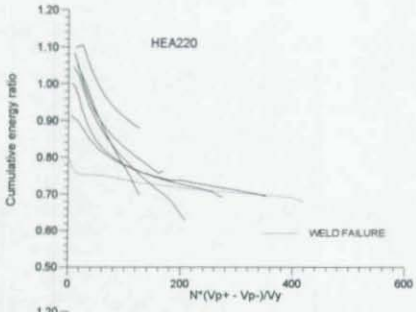

fig. 6.2 HE220A

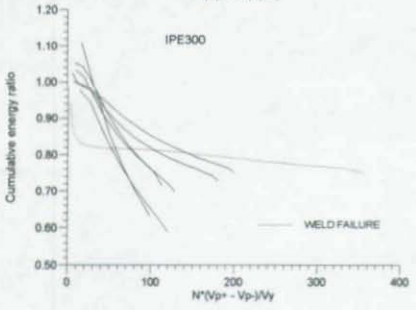

fig. 6.3 IPE300

4. Beam columns

Tests were also carried out with the presence of an axial load. To date, 3 tests were performed on HE120A, with an axial load $P/P_y = 0.05$, 3 tests on IPE300 with $P/P_y = 0.10$, and 8 tests on HE220A specimens, subjected to three different values of the axial load P: $P/P_y = 0.05$, 0.10 and 0.125 (where $P_y = f_y A$ is the plastic strength of the cross section).

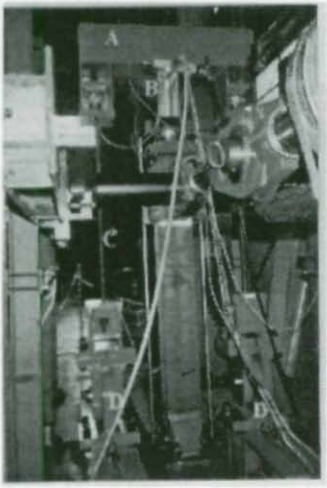

Fig.7 Experimental set up

The axial load was imposed by means of an hydraulic jack (fig. 7-B) positioned between the top of the specimen and a transversal rigid beam (fig. 7-A) connected by means of high-strength tendons (fig. 7-C) to two lateral hinges (fig. 7-D). The axial load in the jack and in the tendons was monitored by means of dynamometers directly connected to the data acquisition unit. The axial load was kept constant during the test by readjusting the oil pressure by means of an hydraulic pump, in order to compensate for specimen shortening due to large deformations and local buckling at plastic hinge location.

The experimental set-up is such that the applied axial load direction is cohincident with the longitudinal axis of the specimen, and during cycling, tilts together with the specimen axis. Hence, no P-Δ effect is induced in the base section by the axial load. Further tests are already programmed, with a modified test set-up, such that it will be possible to keep unchanged the axial load application line during cycling, and investigate the influence of second-order P-Δ effects.

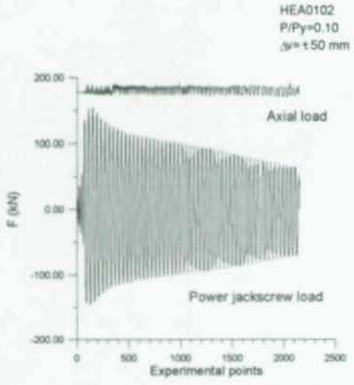

Fig. 8 Variation of axial load and of applied horizontal force during a typical test

Fig. 8 shows the variation of the axial load, as well as of the horizontal force applied by the jack to the specimen, during the whole duration of a typical test. The small fluctuations of the applied axial load are the consequence of both the horizontal cycling of the specimen, as well as (as already said) of the large deformations at plastic hinge and specimen shortening. It can however be noticed that, by operating on the oil pump, it is possible to keep such variations within a sufficently small range.

The presence of an axial load on top of the

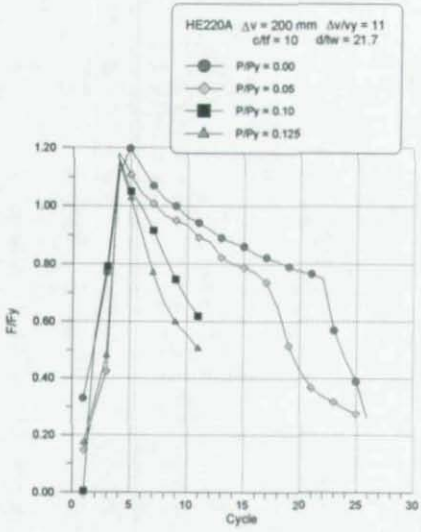

Fig. 9 Effect of axial load on strength degradation

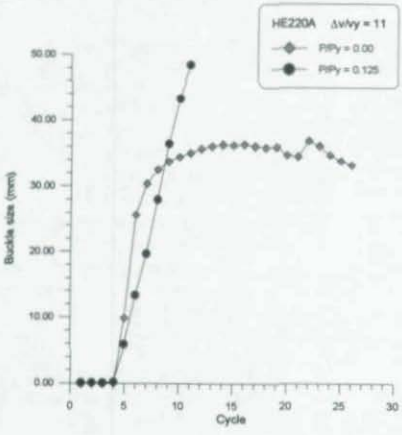

Fig. 10 Effect of axial load on local buckling of flanges

specimens results in deterioration rates larger than in the absence of axial load. This is evident in fig. 9 where the resistance ratio of the load carrying capacity of the specimen at reversal points (normalised on the yield strength) is plotted for HE220A members tested under the same cycle amplitude Δv equal to 200 mm, for different values of the axial load.

It can be noticed that, although the maximum load carrying capacity of the specimen is not much influenced by the presence of the axial load, the rate of deterioration of the specimen load carrying capacity strongly depends on it. In particular, for an axial load P/P_y =0.10 (or greater), the reduction in load carrying capacity of the specimens becomes evident already after the first cycle in the plastic range (i.e. from cycle n.4, as the first three cycles were performed in the elastic range according to ECCS Recommended Procedures [8]).

The following fig. 10 shows the effect of the axial load on the buckling rate of the specimen flanges, in the case of HE220A profiles. It is evident that the stabilization of the buckle size, already discussed in the case of beams, does not occur in the presence of an axial load. The flange of the beam column buckles in the first inelastic cycle, and increases its out-of-plane deflection until failure of the member is reached, although with an initial trend lower than in the case of the beam.

5. Possible failure criteria

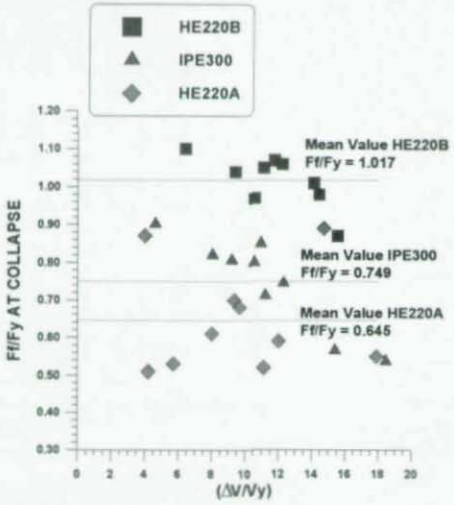

Fig. 11 Mean values of load carrying capacity at failure

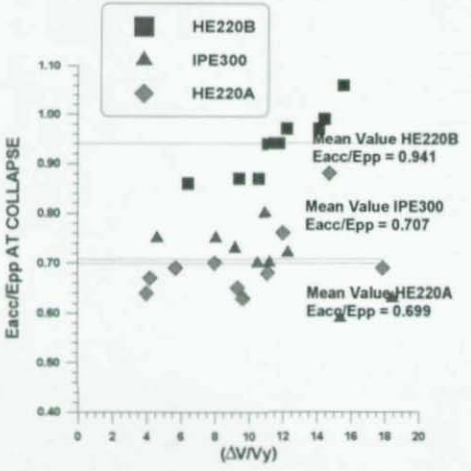

Fig. 12 Mean values of accumulated energy at failure

Examining the experimental results it was noticed that, at collapse, the values of the ratios F_f/F_y of the strength to the yield strength, and cumulative energy ratio E/E_{epp} are strongly dependent on the type of profile. This is clearly evident when examining the following figs. 11 and 12, where for the tests carried out on beams, respectively the ratios F_f/F_y and E/E_{epp} at failure are presented for HE220A, HE220B and IPE300 profiles (at present, too few tests have been performed on other shapes, as HE120A or HE140A, to allow any similar consideration to be drawn for such shapes). By examining figs. 11 and 12, it can be stated that it is not possible to define a common failure criterium, for both HE220A, IPE300 and HE220B profiles, based on the achievement of a limit value by one of the previously defined ratios.

Some authors [20] proposed to adopt as unified failure criterium the reduction of the energy dissipated in a cycle to 50% of that dissipated by a member made of an elastic perfectly plastic material, cycled under the same amplitude. That criterium was formulated based on a number of numerical simulations of the cyclic

behavior of steel members [7]. Presently the experimental results obtained in the present study are currently being reprocessed in order to experimentally validate the criterium proposed in [7].

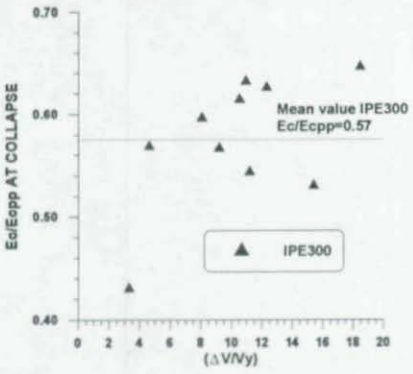

Fig. 13 Values of energy dissipated at last cycle before failure for IPE300 specimens

Fig. 13 shows the preliminary results of such a reprocessing, with reference to IPE300 specimens tested under cyclic bending. It can be noticed that the mean value of experimental data of energy absorbed at the last cycle before failure E_c , normalised on the energy E_{cpp} absorbable in the same cycle by a specimen made of an elastic perfectly plastic material is 0.57. This is in good agreement with the criterium proposed in [7].

It is particularly interesting to formulate some collapse criteria based on the achievement of a given level of deterioration of the mechanical properties of the material.

In fact, by means of such a collapse criterium, the limit state at which the member is considered out-of-service, can be a-priori defined. Such a situation, of course, may not coincide with actual collapse of the member. However, in order to be applied in standard design procedures, such a collapse criterium must allow an assessment of the member failure conditions as close to reality as possible, and always on the safe side.

Considering as parameters governing failure of the member the resistance ratio F_f/F_y , and cumulative energy ratio E/E_{pp} , it is proposed to assume the following collapse criteria:

- for HEA220 profiles:
  $F_f/F_y = 0.7$ or
  $E/E_{pp} = 0.7$
- for HEB220 profiles:
  $F_f/F_y = 1.10$ or
  $E/E_{pp} = 0.95$
- for IPE300 profiles:
  $F_f/F_y = 0.75$ or
  $E/E_{pp} = 0.70$ or
  $E_c/E_{cpp} = 0.50$ (if considering the criterium proposed in [7])

These values can be adopted for a safe assessment of the damage cumulated in the members. Hence, these values are not to be considered as the best fit of experimental results, but can be regarded as possible reference values in damage assessment procedures.

From the carried out tests it was noticed [13] that, for all beams and beam columns tested, the relationships which best fitted the experimental results in terms of cycle amplitude Δv (normalized on the yield displacement v_y) and number of cycles to failure N_f , were exponential functions of the type $N_f = a*(\Delta v/v_y)^b$, with a and b constant parameters to be defined and calibrated on the experimental test results, for the different types of profiles. This kind of relationships are similar to the Wöhler S-N lines [23] usually adopted in high-cycle fatigue design.
By correlating the number of cycles corresponding to the attainment, by the assumed governing parameter (F_f/F_y , or E/E_{pp}), of the "limit" value to the cycles amplitude Δv, it is possible to define a limit (S-N) line associated with a particular collapse criterium.
The definition of the "failure" condition, and in particular of the "limit" value to be assumed by the governing parameter at failure, is particularly important and delicate because inflences the identification of the appropriate S-N line for each detail and involves the assumption of an appropriate safety factor.

Based on the previous results and considerations, it has been shown elsewere [21,22] that, by re-processing data of cyclic tests considering the stress range as the one associated to the real strain range in an ideal member made of an indefinitely linear elastic material, it is possible to fit the low cycle fatigue test data on beams, beam-columns and joints by means of the S-N curves usually adopted for high cycle fatigue. It has also been shown [21,22], that a linear damage accumulation model [19] can be adopted, together with the previously defined S-N lines, for the assessment of accumulated damage in members and connections under seismic loading.

6. References

[1] Bertero V.V., Popov E.P.: "Effects of large alternating strains on steel beams" A.S.C.E., Journal of the Structural Division, vol. 91, n. ST1, Feb. 1965.

[2] Tanabashi R., Yoshitsura Y., Wakabayashi M., Nakamura T., Kunieda H.: "Deformation-history dependent inelastic stability of columns subjected to combined alternating loading", RILEM Int. Symp., Buenos Aires, Sept. 1971.

[3] Hancock, G.: "Local distorsional and lateral buckling of I-beams", ASCE Journal of the Structural Division, vol. 104, n.ST11, Nov. 1978

[4] Popov E.P., Zayas V., Mahin S.: "Cyclic inelastic buckling of thin tubular columns", ASCE Journal of the Structural Division, vol. 105, ST11, nov. 1979

[5] Fukumoto Y., Kusama H."Cyclic bending of plates under transverse loading", ASCE Journal of the Engineering Mechanics Division, vol. 108, n.EM3, June 1982

[6] Kusama H., Fukumoto Y."Cyclic behavior of thin walled box stub-columns and beams", Colloquium on Stability of Metal Structures, Paris, Nov. 1983

[7] Ballio G., Calado L.: "Steel bent sections under cyclic loads. Experimental and numerical approaches", Costruzioni metalliche, n.1 1986

[8] ECCS-TWG 1.3: "Recommended testing procedures for assessing the behavior of structural steel elements under cyclic loads", TC1, Seismic Design, ECCS publ. n. 45, 1986

[9] Ballio G., Zandonini R."An experimental equipment to test steel structural members and subassemblages subject to cyclic loads", Ingegneria Sismica, n.2, 1985

[10] Krawinkler H. et al."Recommendations for experimental studies on the seismic behavior of steel components and materials", The John Blume Earthquake Engineering Research Center, Stanford, CA, Rept. 61, 1983

[11] Castiglioni C.A., DiPalma N.:"Steel members under cyclic loads: numerical modelling and experimental verifications", Costruzioni Metalliche. n.6, 1988
[12] Castiglioni C.A., DiPalma N.:"Experimental behavior of steel members under cyclic bending", Costruzioni Metalliche n. 2/3, 1989
[13] Ballio G., Castiglioni C.A., "Seismic behavior of Steel Sections", J.C.S.R., n.29, 1994, pp. 21-54
[14] Eurocode 8:"European Code for seismic regions", 1988
[15] Seismology Committee, Structural Engineers Association of California: "Tentative lateral forces requirements", October 1985
[16] Gruppo nazionale per la Difesa dai Terremoti (GNDT): "Norme tecniche per le costruzioni in zone sismiche", *Ingegneria Sismica, vol. 2, n.1, 1985*
[17] Kato B., Akiyama H., "Seismic design of steel Buildings", ASCE Journal of the Structural Division, vol. ST8, n.8, August 1982
[18] "Seismic design of steel structures", Selected papers, 1985,1989, by Researchers of the Steel Construction Group, Structural Eng. Dept., Politecnico di Milano, 1990.
[19] Miner M.A., " Cumulative damage in fatigue " - Journal of Applied Mechanics, September 1945
[20] Calado L., Azevedo J., "A model for predicting failure of structural steel elements", J.C.S.R., n.14, 1989, pp. 41-61
[21] Castiglioni C.A., "Seismic damage assessment of steel members and joints", SSRC Proc. ATS&M, Kansas City, March 1995
[22] Ballio G., Castiglioni C.A., "A unified approach for the design of steel structures under low and/or high cycle fatigue", Journal of Constuctional Steel Research, n.34, May 1995, (to appear)
[23] Wöhler A., "Zeitschrift für Bauwesen, vol.10, 1860

7. Aknowledgements

This research has been funded by the Italian Ministry for University and Scientific and Technological Research (M.U.R.S.T.).

STABILITY ISSUES IN THE APPLICATION OF ELASTOMERIC ISOLATION SYSTEMS TO THE SEISMIC RETROFIT OF HISTORICAL BUILDINGS

Ian G. Buckle
State University of New York at Buffalo
National Center for Earthquake Engineering Research

ABSTRACT

Elastomeric seismic isolators have been used in the United States for the earthquake protection of new buildings and bridges for almost ten years. Of particular interest is the use of seismic isolation for the retrofit of historical buildings and the use of elastomeric bearings to decouple these fragile structures from strong ground motions.

Several major public buildings of historic and functional importance have been, or are being, retrofitted using base isolation in the United States at this time. These include the Salt Lake City and County Building in Utah, the Mackay School of Mines at the University of Nevada in Reno, the Oakland City Hall, and the Ninth Circuit United States Court of Appeals in San Francisco. In each case, seismic performance has been improved while protecting the historical fabric of these buildings and reducing the overall reconstruction cost.

Elastomeric isolation systems have been used in three of the four buildings just noted. Their design required careful consideration of material strength, rollover equilibrium, and buckling phenomena at high shear strain. Whereas these limit states are relatively well understood for single bearings, system stability, which involves the interaction of critical and non-critical elements is not so well defined. The successful application of elastomeric isolators to the retrofit of the above buildings required a solution to this problem and the development of improved methods for estimating an overall system factors of safety *against instability*.

INTRODUCTION

Seismic isolation is a design strategy based on the premise that it is both possible and feasible to uncouple a structure from the ground and thereby protect it from the damaging effects of earthquake motions. To achieve this result, while at the same time satisfying all of the in-service functional requirements, additional flexibility is introduced usually at the base of the structure. Additional damping is also provided so as to control the deflections which occur across the isolation interface.

The concept is not new and many proposals have been made since the turn of the Century for "...devices which absorb or minimize shock to buildings arising from earthquake, vibrations caused by heavy traffic or other disturbances of the earth's surface" [1].

In 1906, Jacob Bechtold of Munich, Germany made an application for a U.S. Patent for an Earthquake Proof Building. His primary claim was for "...an earthquake proof building consisting of a rigid base-plate to carry the building and a mass of spherical bodies of hard material to carry the said base-plate freely" [2].

Kelly, in an overview paper [3], has described the 1909 patent of Calantarients, a medical doctor from Scarborough, England who proposed "...a method of building to resist the action of earthquakes" which used layers of talc to isolate the walls and floors from ground disturbances. In correspondence to a Chilean colleague, Dr. Calantarients acknowledged the existence of a Japanese system developed 25 years earlier, in the late 19th century.

Today, there appear to be more than 300 seismically isolated buildings and bridges around the world. Some of this worldwide activity is reported in Reference [4] but since 1990, the date of this particular reference there has been continuing growth in the field and the number and extent of these applications has increased remarkably in the intervening four years. In the United States there are now approximately 76 bridges and 15 buildings which are either completed or under construction using isolation. There are many more in the feasibility and planning stages. Of these 91 structures, more than half are applications to existing structures.

APPLICATION TO BUILDING RETROFIT

Seismic isolation is an attractive alternative to conventional strengthening for existing buildings because in many cases the seismic loads can be reduced to the same order of magnitude as the existing strength of a deficient building. This in turn may eliminate the need for structural work above the isolation level. The advantages here are threefold. When compared with installing a new lateral load resisting system inside an existing building (a steel frame, for example), the alternative of working only in the basement to install the isolation system is very attractive. This option can reduce construction cost, minimize disruption to the occupants of the building (in many cases building operation can continue throughout the retrofit exercise), and preserve the architectural integrity of the existing building. Of these three advantages, the last one is particularly compelling in the case of historical buildings of architectural significance. Conventional retrofit schemes may destroy valuable and irreplaceable interior finishes and also change the external appearance of a building. By contrast, isolation schemes are largely invisible and preserve both the interior and exterior fabric of a building. In the United States, this is particularly important for buildings that are listed on a National Register because the fabric of these structures is protected by federal law and may not be altered during rehabilitation work.

However, the use of isolation may not totally eliminate the need for structural work above the isolators. Some existing buildings are so weak that it is not feasible to reduce the seismic demand to less than the existing (minimal) capacity. As a consequence, some strengthening may be necessary in addition to using isolation, but experience has shown in these circumstances the amount of strengthening required is significantly less than if isolation had not been used.

ISOLATION HARDWARE AND ELASTOMERIC BEARINGS

Today, several different isolation systems are available and these generally fall into three classes: elastomeric systems, sliding (or friction) systems and hybrid systems (combinations of elastomeric and sliding bearings). Of these three, the most commonly used is the elastomeric bearing which consists of alternating layers of elastomer and steel and which is stiff in compression but flexible in shear.

These bearings may be of natural or synthetic rubber and maybe specially compounded to enhance their hysteretic damping. Alternatively the bearings may be structurally modified to include a damping element, such as the inclusion of a lead or granular core on the vertical axis of the bearing.

In a typical building, isolators are located under each column, usually in a sub-basement. In a bridge they are usually placed under each girder at the abutment seats and between the column capbeam and the superstructure. There may be from 40 to 400 bearings in such a structure depending on its size and weight. The individual bearings which make up the isolation system are frequently interconnected by a diaphragm which is rigid in its own plane and which enforces displacement compatibility amongst the various isolators.

STABILITY ISSUES

Of particular interest in the retrofit of large historical buildings is the stability of these elastomeric isolators while subject to varying axial load and simultaneously deformed to high shear strain. Identification of the critical limit state is currently done by examining three separate limit states for each individual bearing; these are the maximum shear strain in the elastomer, the displacement at which rollover commences and the load at which buckling may occur. The shear strain in the elastomer is used as a measure of load capacity since it compares the total strain from all sources (compression, shear and rotation) against the elongation-at-break for the elastomer. The other two limit states are measures of bearing stability. System stability is then estimated by examining the bearing with the lightest axial load, in the case of rollover, and the greatest axial load, in the case of buckling.

However, instability in a single bearing does not necessarily mean that the system as a whole is unstable. Since the axial load varies throughout the structure, it follows that not all isolators are of the same size and stiffness or carry the same axial load. Therefore, while one isolator may reach a limit state, others may not be critical or even close to a critical state and these other isolators may act to restrain the unstable isolator from failure. It follows that system factors of safety related to stability which are based on individual bearing limit states, may be unduly conservative.

System Stability

To gain insight into system stability, it is useful to assume that the load - displacement behavior for the system can be represented by a single curve. Such a relationship is shown in Figure 1, in which the total structure shear force is plotted against shear displacement for the building. Under the above assumption, this building displacement is the same as the displacement for each individual bearing. Characterizing the

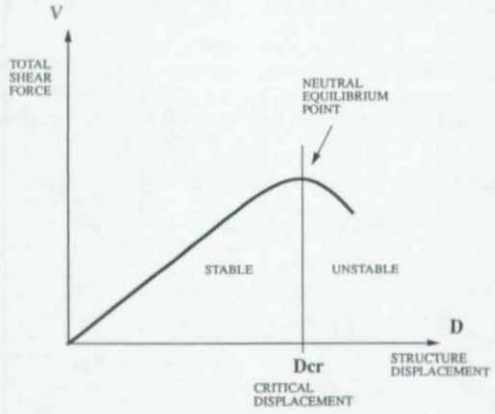

Figure 1 System stability

displacement by a single value is valid provided a rigid diaphragm interconnects all the isolators and torsion about a vertical axis is negligble. It follows that the system load-displacement curve is the sum of the individual bearing load-displacement curves.

The displacement at which the system passes from stable to unstable equilibrium (i.e. through the neutral point) is called the critical displacement for the system. The corresponding shear force is clearly the maximum force that the system can sustain.

A system factor of safety can be calculated using either the critical displacement or the maximum force. If the system is linear, as assumed in Figure 1, both methods will give the same result. Ideally, this is the factor that should be used to estimate system stability, rather than using worst case scenarios from individual bearings.

Bearing Stability

To construct a system load-displacement curve such as that shown in Figure 1, the individual bearing limit states must first be modelled. As noted above, the two limit states affecting bearing stability are rollover and buckling. These are further described below.

The Rollover Limit State *Rollover may occur in bearings which are fastened by dowels* to the masonry and sole plates of the structure. These shear-only connections do not permit the transfer of tension through the bearing which therefore limit tensile stresses in the elastomer to acceptably low levels. Conservative limits on these stresses have been imposed because of the uncertain behavior of rubber in direct tension. However, the absence of a tension connection means that the overturning moment which can be

resisted across the upper and lower faces of the bearing is limited to a finite value and once exceeded the bearing must overturn. Rollover at high shear strains can be prevented by using a bolted connection, but at the expense of higher internal stresses in the bearing.

The theory describing rollover has been previously presented (Reference 5). The essential results are given in Figure 2 and summarized below. A typical bearing on the point of rollover instability is shown in Figure 2a and the corresponding force - displacement curve is given in Figure 2b. The value of the displacement at which rollover commences, unless the shear force is reduced, is given by:

$$\Delta_{ro} = \frac{PB}{(P+Kr.H)} \tag{1}$$

where:

Δ_{ro}	=	rollover displacement
P	=	axial (compressive) load on bearing
B	=	bearing width (shim width)
Kr	=	bearing shear stiffness
H	=	bearing height (includes all shims and rubber layers)

The initial slope is given by Kr, the bearing shear stiffness and is a function of the rubber shear modulus, the bonded area of rubber and the total thickness of deformable rubber layers. The second slope is given by -P/H and is a function of axial load and overall bearing height. It is negative which indicates the need to unload the bearing if it is to remain stable at this displacement.

The Buckling Limit State Elastomeric bearings exhibit buckling phenomena in much the same way that structural columns are susceptible to compressive loads. The buckling theory for these bearings has been developed by Haringx (Reference 6) and Gent (Reference 7). It is also reported in Reference 2. It will be seen that the critical buckling load for an elastomeric bearing is given by:

$$Pc = \frac{R}{2}\left[\sqrt{1 + 4P_E/R} - 1\right] \tag{2}$$

where:

P_E	=	$\pi^2 T/H^2$
T	=	tilting (bending) stiffness for bearing of unit total height
	=	$(E_b I)\ (H/T_r)$
R	=	shear stiffness for bearing of unit total height
	=	$K_r H$
K_r	=	shear stiffness ignoring axial load effects
	=	GA/T_r
G	=	shear modulus of rubber
A	=	bonded area of rubber
T_r	=	total thickness of rubber (excludes shims)
H	=	effective height of bearing (includes shims)
E_b	=	bending modulus
	=	$E_o\ (1 + f_b.S^2)$
E_o	=	elastic modulus of rubber
f_b	=	bending constant

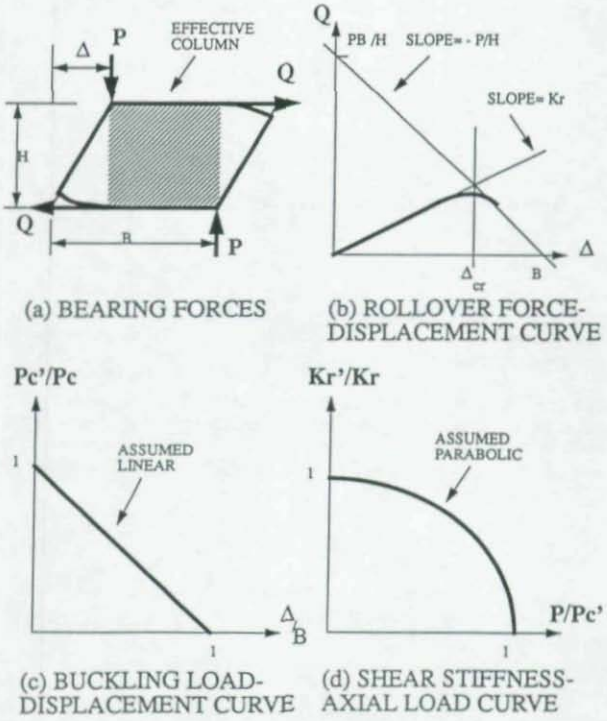

Figure 2 Rollover and buckling limit states for an elastomeric bearing

S = layer shape factor
I = moment of inertia of bearing about axis of bending

However this expression neglects the effect of large shear deformation on the properties of the elastomeric "column". One way to account for these reduced section properties is to use an effective column as shown in Figure 2a. This approximate method simply scales the critical load given by Equation 2, by the ratio of the areas of the effective and actual "columns". The result, for rectangular bearings, is then as follows:

$$Pc' = Pc\left(1 - \frac{\Delta}{B}\right) \tag{3}$$

where: Pc' = modified buckling load
Pc = classical buckling load given by Equation (2)
Δ = shear displacement

This relationship is illustrated in Figure 2c.

Associated with the buckling phenomenon is the corresponding dependence of shear stiffness (Kr) on axial load (a sudden decrease in stiffness may be used to indicate the onset of buckling). This dependence has also been rigorously established (Reference 4) and approximate formulations have been developed which are slightly easier to use (Reference 2):

$$Kr' = Kr\left(1 - \left(\frac{P}{Pc'}\right)^2\right) \tag{4}$$

where: Kr' = modified shear stiffness

This relationship is illustrated in Figure 2d. It will be seen that when the axial load is small compared to the buckling load ($P < 0.3Pc'$), there is less than a 10% reduction in stiffness and in these cases this effect can be neglected. Since most elastomeric bearings have squat aspect ratios, their buckling loads are inherently high at small shear displacements. But, at higher displacements and for bearings with more slender geometries, this reduction in stiffness will be important.

The procedures noted above have been used to estimate the system factor of safety for a number of isolated buildings to date. The advantage gained, for the effort expended, is particularly significant for buildings supported on a large number of isolators such as typically found in historically significant buildings.

CASE STUDY

The first building in the United States to be retrofitted using isolation was the City and County Building in Salt Lake City, Utah. The retrofit was completed in 1988 and since then at least 4 other existing buildings have been (or are being) retrofitted in this way (in the US).

These four buildings are summarized in Table 1 and two are further discussed in subsequent sections of this paper. It is noted that future applications include the City

Halls for both San Francisco and Los Angeles. It is also noted that the 80-year old Parliament House building for the New Zealand Government was recently retrofitted using elastomeric isolators.

Table 1. Retrofitted historical buildings using seismic isolation

Building	Type of Construction	Year Constructed	Year Retrofitted	Isolation System	Additional Strengthening Required?
City and County Building Salt Lake, Utah	unreinforced brick and sandstone	1894	1986/7	lead-rubber bearings	minor
Mackay School of Mines, Reno, Nevada	unreinforced brick, wood floors and roof trusses	1908	1990	high damping rubber bearings and sliders	minor
US Court of Appeals, San Francisco, California	non-ductile steel frame and unreinforced masonry cladding	1905	1993/4	friction-pendulum bearings	yes
City Hall Oakland, California	non-ductile steel frame and unreinforced masonry cladding	1914	1993/4	lead-rubber bearings	yes

City and County Building, Salt Lake, Utah

The City and County Building in Salt Lake City, Utah was completed in 1894. It is located in a moderate seismic zone and has been damaged in past earthquakes. During a complete rehabilitation of the building in 1987, seismic isolation was used to improve its performance in future earthquakes. This description of the building and the isolation system is by Elsesser, Walters and Allen (Reference 8).

The Salt Lake City and County building is a monumental, highly ornamented unreinforced brick and sandstone structure measuring 130 x 270 feet in plan, with five main floors and a 12-story clock tower (Figure 3). The plan is approximately doubly symmetrical (Figure 4).

The seismic vulnerability of the structure, due to its lack of reinforcement, is aggravated by the closeness of the site to the nearby active Wasatch Fault Zone. The building has a record of damage from various earthquakes, the largest occurring in 1934 with a Richter magnitude of about 6.2. Seismic damage to the building includes cracks in the bearing walls and losses of sculptures, roof stones and mechanical equipment form the clock tower.

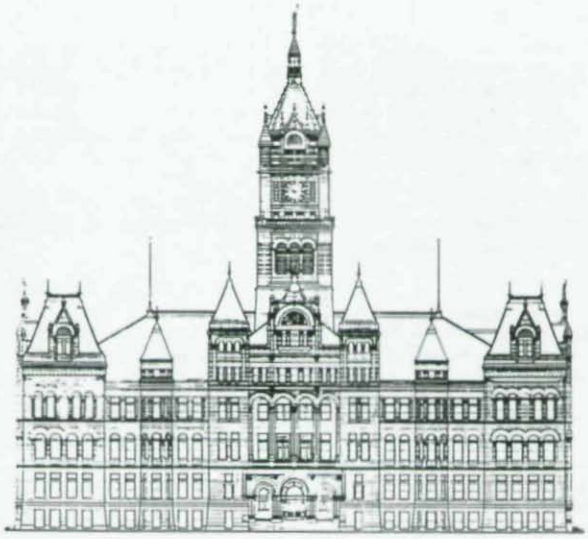

Figure 3 Elevation of City and County Building, Salt Lake City (from Reference 8)

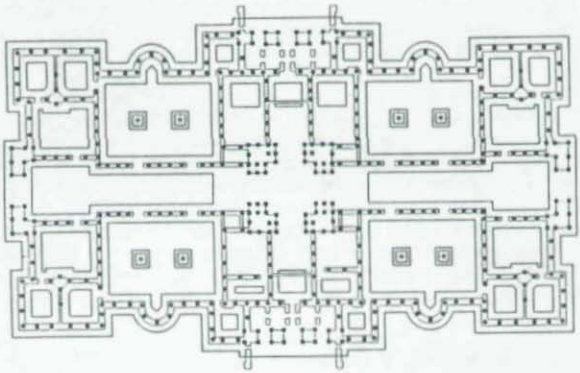

Figure 4 Basement plan showing isolator locations, City and County Building, Salt Lake City (from Reference 8)

The structure is supported by bearing walls of unreinforced brick and sandstone masonry which rest on sandstone plinths and 8'-6" wide continuous concrete footings. The interior brick bearing walls have a maximum thickness of 24 inches at the base. The exterior walls, which have an exterior wythe of sandstone masonry, reach a base thickness of 36 inches. The multiple wythes of brick in each bearing wall are bonded together solely by the original sand-lime mortar, which is quite deteriorated in many locations.

The central unreinforced masonry tower, which is approximately 40 feet square in plan at its base, rests on four solid piers of sandstone masonry which are L-shaped in plan and have a maximum dimension of 13 feet.

The 1st and 4th floors are framed with timber joints and planks, with a wooden floor surface in some locations and a concrete topping in others. The 2nd and 3rd floors are framed with steel beams supporting shallow brick "jack arches", which are covered with stone ballast and a concrete topping. At all levels, horizontal anchorage between the walls and floors is minimal.

In late 1984, the architects, the Ehrenkrantz Group of San Francisco and Burtch W. Beall, Jr., FAIA, of Salt Lake City, considered three different rehabilitation schemes, one of which was base isolation. The other two concepts involved "conventional" reinforcement systems which required the addition of concrete shearwalls and the corresponding removal and replacement of costly architectural wall finishes, such as oak wainscotting and plaster. In addition, conventional methods would have required a substantial amount of reinforcement to tie the walls to the floors and to resist out-of-plane wall loading, all of which would also be disruptive to the finishes. In order to minimize the need for wall reinforcement and replacement of finishes, it was decided to concentrate on developing an economically competitive base isolation scheme. By isolating the structure, horizontal accelerations were reduced substantially, thus minimizing the need for wall strengthening and, thereby, removal and replacement of architectural finishes. Another benefit of base isolation was the reduction in out-of-plane anchorage forces and bending moments in the unreinforced masonry walls.

The installation sequence required that each masonry wall be gripped between a pair of reinforced concrete "side beams" which were then notched into each wall to allow direct bearing, and tied together through the wall by regularly spaced concrete cross beams and ducted prestressing rods. Once these beams were cast and clamped to the wall, portions of brick and plinth below the cross beams were then removed, creating a space in which the isolators and bearing plates were installed to bear on the existing concrete footings (see Figure 5). A similar scheme was developed for the central tower, whereby each of the four sandstone support piers was jacketed with a reinforced concrete collar which was then clamped to the pier leg in each direction by prestressing rods. Pieces of stone plinth below the pier were then removed in stages, starting at the corners, to create space for the new isolators.

In total, there are 447 isolation bearings in the building. Of these, 208 are lead-filled elastomeric bearings using standard natural rubber. They are 17 inches square by about 15 inches tall with a 2.8 inch diameter lead core. The remaining 239 isolators are standard elastomeric bearings of the same overall size but without a lead core.

Average displacements and base shears for two design earthquakes were calculated to be 4.1 inches and 0.085W for the 0.2g event and 10.3 inches and 0.19W for the 0.4g event. Tower base shears were 530 and 840 kips respectively. Since the base shear capacity of the existing masonry was 0.09W and 650 kips respectively, no masonry strengthening was specified. However some floor-to-wall ties were still required and strengthening of the clock tower, above the roof line of the main building, was also performed.

To reduce the effects of elastic axial shortening of the isolators, which was calculated to be about 0.1 inches, the isolators were pre-loaded by flat hydraulic jacks placed beneath the new bearing plates before shimming and grouting the plates. With the isolators installed, the remaining plinth stones were then removed to allow the isolators to translate freely in the event of an earthquake.

CONCLUSIONS

This short paper has briefly outlined some of the stability issues for elastomeric seismic isolators. It has also illustrated the application of these isolation systems to the retrofit of historical buildings by describing a recent case study. The particular advantage of this retrofit technique for this class of building, is the minimal disruption to the interior and exterior finishes and the protection of the architectural integrity of these structures. It is however noted that in each of the cases discussed above, additional strengthening was also required. This was necessary because the original buildings were designed before modern seismic codes were adopted and constructed of non-ductile materials with poor connection details. As a consequence their capacity for seismic load as so weak that isolation could not reduce the demands sufficiently, i.e., to below the existing strength. nevertheless the amount of additional strengthening is less than if isolation had not been used and in some cases it was relatively minor. Further, as contractors develop and refine construction techniques necessary to install isolation systems and strengthen existing buildings, the cost of doing so will decrease. The number of historical buildings that are retrofitted with seismic isolation can be expected to increase in the years ahead.

REFERENCES

1. deMontalk, Robert Wladislas; "Shock absorbing or minimizing means for buildings" *U.S. Patent* No. 1,847,820, 1932, (*New Zealand Patent* granted 1929).

2. Bechtold, Jacob, "Earthquake-proof building" *U.S. Patent* No. 845,046, 1907.

3. Kelly, J.M., "Seismic base isolation; review and bibliography", *Soil Dynamics and Earthquake Engineering*, Vol 5, 1986, pp. 202-216.

4. Buckle, I.G. and Mayes, R.L., "Seismic Isolation: History, Application and Performance - A World View", *Earthquake Spectra*, Vol. 6, No. 2, 1990, pp. 161-202.

5. Buckle, I.G. and Kelly, J.M., "Properties of slender elastomeric isolation bearings during shake table studies of a large scale model bridge deck," *Proc. Second World Congress on Joints and Bearings*, San Antonio, 1986, also in *Special Publication on Joint Sealing and Bearing Systems for Concrete Structures*, American Concrete Institute, SP-94, Detroit, 1986, pp. 247-269.

6. Haringx, J.A., "On highly compressible helical springs and rubber rods and their application for vibration-free mountings, II," *Philips Research Report*, Vol. 4, No. 49, 1949.

7. Gent, A.N., "Elastic stability of rubber compression springs," *J1. Mechanical Engineering Science*, Vol. 6, No. 4, 1964, pp. 318-326.

8. Elsesser, E., Walters, M., and Allen E., "Base isolation of the existing City and County Building in Salt Lake City", *Proc. ASCE Structures Congress*, New Orleans, 1986.

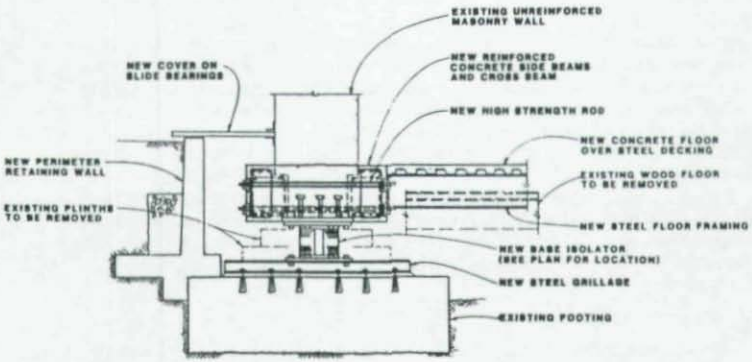

Figure 5 Typical elastomeric isolator installation details City and County Building, Salt Lake City (from Reference 8)

SEISMIC DAMAGE POTENTIAL AND UPGRADING OF STEEL STRUCTURES

Subhash C. Goel
Professor of Civil Engineering
The University of Michigan
Ann Arbor, MI 48109-2125

INTRODUCTION

Unlike lateral forces due to wind, design earthquake forces are somewhat fictitious. Due to resons of economy, code specified lateral seismic design forces are generally a fraction (in the order 1/10) of lateral inertia forces that would be induced in a structure if it were to remain elastic during a design level major earthquake. Therefore, in the event of a design level earthquake, code designed structures are expected to undergo large reversed cyclic deformations beyond the elastic limits, causing severe cyclic yielding and buckling at local and member levels as well as in connection regions. The codes do recognize this fact and make attempt to ensure satisfactory behavior through provisions requiring compactness and lateral bracing. This is particularly true for structures which are designed and detailed for ductility in which case premium is given by specifying smaller design forces. Nonetheless, design calculations proceed in the same manner as for wind forces, namely, checking strength and deflections at specified gravity and lateral force combinations. U.S. design practice does not require explicit checks to show that the structure does possess desired behavior beyond the elastic limits. In fact, design of seismic resistant structures with no ductility is permitted by increasing the specified design forces.

The above mentioned design philosophy has served the profession generally well in the past. That is, no catastrophic failures or collapses of steel structures were observed in major earthquakes with the exception of the collapse of Pino Suarez buildings during the 1985 Mexico City earthquake. However, the Northridge earthquake of January 1994 and the most recent devastating earthquake in Kobe, Japan, in January 1995, showed that severe ground shaking can cause very widespread and severe damage to steel structures. Although no steel structure was reported to have suffered complete collapse during the Northridge earthquake, the Kobe earthquake caused collapse of many steel structures. While it is somewhat comforting that total and catastrophic collapse of steel structures and resulting loss of life have not been too common in the past, recent experiences suggest the need for evaluating the damage potential of existing structures in future major earthquakes, and possible strengthening or upgrading for improved performance and safety. It could be hardly debated that upgrading a structure before it is actually damaged by a major earthquake will generally be much less expensive than waiting for the event and repairing the damage after it has occurred.

Briefly discussed in this paper are some potential problems that may exist in two of the most common types of steel framing systems, i.e., the concentrically braced frames and the moment frames. Many of those problems have been observed in damage caused by past earthquakes, including the Northridge and the Kobe events. Based on available knowledge and past research some possible techniques for upgrading are discussed.

Also included are some thoughts for needed research, and future design practice for new structures.

CONCENTRIC BRACED FRAMES (CBF)

Concentric braced frames (CBF) are among the most efficient structural systems in steel for resisting lateral forces due to wind or earthquakes because they provide complete truss action. However, this framing system has not been considered to be very ductile in past design practice and by codes. The non-ductile behavior of these structures mainly results from early (premature) cracking and fracture of bracing members or connections during large cyclic deformations in the post-buckling range. Instead of requiring the bracing members and their connections to withstand cyclic post-buckling deformations without early premature failures (i.e., for adequate ductility), codes have generally specified increased lateral design forces instead. Numerous studies by the author over the past fifteen years have shown that this design philosophy results in rather poor performance of CBF under severe ground motions [1, 2]. Bracing member and connection failures have been observed in many past earthquakes. However, the two most recent earthquakes - the Northridge and Kobe events - have reconfirmed many findings by the author in a rather graphic manner.

During a severe earthquake, bracing members in a CBF experience large deformations in cyclic tension and post-buckling range which cause reversed cyclic rotations to occur at plastic hinges which form in the member at the ends and mid-length. The braces in a typical CBF should be expected to occur at story drifts of about 0.3 percent to 0.5 percent, which can easily be caused by a moderate intensity ground motion. In a severe major earthquake, however, the braces could undergo post-buckling axial deformations of 10 to 20 times their tension yield deformation. In order to survive such large cyclic deformations without premature failure, bracing members and their connections need to be detailed for adequate ductility.

In September 1993, just prior to the Northridge earthquake of January 1994, the International Conference of Building Officials (ICBO) had accepted a comprehensive code change proposal by the author which introduced provisions for design of CBF based on incorporating ductile behavior for the first time in the 1994 edition of the Uniform Building Code. This class of CBF is referred to as Special Concentric Braced Frames (SCBF) in the UBC [3]. Because there exists a large inventory of "non-ductile" CBF designed by past code provisions, the Northridge and Kobe experience suggests the need for evaluating their potential for damage and possible upgrading for improved performance in future events. Some of the more important aspects are briefly discussed as follows:

Local Buckling of Bracing Members

In the post-buckling range of a bracing member, local buckling of compression elements limits the moment capacity and consequently the compression load capacity of the member. More importantly, however, the extent and severity of local buckling has a major influence on the fracture life (ductility) because of high concentration of reversed cyclic strains at those locations. Therefore, in order to prevent early fracture of bracing

members the limiting width-thickness ratios (compactness) should be smaller than those used in current and past practice. This is reasonable because seismic design relies on the ability of structural members to withstand large reversed cyclic inelastic deformations. Since, the codes have allowed non-compact sections for bracing members, they are prone to very early fractures, thereby, placing heavy flexural demands on columns which are typically not designed to meet those demands.

Hollow rectangular tubular sections are very popular for bracing members. However, they are also very vulnerable to fractures in just a few cycles at modest deformation levels. Studies have shown that filling the tubes with plain concrete can be very effective in mitigating the effects of local buckling in bracing members. Goel and Lee [4] showed that concrete infill can reduce the effective width-thickness ratio of rectangular tubular bracing members by as much as 50%, thereby, increasing the fracture life (ductility) by upto 300%. This is a promising technique for use in upgrading work. However, the related effects, such as increased compression strength, need to be considered in regard to their influence on affected beams and columns.

Stitch Spacing in Built-up Bracing Members

Once again, stitch spacing and strength of bracing members with built-up sections in existing CBF have been determined without considering post-buckling behavior. Such members have been shown to fracture very early due to individual bending of the member components between points of stitches. Stitch spacing and strength need to be such as to ensure integral bending of individual components during cyclic post-buckling deformations. This greatly enhances their fracture life. Doubling the number of stitches in most existing members should result in great improvement.

End Connections of Bracing Members

Single gusset plates are very commonly used for bracing members because of simplicity of connections. Buckling in those members usually occurs out-of-plane, inducing out-of-plane bending in the gusset plate, which has not been considered in past design practice. It is important to allow the gusset plates to develop restraint-free plastic rotations imposed by member rotations. Absence of this freedom results in premature early fractures in gusset plates. It would be extremely difficult to create such freedom in existing connections. One possible remedy is to add cross gusset plates or to create some other means that would prevent flexure of the gusset plates completely, thereby, forcing the end plastic rotations to occur in the member. While this method has beneficial effect on the energy dissipation capacity, the consequent increase in member compression strength needs to be considered for the affected connections and other structural members. More research is needed to develop other corrective details.

Failure of end connections is quite often caused by combined action of axial force and end moments under cyclic post-buckling deformations. This is more critical for in-plane buckling members and bolted connections. Strain concentration and loss of strength due to bolt holes need to be checked more carefully.

Strength and Stability of Beams with Chevron Bracing

Chevron bracing is a very popular pattern used in CBF. Elastic analysis and design methods used in existing practice do not point to the need for checking strength of the related beams for unbalanced force that is induced due to tension in one brace and smaller compression force in the other after buckling. Kim and Goel [6] showed that lack of adequate strength and lateral support of these beams can lead to serious problems during a major earthquake.

MOMENT FRAMES

Unexpected widespread connection failures in welded moment frames during the January 1993 Northridge earthquake have caused much professional and public concern. The January 1994 Kobe earthquake in Japan also caused major widespread damage to a variety of steel structures including connection failures in welded moment frames. Due to the severity of the problem, a comprehensive program of study has been initiated by SAC Joint Venture (a joint partnership of Structural Engineers Association of California, Applied Technology Council, and California Universities for Research in Earthquake Engineering) with major funding from FEMA (Federal Emergency Management Agency). The study program addresses immediate and long-term needs related to solving the observed problems in welded steel moment frames for repair and retrofit of existing frames, as well as improving the overall performance of steel moment frames for future earthquakes. Presented in the following are a couple of ideas by the author which may be applied to upgrading the performance of the existing damaged or undamaged but considered vulnerable steel moment frames:

Addition of Ductile Concentric Bracing

Past studies [2] have shown that addition of ductile concentric braces to non-moment resisting frames can develop excellent strength, ductility and hysteretic behavior, and overall performance in the event of a severe ground motion. This is because of dual line of resistance between the braces and all columns, including those outside the braced bays. It has been found that after buckling and yielding of braces, columns develop considerable shears (upto 25 - 40 percent of total story shears) through flexure even with no moment connection between the beams and columns. It is assumed, however, that columns are continuous over the floor beams, which is common in construction of steel frames. This suggests that adding ductile concentric braces to damaged moment frames in some bays can be an attractive and economical solution in many cases provided other considerations such as foundations, function, and architecture do not preclude their use. In this scheme it is implied that fractured girder flange connections could be left unrepaired, but adequate shear capacity of the web connections must be ensured and any loss of column strength due to cracking is restored. Encasement of columns with Reinforced Concrete can also be considered as an alternate means of strengthening them, where needed and feasible to do so. This scheme has the added advantage that repair of the upgraded structure after a future major earthquake will be much more economical as buckled or yielded braces are much easier and less expensive to replace than detecting and repairing damaged moment connections. In fact, minor buckling or yielding of braces can even be ignored and left unrepaired.

Cutting Rectangular Opening in Girder Webs

This concept is a spin-off of recent development of Special Truss Moment Frames (STMF) with open Vierendeel ductile segment near the middle of the floor truss girders [6]. These frames behave in a truly strong-column ductile girder fashion with "yield mechanism" forming under factored combined loads or design level ground motions through plastic hinges in the chords of the open segments only with no inelastic or ductility demand elsewhere, Figure 1. Such a condition can be created in existing "deficient" or even Ordinary (non-ductile) Moment Resisting Frames (OMRF) by cutting an open panel in the web of the floor girders of W sections. A schematic of this concept is shown in Figure 2. This concept also allows possibility of adding supplemental damping devices in the open panels, if needed for further enhancement of structural performance.

IMPLICATIONS FOR FUTURE DESIGN PRACTICE

Unprecedented widespread damage to steel structures caused by the Northridge and Kobe earthquakes has also raised questions regarding future design practice. As demonstrated by these two earthquakes and also indicated in some seismic risk analysis studies, future major earthquakes are expected to cause heavy economic losses. Therefore, in future seismic design practice increased emphasis is likely to be placed on limiting structural damage (thus, economic loss), in addition to life safety and preventing structural collapse during severe earthquakes. Existing design practice requires strength and deflection checks under applicable design load combinations. The author believes that a third step which ensures formation of pre-selected controlled "yield mechanism" during extreme load conditions, such as during a severe design level earthquake, should be included in future design practice. This would require application of elements of plastic design concepts and selection of desired "yield mechanism" to confine yielding and damage to known and limited structural elements which could be easily repaired or replaced after the extreme event.

SUMMARY AND CONCLUSION

Widespread damage to steel structures caused by the recent Northridge and Kobe earthquakes have reinforced the need for evaluating the damage potential of existing structures in future major earthquakes, and possible strengthening or upgrading for improved performance and safety during future similar events. Some potential problems that may exist in two of the most common types of framing systems, i.e., the concentrically braced frames and the moment frames, are briefly discussed. Some promising techniques for upgrading work are presented which are based on available knowledge and past research. Also included are some thoughts for needed research in this area, and future design practice for new structures. The author believes that future design practice should ensure formation of pre-selected, controlled "yield mechanisms" at extreme load condition representative of a severe design level earthquake, in order to achieve improved performance and repairability.

REFERENCES

1. Goel, S.C. (1992). "Cyclic post-buckling behavior of steel bracing members." Stability and Ductility of Steel Structures under Cyclic Loading, CRC Press, 75-84.

2. Goel, S.C. (1992). "Earthquake resistant design of ductile braced steel structures." Stability and Ductility of Steel Structures under Cyclic Loading, CRC Press, 297-308.

3. Uniform Building Code. (1994). International Conference of Building Officials, Whitier, Calif.

4. Goel, S.C., and Lee, S.S. (1992). "A fracture criterion for concrete-filled tubular bracing members under cyclic loading." Proceedings, ASCE Structures Congress, San Antonio, Texas, 922-925.

5. Kim, H.I., and Goel, S.C. (1992). "Seismic evaluation and upgrading of braced frame structures for potential local failures." Research Report No. UMCE 92-24, Dept. of Civil & Environmental Engrg., Univ. of Michigan, Ann Arbor, Mich..

6. Basha, H. and Goel, S.C. (1994). "Seismic resistant truss moment frames with ductile Vierendeel segment." Research Report No. UMCEE 94-29, Dept. of Civil & Environmental Engrg., Univ. of Michigan, Ann Arbor, Mich.

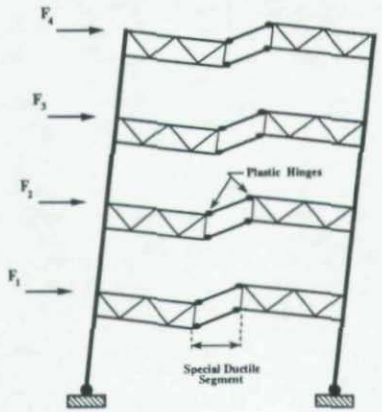

Figure 1. Yield Mechanism of STMF with Open Ductile Segment

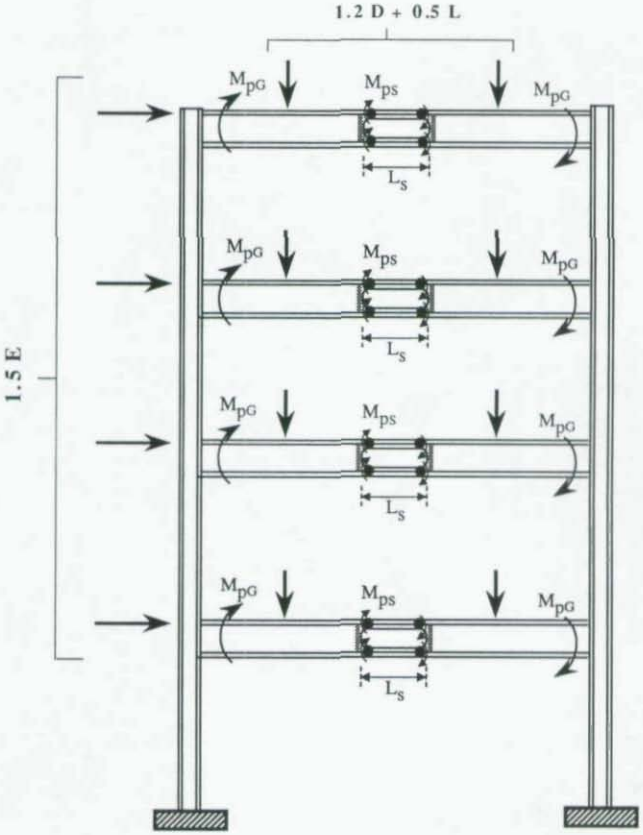

- YIELD MECHANISM @ (1.2D + 0.5L + 1.5E)
- $\xi M_{ps} \leq \left(\frac{L_s}{2L} \right) M_{pG}$

Figure 2. Moment Frame with Ductile Web Opening

TESTING OF STEEL MOMENT FRAMES JOINTS IN RESPONSE TO THE NORTHRIDGE EARTHQUAKE

Michael D. Engelhardt[1] and Thomas A. Sabol[2]

NORTHRIDGE STEEL CONNECTION DAMAGE

The January 17, 1994 Northridge Earthquake caused significant damage at beam-column joints in steel moment resisting frames. This damage was associated primarily with the conventional welded flange-bolted web type moment connection detail widely used in past west coast practice. A variety of different types of fractures were observed at these connections. Fractures in the immediate vicinity of the beam flange groove welds were a common form of observed damage, with fractures near the interface of the beam flange groove weld and the column flange being particularly common. Fractures of the column within the joint region were also observed. These included the pull out of "divots" from the column flange at the groove weld, as well as fractures running across portions of the column flange and web. In some instances, fractures passed through the full depth of the column section. Fractures occurring at or initiating from the beam bottom flange groove weld appear to have occurred far more frequently than at the beam top flange. More detailed damage descriptions are available from other sources [3-5].

Causes of the observed damage have been the subject of considerable discussion [2-7]. It will likely be quite some time before all the contributing factors are clearly identified and understood. Some of the factors considered as possible contributors to the damage are as follows:

Welding Related Factors
- inadequate welding workmanship and inspection;
- lack of adherence to written welding procedure specifications;
- the notch effect created by left in place backup bars;
- detrimental effects of left in place weld tabs;
- use of weld metal with low notch toughness.

Design Related Factors
- overstress of the beam flange groove weld and surrounding base metal regions due to inadequate participation of the bolted web connection in transferring bending moment;
- uneven distribution of stress across the width of the beam flange groove weld;
- highly restrained areas within the joint developing biaxial and triaxial states of tension, thereby inhibiting ductile material response;
- increase in bottom flange stress and strain due to presence of composite floor slab.

Material Related Factors
- actual yield stress of A36 beams considerably in excess of 36 ksi;

[1]Assoc. Professor, Dept. of Civil Eng., Univ. of Texas at Austin

[2]President, Englekirk & Sabol Consulting Engineers, Inc., Los Angeles

- inadequate through-thickness strength or ductility of column flanges;
- inadequate notch toughness of column material;
- high values of yield to tensile strength ratios (F_y/F_u).

It is emphasized that the above list, which is not exhaustive, represents speculation. The role of these and other contributing factors has yet to be definitively demonstrated.

TEST PROGRAM

Within approximately three months following the Northridge Earthquake, a short term intensive testing program was initiated under the guidance of the AISC Task Committee on the Northridge Earthquake [2]. The purpose of this test program was to generate some immediate data on the effectiveness of various measures intended to improve connection performance under earthquake loading. This program was directed towards steel moment frames that were under design or construction at the time of the earthquake, and that were in need of immediate guidance on improved design and construction techniques for moment frame joints. Thus, the test program emphasized connection details for new construction, and was not intended to investigate repair procedures for damaged joints.

Tests were conducted on single cantilever type test specimens, as shown in Figure 1. Slowly applied cyclic loads were applied at the tip of the cantilever. Beam tip displacement was increased until connection failure occurred, or until the limits of the testing apparatus were reached. Test specimen performance was judged primarily based on the level of inelastic deformation achieved in the beam prior to connection failure. All test specimens were constructed of W36x150 beams of A36 steel, and either W14x455 or W14x426 columns of A572 Gr. 50 steel.

A number of different connection details were investigated in the test program. The connections incorporated what were intended to be improvements both in welding and in connection design. For each connection, two replicates were constructed by two different structural steel fabricators in order to gain some confidence in the repeatability of results. A total of sixteen specimens were tested. Highlights for several of these tests are discussed below.

The first connection detail investigated was the conventional welded flange - bolted web detail, designed in accordance with the seismic detailing provisions of the 1991 Uniform Building Code. The detail for this specimen, designated as Specimen 1, is shown in Figure 2. Although the conventional connection detail was used, several improvements were incorporated in the welding, including removal of backup bars and weld tabs, combined with close attention to welding workmanship. Welding was accomplished by the self shielded flux cored arc welding (FCAW) process, as it was for all specimens in this test program. The electrode used for the beam flange groove welds for Specimen 1 was classified as E70T-4, typical of past field welding practice for this connection. This electrode is characterized by very high deposition rates, but can result in weld metal with rather low toughness and ductility.

Both replicates of Specimen 1 showed poor performance, developing only very limited ductility in the beam prior to connection failure. The load-deflection response at the tip of the beam

for one of the two replicates of this detail (designated as Specimen 1A) is shown in Figure 3. Failure of both replicates occurred by sudden fracture at the beam flange groove welds, with the fractures occurring near the weld column interface. No welding workmanship defects were visible on the fracture surfaces. The unsatisfactory performance of these specimens suggests that improving welding workmanship, by itself, may not assure satisfactory connection performance. It may be conjectured that better performance could have been achieved if a different welding electrode or different welding process had been chosen. Unfortunately, there was no opportunity to investigate this hypothesis as part of this test program. The effects of varying weld metal properties, and most notably weld metal toughness, is being investigated in a new test program currently underway by the authors.

The second connection detail investigated in this test program was an all-welded connection. It was similar to the first detail, except that the beam web, rather than being bolted, was welded directly to the column flange. Past test programs have typically shown better performance from all-welded connections, as compared to welded flange-bolted web details. This better performance has been attributed to the improved ability of the welded web connection to transfer bending moment at the connection, thereby reducing stress on the beam flange welds. Unfortunately, both replicates of this connection detail showed poor performance, with fractures occurring at the beam flange groove welds early in the inelastic loading history for the specimens.

The majority of the remaining connection details tested in this program were classified as reinforced connections. The beam flanges were reinforced with cover plates or with vertical "ribs". An example of a connection reinforced with cover plates, designated as Specimen 8, is shown in Figure 4. The intent of these connections is to significantly reduce the stress on the beam flange groove welds and surrounding base metal regions, and to move the location of the beam plastic hinge away from the face of the column. The design goal adopted for the reinforced connection was that the region of the connection at the face of the column should remain essentially elastic under the maximum bending moments and shear forces developed by the fully yielded and strain hardened beams. For the various reinforcement configurations tested, the section modulus of the reinforced cross-section was on the order of 1.6 to 2.0 times the section modulus of the unreinforced beam cross-section. In addition to reinforcing the flanges, different FCAW electrodes were used for some of these specimens, and continuity plates were added for some of the specimens.

Eight of the ten reinforced connections showed excellent performance, developing very large inelastic deformations in the beam without connection failure. The beam tip load versus deflection response for a successful cover plated connection (Specimen 8A) is shown in Figure 5. These connections performed as intended. The beam plastic hinge formed at the end of the reinforcement, away from the face of the column, while the region of the connection near the face of the column remained essentially elastic. The connections were capable of developing the full flexural strength and ductility of the beams.

Two of the connections reinforced with cover plates showed poor performance, experiencing brittle failures at low levels of beam ductility. One cover plated specimen failed by a sudden fracture at the top flange/cover plate weld to the column. This fracture occurred near the weld-column interface, and showed no visible workmanship defects. Inspection data for this specimen suggested that some of the welding parameters (voltage, electrical stickout, etc.) were likely beyond the range specified in the Welding Procedure Specification. Studies of this failure suggest that the improper choice of welding parameters lead to weld metal with unusually low toughness. The replicate of this specimen, with the same connection design and welding electrode, but for which the Welding

Procedure Specification was followed, showed excellent performance. *The Structural Welding Code - Steel*, AWS D1.1-94 [1] requires that welding be executed in accordance with a written and approved Welding Procedure Specification. These test results emphasize the importance of this requirement. They also suggest a relationship between weld metal toughness and overall connection performance.

A second cover plated specimen failed by a sudden fracture within the column flange material at the beam's bottom flange connection, pulling out a portion of the column flange material. The fracture surface suggested a possible problem with through-thickness properties of the column flange. This test specimen indicated that even with a reinforced connection and careful welding practices, material properties may represent a "weak link" for this type of connection.

CONCLUSIONS

The results of these tests suggest that a large improvement in cyclic loading performance is possible at steel moment frame joints by the use of a reinforced connection combined with careful attention to welding. Following this approach, while perhaps not guaranteeing success 100 percent of the time, is expected to provide a much higher level of performance and structural safety, as compared to pre-Northridge practices. It is also clear from these tests that a large number of welding, design, and materials related factors significantly affect connection performance. A long term research effort will be needed to fully resolve all the issues raised by the Northridge Earthquake.

More complete details of this test program are documented in Reference 2, combined with interim design and welding recommendations. Additional information related to steel moment connection performance in the Northridge Earthquake can be found in References 2 to 8.

ACKNOWLEDGEMENTS

The following provided financial support or donations of materials or services: AISC Inc., J. Paul Getty Trust, National Science Foundation (Grant BCS-9358186), PDM Strocal Inc., The Herrick Corp., Lincoln Electric Co., Twining Laboratories, British Steel, TradeArbed Steel, Nucor-Yamato Steel, Gayle Manufacturing Co., and P.V. Banavalker. Members of the AISC Advisory Group on SMRF Research as well as numerous others provided valuable advice. The authors wish to especially thank the late Geerhard Haaijer of AISC Inc. for providing leadership and guidance for this test program.

REFERENCES

1. *Structural Welding Code - Steel*, American Welding Society, Miami, Fla., 1994.
2. *Northridge Steel Update I*, American Institute of Steel Construction, Inc., October 1994.
3. *Proceedings of the AISC Special Task Committee on the Northridge Earthquake Meeting, March 14-15, 1994*, American Institute of Steel Construction, Inc., March 1994.
4. Bertero, V.V., Anderson, J.C., Krawinkler, H., "Performance of Steel Building Structures During the Northridge Earthquake," *Report No. UCB/EERC-94/09*, Earthquake Engineering Research Center, University of California at Berkeley, August 1994.

5. *Proceedings, Invitational Workshop on Steel Seismic Issues, September 8-9, 1994*, Report No. SAC 94-01. Published by the SAC Joint Venture, 555 University Avenue, Suite 126, Sacramento, California 95825 (ph. 916-427-3647).
6. *Steel Moment Frame Connection - Advisory No. 1,* published by the SAC Joint Venture, September 26, 1994.
7. *Steel Moment Frame Connection - Advisory No. 2,* published by the SAC Joint Venture, October 19, 1994.
8. *Steel Moment Frame Connection - Advisory No. 3,* published by the SAC Joint Venture, February 1, 1995.

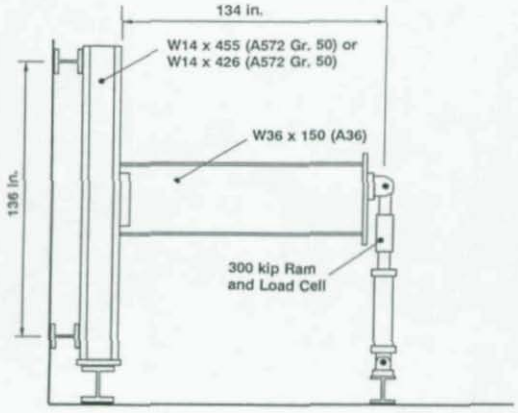

FIG. 1 - TEST SETUP

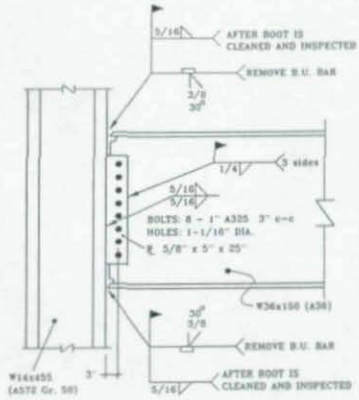

FIG. 2 - SPECIMEN 1 CONNECTION DETAIL

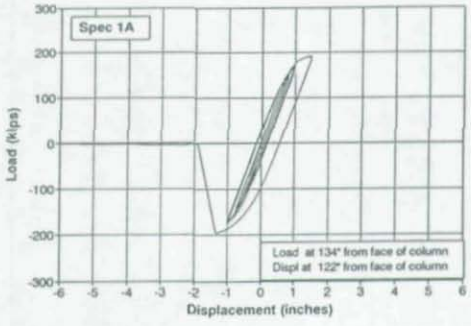

FIG. 3 - LOAD-DEFLECTION RESPONSE FOR SPECIMEN 1A

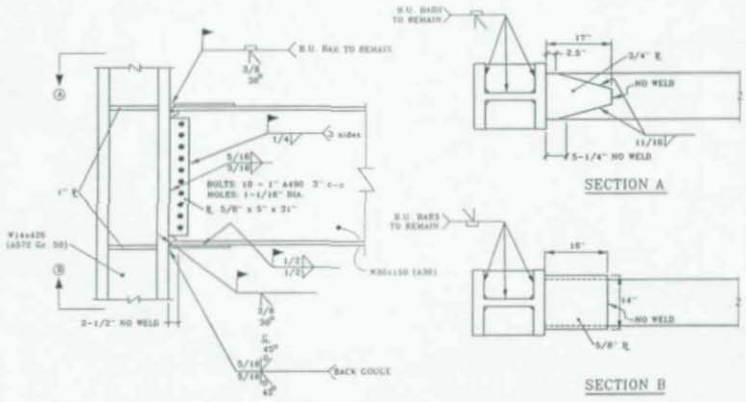

FIG. 4 - SPECIMEN 8 CONNECTION DETAIL

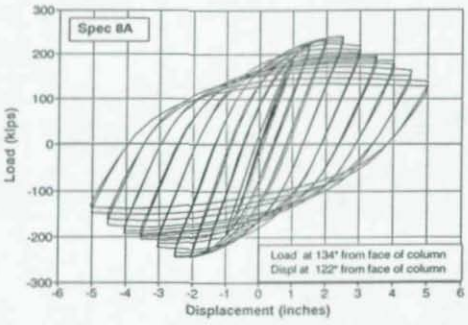

FIG. 5 - LOAD-DEFLECTION RESPONSE FOR SPECIMEN 8A

SESSION 4 - KEYNOTE PAPER

"RELIABILITY APPROACHES TO ANALYTICAL EVALUATION AND FIELD TESTING"

by
Fred Moses
Department of Civil and Environmental Engineering
University of Pittsburgh

ABSTRACT

In-service performance evaluation has received considerable attention in recent years for highway bridges, offshore platforms, dams and other structures. Engineering efforts include inspection, material analysis, nonlinear behavior prediction and field testing. For the design of new structures, reliability methods have been introduced and codified for routine member checking. Applications of structural reliability to the evaluation of existing structures is less advanced due to the varied nature of evaluation requirements. Some recent studies and applications of reliability have occurred for offshore platforms and especially for highway structures. This includes rating assessment of bridges by both analytical methods and use of field testing. This paper emphasizes the use of reliability in developing assessment criteria. Examples in this paper are restricted to highway bridges.

INTRODUCTION

Structural engineers are increasingly faced with the task of evaluating the safety of existing structures. The focus of applications in this paper will be on highway bridges but the techniques illustrated are applicable to other structural systems such as offshore platforms, dams, pipeline networks, aircraft, etc.

The actions that may trigger an evaluation of an existing structure include the following:

a) *Structure deterioration and damage which may reduce* the resistance to design loads. Examples include material corrosion, fatigue cracking, foundation settlements, etc.
b) Increases in the specified structure design loads for that type of system. This may occur as in bridges with increases in more volume and higher legal truck loads or public demand for higher safety as in seismic resistance. Another example is improvements in analytical performance predictions which raise the design loads such as in offshore structures due to better models for wind, wave and current analysis.
c) Accidental events such as fire or collisions,
d) Legal requirements such as Federal regulations which mandate biannual bridge evaluations for highway structures. Such mandates often follow well-publicized failures in bridges, dams, seismic events or airline crashes. These periodic reassessments may affect the continued economic viability of these structures or in some instances lead to increased public investments to ameliorate the public's perceived view of the safety threat. [A properly organized reliability assessment basis would consider relative public

exposures on a more rational basis.]

Structure evaluations require sophisticated analysis and experimental validation to predict structure safety. This is because of greater uncertainties in predicting the structure strength due to in-situ material and structural properties, boundary conditions, member dimensions, connections and foundation condition for a structure that is in service for many years and has suffered damage, deterioration and environmental degradations.

At the same time, the structure evaluator has some advantages in assessment in comparison to new design application. The structure has undergone years of service which may establish a level of confidence in the material properties, construction tolerances and gravity load estimates and load distribution. Further, there an opportunity to make observations and in-situ measurements which would calibrate the analytical performance predictions. Also, the structure has a shorter remaining life than a new design which reduces the probability distribution of extreme events occurring. Finally, a field inspection is possible which could uncover member properties, as-built materials and dimensions, presence of distortions and damage, etc.

EVALUATION APPLICATIONS

The output of an evaluation for an existing structure takes several forms:

1) Allow a structure to be maintained in present operating mode.
2) Reduce operational level as when a bridge is load posted for less than legal loads or the water level in a reservoir is reduced to lower pressures on a dam.
3) Recommend rehabilitation to alleviate distress or to restore or increase structure capacity.
4) Recommend further inspection or structure monitoring and testing to validate performance predictions.
5) Estimate remaining service life and plan for replacement.
6) *Recommend immediate shut-down and reduce exposure to human life* and property.

This paper reviews assessment techniques that have been recently developed and in most cases implemented in evaluation for existing highway structures. The underlying basis for the recommended methods are structure reliability procedures. The actual implementation may be transparent to the reliability analysis in the same way as done in recent LRFD design codes. Examples include:

A) AASHTO Guide Specification for the Strength Evaluation of Existing Steel and Concrete Bridges[1]
B) AASHTO Guide Specification for Safe Life Assessment of Steel Bridges[2]
C)NCHRP Manual for Bridge Rating through Load Testing[3]

The main theme in this paper is the use of reliability criteria as a unifying basis for decisions regarding performance evaluation, rehabilitation needs and operational decisions as well as the provisions for additional evaluation information.

RELIABILITY ANALYSIS

This section briefly reviews reliability methods which have been widely adopted in structural engineering for various specification developments as well as specific project decision tools. Typically, we define random variables, X, which affect load or capacity such as gravity loads, external environmental loads, load analysis uncertainty, geometrical properties, material strengths, etc. Each of the variables is described by a distribution function often with two parameters such as the mean and coefficient of variation(COV). Typically, a failure function, g, is defined such that $g > 0$ means safe and $g < 0$ means failure occurs, where g is a function of the realization of the random variables, X. In most reliability applications, the failure function g is taken on a component basis, for example, a beam-column, connection or pile. In more recent applications the failure modelling is on a total system performance basis[4]. The risk is defined as the probability that g is less than zero. In developing specifications, a measure of reliability is usually introduced known as the safety index, β. For example, in its most simple form the failure function can be written as the margin between the capacity or resistance, R, and the demand or loading, S. Thus:

$$g = R - S \qquad (1)$$

The safety index is expressed as the number of standard deviations that the mean of the function g falls from the failure limit. Thus, for this illustration:

$$\beta = \frac{\bar{R} - \hat{S}}{\sqrt{\sigma_R^2 + \sigma_S^2}} = \frac{\bar{g}}{\sigma_g} \qquad (2)$$

where σ is the standard deviation. If the random variables, R, and S, are normally distributed then β gives an exact expression of the risk when using normal probability tables. If R and S or the other random variables which may form part of the failure function g are not normal then the safety index expression may only be approximately mapped to an actuarial risk value. Recent reliability methods using more accurate advanced procedures or simulation have shown that β does give accurate risk representation and a good basis for risk-based decisions. Typically the β's are in the range of 2-4 which correspond to risks of 10^{-2} to 10^{-5}. With such safety index models, code specification committees throughout the world have introduced via code calibration, Load and Resistance Factor Design (LRFD) type component specifications of the form:

$$\phi R_n = \gamma_D D + \gamma_L L \qquad (3)$$

where ϕ is the resistance factor applied to the nominal resistance(R_n) and γ_D and γ_L are the respective load factors applied to the nominal dead and live loadings. Other load terms may also be added such as temperature, vehicle loads, wind, seismic,etc. The code calibration process used by AISC, AASHTO, API and other code groups selected the load and resistance factors to achieve uniform target reliabilities for components. These factors depend on the specified nominal values as well as their respective uncertainties.

This approach is emphasized herein since the uncertainties at the design stage for new structures may be different than in evaluation for reasons cited above.

ANALYTICAL EVALUATIONS

There are significant differences between the data base and target reliability levels in design and evaluation. For example, Figure 1 compares several distribution cases that may occur. Figure 1a shows the distributions in a design situation. The safety index depends on the high load events occurring combined with the low resistances. Typically, over time there will be changes in the base line distributions that were estimated at the design stage. For example, as illustrated in Figure 1b, the load distribution shifts to the higher values based on higher demands due to greater dead load as well as higher legal loads in bridges. Similarly, the resistance distribution shifts to the lower values. These shifts decrease the safety index over time.

Figure 1c illustrates the influence of a load test during which there is monitoring of response and a validation of the load prediction model. There is lower load effect uncertainty which increases β without change in the overall mean safety margin. Figure 1d illustrates the load and resistance distributions which may result from a proof-load test. The resistance distribution is truncated since there is a basis for knowing the lower level of strength based on the test. Similarly, if there is load response measurements as well is in-situ measurements of material properties and component dimensions, the load and resistance distributions may appear as in Figure 1e. The influence of damage, material deterioration, collision, fire, etc., raises uncertainties and reduces expected safety margins as illustrated in Figure 1f.

Thus, at the evaluation stage there may be different uncertainties and safety margins than existed at the design stage. There is opportunity to integrate (for example, in a Bayesian manner) some of the earlier performance history. Further, there is construction and inspection data which may change uncertainties that existed at the design stage. There is detailed inspection, in-situ material property and dimensional measurements as well as full scale field testing to reduce uncertainties and affect the safety index.

Economic influences also play a role when comparing design and evaluation. The costs of increasing the reliability at the design stage is relatively inexpensive for most structures. On the other hand, increasing the strength of existing structures, especially where damaged, may be very costly. These influences have been historically recognized in highway bridge assessments in which design is at the inventory level but assessment is at the much lower operating levels. For example, many agencies design steel bridges to only 55% of yield while assessing ratings during evaluation at 75% of yield. This considerable difference is to a large extent justified by the marginal costs but also based on other differences cited above.

In order to provide consistent ratings, an NCHRP study by the author and colleagues was undertaken which led to an LRFD-type

format for rating(evaluating) existing bridges[5]. The applications includes the rating factors which are the basis for decisions on load posting, allowable permit levels, rehabilitation needs and eventually bridge closure. The rating format used is the same as given in eq.3 except that the load and resistance factors are site specific based on the information available to the evaluator. Further, if a low rating produces undesirable consequences the evaluator is encouraged to expand the data which may lead to more acceptable ratings. Examples of these adjustments are as follows:

Dead load factor- The dead load factor in design is 1.3 in load factor design procedures. In evaluation, provided an in-situ investigation is made of the overlay thickness, the factor is 1.2. Nominal dead loads should be based on as-built information.

Live load factor- Of major concern is the live load factor to account for vehicle loadings on bridges. The statistics needed to predict maximum vehicle loading effects depends on truck weight distributions, truck volume, spacings between vehicles along with lane occupancy and uncertainties in structural models which predict member load effects from vehicle loadings. The AASHTO load factor design uses a load factor of 2.17. This value is shown in LRFD studies to attain target reliabilities of about 3.5. In the evaluation Guidelines[1], the live load factor depends on: a) truck volume- defined as under 1000 trucks per day and, b) over 1000 trucks per day, and truck weight composition, defined as a) significant control of overloads, and b) significant sources of overloads without effective enforcement. These respective categories provide four possible live load factor values between 1.3 and 1.8. These factors were obtained by simulation of different truck weight spectra and volumes and the prediction of maximum load magnitudes for a two year time interval corresponding to typical inspection/evaluation cycles. These same load simulation studies were used in the new AASHTO LRFD specifications. Unlike the design model which uses the same load factor for a major roadway with high volume as for a secondary roadway, the evaluation specification adjusts the live load factor based on traffic data readily available or obtainable (by say, weigh-in-motion studies) for the specific site being evaluated.

Impact factor- The code uses an impact factor which reaches a maximum value of 1.3. The evaluation Guideline uses a site specific dynamic impact allowance which depends on pavement roughness condition and may vary from 1.1 to 1.3. This approach allows the engineer to recommend resurfacing to reduce dynamic allowance which directly raises the rating.

Live load analysis- Typically, a designer may use alternative analysis procedures ranging from an approximate formula for lateral load distribution to a finite element analysis. The load factor would remain the same. In the Guide Specification for evaluation[1] there is a range of adjustments to the live load factor depending on the accuracy of analysis such as simple formula, finite element, or even field measurements. This approach reflects the respective uncertainties and was calibrated with safety index models.

Target reliability Index - For design, the target reliability for

components is taken to be 3.5. The reason is that the marginal cost to change design strength is relatively small. For example, the cost to increase bridge design loads by 50% would be only 3-5% in most steel or concrete spans. In evaluation, the cost associated with low ratings or with recommended strengthening procedures to restore capacity could be relatively large. In the Guide Specification, the target reliability for redundant designs(more than two load paths) is taken as 2.3, while for nonredundant cases, the target in evaluation is maintained at the design value of 3.5.

Resistance factors - Base case values for resistance factors are given for nondeteriorated redundant components, namely 0.95 for steel members, 0.95 for prestressed members and 0.90 for reinforced concrete. These were based on code calibration to the target reliability values cited. Nonredundant steel members have their resistance factor reduced to 0.80 to bring it in line with the higher target index cited.

Influence of Deterioration - Where the inspection indicates deterioration, the resistance or capacity reduction factor is reduced further. This reflects greater uncertainty in assessing in-situ strength and the greater likelihood there will be further deterioration prior to the next biannual inspection/evaluation cycle. For example, the Guide reduces ϕ by 0.1 for some deterioration and by 0.2 for significant deterioration. To assist the evaluator, this reduction is related to the conventional FHWA condition survey for the superstructure.

Influence of Maintenance - When maintenance is vigorous and likely to correct deficiencies, the resistance factor ϕ may be increased by 0.05.

Influence of Inspection- Where section losses have been carefully estimated for the member being evaluated, the resistance factor may be increased by 0.05. Similarly, where material yield stress is estimated by physical testing the mean test data should be reduced by only 10% instead of the using the smaller nominal yield level.

As shown, this assessment approach encourages the evaluating engineer to obtain more information such as overlay thickness, deck roughness condition, more rigorous analysis tools, site specific traffic data, improved inspection, better maintenance programs, etc. This information sensitive evaluation is tied together in selecting the appropriate load and resistance factors for a reliability rating of the specific structure.

REMAINING LIFE ASSESSMENT

Bridge fatigue and distress due to cracking are phenomena that began to appear some years ago. In particular, welded structures create stress concentrations which may be especially severe for certain types of details, materials and loading conditions. The writer and his colleagues have shown how uncertainties in loading, bridge behavior and material characteristics could create a model for estimating the reliability associated with remaining fatigue lives. This research, sponsored by NCHRP, has led to two AASHTO Guide Specifications including one concerned with the evaluation of

the safe remaining fatigue life of a structure[6].

This AASHTO Guide has been used extensively in the U.S. in conjunction with rating of capacity and decisions regarding strategies for repair, rehabilitation and replacement of steel bridge span structures. The Guide allows either computed stress ranges or measured stress ranges to be used. The latter are especially more accurate when there has been initiation of cracks adjacent to welded details. Often it is observed that substituting the measured stress spectra in the remaining life calculations leads to less severe decisions than using computed values.

Further, the AASHTO Guide allows the input of historical truck traffic information for the specific site being studied into the remaining life estimates. Different factors were also derived based on reliability analysis depending on the source of the data. The specification contains two levels of target reliability. A safety index of 2.0 is used for spans which are redundant, while a higher index of 3.0 was specified for nonredundant structures. These differences are consistent with current design rules which warrant higher reliabilities for nonredundant elements due to possible member failure consequences.

As part of the overall evaluation it is recommended that existing bridges which do not satisfy the target safety criteria should be subjected to more detailed and frequent inspections at locations indicated by the analysis. An alternative control on safety is to modify the details as recommended by Dr. Fisher and others or else to limit the weights of trucks that may use the span.

STRUCTURAL TESTING

Field testing has been increasingly used for verification of bridge capacity for rating. The results of bridge load tests generally show that structures have greater load-carrying capacity than predicted by calculations. Aside from the conservative approach used in design, the actual response of the structure under live loads may be different due to distribution of loads, the interaction of structural (and to a lesser degree, non-structural) components, and the impact of deterioration and repairs.

Numerous organizations including the Ministry of Ontario, FHWA, and DOTs in Florida, Maryland, Alabama, Pennsylvania, Ohio and elsewhere have utilized bridge testing to avoid costly posting or replacement of older structures. Different types of bridge tests have included a)Proof-loading to verify strength capacity, b)testing of structure response under prescribed loads to calibrate and assess behavior predictions and, c) Strain measurements under traffic to predict fatigue life performance.

The potential reduction in the number of structurally deficient bridges through the use of load testing was recognized with the NCHRP Project "Nondestructive Load Testing for Bridge Evaluation and Rating"[3,7]. The research carried out by this writer and colleagues from industry developed a NCHRP "Manual for Bridge Rating Through Load Testing". This manual identifies two types of generic tests including diagnostic and proof-loading. The

diagnostic tests verify bridge behavior models under live loading and are needed when there are uncertainties regarding member support conditions, influence of deterioration, damage and repairs, stiffness properties and participation of secondary members which make it difficult to develop a satisfactory analytical model. For example, steel trusses, concrete T-beams and multi-stringer steel girders. Tests can be use to determine the accurate distribution of loads and stresses within the structure. Such diagnostic tests reduce the analysis uncertainty and allow a more accurate rating. The Manual also discusses methods for applying loads and suitable equipment for making measurements[3].

In a diagnostic test, the load is placed at designated locations on the bridge and the effects of this load on individual bridge members are measured and results compared to effects computed based on structural analysis principles and practices. The basic formula for the theoretical rating of a bridge member, RF, as expressed in AASHTO manuals is as follows:

$$RF = \frac{C - A_1 D}{A_2 L_n (1 + I)} \qquad (4)$$

where C denotes capacity, based on as-built drawings supplemented by inspection and material tests. D is dead load effect supported by on-site estimates, L_n is nominal live load model and I is the dynamic allowance. A_1 and A_2 are factors on dead and live load which depend on level of rating (inventory or operating) and criteria (working stress, load factor or load and resistance factor). These factors are adjusted to reflect the results of the diagnostic testing.

The second area of testing is proof-loading. Proof-loads generally require higher magnitudes of test loads than needed for diagnostic testing and the physical capacity of the structure is verified by the highest load level reached. Proof-tests are needed when the elements of the structure are not known to the rater or when there are serious uncertainties about the material properties and other strength related variables of the structural system. Examples suitable for proof-loading include slab bridges with unknown reinforcement details, or other structures with "hidden" details making it difficult to model strength capacity. In such instances, load is applied in increments to the structure until a maximum static condition is reached.

Proof-testing is an alternative to analytically computing the load rating of a bridge. A proof test "proves" the ability of the bridge to carry its present full dead load plus some factored live load. The rated load should be magnified to provide a margin of safety in the event of an occasional overload during normal operation. The calibration of the proof-load live load factors was done with a reliability model. The uncertainties in dead load, analysis and capacity reflect a situation where the bridge safely carried the factored proof-loading.

The format in the Testing Manual begins with a live proof-load factor, X_p, which is needed to reach an operating rating level of

1.0. The recommended factor is 1.4 which provides the same safety index as the AASHTO Guide Specification[5], namely 2.5. The latter is based on a 1.3 factor on dead load and live load plus impact.

Several adjustments can be made in the proof-load factor X_p, to reflect specific influences that exist in the evaluation of the site. For example, the factor is increased by 15% in the case of a one lane bridge since loading statistics show greater magnitudes of overload in one lane than the corresponding probability of two lanes being simultaneously overloaded.

For spans with fracture critical details, the live load factor is increased by 10% to raise the target reliability and similarly for bridges with single load paths(nonredundant). The factor is increased by a further 10% if bridges are not inspected on two year cycles or are likely to be more poorly maintained. This margin is added to reflect possible further deterioration before the next cycle of inspection and evaluation. If the bridge can be rated by conventional analysis and the proof load validates the modelling then the proof factor can be reduced by 5%. Further, if there are visible signs of distress prior to reaching the target proof-load the test must be stopped. The rating calculation is based on the load reached which is further reduced by 12% to reflect the typical bias between mean material properties and nominal values.

Additional factors including site appropriate traffic intensity, bridge condition and deck roughness category may also be incorporated in the proof-load assessment based on methods discussed above for analytical evaluations.

PROOF-LOAD EXAMPLE - This test was performed to establish the rating capacity of a concrete slab bridge. There are numerous such bridges in the U.S. which cannot be analytically rated due to the absence of detailed reinforcing steel information, skewness, unknown contributions of parapet walls and concrete deterioration. For example, Ohio alone has 8000 such bridges in service.

The criteria cited above were utilized to establish the live load factor for proof-testing. The goal was an operating level rating, so the base case value of X_p of 1.4 was selected. Loads were placed in both lanes simultaneously; there are no fracture critical details, slab deterioration was present, and inspection and evaluation would be repeated within two years, and plans were unavailable. X_p was increased by 5%. The net adjustment is:

$$\text{Target proof-load factor, } X_p = 1.4 \times 1.05 = 1.47 \qquad (5)$$

The target load including the 1.3 dynamic allowance is:

$$\text{Test Load} = 1.47 \times \text{rating load} \times (1 + 0.30) \qquad (6)$$

The rating load is HS 20 , and the magnitude of the test load in each lane of traffic is 61.2 kips to represent the HS20 32kip tandem load. The maximum proof load attained was 63 kips with no apparent signs of distress. (Load is done in increments either by adding load to test vehicles or by staggering the locations of the groups of test vehicles in each lane).

Based on the test, the operating rating load(OPR) is:

$$OPR = \frac{1.0 \times 63/\ 1.47}{32(\ 1+\ 0.3)} = 1.03 \text{ or an HS21 or } 37.1 \text{ tons} \quad (7)$$

CONCLUSIONS

Developments in structural reliability and their acceptance as a basis for calibrating safety factors in design codes have opened up a new avenue for evaluating existing structures. Reliability methods have led to several Guide Specifications for rating existing bridges. A major advance is that the load and resistance factors are selected according to site information and the condition of the structure being evaluated. Site specific data can be used to adjust loadings, analysis models and capacity assessments. Uniform reliability targets can be attained in analytical evaluations. Further, methods of field testing have been introduced for the evaluation operations. Such tests can be routinely done, either for diagnostic validation of behavior calculations or to determine a lower bound to the true bridge capacity by proof-testing. These test methods have been instituted by several agencies on a routine basis and a Manual for conducting rating by testing is available. A major innovation is that such test procedures are also calibrated to safety index models so that the information gained from a test is efficiently used. The evaluator can clearly assess the benefits of reducing uncertainty in achieving higher ratings compared to situations without testing.

The major aim of this paper was to show the benefits in evaluation by the addition of site specific information that can be consistently incorporated in rating with reliability procedures. The actual implementation in practice makes the reliability analysis transparent to the user and operates in the same way as new LRFD-based specifications which accomplish the same purpose.

REFERENCES

1. AASHTO Guide Specification for Strength Evaluation of Existing Steel and Concrete Bridges,Washington, D.C., May 1989.
2. AASHTO Guide Specification for Safe Life Assessment of Steel Bridges, Dec., 1990, Washington, D.C.
3. "Manual for Bridge Rating Through Load Testing" Final Report, NCHRP 12-28(13A), Transportation Research Board, Washington, D.C.
4. Moses, F.,"New Directions and Research Needs in System Reliability Research," Journal of Structural Safely, No. 7 (1990).
5. Moses, F. and Verma, D.,"Load Capacity Evaluation of Existing Bridges,", NCHRP Report 301, Transportation Research Board, Washington, D.C. December, 1987.
6.Moses,F.,Schilling,C.and Raju,K.S.,"Fatigue Evaluation Procedures for Steel Bridges,", NCHRP Report 299, Transportation Research Board, Washington, D.C., November, 1987.
7.Moses,F.,Minervino,C.M.,Dauenheimer,E.,and Lichtenstein,A.G., "Presentation of a Manual For Evaluation of Bridges by Field Testing",Proceedings 10th International Bridge Conference, Pittsburgh, Pa.,June 1993.

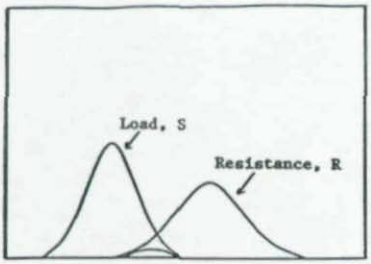

Figure 1a) Conventional Reliability Model ~ Design Case

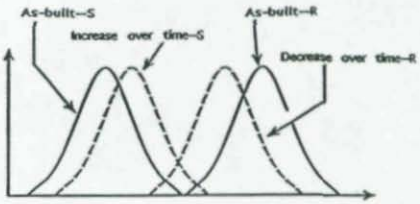

Figure 1b) Illustration of decrease in reliability over time

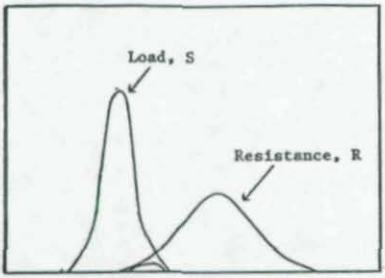

Figure 1c) Reliability model after a load test which validates analysis model and reduces uncertainty of load effects.

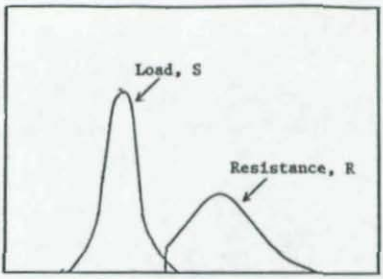

Figure 1d) Reliability model after a Proof-Load Test which reduces load effect uncertainty and truncates resistance distribution

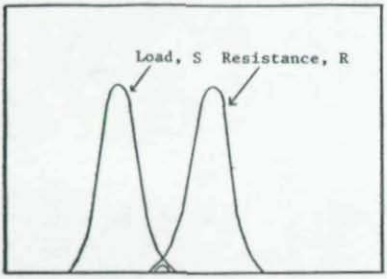

Figure 1e) Reliablity model after considerable site data is obtained which reduces both load and resistance uncertainty

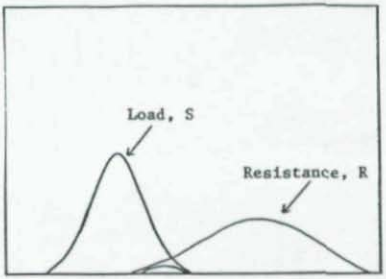

Figure 1f) Reliability model after bridge damage and deterioration with no further information. Increased uncertainty reduces safety index

DETERMINATION OF LATERAL STIFFNESS AND AXIAL LOAD IN RAILS FROM LOW-FREQUENCY FLEXURAL VIBRATIONS

Jean-Guy L. Béliveau , University of Vermont
Thomas Boggs and Thomas M. Murray, Virginia Polytechnic Institute & State University, Blacksburg, Virginia

Presented at the Structural Stability Research Council 1995 Theme Conference
Stability Problems Related to Aging, Damaged and Deteriorated Structures
Kansas City, Misouri, 28-29 March 1995

ABSTRACT

Railroads are an important part of the nation's infrastructure. Thermally-induced lateral track buckling of rails remains one of the most enigmatic problems in the railroad industry. This is particularly relevant for continuously-welded rail which is now used for all new rails all over the world. Currently, there is no convenient method to determine the in situ axial load in the rail nor its lateral stiffness which prevents the instability. An effective method is needed to determine the in situ characteristics and status of the track, such that unnecessary slowdowns can be avoided or so that preventative measures can be undertaken when necessary.

This paper considers the use of low-frequency vibrations of flexural motion having long wavelengths to determine the axial compressive load in rails and the lateral stiffness at the ties. The flexural vibrations in bending are dispersive in nature, with different wavelengths travelling at different velocities. The frequency of vibration depends on the bending stiffness, the lateral stiffness per unit length of the foundation, the axial compression and on the mass per unit length of the rail as well as the wavelength.

A 16' long S4x7.7 beam supported by lateral mechanical springs with two different stiffness located at every 2' was submitted to a measured variable compression load in the laboratory. This beam was impacted laterally with a hammer at various points along its length and the horizontal acceleration at a point was measured. The resonant frequencies of vibration were determined from the frequency response functions.

Contour plots of the measured values of these frequencies as a function of the stiffness and axial compression intersect at the corresponding values of stiffness and axial compression acting on the rail. In particular the intersection of the lowest frequency, with a wavelength of 32', and that associated with a wavelength equal to twice the spacing of the lateral stiffeners, i.e., 4', yields the estimates to the stiffness and axial compression. Additional resonant peaks in the frequency response functions can also be used to determine these two parameters.

INTRODUCTION

Thermally-induced buckling failures of tracks are usually horizontally but can also be vertical on occasion. They often occur on hot days, usually in the early afternoon, with no train on the track, but can also occur when a train is ascending or descending or braking, all of which add to the axial compression in the track. Ironically this buckling is more susceptible to occur after a segment of track has been maintained, before traffic has seeded the ties into the ballast. Since the rails are linked together by ties, both rails buckle together along with the ties as one unit. The phenomenon still defies detection, since current warning systems which signal track failure rely on a small electrical signal which is not broken due to track buckling.

In 1977 alone there were 109 train derailments attributed to buckling of the track [1]. The expense in preheating rails during track laying and the monetary costs associated with slowdown orders for trains on tracks which are thought to be in danger of buckling all add up to important economic considerations. The use of strain gages is not practical for determining the axial stress due to the time and costs involved and since they need a point of reference, i.e. zero strain. Also, the axial strain along the rail is zero in plane strain situation and measurements would need to be based on the perpendicular strain due to Poisson's effect.

Much of the theoretical research on track buckling has dealt either with the analytical considerations of the post-buckling behavior [2], or with the experimental measurement of vibrations at high frequencies [3]. There has been very little experimental research on the elastic pre-buckling behavior of tracks and the measurements of vibrations at low frequencies which are sensitive to the axial load and lateral stiffness.

The most reliable method for obtaining these two critical parameters is based on static force-deflection relationships [4]. First, the spikes which attach the track to the ties over a rail segment are dismantled over the length of a railroad car. This is followed by the application of a static load applied vertically by a hydraulic jack located at the center of the car. A beam-column subjected to axial compression deflects more for a lateral load applied at the middle than a beam with no axial compression. The estimated buckling load is typically on the order of 200 metric tons. The procedure outlined can be as far off as 6 metric tons (12.5 kips).

For lateral stiffness, a hydraulic jack buttressed on one of the rails applies a horizontal force to a tie which has been unfastened from the rail. Graphs of the force versus horizontal displacement for different types of ballast are experimentally obtained, from which both the strength and stiffness of that particular tie can be determined. Using a number of ties, an average value for the track stiffness and strength can be computed.

There currently are no available techniques which can simultaneously assess both the lateral stiffness and the axial load in the rail. Considerable time, effort, and expense are required to unfasten the rail from the tie and perform the static operations described above for both the tie and the rail. Furthermore, these static tests must be repeated many times for a true representation of the track. A more efficient scheme is therefore needed if thermo-buckling of continuously-welded track is to be avoided.

At low frequencies of vibration, the relationship between the frequencies of the flexural motion are highly dispersive, i.e., the velocity depends on the wavelength. Recent field investigation of vertical impact of actual tracks have demonstrated that the resonant frequencies can be determined from frequency response functions [5]. The long wavelengths traveling at relatively slow velocities and vibrating in the low-frequency range are sensitive to both the axial load and the lateral stiffness.

This paper presents results of laboratory experiments which demonstrate the practicality of using measured resonant frequencies of flexural motion in determination of the axial load in beams and the lateral stiffness. The theory of the flexural vibrations of an infinite Euler beam submitted to an axial load and resting on a Winkler foundation is first presented. The boundary conditions at the end of the beam and at the intermediate supports provide equations which lead to a matrix which is singular at the resonant frequencies.

The resonant frequencies can then be plotted on three-dimension plots versus the axial compression and the lateral stiffness at the supports. From these curves, contours corresponding to the measured resonant frequencies are drawn as a function of the stiffness and compression. For a number of measured frequencies, these contours should intersect at appropriate values of the lateral stiffness and axial compression. Measurements of the mode shapes are not used except to determine what mode shape a particular resonant frequency corresponds to.

FLEXURAL VIBRATIONS OF SINUSOIDAL MODE SHAPES OF AXIALLY LOADED EULER BEAM ON WINKLER FOUNDATION

The equations of the forces perpendicular to the original axis of a beam when the rotational inertia is neglected is (See Figure 1)

$$V = \frac{\partial M}{\partial x} + P\frac{\partial w}{\partial x} \tag{1}$$

where V represents vertical force perpendicular to the original axis of the member and not the shear. The bending moment satisfies the equation

$$M = EI\frac{\partial^2 w}{\partial x^2} \tag{2}$$

Newton's equation for vertical motion gives the equation

$$m\frac{\partial^2 w}{\partial t^2} = -\frac{\partial V}{\partial x} - Kw \tag{3}$$

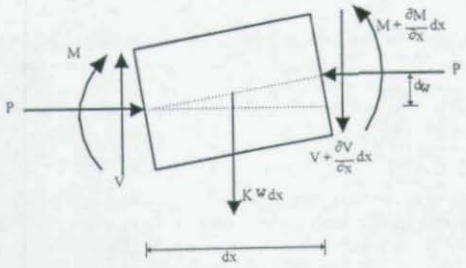

Figure. 1 Beam Element Under Axial Compression on a Winkler Foundation

The partial differential equation for elastic flexural wave vibrations of the lateral motion, w, in doubly-symmetric Euler beam is

$$m\frac{\partial^2 w}{\partial t^2}+EI\frac{\partial^4 w}{\partial x^4}+P\frac{\partial^2 w}{\partial x^2}+Kw=0 \tag{4}$$

The rail material is characterized by the modulus of elasticity, E. I is the moment of inertia of the cross-section about the vertical axis for horizontal motion. m is the mass per unit length, K is the Winkler foundation stiffness per unit length of rail, and P is the axial compression in the rail. For sinusoidal mode shapes in space and time

$$w=W\sin\frac{2\pi}{\lambda}x\sin\omega t \tag{5}$$

There results the following relation between the frequency, ω, and the wavelength, λ,

$$\omega^2=\frac{EI}{m}\left(\frac{2\pi}{\lambda}\right)^4-\frac{P}{m}\left(\frac{2\pi}{\lambda}\right)^2+\frac{K}{m} \tag{6}$$

The elastic stability load of the track is given by

$$P_{CRITICAL}=2\sqrt{KEI} \tag{7}$$

The rail will buckle at a much lower load because of the post-buckling behavior and the fact that the stiffness does not remain elastic[2]. The thermally induced axial load in plane strain situation is

$$\Delta P=EA\alpha\Delta T \tag{8}$$

in which A is the cross-sectional area, E is Young's modulus of elasticity, α is the coefficient of thermal expansion and $\Delta T$is the increase in temperature, and ΔP is the increase in axial compression.

For beams with a finite length, the mode shapes of vibration must satisfy boundary conditions at the ends of the beam. The long wavelengths, associated with small wavenumbers, vibrate at low frequencies. For a member of length L with sinusoidal mode shapes there results

$$\begin{aligned}
\omega_j^2 &= \frac{T}{m}\left(\frac{2\pi}{\lambda_j}\right)^2 && \text{FOR CABLE}\\
\omega_j^2 &= \frac{EI}{m}\left(\frac{2\pi}{\lambda_j}\right)^4 && \text{FOR BEAM}\\
\omega_j^2 &= \frac{EI}{m}\left(\frac{2\pi}{\lambda_j}\right)^4 - \frac{P}{m}\left(\frac{2\pi}{\lambda_j}\right)^2 && \text{FOR COLUMN}\\
\omega_j^2 &= \frac{EI}{m}\left(\frac{2\pi}{\lambda_j}\right)^4 - \frac{P}{m}\left(\frac{2\pi}{\lambda_j}\right)^2 + \frac{K}{m} && \text{FOR RAIL}
\end{aligned} \qquad (9)$$

in which the tension in the cable is the negative of compression, T=-P, and the formula for the beam assumes no axial load. The wavelengths are given are related to the distance between the two ends a distance L apart by the equation

$$\lambda_j = \frac{2L}{j} \quad FOR\ j=1,2,3,\ldots\infty \qquad (10)$$

The frequencies for a cable in tension (EI=K=0; P=-S) are multiples of each other, i.e. they are harmonics, whereas those for a simply supported beam(K=P=0) have ratios of 1, 4, 9, 16, etc. Axial compression decreases the frequencies for a column (K=0), whereas tension, P=-T increases the frequencies. For the rail, the mode shapes with large wavelengths have a frequency equal to $\omega=\sqrt{K/m}$, whereas those with short wavelengths are independent of K, i.e., the square of the frequency decreasing linearly with the axial compression, P.

For the Timoshenko equations with no foundation stiffness, K=0, there results the following partial differential equation for the flexural bending vibrations of a beam including the effect of rotatory inertia and shear deformation [6]

$$\begin{aligned}
&m\frac{\partial^2 w}{\partial t^2} + EI\frac{\partial^4 w}{\partial x^4} + P\frac{\partial^2 w}{\partial x^2}\\
&-\frac{Im}{A}\left[1+\frac{E}{k'G}\right]\frac{\partial^4 w}{\partial x^2 \partial t^2} + \frac{Im^2}{k'A^2G}\frac{\partial^4 w}{\partial t^4} = 0
\end{aligned} \qquad (11)$$

in which the sear factor, k', is

$$k' = \frac{I^2}{A\int_A (Q/t)^2 dA} \tag{12}$$

which for a rectangular section is k'=.833. G is the shear modulus of rigidity

$$G = \frac{E/2}{1+\nu} \tag{13}$$

for ν the Poisson ratio of the rail material. Assuming sinusoidal mode shapes yields the following quadratic equation for the square of the resonant frequency ω^2

$$\frac{Im^2}{k'A^2G}\omega^4 - m\left[1+\left[\frac{2\pi}{\lambda}\right]^2\frac{I}{A}\left[1+\frac{E}{k'G}\right]\right]\omega^2 + EI\left[\frac{2\pi}{\lambda}\right]^4 - P\left[\frac{2\pi}{\lambda}\right]^2 = 0 \tag{14}$$

The lower of the two roots yields a correction factor for sinusoidal wavelengths [8]

$$\omega_j = \frac{\frac{EI}{m}\left[\frac{2\pi}{\lambda_j}\right]^4 - \frac{P}{m}\left[\frac{2\pi}{\lambda_j}\right]^2}{\sqrt{1+\left[\frac{j\pi r}{L}\right]^2\left[1+\frac{E}{k'G}\right]}} \quad FOR\ j=1,2\ldots \tag{15}$$

in which r is the radius of gyration

$$r = \sqrt{\frac{I}{A}} \tag{16}$$

Although Euler theory is adequate for the long wavelengths, it is not for the shorter wavelengths and this correction should be incorporated.

AXIALLY LOADED BEAM WITH DISCRETE SUPPORTS

The previous equations dealt with a beam on a Winkler foundation. Rails, however, are longitudinally, vertically and laterally stiffened at discrete points, i.e., the ties. The flexural vibrations for the wavelengths with shorter mode shapes do not satisfy the previous equations since there is no Winkler stiffness between the lateral supports at the ties. The sinusoidal wavelengths of the eight mode shapes for a 16' S4x7.7 cross-section which was tested in the laboratory are; 32', 16', 10.67', 8, 6.4', 5.33, 4.57' and 4' respectively are shown in Figure 2.

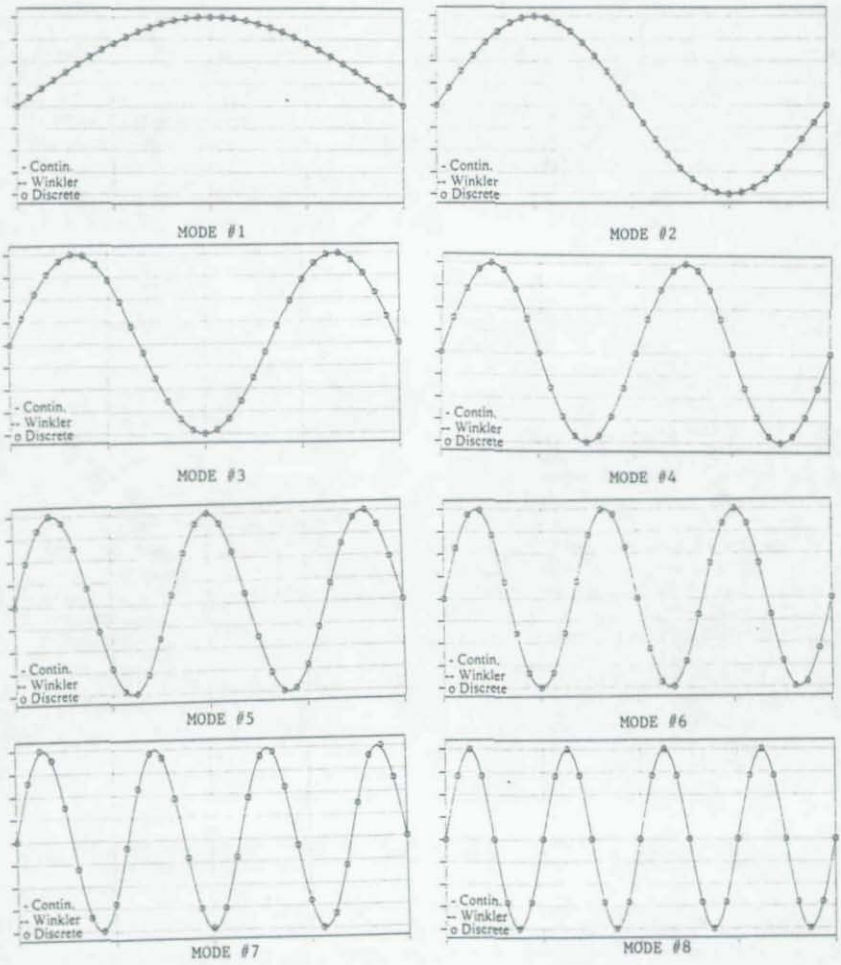

Figure 2. Eight Mode Shapes of Simply-Supported Beam

For a given resonant frequency, ω, α^2 satisfies the quadratic equation

$$EI\alpha^4 - \left[P + m\omega^2\left[1 + \frac{I}{A}\left(1 + \frac{E}{k'B}\right)\right]\right]\alpha^2 + \frac{Im^2\omega^4}{k'AG} = 0 \qquad (21)$$

The two equation at each end of the beam and the four equations at the n-1 intermediate supports can be formulated as 4n equations to solve for the 4n constants of integration, 4 in each beam segment. Furthermore, these equations may be written in a characteristic matrix form

$$AC = 0 \qquad (22)$$

EXPERIMENTS

A 16' long S4x7.7 beam laterally supported about its weak axis every 2' was loaded in compression up to 20 kips[7]. For a beam with 8 segments, A of Eqn.22 is a 32x32 matrix and C is a vector of the 32 constants, 4 per beam segment. Since this is a homogeneous equation, the solution is when the determinant of the 32x32 square matrix is zero, which gives the resonant frequencies of vibration. The C vector is the corresponding eigenvector of the motion. For different combinations of EI, m, P, and k, three dimensional plots of the square of the eight natural frequencies versus the lateral stiffness at the support, k, and the axial compression, P, are given in Figure 4 for wavelengths from twice the distance between the two ends (Mode #1) up to twice the spacing between the supports (Mode #8).

Contour plots of the measured frequencies associated with mode shapes 1,4,5,7, and 8 are given in Figure 5 for two different lateral stiffnesses at loads of 5 and 25 kips in compression for lateral stiffness of 2.7 and 5.4 kips/inch. Modes 3 and 6 had a node near the accelerometer location and were not considered in the data. Similarly, Mode shapes 1 and 2 nearly had the same resonant frequency and were not distinguishable from the data.

The three dimensional plots for the frequencies are adjusted to account for the Timoshenko modification to the higher modes. The end at which the load was applied was relatively flexible since it did not have lateral restraint. A numerical study of lateral stiffness at this end showed that the high frequencies were very sensitive to this lateral stiffness. An estimate to the stiffness was obtained which would account for the high frequency data and incorporated into the three-dimensional plots of the frequencies. Further details are given elsewhere [7].

The contours of the first and the eight mode shapes intersect in the area near the actual values of stiffness and axial compression in all four plots shown in Figure 5. Similar plots at loads of 5, 10, 15, and 20 kips also gave estimates to the parameters. The estimated values of the axial load from the intersection of the first and eight mode shapes is shown versus the applied load in Figure 6, at both 2.7 and 5.4 kips/inch lateral stiffness. The measured resonant frequencies are plotted as a function of the applied load in Figure 7. They match very closely the theoretical values taking account of the Timoshenko beam effect for the high frequencies and the flexibility of the end with the hydraulic actuator.

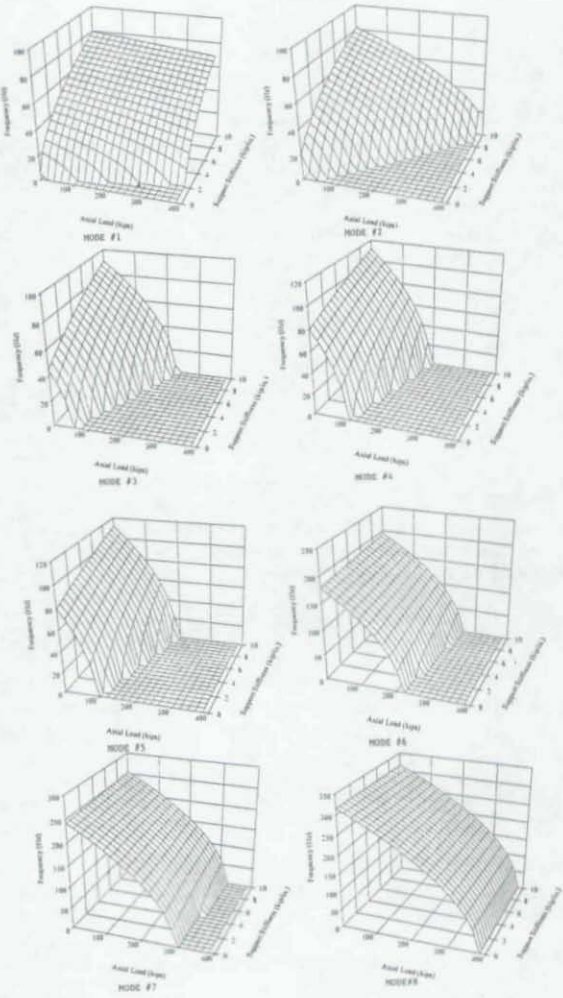

Figure 4. Natural Frequencies for Mode Shapes 1-8 Versus Axial Compression and Lateral Stiffness

CONCLUSION

The measurement of resonant frequencies of vibration can be used in determining the axial load in a member and its lateral stiffness at equally-spaced points along the beam. This procedure provides a tool to assess the in situ lateral stiffness of tracks and the axial load in the rails. With this information the susceptibility to thermally-induced buckling can be better assessed. Good resolution of the resonant frequencies is required to obtain accurate estimates to the axial load and lateral stiffness. Mode shapes are needed to associate the resonant frequencies with the appropriate mode shapes of vibration but need not be used in determining the parameters. Finally, impact testing which generates a broad frequency is appropriate to excite the frequencies of interest. This method is easier to implement in the field than shakers providing a sinusoidal excitation and requires much less time and data analysis.

ACKNOWLEDGEMENTS

The first author wishes to thank Prof. Thomas Murray of VPI&SU for suggesting this topic and for support during a recent sabbatical at VPI&SU where this work was performed. Financial support from the Association of American Railroads and the Volpe National Transportation Systems Center of the Federal Railway Administration is gratefully acknowledged.

REFERENCES

[1] Zarembski, A. M., "On the Nondestructive In-Track Measurement of Longitudinal Rail Force", Proceedings of a Joint Government-Industry Conference on Nondestructive Techniques for Measuring the Longitudinal Force in Rails, Elliott, P.,Editor,1979, pp 1-12.

[2] Kerr, A. D. "Lateral Buckling of Railroad Tracks due to Constrained Thermal Expansions-A Critical Survey", Proceedings, Railroad Track Mechanics and Technology, 1978, pp. 141-169

[3] Lusignea, R., Prahl, F., and Maser, K. "The Effect of Axial Load on the Flexural Dynamic Response of a Rail", Proceedings of a Joint Government-Industry Conference on Nondestructive Techniques for Measuring the Longitudinal Force in Rails, Elliott, P. Editor, 1979, pp 86-109

[4] Samavedam, G. and Kish, A "Continuous Welded Rail Track Buckling Safety Assurance Through Field Measurements of Track Resistance and Rail Force", Transportation Research Record # 1289, Lateral Track Stability- 1991, Transportation Research Board, Washington, DC, 1991, pp. 39-52

[5] Knothe, K.L., and Grassie, S.L., "Modelling of Railway Track and Vehicle/Track Interaction at High Frequencies",Vehicle System Dynamics,Vol. 22,#3-4,1993, pp.209-262

[6] Clough, R. W. and Penzien, J., Dynamics of Structures, McGRaw-Hill, 1993

[7] Boggs, T.," Determination of Lateral Stiffness and Axial Load in Rails from Low-Frequency Flexural Vibrations" Master's Thesis, Virginia Polytechnic Institute and State University, 1994

ULTIMATE STRENGTH ANALYSES OF A NORTH SEA OFFSHORE PLATFORM

James M. Light
Samuel J. DeFranco
Joseph M. Gebara
Bernhard Stahl

Amoco Worldwide Engineering and Construction
Houston, Texas

ABSTRACT

This paper focuses on assessing the mean resistance capacity of an offshore platform in the context of structural assessment practices. The paper presents an overview of structural assessment procedures used in the offshore industry to evaluate fitness for purpose of offshore platforms. An important component of this procedure is the 'pushover analysis' method used to estimate offshore platform mean ultimate strength. The pushover analysis methodology uses explicit modeling of the ultimate strength of platform structural components (bracing members, tubular joints, etc.) in a non-linear, large-displacement, static, finite element analysis to define a global platform collapse load. Results are presented from pushover analyses performed by engineering contractors of an Amoco offshore platform standing in 84 m (275 ft) of water in the central North Sea. These results show significant variability in the predicted ultimate strength as well as surprisingly high predictions of platform collapse load. Results are presented from Amoco in-house analyses of the same platform done in an effort to understand both the high variability in predicted platform ultimate strength and the predicted high reserve strength levels.

Introduction and Background

Ultimate strength analysis is becoming more common, if not routine, in fitness-for-purpose assessment to establish whether existing offshore structures can safely meet their original or modified requirements. Before discussing ultimate strength analysis specifically, it is useful to understand philosophically the function of a fitness for purpose assessment. Figure 1 illustrates a probability density function (PDF) representative of an original structural design. Shown on the plot are the PDFs for both load and resistance, with structural failure representing the probability that the load is greater than the resistance.

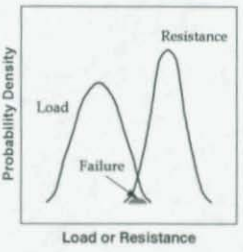

Figure 1
PDF for New Design

Figure 2 illustrates what might happen to the load-resistance PDF over the lifetime of a structure. Damage to the structure or deterioration such as corrosion and fatigue can reduce the strength of the structure, shifting the resistance PDF to the left. It is also possible for the loading on a structure to increase

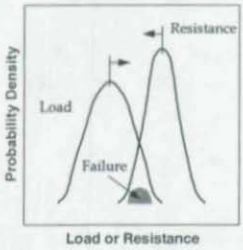

Figure 2
Increased Failure Probability

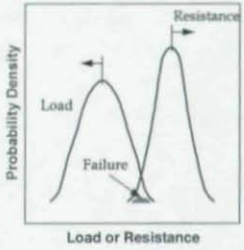

Figure 3
Restoration of Acceptable Failure Probability

beyond its design load, shifting the load PDF to the right. This increase might occur when design criteria of 10 or 20 years ago is shown to be unconservative or when additional equipment or appurtenances are added to a structure. The result of decreased resistance and increased load is an increased probability of failure, as shown in Figure 2. It is this increase (or perceived increase) in risk of structural failure which identifies the need for a fitness for purpose structural assessment. Structural assessment and remedial repair, if necessary, are performed to restore an acceptable failure probability, as shown in Figure 3.

Structural assessment specifically addresses the risk of structural failure, with risk defined as the product of the probability of failure and its consequence. Consequences are often defined in terms of an economic loss. Risk can be controlled in two primary ways:

1. Control consequences: If the probability of failure is high, steps can be taken to reduce the potential for loss of life or property or damage to the environment. In the offshore industry, this might entail removing the operating crew from a platform and operating the platform remotely from shore with occasional visits by personnel. Reduced environmental consequences can be achieved by installing automatic shutdown valves on wells and pipelines to ensure minimal damage to the environment in case of an incident.

2. Use assessment engineering technology to better define the probability of failure and justify that the risk is acceptable. Any or all of the four following means may achieve this goal:

    - Justify increased mean value of structural strength (shift the resistance PDF to the right): This can be achieved by removing conservatism which might be inherent in a 'first pass' estimate of structural strength. If the original structural strength estimate was based on a linear structural analysis, a non-linear analysis including material non-linearity and force redistribution may achieve the desired goal. A large portion of this paper focuses on defining the mean value for structural strength using ultimate strength analysis procedures.

- Justify a reduced coefficient of variation (COV) for structural strength (in the resistance PDF, reduce the spread about the mean): Design code equations for the strength of structural components such as bracing members and tubular joints are formulated to cover a wide variety of component geometry and can include some conservatism. Screening component test data for results most representative of the geometry present in the actual structure may justify reduced variation in component strength and/or increased mean component strength. Reduced COVs for component structural strength can also be justified by performing detailed structural inspection.

- Justify a decreased mean value for loads (shift load PDF to the left): Decreased loads can be achieved by removing equipment and load generating appurtenances as they become redundant or obsolete. Conservative estimates of the loads on a structure are often used in the design process. A detailed study of the actual in-service loads may justify reducing the estimate of loads on the structure. In the offshore industry, a site specific study of the meteorological, oceanographic, or seismic conditions can sometimes identify conservatism in the original design criteria.

- Justify a decreased COV value for loads (reduce the spread about the mean of the load PDF): This may involve studying the approach to defining loads and developing a better understanding of the loads that act on a particular structure or structural component.

It should be observed that the above four means are not independent of each other. Typically the mean values and coefficients of variation must be determined together along with the distribution types (e.g., normal, lognormal, etc.), which can have a significant effect on the results of the analysis.

An increase in resistance and/or decrease in load may be justified by demonstrating that structures have survived extreme loading levels. In the offshore industry, powerful hurricanes can provide the extreme loading. It is important to note that offshore platforms (at least in the Gulf of Mexico) are de-manned during hurricanes so this extreme loading does not pose a risk to human safety.

For typical offshore platforms, it has been shown that the probability of failure under extreme loading conditions can be approximated by considering the load distribution and the MEAN of the resistance [1]. The COV of loading typically dominates the analysis to the extent that the COV of resistance can often be ignored. The focus of this paper is on assessing the mean resistance capacity of an offshore platform using ultimate strength analysis procedures in the context of structural assessment.

Structural Assessment: A Step-wise Process

There are three primary steps in a structural assessment: (1) inspection of the structure to determine its in-service condition, (2) definition of assessment criteria or 'failure', and (3) analysis of structural strength which typically involves finite element structural analysis. It

is tempting for engineers to perform the third step without recognizing the importance of the first two steps. The three step assessment procedure proposed by the writers is in line with a similar step-wise approach to structural assessment recommended in Draft Section 17 to API RP-2A [2,3].

Detailed inspection of a structure should identify its present condition, noting specifically the as-built condition and any damage or deterioration that has occurred with time. These data are often used to build a finite element computer structural analysis model appropriate for the assessment, which can be significantly different than a structural analysis model typical for new design.

It is important that the assessment criteria be defined before starting any assessment calculations. This effort might involve selecting appropriate loading criteria such that a structure shown to withstand this loading criteria passes the assessment. The assessment criteria could also be a definition of 'failure' or it could be a specific process for performing an ultimate strength structural analysis.

Assessment engineering involving calculation of the loads on the structure and the structural resistance constitutes the third assessment step. These calculations can range from relatively simple linear-elastic analyses to satisfy predetermined loading criteria, to progressively more complex inelastic ultimate strength analyses, to explicit platform reliability analyses.

A step-wise approach to structural analysis for assessment, such as that proposed for offshore structures the Draft Section 17 to API RP-2A [2,3], is highly recommended. The step-wise analysis method is generally efficient, with each successive step involving more engineering effort to characterize platform performance. The step-wise procedure is generally followed only until the structure is shown to pass its pre-defined assessment criteria. A typical approach to assessment structural analysis of an offshore platform might be as follows:

1. Design level linear-elastic analysis using typical design procedures and component strength formulations, including all factors of safety. This analysis is extremely useful for identifying critical components and focusing the efforts of later, more complex analyses.

2. Design level linear-elastic analysis removing factors of safety from component strength formulations.

3. Member removal analyses using linear-elastic analysis and removing 'critical' components from the model to investigate load redistribution through the structure. In some cases the components shown to be critical in design-level analyses can be entirely removed from a structural analysis model without any adverse effect on overall structural strength. These 'critical' components can thus be shown to be non-critical in terms of platform ultimate strength.

4. Local ultimate strength analysis modeling the localized non-linear effects of component failures with the rest of the analysis model linear-elastic.

5. Global ultimate strength analysis using non-linear structural analysis procedures to model numerous component failures and component post-failure strength. The remainder of this paper focuses on 'pushover analysis', a particular method of global ultimate strength analysis common in the offshore industry.

Static Pushover Analysis

The de-facto standard for ultimate strength analysis in the offshore industry has developed as "static pushover analysis", a term referring to three-dimensional, non-linear, large displacement, static finite element analyses in which the horizontal forces on a platform (representative of wave forces) are increased until structural collapse. The failure and post-failure behavior of platform components such as brace members and tubular joint connections are modeled explicitly. Significant effort has been devoted over the years by the offshore industry to developing specialized software to perform these analyses and to calibrating the method to 'real world' behavior.

The underlying assumptions in a static pushover analysis are that the failure of an offshore platform occurs when a single large wave strikes the platform and that the wave period is sufficiently longer than the natural period of the structure so that dynamic effects are negligible. For most fixed platforms these are reasonable assumptions since wave forces dominate the structural loading and considering that the typical offshore platform has a natural period of vibration less than 3 seconds and a design-level or ultimate strength-level ocean wave has a wave period greater than 12 seconds.

The analysis tools and methodologies used in the offshore industry for pushover analysis have resulted from significant joint industry funded research over a number of years. Numerous full scale laboratory tests have been performed of typical offshore platform components to develop and calibrate analytical models of component failure loads and post failure behavior. Most recently, a calibration effort of the entire pushover analysis process was undertaken using experience from Hurricane Andrew [4,5]. This 'design level' storm passed through the Gulf of Mexico in August of 1991 and caused structural damage to a few offshore platforms. The calibration effort focused on performing pushover analyses of select offshore platforms and comparing predicted strength to observed behavior during Andrew. In general the static pushover analysis methodology was shown to be conservative [4,5].

Amoco is developing a 'recipe' for performing static pushover analyses of offshore platforms. This recipe, while still evolving, is based heavily on the experience from the Hurricane Andrew calibration effort. The recipe specifically addresses the following issues:

- Recommendations for typical steps in an investigation of platform ultimate strength, i.e. the levels of complexity in the analysis series building up to a full non-linear collapse analysis.

- Methods for modeling platform component strength and post-failure behavior, including the buckling strength of platform braces, the ultimate strength of tubular joint connections, the residual strength of damaged members, and mean (as opposed to lower bound) material properties.

- Methodology for characterizing soil strength and procedures for modeling soil/pile/structure interaction.

- Methods for calculating wave forces on platform members and increasing these wave forces to platform collapse.

- Methods for calculating wave forces on platform decks and deck equipment.

Amoco UK 'Lomond' Platform

The impetus for writing this paper and developing an ultimate strength analysis 'recipe' came primarily from a series of ultimate strength analyses which were performed for the Amoco UK 'Lomond' platform. This platform stands in 84 meters of water in the central North Sea, approximately 250 kilometers offshore due East of Aberdeen, Scotland. The platform was installed in 1992 and was designed to support 21 wells, 3 pipeline risers, and a topsides production deck weighing 16,500 metric tonnes. Total jacket structural steel weight is approximately 4,800 tonnes with approximately 5,400 metric tonnes of piles.

The Lomond platform is a 4-leg tower structure with 4 leg piles and 8 skirt piles. The structure has four vertical X-braced bays (without horizontals) on the four platform faces and secondary X-bracing at five horizontal levels at the top and bottom and between each vertical bay. Figure 4 is a plot of a finite element model of the platform which illustrates the major platform framing. It should be noted that the deck framing shown in Figure 4 is simplified for the finite element analyses. Figure 4 also shows the piles extending below the seabed at the bottom of the platform.

Original Ultimate Strength Analyses

The original ultimate strength analyses of the Lomond platform were performed as part of an effort to define the appropriate time interval between underwater inspections of the platform [6]. This required pushover analyses of the platform in its intact state and various damage states (members removed).

The original ultimate strength analyses of the Lomond platform incorporated several simplifying assumptions, particularly in that the platform foundation was modeled with equivalent linear springs and tubular joint failure modes were neglected. This effectively eliminated two very important parameters which have since been shown to influence the collapse strength of the platform. Also, the methods for modeling brace failure were somewhat simplified and these methods were not proven to be conservative. The original analyses showed that the Lomond platform had a Reserve Strength Ratio = 4.99. Platform ultimate strength is often characterized by this Reserve Strength Ratio (RSR), which is defined as follows:

$$RSR = \frac{\text{(Lateral Force at Platform Collapse)}}{\text{(Lateral Force Calculated Using Current Design Procedures)}}$$

The value of RSR = 4.99 seemed extremely high to Amoco engineers. Other engineering firms were retained to perform a similar analyses, producing RSR values ranging from 2.90 to 5.08. Analyses A through E in Figure 5 show load-displacement plots from these initial analyses. All results shown in Figure 5 are for forces from the platform West direction and all RSR values have been calculated using a common 'design lateral load' denominator of 35,014 kilonewtons.

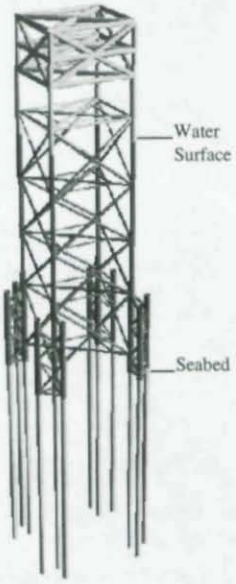

Figure 4
KARMA Model of Lomond Platform

The Figure 5 plot clearly illustrates the variability that can result from ultimate strength analyses when the input parameters and analysis assumptions are not closely controlled. It is interesting to note on the plot both the significant variability in predicted ultimate strength and the significant difference in initial stiffness. Similar variability has been shown in recent joint industry project work in which a number of companies performed ultimate strength analyses of a single platform [7,8].

The writers were asked to investigate the initial ultimate strength results and to supplement these results with in-house analyses. In-house analyses were first performed using simplifying assumptions similar to those of the original engineering consultant in order to better understand the work that had been done. These in-house analyses showed that RSR values from 4.02 to 5.78 can be produced simply by varying certain input

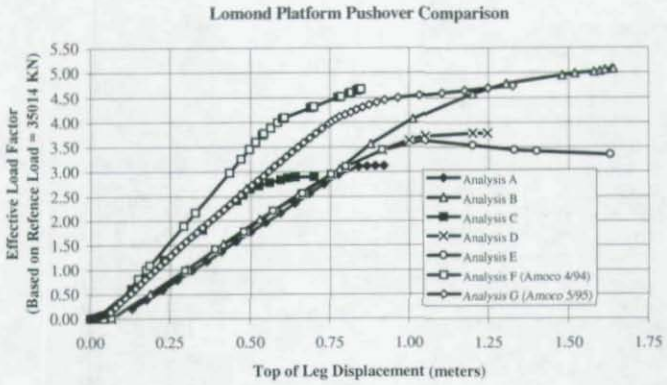

Figure 5
Load-Displacement Plots for Lomond Pushover Analyses

assumptions related to member failure. Analysis F on Figure 5 illustrates results from one early Amoco in-house pushover analysis.

Subsequent Ultimate Strength Analyses

Subsequent to this initial series of analyses, certain of the contractors involved were asked to re-run analyses including more detail in the model to represent their best practice for performing ultimate strength analyses. Specifically, a full foundation model and better attention to joint failure were included in the analyses. These analyses are being finalized *as this paper is being written.*

Amoco has performed subsequent in-house analyses using our evolving ultimate strength analysis 'recipe'. This analysis work and the development of the analysis 'recipe' are still in progress, but preliminary results have been produced for wave forces from the Platform West direction. These results are included on the Figure 5 plot as Analysis G.

The RSR value predicted by the Amoco in-house analysis for the Platform West wave approach direction is shown as 4.7. However, this value may reduce somewhat as appropriate care has not been fully taken in characterizing tubular joint strength and brace member ultimate ductility levels. Figure 6 shows the deformed shape of the Lomond platform at ultimate strength with displacements magnified 10 times for illustration purposes.

The platform collapse sequence from Analysis G is summarized as follows, with each item number corresponding to a number label in Figure 6:

1. *First inelastic response in the analysis occurs in the deck legs at the bottom level of the* deck. Since neither the deck framing nor the load distribution on the deck is modeled very accurately, this event is not of significant concern.

2. The second series of events involves yielding in the top brace between the legs and the skirt pile sleeves. This is a bending/compression yielding in a minor brace. Load paths are available for load redistribution.

3. The next event is the onset of yielding in the piles below the seabed. First yield occurs in the skirt pile with the highest compression load as a combination of bending and axial compression stress. Yielding follows in other skirt piles and the main leg piles. As the load increases, yielding extends along increasing lengths of the piles.

4. The first primary X-brace member fails in compression. This member is in the second bay from the bottom of the platform. This failure is followed fairly quickly by similar compression X-brace failures in the same bay on opposite sides of the platform. It is interesting to note that even with compression all compression X-braces buckled in one bay the platform is still able to carry additional load in portal frame action supplemented by the tension capacity of the remaining X-brace members.

5. Compression X-braces fail in the third framing bay from the bottom.

6. The next significant event is the yielding of the first tension X-brace member in the second bay from the bottom of the platform. This is followed by similar failures on opposite sides of the platform, buckling of compression X-braces in other platform bays, and continued tension X-brace failures. At this point the structure is resisting loads primarily through portal frame action. Significant softening and large displacements are evident in the global load-displacement plot shown in Figure 5.

7. Final collapse is caused by bending/compression failure of a main leg member after numerous vertical X-brace failures cause significant portal frame action.

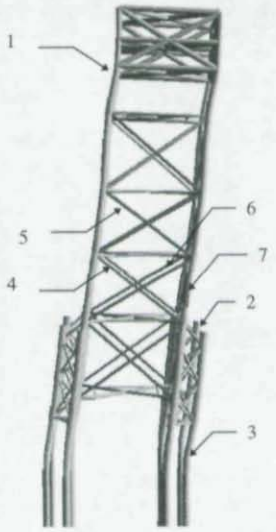

Figure 6
Displaced Shape at Platform Collapse
(Displ. magnified 10x)

Significant inelastic behavior is experienced in the pile foundation but no foundation failure mechanism is formed.

Wave Force Profile

Common industry practice in modeling lateral forces for static pushover analyses is to use a force pattern based on a design wave height and linearly scale this force pattern to platform ultimate collapse. Increasing wave forces on a platform, particularly of the magnitude required to produce collapse level loads on the Lomond platform, can only come from increased wave height. Calculations were performed to show that for Lomond, collapse level loading can only be achieved when waves are high enough to hit the platform deck levels. When the wave reaches the blocky areas of the deck, very large forces are exerted at the deck level, resulting in a significant change in the wave force pattern. Wave-in-deck forces and the associated change in wave force pattern were not included by any of the engineering contractors in their Lomond analyses. This factor was included in the latest Amoco analysis and it is the feeling of the writers that this effect should be included in a pushover analysis.

Sources of High Reserve Strength

One might reasonably question why a platform might be predicted to be able to withstand forces on the order of four times its design level loading. It might seem that the platform was over-designed and that some cost savings could have been achieved by optimizing the design. The writers have attempted to understand the sources of this high reserve strength and have come to the following conclusions:

- The Lomond platform components were in general not designed to code strength interaction ratios of exactly 1.00. The tubular joint connection designs were generally controlled by fatigue, which resulted in the brace ends being over-sized for strength. To ease fabrication, it is believed that the entire length of the brace was increased to the wall thickness required at the brace end. This resulted in a number of members having strength interaction ratios on the order of 0.5 to 0.6 under design level loading.

- The platform design process included a large number of load cases: extreme storm environmental conditions from eight approach directions, a variety of topsides production equipment layouts (both present and future), loads from the drilling rig located over a number of different wells, fabrication and lift forces, transportation and installation forces, etc. Each platform member was sized for the worst load case for that particular member, with the resulting composite structure being perhaps overdesigned for any single load case.

- A three-dimensional X-braced structure, by its very nature, has a tremendous number of redundant load paths and can tolerate numerous component failures before global platform collapse.

- Fully optimizing structural steel weight for the Lomond platform may not have been a major project objective. Economic analyses of construction projects for offshore hydrocarbon production often show that more benefit can be gained by reducing the time spent designing, fabricating, and installing a platform (thereby reducing time to first hydrocarbon production) than can be gained by spending extra time in design and fabrication optimizing structural steel weight.

Conclusions

The analyses of the Lomond platform have been an interesting project for the writers. The Lomond platform is probably atypical of the platforms for which structural assessment and ultimate strength analyses are generally performed, since it was designed and installed so recently (1991-92). The motivation for these studies was inspection planning, not assessment for service life extension. However, the platform proved an excellent test of state-of-the-art ultimate strength analysis procedures and the project showed that the offshore industry needs to devote further effort to reducing the variability in the results of these complicated analyses.

The authors believe that ultimate strength analysis (in the sense of something beyond design level linear analysis) is a vital part of the structural assessment procedure. It is highly recommended that a step-wise approach similar to the one proposed in this paper or in API RP-2A Draft Section 17.0 [2,3] be used in building up to an ultimate strength analysis from a design level linear analysis.

All assumptions taken in ultimate strength analyses must be reasonable and justified. These assumptions are numerous in a fully non-linear analysis and unreasonable assumptions or neglected component failure modes can drastically alter the predicted platform collapse strength and lead to high degrees of variability in the analysis results. Guidelines for ultimate strength analysis are needed to assist designers and engineers whose experience lies primarily with linear-elastic analyses.

Where appropriate in static pushover analyses, changes in wave force profile should be included. For the platform discussed in this paper, it can be shown that collapse level loading is only possible if the wave reaches the platform deck elevation. This causes a significant shift in the lateral force profile that was not accounted for by any of the engineering contractors. Increasing the lateral load by scaling a single wave force profile, a procedure followed by most analysts in the industry, should not be used when the possibility of waves reaching the deck exists.

Modern offshore platforms with three-dimensional X-braced framing can be expected to exhibit high levels of reserve strength due to the high number of redundant load paths provided by this framing geometry.

Acknowledgments

The writers appreciate the support and encouragement of John K. Smith of Amoco (UK) in the preparation of this paper. The writers also appreciate the openness of the engineering contractors involved in the Lomond analyses in sharing their thoughts and engineering talents.

References

1. Cornell, C. A., "Structural Reliability - Some Contributions to Offshore", OTC 7753, *Proceedings, Offshore Technology Conference, 1994.*

2. American Petroleum Institute (API), *Recommended Practice for Planning, Designing, and Constructing Fixed Offshore Platforms - Working Stress Design*, API RP-2A WSD, Twentieth Edition, July 1, 1993.

3. API Task Group 92-5, *Draft API RP-2A WSD Section 17.0 - Assessment of Existing Platforms*, working draft supplement to API RP-2A WSD, April 29, 1994.

4. PMB Engineering, Inc., *Hurricane Andrew - Effects on Offshore Platforms*, final report to joint industry project participants, October 1993.

5. Puskar, F. J., Aggarwal, R. K., Cornell, C. A., Moses, F., and Petrauskas, C., "A Comparison of Analytically Predicted Platform Damage to Actual Platform Damage During Hurricane Andrew", OTC 7473, Proceedings, Offshore Technology Conference, 1994.

6. Onoufriou, T., Fowler, D., and Smith, J. K., "Reliability Based Optimised Inspection Planning", Proceedings, BOSS Conference, 1994.

7. PMB Engineering, Inc., *Benchmark Analysis - Trial Application of API RP-2A WSD Draft Section 17*, final report to joint industry project participants, December 1994.

8. Digre, K. A., Puskar, F. J., Aggarwal, R. K., Irick, J. T., Krieger, W. F., and Petrauskas, C., "Modification to and Applications of the Guidelines for Assessment of Existing Platforms Contained in Section 17.0 of API RP 2A", OTC 7779, Proceedings, Offshore Technology Conference, 1995.

BRIDGE EVALUATION THROUGH EXPERIMENTAL FIELD TESTING

Michael J. Chajes, Dennis R. Mertz, and William M. Edberg
Department of Civil Engineering, University of Delaware, Newark, DE 19716

Jeffrey L. Schulz
Bridge Diagnostics, Inc., 5398 Manhattan Circle, Suite 280, Boulder, CO 80303

ABSTRACT

In this paper, nondestructive methods for experimental field testing of bridges are discussed. Procedures currently available can be used to evaluate the many aging and deteriorating bridges on our roads and interstates. Using a diagnostic field test, a posted, three-span, steel-girder-and-slab bridge was recently evaluated. This paper will present an overview of the testing which took place, as well as how the load test data was used to evaluate the bridge's load-carrying capacity.

INTRODUCTION

A posted bridge, a bridge which is signed to restrict traffic crossing it based upon a weight limitation below the normal legal limit, represents an economic hardship to the regions served by the bridge. The costs to society of the posted bridge can be measured in terms of miles and minutes of the detour required for commercial traffic, as well as the traveling public.

The cost of replacing all of the nations' deficient bridges is prohibitive. One alternative to replacement is to strengthen or rehabilitate sub-standard bridges. However, before this option is exercised, it is useful to be able to evaluate the actual load-carrying capacity and stability of the bridge in question.

Traditionally, a bridge's load-carrying capacity has been based upon conservative, non-site specific, calculations. As a result, many bridge-specific strength and stability considerations can not be accurately addressed. One method of more fully evaluating a bridges safe load-carrying capacity involves field experimentation. Due to technological advances in this area, the cost of field testing bridges is now relatively small in comparison with the cost of rehabilitation, or the societal costs associated with restricting traffic on a posted bridge.

Through research supported by the Delaware Department of Transportation, the authors have evaluated the use of experimental bridge testing to determine accurate capacities of posted bridges, and have conducted a diagnostic load test on one of Delaware's posted bridges.

This paper will briefly review the current state-of-the-art in experimental field testing of bridges, and present one method for evaluating a bridges load-carrying capacity based on a recently conducted field test.

BACKGROUND

Currently, most bridges are evaluated using simplified models that rely on structural dimensions and properties determined from original design plans and/or observations made during on-site inspections. As a result, current ratings may not always accurately reflect a bridge's safe load-carrying capacity. In fact, researchers have found that traditional load rating methods are

typically quite conservative (Aktan et al., 1993; Bakht and Jaeger 1990; Commander 1989; Lichtenstein 1995).

Even if an advanced analysis of a bridge is performed, many sources of capacity are too bridge-specific to be included without field experimentation. These sources include the unexpected existence of composite action, unintended support fixity, better-than-expected lateral distribution of live loads, participation of secondary and non-structural components, effects of geometry, and effects of two-way action.

One method for quantifying bridge-specific sources of capacity, and more accurately determining a bridge's load-carrying capacity, is to conduct an experimental field test (Schulz 1993). A state-of-the-art survey of experimental field testing of bridges by Edberg (1995) indicated that many researchers are actively working in this area including Aktan and Raghavendrachar (1990), Bakht and Jaeger (1990, 1992), Burdette and Goodpasture (1988), Fu and Tang (1992), Goble et al. (1992), Moses et al. (1994), and Pinjarkar et al. (1990). Work on developing appropriate, nondestructive test methodologies for bridge testing by these researchers and others, combined with the increasing capability and affordability of testing equipment (Schulz 1989), has made the prospect of conducting routine bridge load tests a reality. In recognition of this, a "Manual For Bridge Rating Through Nondestructive Load Testing" has recently been written (Lichtenstein 1995a). In fact, the Florida Department of Transportation (El Shahawy and Garcia 1989), the New York Department of Transportation (Fu et al. 1992), the Ontario Ministry of Transportation (Bakht and Csagoly 1979; Bakht and Jaeger 1990), and Switzerland (Markey 1991) are already making extensive use of experimental field testing to rate bridges.

DIAGNOSTIC AND PROOF LOAD TESTING

Experimental field testing of bridges can be divided into two categories, diagnostic tests, and proof test. In a "semi-static" diagnostic test, a truck having a predetermined weight, typically near the bridge's rated capacity, is slowly driven across the bridge on several different paths and the bridge response is measured. The use of demountable strain transducers, described by Schulz (1989), makes it possible to fully instrument and test most short-to-medium span bridges in a single day. The transducers consist of four foil resistance strain gages in a modified Wheatstone bridge configuration embedded in an aluminum ring. The ring has brackets which allow the gage to be attached to a bridge member either by clamping the brackets directly to the member, or by bolting metal tabs to the brackets and then adhering the tabs to the member with a quick setting two-part epoxy. The transducers can be attached to concrete members using epoxy in the same manner as used with steel. In this case, an extension is used to provide a longer gage length. Using this method, a wide variety of bridges can be evaluated including steel (rolled sections, plate-girders, and boxes) prestressed concrete (I-sections, boxes, etc.), and reinforced concrete (slab, and box girder). Once the field test has been completed, the measured response is used to develop an accurate numerical model of the bridge, and the model is used to estimate the maximum allowable load.

In a proof test, incremental loads are applied to the bridge until either a target load is reached or a predetermined limit state is exceeded. To apply the required load, a special loading vehicle is required. The same type of instrumentation used in a diagnostic test can be used in a proof test. In addition to measuring strains, deflection are often monitored during a proof test. To ensure that no damage occurs due to the test, after each increment of load is applied to and removed from the bridge, the recovery of the bridge is carefully monitored. Using the maximum load applied, a safe capacity for the bridge can be determined. For the proof test, the safe carrying capacity can be determined with less instrumentation and without the need for extensive analysis.

Both of these methods are currently being used to evaluate bridges. Each method has advantages and disadvantages. While results from "semi-static" diagnostic tests must be

extrapolated in order to estimate a bridge's capacity, compared to proof tests they are less expensive to perform, require a shorter testing time, and cause less disruption to traffic. The advantages of proof tests include the ability to rate bridges with less extensive analysis, as well as the ability to evaluate bridges for which little information about the as-built condition is available.

With regards to issues of stability, diagnostic testing is preferable. Since instability is a sudden phenomena, the basic proof test philosophy of incrementally applying loads until a target load is achieved, is not desirable. Rather, by applying a "safe" predetermined load and conducted a diagnostic test, a substantial amount of information regarding the structural condition and behavior of the bridge can be gathered. This information can in turn be used to numerically investigate issues of stability. The remainder of the paper will summarize the evaluation of a posted bridge through the use of a diagnostic field test.

FIELD TESTING OF A POSTED BRIDGE

The steel-girder-and-slab bridge tested in this study was built in 1940. It is located on the heavily traveled Lancaster Pike, and carries traffic across the Red Clay Creek in Wilmington, Delaware. The average daily traffic and average daily truck traffic for the bridge are 17,600 and 900 respectively. The superstructure consists of three, simply supported spans, each consisting of nine non-composite rolled steel girders. The fascia girders consist of rolled sections encased in concrete. On the center span, four equally spaced beams act as end and intermediate diaphragms. The original roadway consisted of a 216-mm-thick concrete deck with a 50.8-mm-thick asphalt overlay. Section, plan, and elevation views of the bridge are shown in Fig. 1.

Over the history of the bridge, a variety of repairs have been made. Corrosion of diaphragms has been repaired with field-welded plates. One of the steel girders has also experienced corrosion in the region below an expansion joint and was also repaired with a field-welded plate. To prevent further corrosion damage to the girders, they have recently been re-painted. In another repair, the ends of the beams of the center span were welded to their bearing plates, thereby restraining relative movement. This condition has led to some cracking of the pier caps just below the support locations. The parapets have experienced a considerable amount of concrete spalling, exposing some of the reinforcing steel. Finally, additional asphalt overlays have been added to the bridge, covering the expansion joints and bringing the thickness of the current wearing surface to approximately 280 mm.

In March of 1994, the bridge was analyzed and rated by the Delaware Department of Transportation using BRASS (1987). The analysis, which incorporated an estimate of the corrosion damage to the girders, indicated that load restrictions were needed. The computed inventory, operating, and posting rating factors for Delaware's seven rating vehicles are shown in Table 1. The rating factors for posting range from 0.72 to 1.39. In Delaware, rating factors for posting are taken to be equal to two-thirds of the inventory rating plus one-third of the operating rating. All ratings were governed by insufficient midspan moment capacity of the center span. As a result of the analysis, the bridge was posted for several vehicle types, partially restricting truck traffic.

Based on the fact that the center span controls the current posting, only this span was instrumented. Demountable strain transducers were attached to all girders at midspan and to selected girders at locations halfway between the end of the girder and the first internal diaphragm. The transducers were connected to a digital data acquisition system, which recorded strain histories caused by the loading vehicle. All transducers were mounted using either c-clamps or a quick-setting adhesive applied to special mounting tabs. In all, 32 strain transducers were used. The location and number assigned to each transducer are shown in Fig. 2. For the numbering, T signifies that the transducer is attached to the top of the girder and B to the bottom.

The loading vehicle used was a three-axle, single-unit truck (S335) weighing 223 kN. This weight was slightly less than the rated posting (231 kN) for the three-axle configuration. With the bridge temporarily closed to traffic (a few minutes at a time), the truck was slowly driven across the bridge (at approximately 8 km/hr) and strain data, as a function of truck location, was recorded for each channel at 32 Hz. After each truck pass, strains were monitored to ensure that they went back to zero (i.e., no permanent deformation). In order to obtain meaningful data regarding both transverse and longitudinal load distribution, the truck's driver-side wheels were driven along three marked paths denoted P1 - P3 (see Fig. 2), each having a different transverse position on the deck. In order to ensure consistent results, measurements were taken as the truck made two passes along each path. Six truck passes were needed to collect all of the data, and the entire field test was completed in a single day.

A typical strain history measured by transducers on a girder's top and bottom flanges at midspan is shown in Fig. 3. Note that positive strains indicate tension. During the field test, the maximum strain recorded was 73 microstrain. This value of strain corresponds to a tensile stress of 14.5 MPa (2.1 ksi), well below the steel's allowable tensile stress.

BRIDGE ANALYSIS

In order to estimate a safe load rating for the bridge, a finite element model was created based upon the data from the diagnostic test. A planar grid model of the main structural elements, combined with a plate element representing the deck, was used. The plates allowed accurate transverse distribution of wheel loads to the girders.

From the measured data, two important characteristics of the bridge were identified. First, under the loads applied, it was evident that unintended composite action between the girders and the deck was occurring (see Fig. 3). Second, the longitudinal strain distribution observed along the girders indicated that some degree of support restraint, referred to by Bakht and Jaeger (1990, 1992) as bearing restraint forces, was developed.

The determination of composite section properties for the girders involved a series of steps including (1) the identification of the neutral axis location from the measured strain data, (2) the determination of an effective deck thickness, and (3) the final calculation of section properties including the composite moment of inertia.

Even though the bridge was designed to have pin-and-roller joints, modifications to the supports by maintenance forces (which involved field-welding of the bearing plates to the ends of the girders) introduced a measurable amount of restraint. One way to model bearing restraint forces is to incorporate a rotational spring into the model at the supports. To determine the appropriate rotational spring constant, one can begin by looking at strain measurements along the length of a girder when the centroid of the loading vehicle is at midspan. If there were no end restraint (ideal pin-roller boundary conditions), the strains would go to zero at the reaction. In this case the absolute value of the end-to-midspan strain ratio would be equal to zero. If the ends of the girder were completely restrained (fixed boundary condition), the absolute value of the end-to-midspan strain ratio would be equal to one. By computing the measured end-to-midspan strain ratio, the degree of restraint or percent of fixity can be determined, and an appropriate rotational spring stiffness, k_s, can be found. In this case, the measured end-to-midspan strain ratio was estimated to be 0.20 (i.e., 20 percent fixity) for both interior and exterior girders.

Once all of the parameters for the model were established, the test truck was placed on the model at 11 discrete locations along each of the three loading paths (a total of 33 truck positions). For each truck position, an analysis was performed. In order to compare the computed results to those measured in the field, computed moments were used to find strains at each of the gage locations. Fig. 4 illustrates the accuracy of the model in predicting the longitudinal load

distribution by comparing measured and computed strains along the bottom face of girders 2 and 4. To see how well transverse load distribution is predicted, Fig. 5 compares the measured and computed strains on the bottom face of each girder at midspan. In both cases, the finite element model does a good job of capturing the recorded bridge response.

In addition to the visual data comparison, the accuracy of the model was also evaluated statistically. By utilizing 1,056 comparisons between measured and computed strains (33 truck locations times 32 strain transducers), absolute error, percent error, scale error, and a correlation coefficient were computed. The absolute error was 1850 microstrain (on average, this represents an error of less than 2 microstrain per reading). The percent error and scale error were 7.9 and 10.0 percent respectively, and the correlation coefficient was 0.97. These values, like the visual comparisons, indicate the high degree of accuracy of the numerical model.

BRIDGE LOAD RATING BASED ON FIELD TEST RESULTS

Having developed an accurate numerical model of the center span, the bridge could now be load rated. However, because the applied load was limited to a 223 kN truck, two important decisions regarding modeling assumptions needed to be made in order to extrapolate results to higher loads. The decisions were whether unintended composite action and/or unintended support restraint should be counted on at the higher loads.

Several factors should be considered in deciding whether or not to utilize the additional strength caused by unintended composite action. These factors include the current condition of the bridge, its past and future traffic history, the amount of structural redundancy, and the potential for future nondestructive structural evaluation. In this case, the condition of the deck and girders was relatively good. Neglecting the three months immediately prior to the load test during which the bridge had been posted, there was no reason to expect a change in traffic patterns from earlier years if the bridge were unposted. Since the bridge had maintained composite action to date, there was nothing to suggest that it would abruptly lose composite action in the future. Furthermore, since nine longitudinal girders carry two lanes of traffic, the bridge has a high degree of redundancy, and a loss of composite action would be likely to occur gradually and not result in a sudden failure.

Based on this evidence, it appears reasonable to include the effects of composite action in the final load rating of this particular bridge. If the bridge rating is to be based on unintended composite action, a relatively frequent inspection program is recommended. Future inspections should include examination of the deck-girder interface. If integrity of the composite action is ever in question, additional load tests using ambient traffic should be performed to determine neutral axis locations.

With regard to the supports, it may not be as reasonable to rely on this unintended restraint at higher load levels. The restraint is a result of repair work done to the bridge, which involved welding the ends of the beams to their bearing plates. This restraint has led to cracking of the piers just below the support locations. Because of the poor condition of the piers, which implies that significant bearing forces can develop, it seems reasonable to base the final load rating of this bridge on a model that neglects support restraint (i.e., has simply supported boundary conditions). In fact, by repairing the supports and restoring simply supported conditions, further damage to the piers may be prevented.

Based on this reasoning, a finite element model incorporated composite section properties and simply supported ends (i.e., no support restraint) was used to evaluate and rate the bridge. Rating factors (RF) for each bridge element were computed based on the equation

$$RF = \frac{C - A_1 D}{A_2 L (1 + I)} \quad (1)$$

where C is the member capacity based on a specified stress limit, D is the maximum stress developed due to dead loads, L is the maximum stress developed due to live loads, I is the impact factor, and A_1 and A_2 are the dead-load and live-load factors for LFD rating respectively. Results from the load test and the finite element analyses were used to determine the terms in Eq. 1. Member capacities were defined based on the measured neutral axis location and the inventory and operating stress levels. In this case, limiting values for inventory and operating stresses for the steel girders were taken to be 124 MPa (18 ksi) and 172 MPa (25 ksi) respectively. These values were based on an assumed steel yield strength of 227 MPa (33 ksi), which was chosen due to the age of the structure. An impact factor of 27 percent, as suggested in AASHTO (1989), was used. Live-load and dead-load effects were computed using the finite element model. Since the entire bridge is modeled as a system, the use of a distribution factor to determine load effects on a particular beam was not necessary. Instead, to account for multiple-lane loadings, several truck paths were defined for the rating vehicles, and stresses computed for each path were superimposed to obtain the maximum live-load response.

For each of Delaware's seven rating vehicles, critical inventory and operating rating factors were computed . Based on the analyses, rating of the exterior girders was controlled by two lanes being loaded, while three lane loads combined with the 10 percent reduction (AASHTO 1989) controlled the rating of the interior girders. In all cases, the final load ratings were governed by flexural stresses in the interior girders. The computed rating factors are given in Table 1.

Since unintended composite action was utilized, values of horizontal shear stresses at the concrete slab/steel flange interface were checked and found to acceptable based on recommendations made by Lichtenstein (1995). These recommendations suggest that limiting bond strengths of 0.48 MPa (70 psi) for non-imbedded flanges, and 0.69 MPa (100 psi) for partially or fully embedded flanges, can be conservatively used.

SUMMARY AND CONCLUSIONS

Nondestructive methods for experimental field testing of bridges have been discussed. Existing methods are relatively simple to conduct, and results can be used to gain a better understanding of a bridge's structural condition and behavior. Using information gathered during a field test, engineers can evaluate the bridges load-carrying capacity. In addition, data gathered during a diagnostic field test can be used to develop accurate mathematical models of a bridge, which in turn can be used to numerically investigate stability issues.

Also presented in this paper is a summary of a diagnostic field test of a posted, three-span, steel-girder-and-slab bridge. Using the test results, bridge inspections reports, field observations, and engineering judgment, inventory and operating load ratings for Delaware's seven load vehicles were computed and found to range from 0.99 to 1.83 and 2.16 to 4.00, respectively. Using these ratings, the posted rating factors range from 1.38 to 2.55. These results indicate that the bridge's load-carrying capacity may be substantially higher than the current load levels indicate (recall that the current posted rating factors range from 0.72 to 1.39) and suggest that the posting levels on the bridge may be unnecessary.

ACKNOWLEDGMENTS

The authors are grateful for support of this work provided by the Delaware Department of Transportation through the Delaware Transportation Institute (Grant No. TRA/DTI-4222312018). The authors would also like to acknowledge the help of the Delaware Department of Transportation

with special thanks being extended to Chao Hu, Muhammad Chaudhri, Dennis O'Shea, Chuck Lightfoot, and Steve Bunting for their contributions. We would also like to thank graduate students William Finch, Jr., Scott Holsinger, Ted Januszka, and Ted Thomson, Jr., who helped during the instrumentation and field testing of the bridge. Finally, we would like to recognize the efforts of undergraduate students Cortney Dula and Cory Farschman, who not only helped with the bridge testing, but also spent many hours analyzing data and developing preliminary computer models.

REFERENCES

AASHTO (1989). "Standard Specification for Highway Bridges." Washington, D. C.

Aktan, A. E., and Raghavendrachar, M. (1990). "Nondestructive Testing and Identification for Bridge Rating: Pilot Project." FHWA/OH-90/005 Final Report.

Aktan, A. E., Chuntavan, C., Lee, K. L., Toksoy, T. (1993). "Structural Identification of a Steel-Stringer Bridge." *Preprint, TRB Paper 930560*, Transportation Research Board, 72rd Annual Meeting, Washington, D. C.

Bakht, B., and Csagoly, P. F. (1979). "Bridge Testing." Ministry of Transportation and Communication, Ontario, Canada.

Bakht, B., and Jaeger, L. G. (1990). "Bridge Testing - A Surprise Every Time." *J. Struct. Engrg.*, ASCE, 116(5), 1370-1383.

Bakht, B., and Jaeger, L. G. (1992). "Ultimate Load Test of Slab-on-Girder Bridge." *J. Struct. Engrg.*, ASCE, 118(6), 1608-1624.

BRASS 4.2, Wyoming State Highway Department, Cheyenne, WY, Copyright 1987.

Burdette, E. G., and Goodpasture, D. W. (1988). "Correlation of Bridge Load Capacity Estimates with Test Data." NCHRP Report 306, Transportation Research Board, Washington, D. C.

Commander, B. C. (1989). "An Improved Method of Bridge Evaluation: Comparison of Field Test Results with Computer Analysis." Master Thesis, University of Colorado, Boulder, CO.

Edberg, W. M. (1994). "State-of-the-Art Survey in Experimental Load Rating of Bridges." Master Thesis, University of Delaware, Newark, DE.

El Shahawy, M., and Garcia, A. M. (1989). "Structural Research and Testing in Florida." Structural Research Report No. SRR-01-89, Florida Department of Transportation, Tallahassee, Florida.

Fu, G., Sardis, P., and Tang, J. (1992). "Proof Testing of Highway Bridges." Research Report 153, Engineering Research and Development Bureau, New York State Department of Transportation.

Fu, G., and Tang, J. (1992). "Proof Load Formula for Highway Bridge Rating." *Transp. Res. Record*, 1371, Washington, D. C., 129-141.

Goble, G., Schulz, J., and Commander, B. (1992). "Load Prediction and Structural Response." Final Report, FHWA DTFH61-88-C-00053, University of Colorado, Boulder, CO.

Lichtenstein, A. G. (1995a). "Bridge Rating Through Nondestructive Load Testing." Final Report, NCHRP Project 12-28(13)A.

Lichtenstein, A. G. (1995b). "Bridge Rating Through Nondestructive Load Testing." Technical Report, NCHRP Project 12-28(13)A.

Markey, I. (1991). "Load Testing of Swiss Bridges." Steel Constr. Today, 5(1), 15-20.

Moses, F., Lebet, J. P., and Bez, R. (1994). "Applications of Field Testing to Bridge Evaluation." *J. Struct. Engrg.*, ASCE, 120(6), 1745-1762.

Pinjarkar, S. G., Guedelhoefer, O. C., Smith, B. J., and Kritzler, R. W. (1990). "Nondestructive Load Testing for Evaluation and Rating." NCHRP Project 12-28(13) Final Report.

Schulz, J. L. (1989). "Development of a Digital Strain Measurement System for Highway Bridge Testing." Master Thesis, University of Colorado, Boulder, CO.

Schulz, J. L. (1993). "In Search of Better Load Ratings." *Civil Engineering*, ASCE 63(9), 62-65.

Table 1. Current and Computed Rating Factors

Rating Vehicle	Inventory		Operating		Posting	
(GVW kN/tons)	Current	Computed	Current	Computed	Current	Computed
HS20T (320/36)	0.51	1.11	1.43	2.42	0.82	1.55
S220 (178/20)	0.86	1.83	2.43	4.00	1.39	2.55
S335 - (312/35)	0.46	1.01	1.29	2.20	0.74	1.41
S437 - (325/36.5)	0.45	0.99	1.27	2.16	0.72	1.38
T330 - (267/30)	0.70	1.57	1.98	3.43	1.13	2.19
T435 - (312/35)	0.64	1.33	1.80	2.91	1.03	1.86
T540 - (356/40)	0.57	1.20	1.59	2.61	0.91	1.67

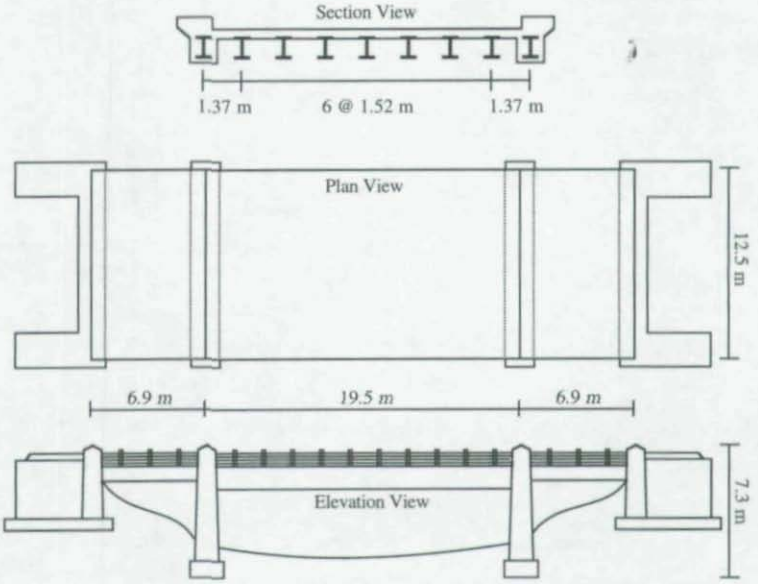

Figure 1. Section, Plan, and Elevation Views of Test Bridge

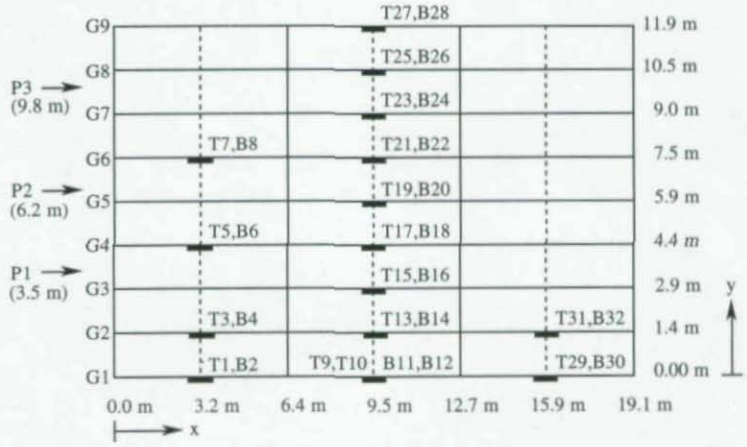

Figure 2. Location of 32 Transducers and Three Paths for Loading Vehicle

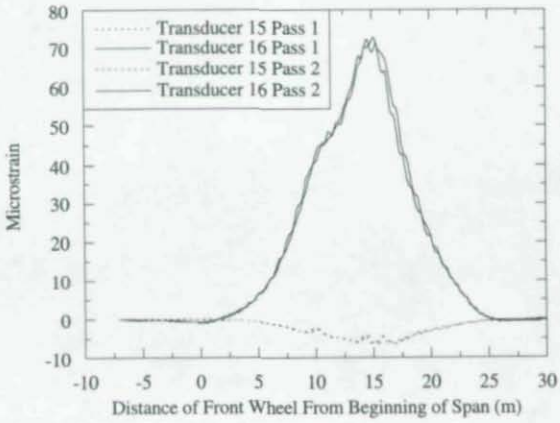

Figure 3. Recorded Strains at Midspan of Girder 3 Due to Loading Vehicle on Path P1

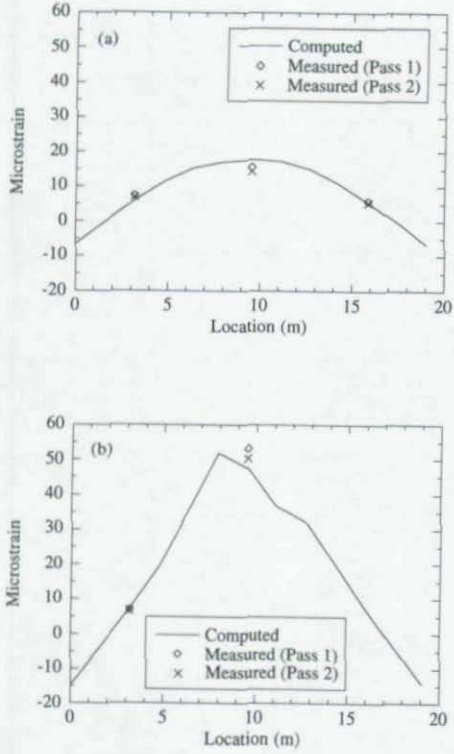

Figure 4. Comparison of Measured versus Computed Strains Along Girders Due to Loading Vehicle on Path P2 with its Centroid at Midspan: (a) Girder 2; (b) Girder 4

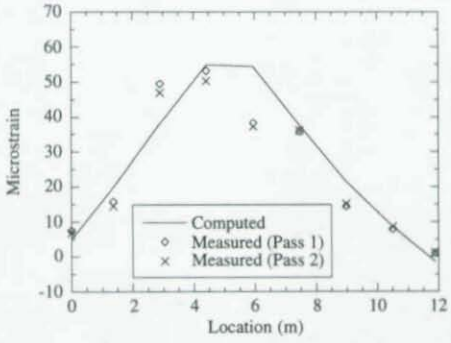

Figure 5. Comparison of Measured versus Computed Strains Across Midspan Due to Loading Vehicle with its Centroid at Midspan on Path P2

BRIDGE DETERIORATION

John T. DeWolf
Professor of Civil Engineering
University of Connecticut
Storrs, Connecticut, U.S.A.

INTRODUCTION:

The National Science Foundation has noted the need for the development of a cohesive strategy for renewal of the U.S. civil infrastructure. Four key research areas are deterioration science, assessment technologies, renewal engineering and institutional effectiveness and productivity. Included in these is the enhancement of system performance and ensuring the longevity of existing and future infrastructure systems. As noted by Bordogna (1), current methods are relatively primitive and unreliable, prompting conservative, often costly decisions. He further notes the need for research in nondestructive evaluation techniques.

With few exceptions, bridges are presently monitored with visual techniques. It is not always possible to see all critical areas, with the result that problems go unnoticed until they become serious. This approach also does not provide information between inspections. A bridge with a problem would require more frequent inspections, requiring additional manpower. Fortunately, failures have been limited. Those that have occurred have been disastrous (Mianus bridge in Connecticut in 1983 and the Schoharie bridge in New York in 1987 are examples).

Work during the past decade at the University of Connecticut has been directed toward field monitoring of bridges, involving both strain measurements and vibrational studies. We presently have a fully operational monitoring system mounted on a Connecticut bridge and portable equipment for short term studies, as needed. This work has resulted in substantial savings to the State of Connecticut by providing information in the continued efforts to renew and maintain the state's bridge infrastructure. It has also provided research information in field monitoring. This paper reviews some of the efforts at developing vibrational techniques which can be used for a systems approach to the continuous monitoring of bridges under normal traffic loading.

VIBRATIONAL MONITORING:

Many techniques are available for bridge monitoring. Those involving deformations include strain measurements and determination of deflections. These are most useful where there is a known problem so that the sensors may be located to determine specific information. They do not provide for global monitoring, which both requires that a major portion of the structure be under surveillance and requires evaluation of different potential failure mechanisms. Furthermore, since changes in strains and other deformations are relatively small, even when there is a major change in the bridge's structural integrity, these localized measurements of strains and deflections are unlikely to indicate a problem exists.

Vibrational measurements have been successfully used in many different applications for global evaluations. Manufacturing plants rely on this approach to prevent breakdowns in critical equipment which can result in serious loss to production capacities. Power plants also use vibrational measurements to maintain continued power generation. One of the benefits in using vibrational data is the wide variety of ways in which the information can be processed. This allows for development of techniques which can magnify the changes which occur when the structural integrity is compromised.

An essential requirement in bridges is the need to use continuing excitation for evaluation. A monitoring approach which requires use of a test vehicle, or other specialized loading, is limited to use only when sufficient manpower is available to operate the system. This type of inspection technique normally requires closing of the bridge to conduct the monitoring. This is not readily done with many of the more heavily trafficked bridges on the nations's highway system.

A significant portion of the work at the University of Connecticut during the past decade to adapt vibrational monitoring to bridges has involved development of new equipment and adaption of evaluative techniques. What has been done for machinery and power plants, while providing a basis of this work, has not been directly applicable to bridges. Typically, bridges are more complex than parts of manufacturing plants, with members which are neither homogeneous nor always rigidity connected together. The frequency ranges for bridges are much lower than most other applications, requiring special sensors. Loads, i.e. traffic loading, is highly variable, with different vehicle weights/sizes, vehicle suspension systems, speeds and travel lanes. The exterior environment, with all kinds of weather conditions, necessitates careful design for long-term use. Much greater care is needed in developing ways to process the data so that the vibrational signature is

able to reflect that there has been a change in the structural integrity.

The following is a review of some of the studies which are providing researchers at the University of Connecticut with some of the key components needed for a fully operational continuous monitoring system.

FIELD MONITORING STUDIES IN CONNECTICUT:

Research in vibrations at the University of Connecticut began with a study of a four span continuous steel plate girder bridge (2). The bridge longitudinal view and cross section are shown in Fig. 1. Both test vehicles and normal traffic were used to describe the vibrational behavior, determine the significance of the vibrations on the structural integrity of the bridge and make recommendations if needed on what might be done to reduce the vibrations should they have a negative influence on the bridge's structural capacity.

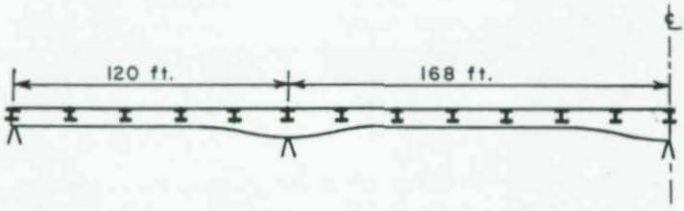

(a) Bridge Longitudinal View (Half of Symmetrical Bridge)

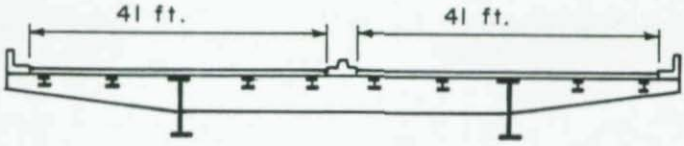

(b) Bridge Cross Section

Figure 1 Four Span Continuous Bridge

In addition to characterizing the behavior and concluding that the vibrations were not detrimental to the long-term performance of the bridge, this study of a large indeterminate bridge indicated that normal traffic could be used to characterize the global performance. The natural frequencies and mode shapes for the lowest natural frequencies were discernable from normal traffic loading. Portions of this information do no change with different vehicles, speed or travel lanes. The study also demonstrated that vibrational equipment, both sensors and processing hardware and software, needed further development for application to bridge studies. The main conclusion was that vibrational monitoring had possibilities for continuous, long-term bridge monitoring. In addition, extensive analytical work followed the field study to gain a better understanding how different factors influence the vibrational performance.

A model study was developed to learn more about how vibrational monitoring might be applied to bridges (3,4). An aluminum plate girder structure was built, consisting of two I-sections made from elements, allowing for replacement of different elements as cracks were introduced. The bridge was tested as both a single span and a two span structure. The model bridge is shown in Fig. 2. Different vehicles were pulled across the bridge at different speeds while accelerations were recorded. The ambient vibration method was employed to define the resulting behavior.

Degradation tests included both introduction of a crack into one of the I-sections and movement of different supports. The conclusions were that the ambient vibration method could be used for natural frequency and modal shape determinations, that both natural frequencies and mode shapes exhibited changes when cracks and support displacements occurred, and that the approach had potential for bridge monitoring.

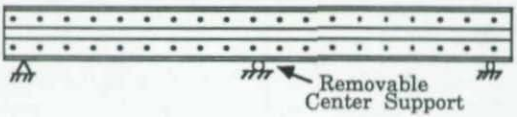

(a) Bridge Longitudinal View

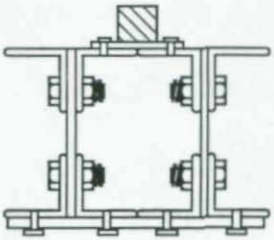

(b) Bridge Cross-Section

Figure 2 Model Bridge

Additional field tests were conducted to determine whether vibrational signatures in the form of frequency response plots were obtainable for a full scale bridge using the same equipment and methodology employed in the laboratory model study. These were also used to define requirements for both sensors and the hardware needed for interaction with the sensors in order to apply the vibrational technique to long-term bridge monitoring.

A prototype monitoring system was next developed for continuous, long-term installation on bridges. This work was carried out with support from a State of Connecticut economic development initiative in conjunction with Vibra•Metrics, a Connecticut Company specializing in manufacture of vibrational equipment. The

design of the system included development of specific sensors for use on bridges and a complete package of hardware and software for collecting the data. The system is remotely controlled and capable of collecting data on a continuous basis. The system has 16 accelerometers which provide for determination of the bridge's modal performance.

The monitoring system was first placed on a newer Connecticut single span bridge (5). The cross-section and the framing plan with accelerometer locations are shown in Fig. 3.

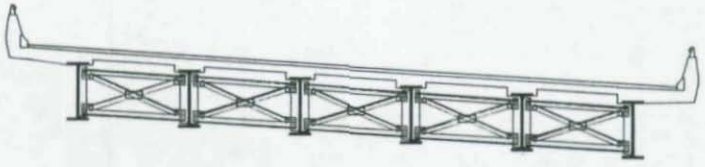

(a) Bridge Cross-Section

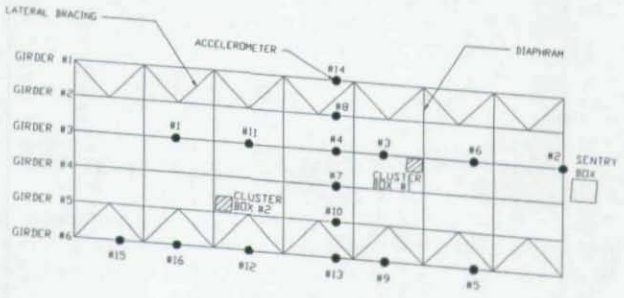

(b) Framing Plan and Accelerometer Locations

Figure 3 Bridge with Prototype Monitoring System

An example of a response spectrum is shown in Fig. 4. This spectrum plots volts (proportional to the acceleration levels) versus natural frequencies, based on data processed from a small time period. Generally, major peaks in the response spectrum correspond to natural frequencies. In bridges, only the lowest natural frequencies are measurable. The levels of excitation for higher frequencies is below the system noise levels. Different spectrum clean up techniques can reduce the noise levels and improved system resolutions can aid in determination of higher frequency levels. Most smaller and medium span bridges do not exhibit more than about 5 natural frequencies. In this study, the three lowest natural frequencies, at 2.01 Hz, 2.37 Hz and 4.16 Hz, were decipherable at most sensors in most tests. Others occurred sporadically.

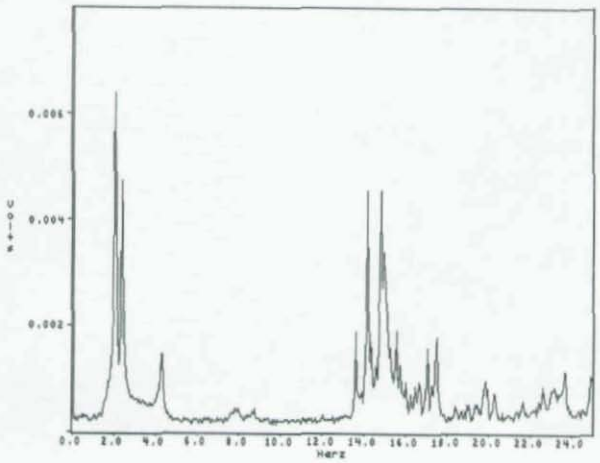

Figure 4 Example Response Spectrum

The frequency spectra for different sensors along with phase information can be processed to produce mode shapes. There are both flexural mode shapes, with longitudinal variations in displacement, and torsional mode shapes, with both longitudinal and transverse variations in displacements. The mode shapes for the first flexural and first torsional natural frequencies are shown in Figs. 5 and 6, respectively.

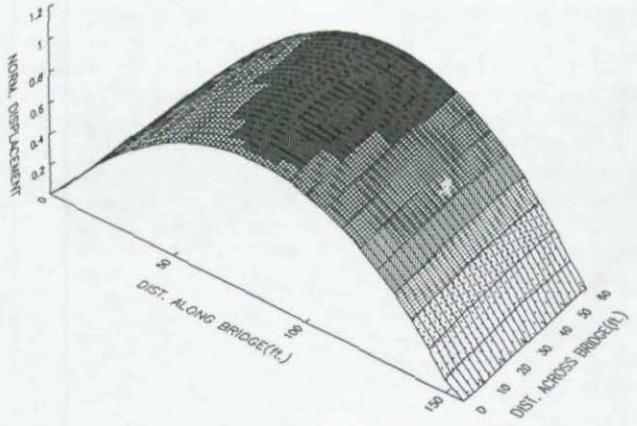

Figure 5 Mode Shape for First Flexural Mode

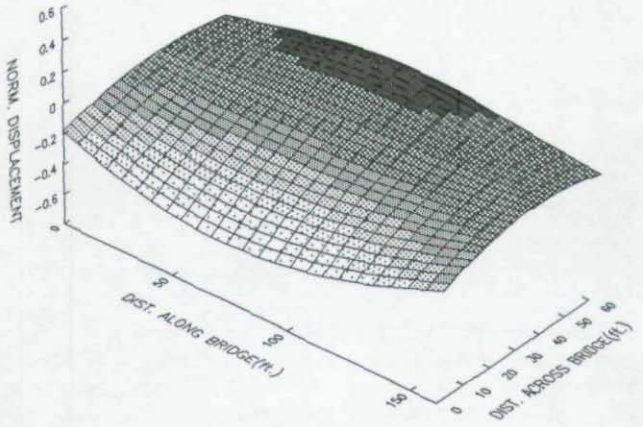

Figure 6 Mode Shape for First Torsional Mode

Both the natural frequencies and mode shapes were used to characterize the bridge, i.e. to develop a vibrational signature. The data collected during a year was analyzed statistically for stability.

Another study (6), conducted by Lauzon for the Connecticut Department of Transportation and in which researchers at the University of Connecticut participated, involved introduction of a crack into a full-scale highway bridge scheduled for replacement. The cross-section of the test span, using a portion of the width, is shown in Fig. 7. The crack was introduced into girder C near the center of the span.

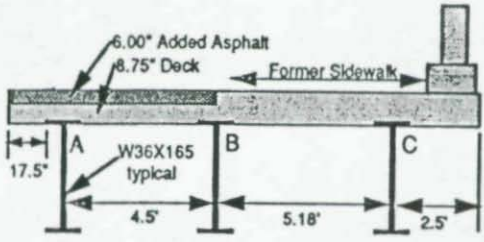

Figure 7 Cross-Section of Test Span with Failure Mechanism

The results from Lauzon's study are being evaluated to determine how actual field vibrational information can be used to predict major changes in structural integrity. Preliminary results (6) have demonstrated that changes in specific natural frequencies are not sufficient to indicate a change in the structural integrity has occurred. However, additional frequency peaks develop and can be used in this prediction. There are also substantial changes in modal shapes which can be used for monitoring purposes.

The prototype monitoring system is presently mounted on an older, continuous two-span steel girder bridge. The system resolution has been increased, allowing for better determinations of the response information. One of the considerations involved in this study is how temperature changes and frozen bearings modify the vibrational results. This work will be reported on shortly.

CONCLUSIONS:

Vibrational monitoring, based on use of normal traffic excitation, can be used to develop a signature for the bridge. The goal of this continuing work has been to use this signature as a basis for continuous monitoring to prevent catastrophic consequences.

It has been necessary to design special equipment for the vibrational monitoring in the bridges studied. It has also been necessary to use appropriate evaluative techniques. This includes the choice of software used and determination of those items which will change as the bridge's structural integrity changes. Frequency based comparisons are in themselves not adequate. The modal shapes offer more information for monitoring purposes. Statistical evaluation of the resulting data must be used with carefully developed evaluative techniques. These are now under development.

ACKNOWLEDGMENTS:

This continuing research at the University of Connecticut was conducted with assistance from the State of Connecticut thorough their economical development efforts, the Connecticut Department of Transportation and Vibra•Metrics, Hamden, Connecticut. Graduate students contributing to this effort have included Jine-Wen Kou, Andrew Rose, Robert Lauzon, David Mazurek, Ronald Paproski, Patrick O'Leary, Dean Bagdasarin and Patricia Conn.

REFERENCES:

1. Bordogna, J., "Intelligent Renewal Keeps Infrastructure Civil," Civil Engineering, March 1994, p. 6.

2. DeWolf, J.T., Kou, J.W. and Rose, A.T., "Field Study of Vibrations in a Continuous Bridge," Third International Bridge Conference, Pittsburgh, Pennsylvania, June 1986, pp. 103-109.

3. DeWolf, J.T., Lauzon, R.G. and Mazurek, D.F., "Development of a Bridge Monitoring Technique," Proceedings: Bridge Research in Progress, Iowa State University, Ames, IA, September, 1988, pp. 65-68.

4. Mazurek, D.F and DeWolf, J.T., "Experimental Study of Bridge Monitoring Technique," Journal of Structural Engineering, ASCE, Vol. 116, No. 9, September, 1990, pp. 2532-3549.

5. O'Leary, P.N., Bagdasarian, D.A. and DeWolf, J.T., "Bridge Condition Assessment Using Signatures," Proceedings of Conference on Nondestructive Evaluation of Civil Structures and Materials, University of Colorado, Boulder, Colorado, May 1992, pp. 171-179.

6. Lauzon, R.G. and DeWolf, J.T., "Full-Scale Bridge Test to Monitor Vibrational Signatures," Structural Engineering in Natural Hazards Mitigation, ASCE Structures Congress, 1993, pp. 1089-1094.

EXPERIMENTAL EVALUATION: Aging, Deteriorated and Damaged Structures

Peter C. Birkemoe[1]

INTRODUCTION

The purpose of this paper is to help define the role of **"experimentation"** in the general area of maintenance, rehabilitation and repair and in the particular area of structures which through wear, time or catastrophe require engineering evaluation and solutions to maintain safe operation or extend the use of the structure to new functions. Another aspect of the discussion is that only problems related to the stability of metal structures are addressed.

Experimentation and measurement are viewed as synonymous in this context and thus whether a laboratory controlled study or the measurement of geometric properties of a structure for engineering evaluation, similar principles and goals are involved. And it can be shown that laboratory and field measurements both contribute to the general knowledge of structures and have a global effect on engineering practice through the modification and interpretation of codes and standards.

The evaluation of structures with significant information often permits more sophisticated analytical techniques which remove conservatism associated with uncertainties that were present in the original design time. Analytical modelling methods which are often evaluated through direct comparison with physical modelling can now be used to advantage to obtain, for example, improved evaluations of residual strength, including many parameters explicitly known through measurement.

STRUCTURAL CHANGES

The changes that tend to affect stability related behavior are those which affect dimensions and/or stiffness, and an important aspect that separates this topic from conceptual design is the fact that we are dealing with an existing structure and thus have more information of a specific nature than one generally has at hand in original designs. Structural changes that cause reason for any evaluation can be classified broadly as follows:

- USAGE

  Functional requirements change with owners, activities, markets etc. and generally have increased demands on the structure from the standpoint of load magnitude, frequency and location. Increases in dead load through repairs and maintenance as well as major reductions resulting from alternative materials contribute to the structural changes associated with use.

- VOLUME

  Material loss through wear or corrosion essentially produces a structure which is weaker and

---

[1] Professor, Department of Civil Engineering, University of Toronto
35 St. George Street, Galbraith Bldg. 213, Toronto, Ontario M5S 1A4 CANADA
Telephone (416) 978-5908 Fax (416) 978-6813

more flexible as the result of volume/thickness changes. Although not in the same realm, structural modification such as the removal of portions of the structure to accommodate an unrelated activity can be included in this category.

- SHAPE

The configuration of a structure may be changed enough to render it globally or locally weaker than it was in its initial configuration; similarly material properties may be changed and although not "geometric" the results may be similar. Examples of changes in this category include distortion by fire, collision and overload. The nature may be local (dented or partially collapsed cross sections), global (frames over loaded in a storm or collision to cause permanent deformations) and material response (altered yield strength or ultimate strength in metal structures) as a result of fire or strain hardening from a seismic event.

Thus the changes in geometry, stiffness and loading while within these broader changes in structures can be in turn related to stability considerations which must be addressed to provide a reliable performance and adequate safety. From the point of view of stability, these structural changes which are of concern in most structural designs must be addressed in light of the evaluations of the conditions that exist in the structure rather than those established as the norm or defined in terms of accepted standards or tolerances. It is here that the measurement of the condition of the structure becomes an essential element of the evaluation and solution.

MEASUREMENT / EXPERIMENTATION

Measurement is the substance of what one does in experimentation and thus it can be viewed as part of the evaluation and assessment process and may become an integral part of the design. Three specific "areas" or "examples" will be cited here to show the association. Others could be added, but these were chosen to cover the situations described above and to relate to the theme of "aging, deteriorated and damaged structures."

- Structures "as built" and "as they are after a while"

Steel bridge design is an exercise in functional geometry applied to pedestrian, highway and rail transport. In fabrication the geometric specifications (tolerances) have a major impact on the economy, rate and cost. Bridge standards generally have very stringent tolerances some of which are not always achieved in practice.

Korol and Thimmhardy[2] followed the fabrication and erection of several major bridges to determine the nature of the "as-fabricated and as constructed" imperfections in plate and box girder bridge construction. They devised some laboratory equipment which had a degree of simplicity and certainty that made measurements of the geometry of plates and stiffeners quite accurate and straight forward. This study showed, as others have, that many techniques of

[2] Thimmhardy, E. G. and Korol, R. M., "Geometric imperfections and tolerances for steel box girder bridges, Canadian Journal of Civil Engineering, Vol. 15, No. 3, 1988, pp437-442.

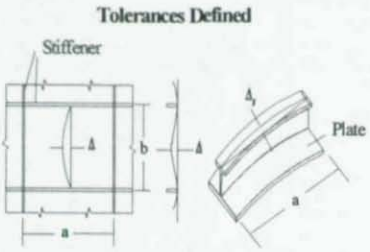

Fig.1 Measurements of Distortion

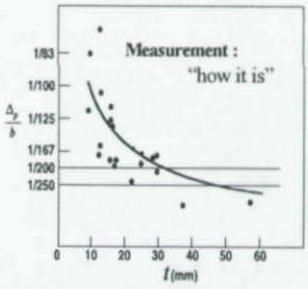

Fig. 2 Distortion as a Function of Thickness

measurement developed for the laboratory environment have direct application to field problems. Their study followed the fabrication and erection of bridges and compared the several Canadian bridges to the prescribed tolerances. The deviations from the ideal were generally measured as they are prescribed in terms of an amount relative to the nominal length of the element involved, see Fig 1. A sample of their findings, in Fig.2, illustrates what is often found in field measurements: the nature and/or magnitude of the distortion is not as indicated by the tolerances which are prescribed in specifications. The out-of-straightness, as a function of the panel width, is shown to exceed typical specification requirements of 1 in 200 as the thickness of the plate decreases. The results of studies of this nature should influence the revision of standards to reflect the reality of what can be achieved and may, as well, lead to modifications in specification formulas for design.

- CORROSION "a slowly changing geometry"

The long term effect of corrosion of metal structures are many, but from the stability and strength standpoint it is a simple dimensional reduction which increases stresses and generally causes a degradation in stiffness parameters which in turn reduce buckling strength. Current examples of corrosion problems are found in the offshore oil production industry and in the transportation industry.

In current research at Lehigh University under the direction of Ostapenko and Ricles, the corrosion effect on tubular members in offshore platforms are being quantified through experimentation on members removed from structures taken out of service. This work provides an example of experimentation which, unlike the previous example which involved laboratory measurements in the field, brings the reality of the field into the test laboratory. Rigorous measurement of the ansata geometry is being correlated with measured strength while models for the analytical determination are being developed to assess strength reduction and to determine the need and feasibility of repair. This joint industry sponsored research also is examining methods of repair for field application; again, experimental and analytical evaluation

are being carried out to provide a comprehensive solution. One of the biggest challenges has been the characterization of the corrosion which may be uniform but is more commonly characterized by a random thickness reduction with local perforation. Mapping of the corrosion condition in the field will be a major consideration in the evaluation of the safety of existing structures. Experimental techniques developed in the laboratory will provide guidance for these procedures.

The research described above is directed toward tubular members, but the approach can also being used for the evaluation of bridge and building structures which have been exposed to a corrosive environment.

- DENTING and DISTORTION "assessing visible damage"

The third example of experimental applications deals with the damage through denting and distortion of members which results from impact with an object or the experience of an excursion of overload which causes permanent large deformations in the member or structure. The experimental evaluation of dented tubular member has been underway for the past two decades, spurred principally by the offshore oil and gas industry. Here, damage of members in heavily redundant structures does not lead to collapse but rather a potential weakening and the assessment of theat weakening is a major economic and safety consideration.

Recent examples of "partially" failed structures and structural elements in the earthquake in Japan indicate that a general need exists for the evaluation structures which have been damaged. In the damage aftermath numerous examples of buckled structures which were still standing showed that knowledge of the postbuckled strength could be of great benefit in safety assessment; classical buckling distortions could be related to experimental studies which had measured and led to the development of models. Field measurement of the configuration of damaged structures is necessary for modelling the subsequent behavior and techniques and guidelines must be developed in this "new surveying."

SUMMARY

Through a few selected examples, the relationship has been between "experimentation" and the evaluation of "structures that have changed" has been illustrated. An attempt has been made to show that the classical techniques of the laboratory can be extended to the field and that anywhere measurement is involved one has the essential element of experimentation. With the growth of sophistication in analytical capability potential practical benefits require the need for more "real" information through measurement. Some industries have been dealing with this problem and have provided insight for applications to other areas. In dealing with aging, deteriorated and damaged structures the paramount need for quantitative field assessment has been reinforced.

AN ANALYTICAL/EXPERIMENTAL VERIFICATION STUDY FOR LOCATING DAMAGE IN STRUCTURAL SYSTEMS

John B. Kosmatka[1] and James M. Ricles[2]

ABSTRACT

A methodology is presented for detecting structural damage in structures by nondestructive means. The procedure is based on using experimentally measured modes in conjunction with a procedure that used vibratory residual forces and a weighted sensitivity analysis to estimate the extent of mass and/or stiffness variations. The method was applied to a ten-bay space truss, and is shown to accurately predict the severity of stiffness change as well as any change in mass for four different damage scenarios.

INTRODUCTION

Structural systems are susceptible to structural damage over their operating lives due to impact, operating loads, fatigue, and corrosion. Undetected member damage can result in the failure of the components of the structure, including fracture in tension or instability under compression. Consequently, the structural system's integrity and safety can become jeopardized. In the past, numerous damage inspection methods and monitoring systems have been developed. Examples include: x-ray; electron scanning; ultrasound; magnetic resonance imagery; coin tapping; dye penetration; visual inspection. These methods tend to be time consuming for they are local assessments, often requiring the exposure of structural elements to the inspector and equipment for detecting damage.

As an alternative, and which forms the basis for the current study, is to recognize that modal vibration test data (structural natural frequencies and mode shapes) characterize the state of a structure [Ewins 1984]. Therefore, modal data acquired at different periods during a structure's life can be used to distinguish whether change (e.g. damage) has occurred, by comparing these data with a set of baseline data. Modal testing as a means of inspection has many advantages, which lead to a reduction in schedule and costs. Included among these advantages are that the direct exposure of the structural elements is not required while more of the complete structure can be inspected in one modal test.

The past use of modal test data to locate structural damage has been utilized to evaluate the integrity of offshore oil and gas platforms [Vandiver 1975; Coppolino and Rubin 1980], composite laminates [Crawley and Adams 1979a], continuum structures [Adams et al. 1978, Crawley and Adams 1979b; Park et al. 1988; Stubbs and Osegueda 1990], and recently large space structures [Smith and Hendricks 1987; Chen and Garba 1988; Stubbs et. al. 1990]. All of this previous work have a severe limitation, for they are based on an approach that assumes the

[1]Associate Professor of Applied Mechanics, Department of Applied Mechanics and Engineering Sciences, University of California, San Diego, La Jolla, CA.
[2]Associate Professor of Civil Engineering, Department of Civil and Environmental Engineering, Lehigh University, Bethlehem, PA.

system's mass is constant and changes in vibration characteristics are associated with only stiffness variations. Furthermore, these approaches do not account for variations in the mode shapes, uncertainty in structural parameters, as well as instrumentation accuracy.

Presented in the current study is a new methodology for non-destructive detection of damage in flexible structures [Ricles and Kosmatka 1992, Kosmatka and Ricles 1993]. This methodology uses measured modal data along with a correlated analytical structural model to: (1) first locate potentially damaged regions using residual modal force vectors (based on Chen and Garba 1988); and then, (2) to conduct a weighted sensitivity analysis (based on Collins et al, 1974) to assess the extent of mass and/or stiffness variations, where damage is characterized as a reduction in stiffness. The current approach is unique among all existing approaches, in that it accounts for: (1) variations in a system's mass, stiffness, and center of mass locations; (2) perturbations of both the natural frequencies and modal vectors; and, (3) statistical confidence factors for the structural parameters and potential experimental instrumentation error. Results associated with four structural damage configurations for a ten-bay space truss are presented. These results illustrate the potential of the approach and serve to validate its reliability.

THEORETICAL BACKGROUND

The methodology for the nondestructive damage detection procedure is shown in Fig. 1, where the algorithm is shown to consist of three main steps: (1) modal testing and correlation; (2) location of potential damage regions; and, (3) assessment of the severity of damage. In the modal testing and correlation phase, an experimental modal survey is performed on the baseline (undamaged) structure to obtain measured system vibration properties Λ_0, which includes the natural frequencies ω_0 and modes shapes Φ_0. These measured properties are subsequently used to develop a correlated (baseline) analytical model using a system identification technique, which is similar to that for assessing the severity of damage and will be discussed more later. The corresponding analytical vibration properties are noted as Λ_a and include modes shapes (Φ_a) and frequencies (ω_a). This analytical model is used as a basis for comparison in the remaining two steps of the algorithm. The second step of the algorithm involves conducting a modal survey on the structure after it has been in service, in order to measure the vibration properties Λ_d, which includes natural frequencies $\mathbf{w}_d$ and mode shapes Φ_d. The subscript d is used to designate the structural configuration that includes the potential damage. The properties Λ_d are used to identify regions in the structure where potential damage is located. The final step in the procedure is to assess the severity of damage, by calculating structural parameters $\mathbf{r}_d$ in damaged regions using a sensitivity analysis. The sensitivity analysis involves the use of the vibration properties Λ_a and Λ_d.

The selection of modes that are used to develop the correlated analytical model are based on three criteria: (1) a smaller frequency $\Delta\omega$ between Λ_0 and Λ_a compared to Λ_0 and Λ_d; (2) a superior set of modal assurance criterion (MAC) values between Λ_0 and Λ_a compared to Λ_0 and Λ_d; and, (3) an adequate cross-orthogonality vector check (COR) between Λ_0 and Λ_a. Considering the ith mode, and Λ_0 and Λ_d, the frequency shift and MAC values are:

$$\Delta\omega_i = (\omega_i)_0 - (\omega_i)_a \tag{1}$$

$$MAC_i = \frac{\left[\sum_{j=1}^{N} (\phi_{ji})_0 (\phi_{ji})_a\right]^2}{\sum_{j=1}^{N} (\phi_{ji})_0^2 \sum_{j=1}^{N} (\phi_{ji})_a^2} \tag{2}$$

and for all modes

$$COR = \Phi_0^T \mathbf{M}_a \Phi_a \tag{3}$$

in which $\mathbf{M}_a$ is the analytical mass matrix, and j the instrumentation measurement location in the modal survey. The assessment for Λ_0 - Λ_a is performed by replacing Λ_a with Λ_d in Eqs. (1) through (3). The first criteria (e.g. Eq. (1)) is sometimes difficult to satisfy, and can be omitted if the MAC and cross-orthogonality vector check values are superior in nature.

Location of Damaged Regions

Identifying the location of damage in the structure is based on differences in measured modal properties (Λ_d) and the baseline (Λ_0) values through the use of an extended application of the residual force method [Chen and Garba 1988]. In concept, the experimental natural frequencies and modes shapes must satisfy an eigenvalue equation, where considering the ith mode of the potentially damaged structure

$$\left(\mathbf{K}_d - \lambda_{d_i} \mathbf{M}_d\right) \phi_{d_i} = 0 \tag{4}$$

in which $\mathbf{K}_d$ and $\mathbf{M}_d$ are the experimental (unknown) stiffness and mass matrices associated with the damaged structure, respectively, and λ_{d_i} is the experimental measured eigenvalue corresponding to the experimental measured ith mode shape ϕ_{d_i} of the damaged structure. Assuming that the stiffness and mass matrices associated with the damaged structure are defined as

$$\mathbf{K}_d = \mathbf{K}_a + \Delta\mathbf{K} \tag{5a}$$

$$\mathbf{M}_d = \mathbf{M}_a + \Delta\mathbf{M} \tag{5b}$$

where $\mathbf{K}_a$ and $\mathbf{M}_a$ are the baseline stiffness and mass matrices of the analytical model, respectively, and $\Delta\mathbf{K}$ and $\Delta\mathbf{M}$ are the unknown changes in the stiffness and mass matrices as a result of damage, respectively. Substituting Eq. (5) into Eq. (4) and rearranging, one arrives at the definition of the residual force vector for the ith mode ($\mathbf{R}_i$):

$$\mathbf{R}_i = -\left(\Delta\mathbf{K} - \lambda_{d_i} \Delta\mathbf{M}\right) \phi_{d_i} \tag{6a}$$

$$= \left(\mathbf{K}_a - \lambda_{d_i} \mathbf{M}_a\right) \phi_{d_i} \tag{6b}$$

where the right-hand side of Eq. (6b) is known and will only be equal to zero if λ_{a_i} and ϕ_{a_i} are equal to the undamaged values of λ_{a_i} and ϕ_{a_i}, respectively. Regions within the structure that are potentially damaged correspond to the degrees of freedom that have large magnitudes in $\mathbf{R}_i$. It

should be emphasized that one should calculate the residual force $\mathbf{R}_i$ using a number of different modes, for if a damaged member is located near a node line, then the modal displacement is near zero and the residual force will also be near zero.

Magnitude of Damage Severity

The magnitude of the damage severity is determined by establishing a relationship between the measured vibration characteristics and the structural parameters (member mass, stiffness, and section geometry) in the damaged region using a first-order Taylor series expansion:

$$\Lambda_d = \Lambda_0 + \mathbf{T}\left(\mathbf{r}_d - \mathbf{r}_0\right) + \varepsilon \tag{7}$$

where Λ_0 and Λ_d are arrays containing the selected experimental measured natural frequencies and mode shapes of the initial (undamaged) and damaged structures, respectively, $[\Lambda^T = (\omega^2, \Phi)^T]$; $\mathbf{r}_d$ is an array of the unknown structural parameters in the damaged region; $\mathbf{r}_0$ the array of the initial (known) structural parameters in the same damaged region; and ε an array containing the values of testing error associated with each measured parameter (i.e. mode shape amplitudes and natural frequencies). The matrix $\mathbf{T}$ is a sensitivity matrix that relates the change in the structural parameters to changes in the vibration properties (natural frequencies and mode shapes):

$$\mathbf{T} = \begin{bmatrix} \dfrac{\partial\omega^2}{\partial\mathbf{K}} & \dfrac{\partial\omega^2}{\partial\mathbf{M}} \\ \dfrac{\partial\Phi}{\partial\mathbf{K}} & \dfrac{\partial\Phi}{\partial\mathbf{M}} \end{bmatrix}_0 \begin{Bmatrix} \dfrac{\partial\mathbf{K}}{\partial\mathbf{r}} \\ \dfrac{\partial\mathbf{M}}{\partial\mathbf{r}} \end{Bmatrix}_0 \tag{8}$$

where the subscript 0 is associated with the initial (baseline) configuration. The four submatrices in the first matrix of $\mathbf{T}$ represents partial derivatives of the eigenvalues and mode shapes with respect to the coefficients of the system's stiffness and mass matrices, whereas the second matrix of $\mathbf{T}$ represents the partial derivatives of the stiffness and mass matrices with respect to structural parameters $\mathbf{r}$.

The derivatives of the eigenvalues and modes shapes are determined using the experimentally measured vibration properties of the initial (undamaged) structure Λ_0 and baseline analytical mass matrix $\mathbf{M}_a$, where for mode k and considering instrumentation points i and j it can be shown [Collins et al. 1974, Fox and Kapoor 1968, Nelson 1976]

$$\frac{\partial\omega_k^2}{\partial\mathbf{K}_{ij}} = \frac{\phi_{ik}\phi_{jk}}{\phi_k^T\mathbf{M}_a\phi_k} \tag{9a}$$

$$\frac{\partial\phi_{rk}}{\partial\mathbf{K}_{ij}} = \sum_{n=1}^{q}\left[\frac{\phi_{in}\phi_{jk}\phi_{rn}}{\left(\omega_k^2 - \omega_n^2\right)\phi_n^T\mathbf{M}_a\phi_n}\right]\left(1 - \delta_{nk}\right) \tag{9b}$$

$$\frac{\partial\omega_k^2}{\partial\mathbf{M}_{ij}} = -\frac{\omega_k^2\phi_{ik}\phi_{jk}}{\phi_k^T\mathbf{M}_a\phi_k} \tag{9c}$$

$$\frac{\partial \phi_{rk}}{\partial \mathbf{M}_{ij}} = \sum_{n=1}^{q} \left[\frac{-\omega_k^2 \phi_{in} \phi_{jk} \phi_{rn} \left(1 - \delta_{nk}\right)}{\left(\omega_k^2 - \omega_n^2\right) \phi_n^T \mathbf{M}_a \phi_n} - \frac{\phi_{in} \phi_{jk} \phi_{rn} \delta_{nk}}{2 \phi_n^T \mathbf{M}_a \phi_n} \right] \tag{9d}$$

in which q is the number of retained modes in Λ_0 for the assessment and n is the index to identify the mode number. For structures having repeated natural frequencies, the calculated eigenvector derivatives of Eqs. (9b) and (9d) are no longer valid and one must use an approach developed by Mills-Curan [1988].

The goal of the damage severity assessment is to determine $\mathbf{r}_d$ in Eq. (7). This is accomplished by first treating the difference ($\mathbf{r}_d$ - $\mathbf{r}_0$) for all structural parameters as normally distributed random variables, having a zero mean and a specified covariance $\mathbf{S}_{RR}$ to deal with the uncertainty in the damage assessment. Treating the test measurement error also as a random variable with a zero mean and specified covariance $\mathbf{S}_{\varepsilon\varepsilon}$ leads to the solution for $\mathbf{r}_d$ from [Collins et al. 1974] as

$$\mathbf{r}_d = \mathbf{r}_0 + \mathbf{S}_{RR}^* \mathbf{T}^T \left(\mathbf{T} \mathbf{S}_{RR}^* \mathbf{T}^T + \mathbf{S}_{\varepsilon\varepsilon} \right)^{-1} \left(\Lambda_d - \Lambda_0 \right) \tag{10a}$$

where

$$\mathbf{S}_{RR}^* = \mathbf{S}_{RR} - \mathbf{S}_{RR} \mathbf{T}^T \left(\mathbf{T} \mathbf{S}_{RR} \mathbf{T}^T + \mathbf{S}_{\varepsilon\varepsilon} \right)^{-1} \mathbf{T} \mathbf{S}_{RR} \tag{10b}$$

Values for the diagonal terms (e.g., variances) in $\mathbf{S}_{RR}$ are assigned in conjunction with the results of the residual force analysis and all off-diagonal terms are set equal to zero. Only those members suspected of damage are given nonzero variances, and therefore these are the only members that are emphasized in the damage severity assessment. Hence, the diagonal terms in $\mathbf{S}_{RR}$ are in effect weighting factors for the sensitivity analysis. In the current study, all suspected members with damage were given equal variances of a value of 1.0. It should be noted that uncertainties associated with the structural parameters of the analytical model can also be considered by assigning nonzero variances. The matrix $\mathbf{S}_{\varepsilon\varepsilon}$ is usually treated as diagonal since the measurement errors are statistically independent. The magnitude of the diagonal value of $\mathbf{S}_{\varepsilon\varepsilon}$ can sometimes be difficult to estimate, and it is important to be conservative.

If the relationship between the stiffness and mass components and the structural system is linear, the current method [Eq. (10)] will converge in one step. However, the partial derivatives of the eigenvalues with respect to the stiffness and mass coefficients are nonlinear if enough damage has occurred to cause a significant frequency shift, as illustrated in Fig. 2a. To obtain a more accurate assessment of the severity of damage, it is necessary either to continuously monitor the system or to use the correlated analytical model to update the damage assessment to converge to Λ_d, as illustrated in Fig. 2b, where the subscripts 0, 1, and 2 refer to the linearization points during updating. Each update involves evaluating $\Delta \mathbf{r}_i = \mathbf{r}_d$ - $\mathbf{r}_i$, which represents the change in the structural parameters where $\mathbf{r}_d$ is from Eq. (10) considering the current structural state of $\mathbf{r}_0 = \mathbf{r}_i$, $\mathbf{T} = \mathbf{T}_i$, and $\Lambda_0 = \Lambda_i$. Here $\mathbf{r}_i$ is the current value for the structural parameters, which reflects the accumulated changes from the previous updates and $\mathbf{T}_i$ is the sensitivity matrix based on the vibration characteristics of the updated baseline analytical model (or in the case of an on-line monitoring system the measured characteristics at that time point). Convergence is achieved

when $\Delta \mathbf{r}_i$ during an update becomes less than the tolerance for convergence, with the predicted extent of damage equal to the sum of $\Delta \mathbf{r}_i$ for all update cycles, as indicated in Fig. 2b.

EXPERIMENTAL STUDY

A light-weight ten-bay statically indeterminate space truss consisting of 135 members and 44 joints (see Fig. 3(a)) was constructed. Each bay had outer dimensions of 356 by 356 mm, with the truss having an overall longitudinal length of 3327 mm. The members of the truss were fabricated from Aluminum tubing, having a nominal outer diameter and thickness of 19 mm and 4.8 mm, respectively. Each truss joint included a 25 mm diameter Aluminum ball, having 16 pre-drilled and tapped holes to accept threaded aluminum axial pins. The connection of a truss member to a joint was made by placing a tight fitting hollow truss member over an axial pin threaded into the joint, as shown in Fig. 3(b), using two set screws to secure the truss member to the joint. This method of construction was used because it enabled the truss geometry to be accurately controlled, while eliminating any initial internal member forces that could be present as a result of assembly. In addition, it permitted members to be easily replaced without disassembling the entire truss.

The boundary conditions imposed were that of a free-free support. This was achieved by suspending the structure horizontally from a test frame using elastic surgical tubing (weighing 1.68 gr/mm) which was attached to axial pins threaded into four truss joints (see Fig. 4).

Damage was simulated in the experimental model by altering Member A, which was a horizontal member in an end bay (see Fig. 3(a)), or its joints, resulting in four different experimental set-ups. These four cases of damage included:

Case A - The set screws that securely held Member A to the joints were loosened, so that the member was free to rotate on the axial pin of the joint and could only transmit compressive loads. This test simulated damage to the joints of a structure.

Case B - Member A was replaced with another Aluminum member, where this member had a series of four cross drilled holes of 12.5 mm diameter to reduce both the member's axial and bending stiffness. The new member was firmly attached to the truss joints. This test simulated damage to an individual member.

Case C - Member A was replaced with a hollow copper member, which was firmly attached to the joints. This test simulated damage to an individual member, where the copper member had a different axial stiffness, bending stiffness, and mass than the original Aluminum member.

Case D - A concentrated lead mass (58.7 grams in weight) was added to the mid-length of Member A. This test was intended to produce a reduction in measured natural frequency, as in the above three damage cases. The results of this test were used to validate the robustness of the current approach (e.g., assess whether the procedure can identify the difference between a change in localized stiffness and [illegible]alized mass).

EXPERIMENTAL RESULTS

The modal testing was performed using a small Kistler accelerometer, weighing 0.5 grams and placed at the far end of the truss in the Y-direction (see Fig. 4), along with a PCB modal impact hammer and a 16 channel Tektronic spectrum analyzer to record and process the input and output signals. The structure was excited in the X-Y-Z directions, whenever possible, using the modal hammer at each of the joints. At least 10 averages were taken at each excitation point during modal testing in order to minimize uncorrelated noise. The quality of the measured frequency data was assessed using the coherence functions, which were consistently above 0.95 at the modal peaks. A typical transfer function is plotted in Fig. 5, where the first two lower peaks near the frequency of f = 97 Hz. are associated with the first two bending modes. The second peak in the transfer function at 136 Hz. corresponds to the first torsional mode, while the wide set of peaks in the range of 220 to 230 Hz. includes the second torsional mode along with the third bending and first axial modes. The peaks above a frequency of 250 Hz. are associated with local member modes.

The SMS STAR Modal software package [STAR 1991] was used on an AST/386 computer to reduce the measured data to acquire the frequency response functions. A modal peaks search was performed on the data as well as a visual inspection to locate all possible modes. The data was then banded and curve fit in order to extract natural frequency and mode shape information for all of the configurations. Using the measured baseline modal information and the analytical finite element model, the Young's modulus (E) for the truss members and the mass of the truss joints (m) were determined by performing a separate global sensitivity analysis (i.e. model updating). The convergence criteria which was utilized involved requiring that the first bending mode of both the experimental and analytical models were nearly identical, while attempting to minimize the amount of error in the higher modes. The resulting values for E and m were 64.516 GPa and 629.9 kg, respectively.

In the current study, the residual force calculation damage severity assessment was based upon the modal information from the first-two bending and torsional modes. These four modes were selected over the higher frequency local member modes because they exhibited global deformation behavior having a measurable amount of strain and kinetic energy in each of the truss members. The experimentally measured natural frequencies of the first four modes, corresponding to the first and second bending and torsional modes, respectively, are presented in Table 1 for the baseline (undamaged) truss structure (see column 2) and for the four damage cases (columns 5 to 8). The subscript *0* and *d* are used to designate the measured frequencies for the baseline and damaged models, respectively. The baseline case includes results from both an uncorrelated and correlated analytical model with respect to the first four experimental measured modes (see columns 3 and 4). The subscripts *a,u* and *a,c* have been used to designate frequencies from the uncorrelated and correlated analytical models.

The finite element analytical model of the three-dimensional space truss was developed using MSC PAL/2 [MSC 1987], where each truss member was modeled using a beam-type element, and the joints were modeled as discrete (lumped) masses. The resulting model had 132 degrees of freedom. The natural frequencies ω_a and modes shape Φ_a of the analytical model were calculated by performing an eigenvalue analysis of the free-free structure.

The MAC values and COR result associated with the uncorrelated as well as correlated baseline analytical models are summarized in Tables 2, 3 and 4. These results indicate that an excellent agreement exist between the experimental results and the uncorrelated as well as correlated models' first-four modes. The residual forces associated with the X-axis (longitudinal axis) for the uncorrelated analytical model are shown in Fig. 6(a). Residual forces are seen to exist at all measurement points which indicate the possible need to further update (e.g., correlate) the analytical model. The results of this update is shown in Fig. 6(b), where the residual forces have become very small.

Using the calculated residual force vectors and previously described sensitivity method, the change in the stiffness and/or mass of the individual truss members for each of the four cases of damage was performed. In the current study, the variables in the sensitivity analysis included the Young's modulus E and mass density ρ for each of the 135 truss members. It was further assumed the test measurement error matrix $\mathbf{S}_{ee}$ was taken as the identify matrix (e.g., full confidence in all data). Carrying out the sensitivity calculation for the four altered set-ups produced convergence after a few iterations, where the change in stiffness and mass was negligible for all members except Member A.

The residual forces for the four cases is shown in Figs. 7 to 10, which are based on the uncorrelated analytical model. For Cases A, B, and C the X-axis forces are shown, while for Case D the Y-axis (vertical direction) are shown. In each case, larger residual forces are shown to exist at nodes 4 and 12 compared to the other nodes, as well as the baseline results shown in Fig. 6. Note that the vertical axis scale in Figs. 6 to 10 varies in order to accommodate the magnitude of the residual forces for each case. The residual forces for each mode associated with the first three damage cases are shown to be paired, where a modal residual force at node 4 is equal and opposite to that acting at node 12. The relatively larger paired residual forces at nodes 4 and 12 indicate that Member A, which spans between these two nodes, has developed damage. For the fourth case, Case D, large peak residual forces are shown to exist at nodes 4 and 12, indicating a change has occurred in the region of member A. Thus, even though the analytical model is not completely correlated to the baseline experimental results, the residual force vectors are able to locate the regions within the truss containing damage associated with stiffness and/or mass change.

The percent change in stiffness (E) and mass (ρ) for Member A in relation to the baseline values are presented in Figs. 11 to 14 as well as Table 5 for the four cases of damage. The actual change in the mass of Member A for each setup (e.g. Cases B, C, and D) was determined by weighing the member, whereas the actual change in stiffness of Member A (Cases B and C) was established by performing a modal analysis on the individual member suspended in a free-free state to determine its vibration properties, from which the stiffness (E) could be calculated.

For Case A, which is the loosened screw set that attached Member A, the calculated sensitivity values (E, ρ) plotted in Fig. 11 show a small reduction only in stiffness (E). None of the other members were found to have neither a change in mass nor stiffness. The reduction in stiffness was obtained in a single iteration. Thus, the approach is able to locate damage, such as a loose joint, on a truss structure and estimate its effective stiffness reduction, even with analytical models which are not completely correlated to a baseline experimental model.

For Case B (see Fig. 12), which involved replacing Member A with the cross-drilled Aluminum member, it is observed that the current approach does an outstanding job in estimating both the actual reduction in member stiffness and mass of -38 percent and -10 percent, respectively. The correlated model predicts closer to the actual results, being within 1 percent for both stiffness and mass reduction. The uncorrelated model produced results within 7 percent and 2 percent for stiffness and mass reduction, respectively. The results of the sensitivity analysis for Case C, involving replacing Member A with a copper member, are shown in Fig. 13 and indicate that the current approach does an outstanding job in estimating the large actual change in mass of Member A (+28 percent) relative to its stiffness (+0.9 percent). The correlated model does a better job than the uncorrelated model, where the former is within 1 percent and 1.5 percent of the actual change in mass and stiffness, respectively, of Member A. The uncorrelated model estimates a change in mass and stiffness of Member A that is within 2 percent and 4.6 percent, respectively, of the actual change. It is noted that for both Cases B and C that more iterations are required until convergence occurs. This phenomena is associated with the simultaneous change that occurs in both the mass and stiffness for these two cases.

For Case D, involving the addition of a discrete mass to the mid-length of Member A, it is observed in Fig. 14 that the current approach converges towards the exact solution for a change in mass of 120 percent and within 1.6 percent of the actual stiffness change of 0 percent for Member A when the correlated analytical model is used. The uncorrelated model converges towards a solution that is within 10 percent and 2.1 percent of the actual change in mass and stiffness of Member A.

CONCLUSIONS

A methodology for detecting structural damage has been presented. Experimentally obtained measured modal test data along with an analytical model are used to first locate potentially damaged regions of the structure using residual force vectors. The test data and residual force vector information is then used to conduct a sensitivity analysis to assess the extent of mass and /or stiffness variations. The current approach is unique among all existing ones in that it accounts for (1) variations in a system's mass, stiffness, and mass center locations; (2) perturbations of both the natural frequencies and modal vectors; and, (3) statistical confidence factors for the structural parameters and potential experimental instrumentation error.

Based on a verification study involving a three-dimensional 10-bay space truss, the following conclusions are noted:

(1) The method is able to successfully determine the location of potential damage, as well as estimate its magnitude. The approach works exceptionally well, even if the frequency shift due to damage is small.

(2) A simultaneous determination can be made of any changes in both mass and stiffness.

(3) A fully correlated analytical (finite element) model is not necessary in order to obtain a reasonable solution. Modal assurance criterion (MAC) values and a cross-orthogonality check (COR) can be used to determine which modes to utilize in the approach. However, an increased

correlation of the analytical model to the baseline improves the accuracy of the method in estimating the severity of damage.

ACKNOWLEDGMENTS

The research study was partially supported by the NASA Johnson Space Center (JSC). The authors would like to extend their thanks to JSC for the support, and in particular their appreciation to David Hamilton of NASA/JSC for his interest, valuable recommendations, and encouragement during the course of this study.

REFERENCES

1.) Adams, R. D., P. Crawley, C. J. Pye, and B. J. Stone, (1978). "A Vibration Technique for Non-Destructively Assessing the Integrity of Structures," Journal of Mechanical Engineering Science, Vol. 20, pp. 93-100.

2.) Chen, J.C. and Garba, J.A., (1988). "On-Orbit Damage Assessment for Large Space Structures," AIAA Journal, Vol. 26, No. 12, pp. 1119-1126.

3.) Chen, T. Y. and B. P. Wang, (1988). "Finite Element Model Refinement Using Modal Analysis Data," Proceedings of the AIAA/ASME/ASCE/AHS 29th Structures, Structural Dynamics, and Materials Conference, Vol. II, pp. 1219-1229.

4.) Collins, J. D., G. C. Hart, T. K. Hasselman, and B. Kennedy, (1974). "Statistical Identification of Structures, AIAA Journal, Vol. 12, No. 2, pp. 185-190.

5.) Coppolino, R. N. and S. Rubin, (1980). "Detectability of Structural Failures in Offshore Platforms by Ambient Vibration Monitoring," Proceedings of the Offshore Technology Conference, Vol. 1, Paper OTC-3865, pp. 101-110.

6.) Crawley, P., and R. D. Adams, (1979a). "A Vibration Technique for Non-Destructive Testing of Fibre Composite Structures," Journal of Composite Matls, Vol. 13, pp. 1161-175.

7.) Crawley, P. and R. D. Adams, (1979b). "The Location of Defects in Structures from Measurements of Natural Frequencies," Journal of Strain Analysis, Vol. 14, Apr, pp. 49-57.

8.) Ewins, D. J., (1984). Modal Testing: Theory and Practice, John Wiley and Sons, Inc., New York, N. Y.

9.) Fox, R. L., and M. P. Kapoor, (1968). "Rates of Change of Eigenvalues and Eigenvectors," AIAA Journal, Vol. 6, No. 12, pp. 2426-2429.

10.) Kabe, A. K., (1985). " Stiffness Matrix Adjustment Using Mode Data," AIAA Journal, Vol. 23, No. 9, pp. 1431-1436.

11.) Kosmatka, J.B., and Ricles, J.M. (1993). "Nondestructive Damage Determination Using Vibratory Residual Forces and Weighted Sensitivity - Analytical and Experimental

Verification Studies," Structural Systems Research Report No. 93/09, University of California, San Diego.

12.) Mills-Curan, W. C., (1988). "Calculation of Eigenvector Derivatives for Structures with Repeated Roots," AIAA Journal, Vol. 26, No. 7, pp. 867-871.

13.) MSC PAL/2 Advanced Stress and Vibration Analysis, (1987). MacNeal-Schwendler Corporation, Version 3.0.

14.) Nelson, R. B., (1976). "Simplified Calculation of Eigenvector Derivatives," AIAA Journal, Vol. 14, No. 9, pp. 1201-1205.

15.) Park, Y. S., H. S. Park, and S. S. Lee, (1988). "Weighted-Error-Matrix Application to Detect Stiffness Damage by Dynamic Characteristic Measurement," Journal of Modal Analysis, July, pp. 101-107.

16.) Ricles, J.M., and Kosmatka, J.B., (1992). "Damage Detection in Elastic Structures Using Vibratory Residual Forces and Weighted Sensitivity," AIAA Journal, Vol. 30, No. 9, pp. 2310-2316.

17.) Smith, S. W., and S. L. Hendricks, (1987). "Evaluation of Two Identification Methods for Damage Detection in Large Space Trusses," Proceedings of the 6th VPI&SU/AIAA Symposium on Dynamics and Controls for Large Space Structures, Blacksburg, VA., pp. 127-142.

18.) STAR Modal Analysis Package, (1991). Structural Measurement Systems, Version 3.0.

19.) Stubbs, N., T. H. Broome and R. Osegueda, (1990). "Nondestructive Construction Error Detection in Large Space Structures," AIAA Journal, Vol. 28, No. 1, pp. 146-152.

20.) Stubbs, N., and R. Osegueda, (1990). "Global Non-Destructive Damage Evaluation in Solids," International Journal of Analytical and Experimental Modal Analysis, Vol. 5, No. 2, pp. 67-79.

21.) White, C. W., and B. D. Maytum, (1976). "Eigensolution Sensitivity to Parametric Model Perturbations," Shock and Vibration Bulletin, Vol. 46, No. 5, pp. 123-133.

22.) Vandiver, J. K., (1975). "Detection of Structural Failure on Fixed Platforms by Measurement of Dynamic Response," Proceedings of the Offshore Technology Conference, Vol. 2, Paper OTC-2267, pp. 243-252.

Table 1. Natural Frequencies of Experimental and Analytical Models.

Mode	Natural Frequency - f (Hz.)						
	Baseline Model			Damaged Experimental Model			
	Measured f_0	Uncorr. Anl. $f_{a,u}$	Corr. Anl $f_{a,c}$	Case 1 f_d	Case 2 f_d	Case 3 f_d	Case 4 f_d
1	96.76	102.60	99.20	94.45	90.77	96.10	94.88
2	98.46	104.04	101.10	95.76	93.10	98.21	97.13
3	136.05	150.60	140.70	130.76	127.34	135.61	132.10
4	220.60	310.10	235.20	210.16	210.51	218.30	222.10

Table 2. Modal Assurance Criteria (MAC) Values - Case A.

Mode	MAC		
	$\phi_0,\phi_{a,u}$	$\phi_0,\phi_{a,c}$	ϕ_0,ϕ_d
1	0.999	0.999	0.999
2	0.998	0.999	0.998
3	0.996	0.998	0.995
4	0.995	0.995	0.993

Table 3. Cross-orthogonality Check - Measured and Uncorrelated Baseline Finite Element Model.

		FEM $\phi_{a,u}$			
	Mode	1	2	3	4
Measured ϕ_0	1	0.996	0.001	0.003	0.006
	2	0.002	0.996	0.004	0.008
	3	0.002	0.004	0.961	0.010
	4	0.004	0.006	0.012	0.911

Table 4. Cross-orthogonality Check - Measured and Correlated Baseline Finite Element Model.

		FEM $\phi_{a,c}$			
	Mode	1	2	3	4
Measured ϕ_0	1	0.999	0.001	0.001	0.003
	2	0.001	0.999	0.002	0.002
	3	0.002	0.002	0.988	0.004
	4	0.002	0.002	0.006	0.963

Table 5. Percent Change in Stiffness and Mass of Member A of Actual Experimental Model and That Calculated by Sensitivity Analysis.

Experimental Setup	Actual		Sensitivity Analysis			
			Uncorrelated Model		Correlated Model	
	Stiffness (%)	Mass (%)	Stiffness (%)	Mass (%)	Stiffness (%)	Mass (%)
Baseline	0	0	0	0	0	0
Case A	n/a	0	-0.675	0	-0.475	0
Case B	-38	-10	-45	-8	-39	-9.75
Case C	+0.9	+28	-3.7	+26	-0.6	+27
Case D	0	+120	+2.1	+110	+1.6	+120

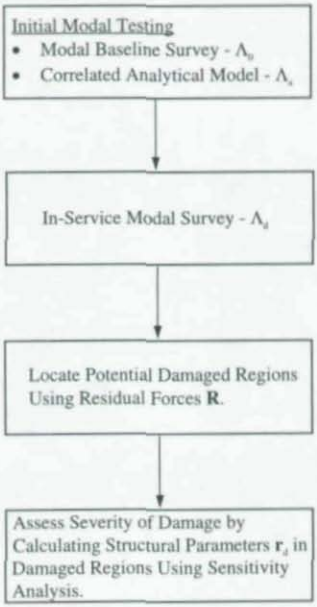

Figure 1 Damage Detection Algorithm.

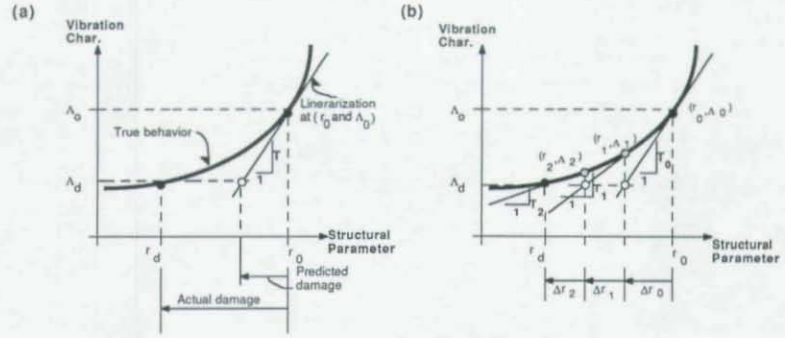

Figure 2 (a) Linearization of The Nonlinear Vibration-Structural Parameters Relationship, and (b) Updating to Obtain Convergence.

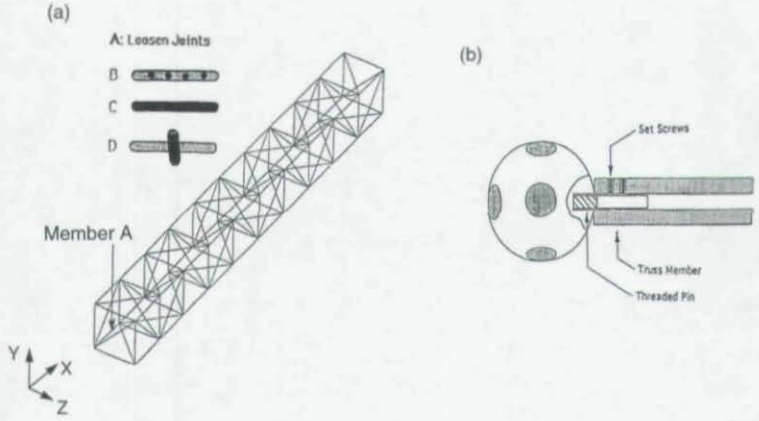

Figure 3 Ten-Bay Space Truss for Experimental Study: (a) Structural Configuration, and (b) Joint Assembly Detail.

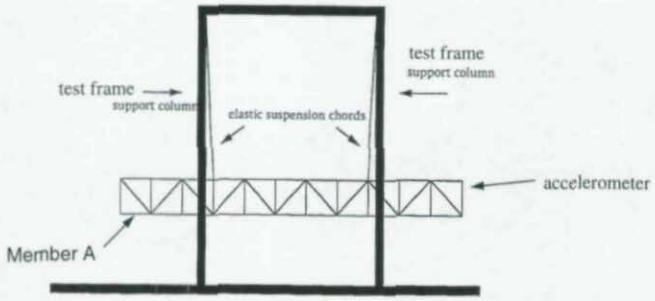

Figure 4 Experimental Test Setup.

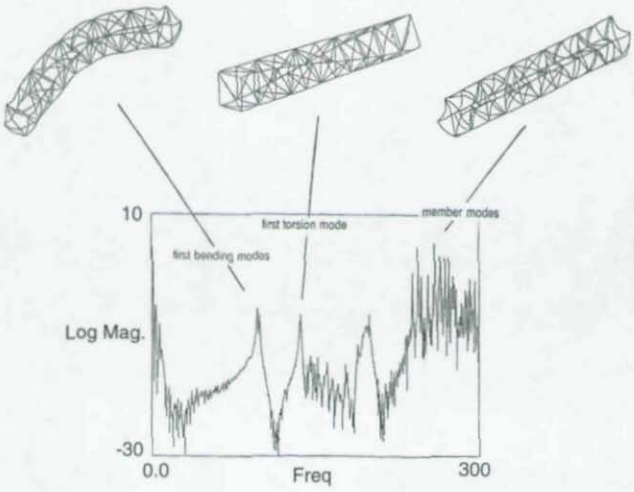

Figure 5 Transfer Function Plot for Ten Bay Space Truss.

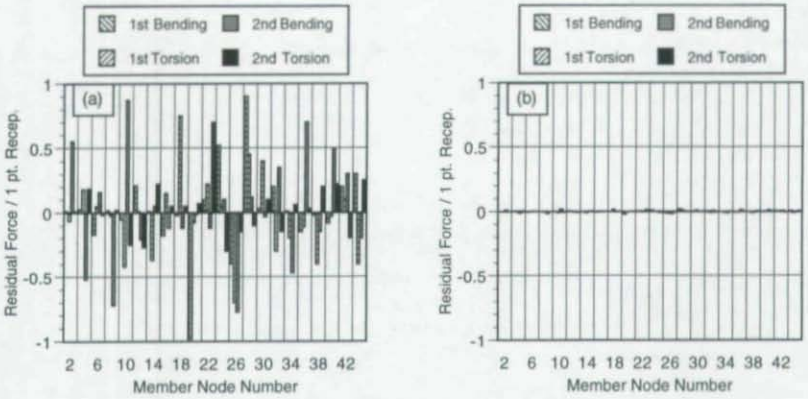

Figure 6 X-Axis Residual Forces for (a) Uncorrelated, and (b) Correlated Baseline Analytical Model.

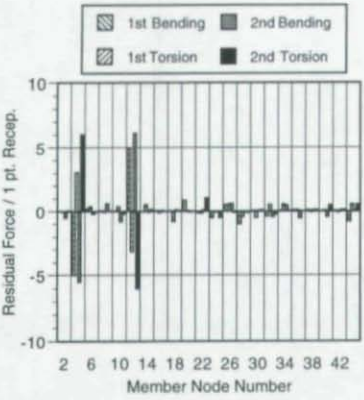

Figure 7 X-Axis Residual Forces - Case A.

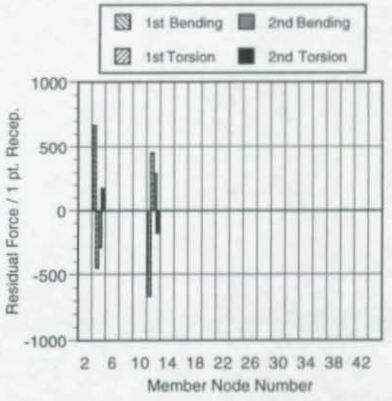

Figure 8 X-Axis Residual Forces - Case B.

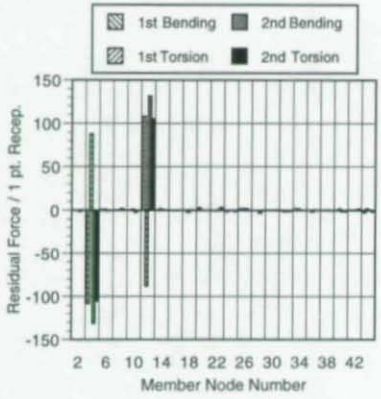

Figure 9 X-Axis Residual Forces - Case C.

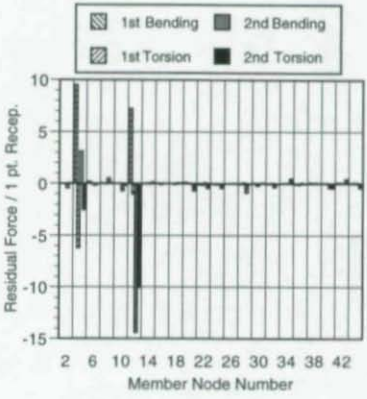

Figure 10 Y-Axis Residual Forces - Case D.

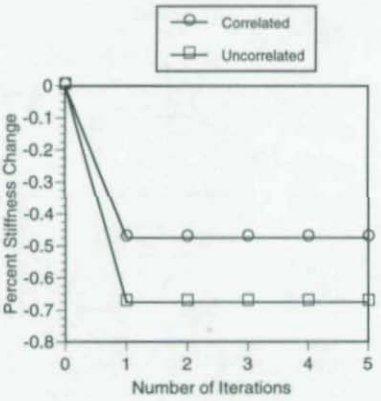

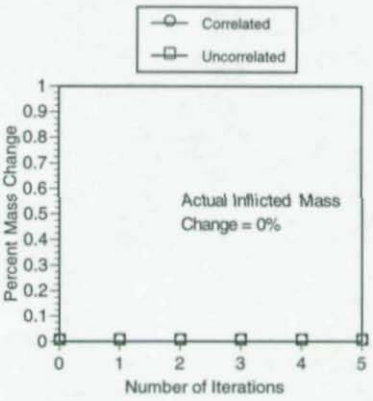

Figure 11 Change in Stiffness and Mass in Member A Predicted by Damage Severity Algorithm - Case A.

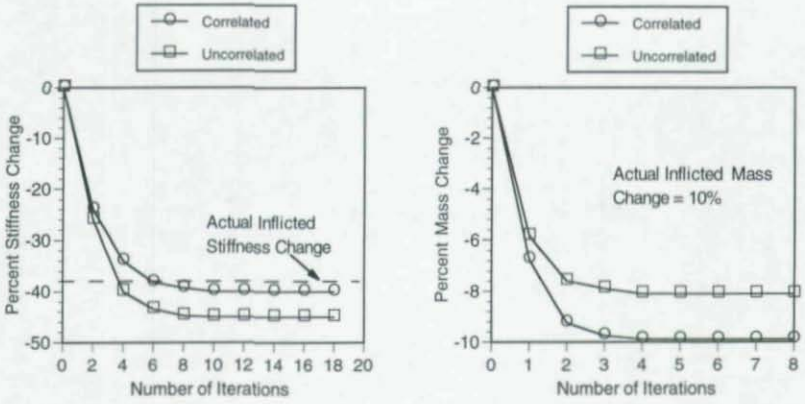

Figure 12 Change in Stiffness and Mass in Member A Predicted by Damage Severity Algorithm - Case B.

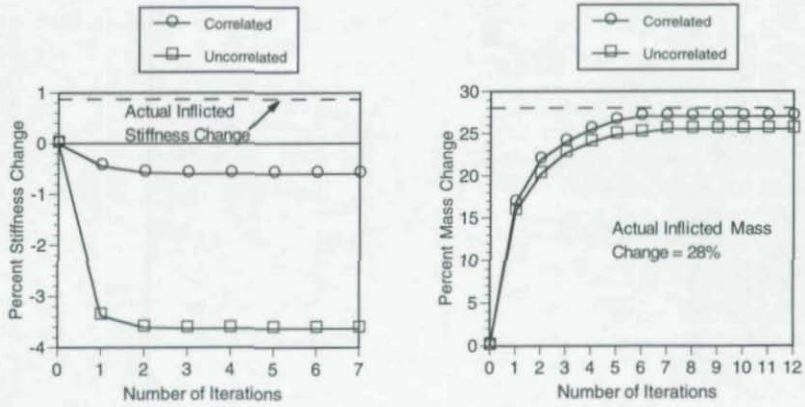

Figure 13 Change in Stiffness and Mass in Member A Predicted by Damage Severity Algorithm - Case C.

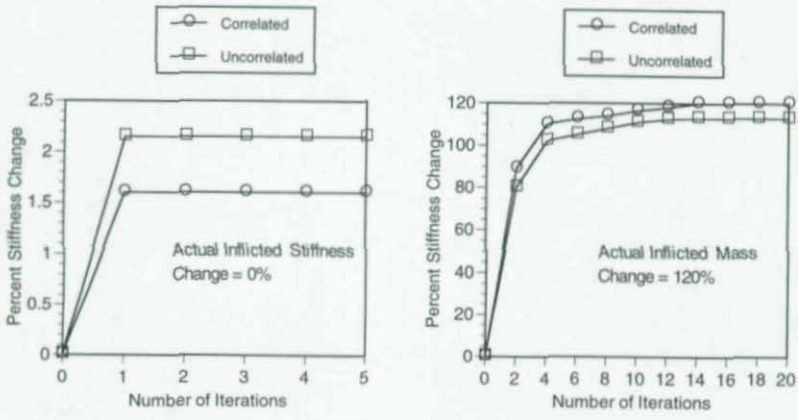

Figure 14 Change in Stiffness and Mass in Member A Predicted by Damage Severity Algorithm - Case D.

THE REPAIR OF GULF WAR DAMAGED STEEL BRIDGES

Khalid S. Dinno, Ph.D
Visiting Professor
Department of Civil Enginering, University of Toronto
Toronto, Ontario M5S 1A4, Canada

Abstract

The paper describes the structural damage caused to two steel bridges situated near the City of Basrah in the south of Iraq, as a result of several direct air strikes during the Gulf War of 1991. One of the bridges is a through type truss railway bridge and the other a deck type highway bridge, both were rotatable for navigational purposes. In addition to severe component damage, the overall stability of both bridges was seriously endangered. The paper describes the strategy formulated and adopted for the repair and rehabilitation of each facility operating within severe constraints on resources.

1. AL-FAYHA RAILWAY BRIDGE

1.1 Brief Description of Bridge

This 2-track railway bridge is situated 30 kms west of Basrah and spans the Shatt A-Basrah waterway. The bridge which has a total length of 238 m consists of 10 spans : 2 central spans of steel truss type with span length of 38.7 m and 8 spans of prestressed concrete deck construction of length 20.00 m each which are symmetrically disposed on both sides of the steel spans. see fig.1.1 .The 2 steel spans form a 77.4 m long continuous steel bridge which is rotatable about the central pier for navigational purposes. The steel bridge comprises 2 main lohgitudinal side trusses placed at 10500 mm apart, a deck floor of cross and logitudinal beams and a system of top level bracing . The chord members have box sections of typical dimensions 550 x 800 mm made of 16-20 mm thick plates. The verticals, diagonals and bracing members are of fabricated I sections of typical dimensions 500 x 500mm. The truss joints contain some 22000 high strength friction grip bolts.The sub-structure consists of solid R.C. wall type piers except for the central pier which is a hollow cylinder having a mean diameter of 12 m . The roof slab of this pier acts as a platform which houses the equipment for supporting and rotating the bridge. The pier extends down to river bed level and like all the other piers is founded on 1000 mm diameter bored piles.

1.2 Damage Due to War

At least 4 air to surface missiles hit the bridge causing extensive damage to 2 concrete spans, namely spans 3 & 7 and to piers P5, P6 as well as to the steel spans. Of interest here is the damage caused to the steel spans and to their supporting piers P5 (the central pier) and P6 . This damage, caused by 2 missile hits, is briefly described here, with reference to Fig. 1.2 in which discontinuous lines indicate seriously damaged members, and to the pictures in Figs. 1.3 to 1.7

The first missile hit was near the span end at pier P6. The force of impact against the steel members and subsequent explosion on impacting pier P6 caused the following : loss of members 1' - 2' , 1' - 3' on the downstream side, loss of the end cross beam on axis 1' as well as of 3 - 5 m lengths of 5 longitudinal beams close to that axis. The hit caused severe disintegration of pier P6 and the resulting wide vertical cracks extended fully down through the pile cap. Subsequent demolition of the pier and examination of the pile heads showed that these had been displaced by amounts varying from 370 to 2080 mms.

The second missile impacted the steel bridge near axis 7 on the upstream side before reaching and exploding against the cylindrical central pier. The entire pier was toppled and a large hole of approximate size 3 x 4 m was created in its wall at the water line. As a result of that and of the serious damage in the vicinity of pier P6, the two span truss bridge suffered gross dislocation . It rested critically on pier P4 and on the toppled central pier with a longitudinal tilt that caused the bridge end near pier P6 to descend about 8.0 m from its normal position. A transverse tilt of 10 % was also produced across the deck. The damage to the steel bridge resulting from the second hit can be summarized as follows :

. Extensive tearing and / or twisting of members 6-7, 7-9, 5-7, 8-7 and 8-9 on the upstream side.
. Twisting of bottom flange and web of the cross beam at axes 7, 12, and 4'
. Out of straightness in the upper downstream chord with a lateral displacement of 140 mm , principally caused by a lateral kink at joint No.5. A similar situation was found to exist in the upper, upstream chord with a max. lateral displacement of 125 mm .

The two missile hits also caused rupture and connection failures in more than 50 % of the top bracing members as well as numerous local damages including shrapnel holes to several members.

1.3 Repair Strategy

1.3.1 Overriding Constraints:

The severe post Gulf War conditions created correspondingly severe constraints on material resources. That had a strong impact on the formulation and the implementation of the solution. . The possibility of dismantling the bolted steel truss bridge to straighten up or replace every member neatly was ruled out, as it was impossible to replace the 22000 bolts involved. It was also quite unfeasible to replace full lengths of damaged members due to scarcity of steel plates and sections. The shortages also extended to jacks and related equipment .Such was the task and the inherent challenge.

A separate basic issue concerning the working environment had to be addressed from the beginning as it had an impact on the approach to solving other issues. This was whether to work in a water environment or on dry land by filling across the waterway. This choice was possible because the waterway was inactive at that time due to the damage caused during the Gulf War to navigational locks further downstream. Working in a water environment would have the advantage of making it possible to load the whole of the truss bridge onto two large pontoons and to move it to a suitable location downstream or upstream for repair using the pontoons as workshops allowing, in the meantime, work to proceed on the central pier. Such disengagement of functions could shorten completion time considerably. In this case however, a dry enclosure

must be formed by, say, sheet piling around the toppled pier. Working in dry conditions , on the other hand would eliminate the need for the scarce sheet piles and enable easier access and working conditions. A detailed appraisal of the two alternatives taking into account, availability of resources and the logistic problems of bringing in large pontoons, led to a decision in favor of filling the waterway and working in the resulting dry environment.

In considering the major stages of work, stabilizing and lifting the truss bridge clear of the damaged piers was an important critical first step in the re-construction effort. Concluding that successfully would enable work to start on the supporting piers. The stabilizing and lifting task is briefly described later.

1.3.2 Objectives of Steel Repairwork:

1. The achievement of structural stability throughout the various phases of repair, and the assurance that while a member is being replaced or repaired the others are not over stressed.
2. The achievement of an acceptable geometry (i.e. alignment and levels) in the final structure. The question arises here as to what is an acceptable geometry. In a simply supported span an acceptable geometry is principally provided by a functionally and aesthetically suitable profile. In statically indeterminate construction the geometry must also produce the intended distribution of reactions between the supports. In the present case, where the bridge must retain the capability to rotate , a further requirement exists, namely the assurance that the repaired bridge can disengage freely from the end piers and rotate in a true horizontal plane about the central pivot.

1.3.3 Technical Criteria for Repair :

In considering a damaged component a criterion had to be established as to what constituted an acceptable deviation from straightness, planarity and squareness and what did not. Review of available technical literature showed how very few norms existed to aid in this kind of situation. Eventually it was decided to adopt the tolerance limits given in BS 5400 Part6 .

The next step was to decide on the action to take with respect to a component that did not conform to the adopted tolerance limits. Replacing a damaged component with a new one would be the easiest and safest course of action to take. But in view of the scarcity of material resources, that option could only be invoked if there was no alternative. Although some technical standards permit the use of limited heating for repair, this procedure was not followed here due to the difficulty of closely monitoring and enforcing the max. limit on temperature. Cold pressing of gentle curves was permitted. Components containing sharp kinks or other severe local deformations were identified and marked for replacement. Due to scarcity of bolts, cuts had to be made outside the bolted joints and weld connection details had to be elaborated to transmit the internal forces, paying due attention to residual effects and fatigue rating.

Quality control of fabrication and welding in particular was considered critical for the success of the whole repair effort. Only welders with recognized qualifications were employed. Radiographic testing was extensively used. Regions involving welding of 40 mm or thicker plates were given post-heat treatment using electric heating coils. Hardness of the heat affected zones was measured before and after the heat treatment in order to verify the adequacy of the treatment.

1.4 Stabilizing and Lifting the Truss Bridge

A careful study was made of the damaged state of the members and of the way the bridge lay and was supported, in order to determine the most suitable method of lifting it, considering overall stability and stress levels in members. Consequently it was decided to support and subsequently lift the bridge at the two axes 7 and 7' . However this required strengthening, temporarily, key elements of the damaged truss such as chord elements 6-7, 7-9 diagonal elements 5-7 and 8-7 and vertical element 8-9, all on the upstream.

The arrangement for supporting and lifting the 800 ton bridge consisted of introducing steel girders transversely underneath the bridge at axes 7 and 7' to support the upstream and downstream trusses at their lower chords. The steel girders were end supported on groups of 6-700 mm dia tubular steel piles which were driven just outside the overlying steel bridge. The contact detail between the lower chord box and the supporting girder incorporated a curved bearing which protected the contact surfaces from damage due to concentrated point action. The support arrangement of the lifting girders at each pile group involved a bearing beam assembly which accommodated a jack and two temporary supports. The latter were used to support the load temporarily while the jack was being reset as it came to the end of its stroke. For stability reasons the height of the temporary supports was limited to about 1000 mm and represented a sub-stage in the jacking up process. At the end of each sub-stage the bearing beam assembly was re-installed at a higher level on brackets projecting from the pile assembly, ready for the next series of sub-stages.

Prior to commencing the jacking up process precautionary measures had to be taken to stabilize the bridge longitudinally by tying it to the pier P4 by steel wire ropes which incorporated adjustable turn-buckles.This was particularly necessary as the jacking up proceeded to the stage when the bridge was disengaging from the central pier which had been providing the restraint against longitudinal sliding. The tension in the wire ropes was continually maintained during the jacking process.

The transverse tilt of the bridge was first targeted for correction by operating the jacks on the lower (upstream) side, during which process temporary retracting jacks were operated on the downstream side.The jacking up process, especially for correcting the longitudinal tilt, proceeded slowly but quite smoothly . There was a point of some anxiety, however, when the steel bridge was about to disengage from the central concrete pier. The two were entangled in a complicated way and it was necessary to ensure that they separated without causing abrupt forces that could endanger stability. This was done by breaking the concrete at the junction using hydraulically operated pneumatic hammers, that worked their way around the entangled parts. The whole bridge was eventually raised to a horizontal level, see Fig.1.8 . The raised level was 1.0 m higher than the final correct level in order to provide enough room for re-constructing the central pier.

1.5 Phases of Steel Repairwork :

To meet the objectives of the repairwork, it was important to recognise the need for careful planning of the work into phases such that the work of each phase did not adversely affect the repair objective of the other phases. To rectify the lateral kink in the two upper chords for

example, it was important that the upper level horizontal bracing was just adequate for stability of the chords yet was as flexible as possible in order to enable the required repair to be carried out with manageable repair jacking forces, and min induced residual stresses. With considerations such as this in mind the main phases of work were :

Phase I : Fabrication and erection of the bridge end members near pier P6 in order to establish a support capability on the re-constructed pier.

Phase II : Rectification of the out of straightness in the upper chords.

Phase III : Expanding the structural support system of the bridge from that initially established along axes 7 and 7' by introducing 14 other supports which had two aims :

1. Ensuring stability of the bridge as a whole and in part and maintaining acceptable levels of stresses as key members near axis 7 were replaced.
2. Providing the means to adjust the levels (profile) of the bridge before erecting and welding into position the key truss members near axis 7. Failure to make this adjustment would result in a geometric configuration that does not allow the bridge to function as a rotating bridge. This phase had to be performed after completing the re-construction of piers P5 and P6 and lowering the steel bridge down to these and onto pier P4. The expanded support system comprised 18 supports as follows:

4 permanent supports along axis 12 on the central pier
2 " " " each of piers P4 and P6
2 temporary supports introduced by transverse girders at each of axies 4 , 7 and 7'
2 temporary supports over the central pier at each of cross beams 10 and 10'

Phase IV :

1. Introducing temporary strengthening to the upstream truss around node 7 to enable the phased replacement of the damaged key members around that node.
2. Implementing the phased replacement of the damaged key members around node 7 and removing the temporary strengthening .
3. Completing the bridge repair, including main floor members and upper level bracing .

Phase V : Restoration of position, alignment and level of steel bridge and anchorage to bearings .

1.6 Structural Analysis for Field Repair & Erection :

The analytic basis for achieving the desired final levels may be clarified with the aid of schematic representation shown in Fig.1.9 .

Curve 1 represents the deflected shape of the undamaged structure,having overall stiffness K_1, under dead weight .

Curve 2 represents the deflected shape of the damaged structure,having a reduced overall stiffness K_2 ,under dead weight.

Applying the forces P_j where j is typical of the n jacking points, causes a deflection V_{1i} at support point i, and leads to the modified geometry represented by curve 3. The repair work is to be carried out at this geometry , thereby upgrading the stiffness from K_2 to K_1. The structure must be locked at that geometry.In the present case this is done by the proposed temporary strengthening around node 7. If the temporary supports are now removed, i.e. applying P_j in the reverse direction a corresponding deflection V_{2i} at support point i will result indicating return to the original geometry (curve 4). Putting the above in symbolic form :

$$V_{1i} = \sum_{j=1}^{n} C_{ij} P_j \qquad \text{.....(1)}$$

$$V_{2i} = \sum_{j=1}^{n} D_{ij} P_j \qquad \text{.....(2)}$$

$$v_i = V_{1i} - V_{2i} \qquad \text{.....(3)}$$

$$v_i = \sum_{j=1}^{n} C_{ij} P_j - \sum_{j=1}^{n} D_{ij} P_j \qquad \text{.....(4)}$$

Where C_{ij} and D_{ij} are the deflection coefficients associated with the damaged and initial stiffnesses K_2 and K_1 respectively and v_i is the additional self weight deflection at point i caused by the drop of stiffness from K_1 to K_2 as caused by the damage.

Now in order to repair the key members close to axis 7, the bridge had to be lowered down and supported on the central pier along axis 12 yielding n = 14. These supports represented reaction points and the quantities C_{ij} , D_{ij} and v_i were calculated by stiffness analysis for such boundary conditions. Evaluating the undeformed stiffness K_1 was standard enough, but evaluating the stiffness K_2 of the damaged state required paying careful attention to modeling the residual stiffness of a partially damaged member ; say a box or an I section with a partial damage to a web or to a flange along part of its length . The models were tested by comparing calculated values of v_i with observed values in order to assure that important modeling errors were not made.

The solution of the 14 simultaneous equations (4) gives the forces P_j that would bring the n pre-selected points back to the original (undeformed) configuration.At this point 2 remarks merit specific mention. The first concerns the number of points n. In order to get the bridge back to the original geometry everywhere, an infinite number of points with applied forces would be needed . Hence a practical situation calls for a prudent selection of the salient points which should fall on the required profile. Bridge bearing points are amongst such points. The second remark concerns the nature of the numerical results. Different trial runs showed that the P forces were quite sensitive to the prescribed displacements. A trade off has had to be made between accuracy of levels and the magnitude and sign of the forces that could be supplied by available jacks. Such tradeoff eventually led to a manageable set of jacking forces having max value of 350 tons. Upon final setting of the bridge on its central bearing the cantilever deflections at piers P4 and P6 were found to deviate by not more that 20 mm (representing 15%) of the designated values in the original design. The magnitude of this deviation was well within the tolerance limit of 75 mm that would impede deck rotation.

1.7 Position Restoration of the Steel Bridge :

Upon completion of the steel bridge repairs the final task was to restore proper location and alignment. The center of the bridge had to be moved 270 mm longitudinally, 570 mm laterally and be rotated about 4 degrees about the central pivot . A system of 150 mm diameter steel rollers was designed and manufactured from hardened steel for this purpose. The horizontal movements

were produced by horizontal jacks of up to 100 ton capacity reacting against steel frames which had been constructed and anchored into the concrete of piers P5 and P6 for this purpose. The same rollers were used in producing orthogonal movements by raising the whole bridge on the central pier by 500 ton jacks and turning round the rollers. The bridge was finally anchored down to a set of temporary bearings pending their future replacement by the pivot and wedge bearing units that would then form part of the bridge rotating equipment , see Fig. 1.10 & 1.11 .

That concluded the last major step in a re-construction effort that started in July 1992. The bridge passed a load test with a 94 % elastic recovery and was re-opened on Dec.28, 1993. Periodic inspections since then have shown no signs of problems.

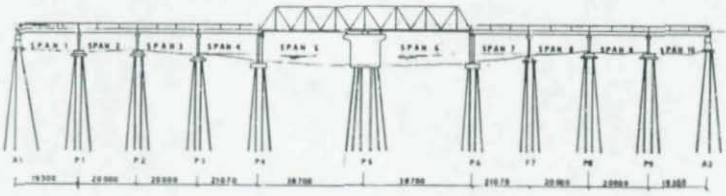

Fig. 1.1 AL-FAYHA RAILWAY BRIDGE

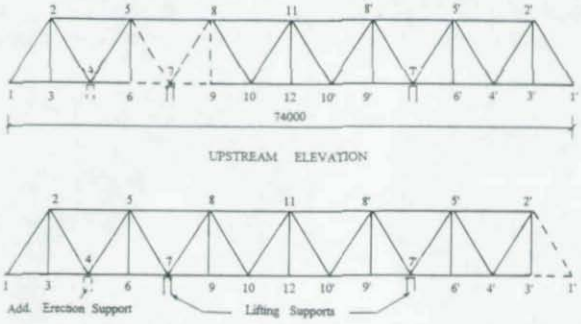

Fig. 1.2 OUTLINE OF STEEL BRIDGE

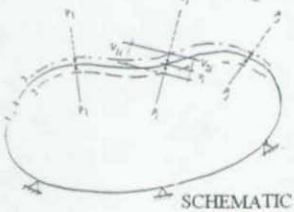

Fig. 1.9

SCHEMATIC REPRESENTATION FOR ANALYSIS

Fig. 1.3

Fig. 1.4

Fig. 1.5

Fig. 1.6

Fig. 1.7

Fig. 1.8

Fig. 1.10

Fig. 1.11

2. FIRST GARMAT ALI HIGHWAY BRIDGE

2.1 Brief Description of Bridge

This bridge is located just to the north of the southern City of Basrah on Garmat Ali, a tributary of Shatt Al-Arab River. The 407 m bridge consists of 9 - 37 m long simply supported prestressed concrete spans and 2 central navigational continuous twin steel spans, of total length of 74 m, see Figs 2.1 & 2.2 . The steel spans basically consist of 2 longitudinal girders , cross beams and a deck plate which is longitudinally stiffened by trough stiffeners. The steel construction comprises 7 segments of shop fabricated welded construction, except for the bolted cross beams. The segments were site bolted on erection. The steel spans are supported on to the central pier through a 10500 mm dia 1100 mm deep circular steel girder which had a turning capability on a circular rail mounted on top of the supporting central pier. The two supporting end piers which are wall type and the central pier which is a hollow cylinder are of reinforced concrete construction and are founded on 1000 mm diameter vertical and inclined piles.

2.2 Damage Due to War

The bridge was hit by several air to surface missiles which caused serious damage to two concrete spans and to the steel spans. Attention is confined here to the steel spans .The damage to these was caused by a single missile hit which penetrated the web of the circular steel girder and exploded in the space enclosed by that girder ; a space which housed the rotating mechanism of the bridge. The resulting damages may be summarised as follows, see Fig. 2.4 & 2.5 .

. Destruction and twisting of the hydraulic jacks and other mechanical equipment .

. Complete derailment of the circular steel girder and hence the whole of the steel bridge (steel spans) from its proper location on the central pier.. The derailment and side shift caused an overall body shift of the steel bridge horizontally and vertically as well as a lateral tilt of the deck about 20% .The horizontal shift at the central pier was 1750mm and at one pier P8 was 3750mm.The configuration of the steel bridge considering the way it was supported was quite unstable .

. Bulging of the web of the circular girder in many locations around the circumference in addition to the hole created by missile penetration. The flanges also developed ovality and gentle twisting.

. Disconnection and complete destruction of 18 radial beams that connected the circular girder to the central pivot

. Extensive damage in the form of severe twisting to the cross beams above the central pier P7. The cross beam over pier P8 developed a sharp kink as result of the abnormal bearing situation to which it was subjected.

. Extensive damage in the form of tearing and bulging to the deck plate and its longitudinal trough- type ribs over the area of the explosion to an extent of 16 m length .

. Various local damages in the flanges and webs of the two longitudinal steel girders.

. Extensive damage to the central R.C. cylindrical pier characterised by disintegration and heavy cracking in the roof of the pier and complete failure of the connection between the pier and 11 of the 12 supporting piles including snapping of pile reinforcement which was originally anchored in the pier. The pier leaned out of vertical as it rested on only one vertical pile .

2.3 Repair Strategy

The constraints on material resources described for the Al Fayha Bridge apply here to a large extent except that with the implementationof this work being carried out earlier, shortages were not as severe. In view of the serious damage to the central pier and to some of its supporting piles, dismantling of most of the steel bridge and demolition of the pier was necessary. Dismantling would also enable a better repair of the badly damaged steel components. However the first and most important task was to address the question of the stability of the steel bridge. This is considered next.

2.4 Stabilizing the Steel Bridge :

In view of the unstable configuration of the damaged steel bridge, it was first necessary to design and execute measures that would ensure the stability of the structure then and also during the subsequent dismantling stages. In addition to tying the deck at various locations to existing fender piles by steel wire ropes, two temporary support zones were set up: Zones AB and CD (see Fig.2.3). Support Zone AB consisted of steel platform supported on 10 -700 mm dia tubular steel piles . 2 - 100 ton jacks were mounted on the platform to form part of the lifting set up. Support Zone CD consisted of 2 steel girders which were erected underneath the bridge deck, close to the bolted joint between parts 2 and 3, and supported on 8 tubular steel piles at each end. Jacks were also supplied over this zone to facilitate lifting, dismantling and subsequent re-erections. In addition to Zones AB and CD, locations E1, E2 and F provided further jacking points.
The 350 ton steel bridge was restored to level position prior to dismantling using the following jack configuration.
a) Lifting jacks J1 and J2 and retracting jacks J3 and J4 were positioned at the four original points which were allocated for the lifting of the whole deck during routine bridge maintenance .
b) Jacks J5 to J8 were mounted in the temporary Support Zone CD .
c) Jack J9 was mounted under the dislocated end corner F of the longitudinal girder at pier P8 .
The jacks were operated manually and their action was carefully coordinated to fulfill two purposes. The lifting required at J1 and J2 was of the order of 1500 mm and it was not possible to achieve that in one stroke with the available jacks which had a max stroke of 150 mm. It was also necessary to install temporary supports TS1, TS2 and TS9 to enable the re-setting of jacks J1, J2 and J9 respectively. As lifting progressed the tension in the steel wire ropes became slack and had to be continuously tensioned until final stable configuration was obtained. The pictures in Figs. 2.6 & 2.7 show the stabilized position of the bridge.

2.5 Dismantling of Steel Bridge

A detailed examination of the steel deck showed that segments 1 and 2, although were dislocated from their proper position, were basically undamaged except for shrapnel holes. For this reason it was decided to keep them in position and to re-locate them to correct position at a subsequent stage. The erection / splice joints between the various segments were the natural locations for dismantling. The size and weight of the dismantled segments was dictated by the safe lifting capacity and maneuverability of the cranes which were available to operate from river craft. Dismantling proceeded in the following order : Segments 1' , 2' , 3' , 4 , 3 and circular central girder. The joint between each 2 segments had high strength friction bolts in the bottom flanges

and webs. The longitudinally stiffened deck plate also acted as top flanges for the 2 longitudinal girders. The deck plate was welded at the joint. Starting from segment 1', certain proportion not exceeding 50% of the bolts were removed before the segment was supported by 2 cranes from pre-chosen 4 strong points. The removal of the remaining bolts and the gouging of the deck plate weld was done with crane ropes being just or slightly taut until complete separation. The tension in the steel ropes had to be carefully monitored and controlled to take account of the tidal effects and associated change of water level. Dismantling of the other segments proceeded in a similar manner.

2.6 Repair of the Steel Components

The dismantled bridge segments were set up on a level concrete base where careful re-examination of their damages was made and documented. The criteria and procedures cited for the Fayha Bridge concerning acceptable tolerances for deviation from straightness, planarity and squareness and as to the method of repair of componentswere followed in the present case too. Based on these criteria the following components had to be substantially re-fabricated :

. the cross beam over pier P8 and the three cross beams over the central pier

. deck plate and its longitudinal stiffening for most of segments 3' and 4.

. Extensive repair to circular girder under segment 4. This also involved replacement of large areas of web and the completely destroyed radial beams by new ones. Due to deformation of the flanges, their repair was only possible after completely disconnecting web from flanges. The weld was removed by gouging. Restoring this girder with its 25 mm web & 40 mm flanges to proper circularity, plane upper and lower flange faces and flange to web squareness was a considerable challenge to the fabrication team. Figs 2.8 and 2.9 show pictures of this girder during and after repair.

In view of the severity of the damage that occurred to the electro/mechanical equipment required for rotating the bridge, it was decided to utilize the bridge in a fixed form and yet retain the potential for future capability for rotation. The steel roller and rail arrangement were therefore replaced by an arrangement of 18 equally spaced fixed stub steel columns.

2.7 Erection

Erection started by fixing the 18 stub columns around the upper wall of the central pier. Their bolts were anchored in pre-prepared holes. The circular steel girder was then lowered and fixed on the stubs. Erection of the bridge units proceeded in a cantilever manner starting with segment 4, and was followed symmetrically with segments 3 and 3'. The combined segments 1 and 2 were then re-aligned into final position and connected to segment 3 . Fine level adjustment was made by the jacks J5 and J7. These jacks were then utilized to take a pre-calculated share of the weight of that span until the erection of segments 2' and 1' was completed.

Hoisting and erection of each of the cantilever segments 3, 3`, 2`, 1` was carried out by crawler cranes operating from the platform of floating pontoons. Web splice bolts were inserted and loosely tightened first, followed by bottom flange bolts, simultaneously with which steel lugs were welded across the transverse joint gap of the deck plate. The lugs were of sufficient size and weld to supply temporarily and in conjunction with the lower flange the moment resistance for the

cantilever action. The percentage of bolting and welding that had to be achieved before the cranes could be relieved was calculated and specified. Figs. 2.10 and 2.11 show intermediate and final stages of erection.

The original splice bolts were 24 mm dia class 10.9 high strength friction bolts. At the time of reconstruction of this bridge it was still possible to obtain new replacement for most of the bolts. Flange splice bolts were available. There was however a deficiency of about 25% of web splice bolts. The question of utilizing re-use bolts was examined, in the light of research work by Boyd and Hyler[1] which forms the background to the AISC recommendations. According to these recommendation, ungalvanised A 325 bolts may be re-used for up to 3 times while A490 bolts are not recommended for re-use. With bolts grade 10.9 being closer to A490 than to A325 bolt quality it was decided to search for an alternative to re-using these bolts. A 325 bolts were eventually found. To supplement their strength it was decided, after consultation with the Client, to adopt a hybrid connection involving fillet welding in addition to the A325 bolts. BS 5400 part 3 permits this type of connection. The weld size was in fact conservatively designed to carry the whole load.

The tip elevation of each erected segment was measured in order to verify that it did not depart significantly from calculated values. It was important to ensure that the cantilever elevation of the end segments 1 and 1' was within prescribed tolerances that assured the functionality of the bridge as a turning bridge. With the damage to the main longitudinal girders being only local, it was not difficult to preserve accurate vertical profile and no problems were encountered in meeting the aforementioned tolerances.

The bridge passed a standard load test with 96 % elastic recovery. The work on this bridge started in June 1991 and the bridge was re-opened on May 4, 1992 . Periodic inspection since then showed no signs of problems.

Concluding Remarks

In the aftermath of the Gulf War of 1991, an urgent need arose in Iraq for the repair, re-habilitation and re-construction of vital infra-structure facilities such as bridges, electric power stations and refineries. The structural failures were of a nature quite unencountered in modern history. The methodology of repair and its associated engineering problems were also intrinsically different from the well trodden path of standard new construction. New areas of research became immediately apparent. Such areas include the study of the performance of different structural systems under catastrophic forces, the structural lessons to be learnt from the nature of failures, finding answers to technical problems associated with the repair process and the appraisal of the technical solutions adopted for these repairs. Most of these aspects will be increasingly relevant to the future re-habilitation of infra-structures that may be subjected to deterioration by various causes, natural or otherwise.

References

1. Boyd & Hyler, J.Struct.Div.ASCE Vol. 99, 1973

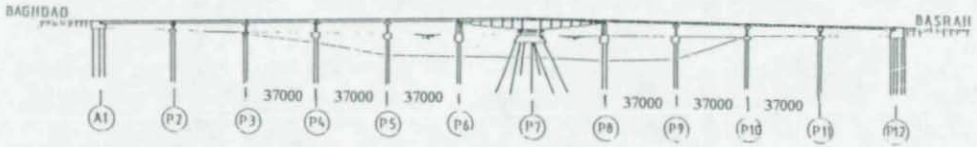

Fig. 2.1 FIRST GARMAT ALI HIGHWAY BRIDGE

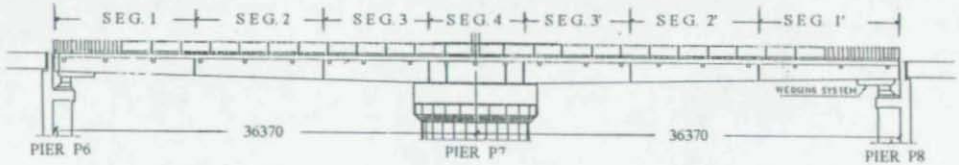

Fig. 2.2 ELEVATION - STEEL BRIDGE

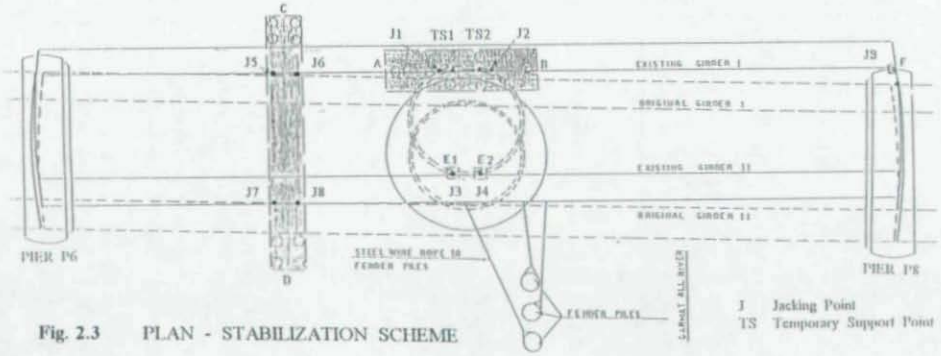

Fig. 2.3 PLAN - STABILIZATION SCHEME

Fig. 2.4

Fig. 2.5

Fig. 2.6

Fig. 2.7

Fig. 2.8

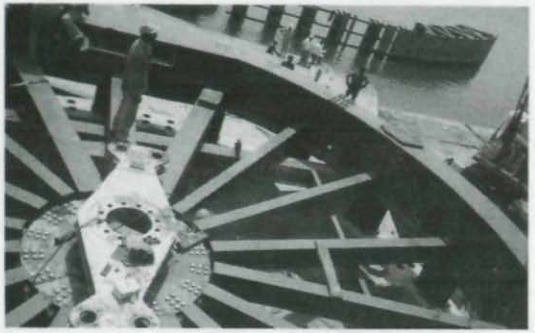

Fig. 2.9

Fig. 2.10

Fig. 2.11

STRUCTURAL REPAIRING AND UPGRADING OF LARGE SHIP UNLOADERS

Ronaldo C. Batista and Eliane M. L. Carvalho
COPPE - Federal University of Rio de Janeiro
C. Postal 68506, CEP 21945-970, RJ, Brazil

Abstract

Ship unloaders are normally subjected to a very heavy duty and therefore wear and cracks are not uncommon in their steel structures which often need some repairing and upgrading. This paper focus on the interactive theoretical-experimental-numerical procedure which was used to model the structural-mechanical system and the dynamic loading, to then assess the structural behavior, forecast fatigue-cracks and estimate the ulterior service life of two similar large ship unloaders that were on duty for a period of 10 years. A summarized account is given on how, after the occurrence of one the predicted cracks, the same procedure was used to design the needed structural reinforcing/stiffening details which were carried out to upgrade these large machines.

1 Introduction

Steel structures of large machines such as ship unloaders in busy ports are subjected to a very severe duty and therefore should be designed under rigorous dynamic criteria if its fatigue life expectancy in years is taken as one of the main indexes to measure its structural performance. Wear of the moving parts and cracks in the steel structure resulting from heavy duty are not uncommon in these large structural-mechanical systems which often need some repairing and upgrading. In some cases fractures may propagate quickly and widely, decreasing drastically local strength and leading to localized buckling and even collapse. The latter event excluded this was the case of the analysed unloader's steel frame structure (see Fig. 1) composed of large and slender thin walled box-section members.

This paper focus on the main aspects of the interactive theoretical-experimental-numerical procedure which was used to model the structural-mechanical system and cyclic loading; assess the structural dynamic behavior and to estimate the ulterior service life of two similar unloaders that were on duty for a period of 10 years. These latter estimates were then used to forecast the occurrence of fatigue cracks in major box sections that could have led to the collapse of the whole structure of one of the unloaders. Under the repeated action of heavy moving parts the undetected (although predicted) crack grew to dangerous proportions, and this severely weakened the structure. This occurred extensive fracture, caused by fatigue and initiated at a point of high stress concentration, corroborated initial predictions and compelled to design the needed structural reinforcing and stiffening details which were carried out to upgrade these two large machines.

It is shown how the dynamic characteristics of the steel structure and of the moving parts of the machine were first identified by experimental measurements, which in their turn were used to formulate a theoretical model for the dynamic load and to calibrate the FEM model of the

whole structural-mechanical system, in terms of natural vibration frequencies and mode shapes and also in terms of time response amplitudes. Moreover, it is shown how the most stressed box section was modeled and analysed by combining finite element techniques and experimental strain measurements, and how the resultant stresses were used to design the needed structural strengthening. Correlation of experimental and numerical results are given to demonstrate the effectiveness of the used interactive approach to this engineering problem.

2 General description of the structural-mechanical system

A side view and overall geometry of the unloader's steel structure is shown schematically in Fig.1 together with some of its main accessories: bucket and trolley, hopper and apron feeders. The material (e.g. coal or iron ore) is unloaded from the ship in the following operation sequence: the bucket is lowered into the ship and bites the material, then is lifted and transported by the trolley along the boom to throw the material inside the hopper, returning then empty to restart the unloading operation.

When the bucket filled with material and hanging by cables from the trolley is transported to the hopper, it performs a coupled pendular-translational motion that creates a dynamic force that makes the unloader to oscillate. In its way back towards the boom tip the now empty bucket creates a similar force of opposite sign and half magnitude. Structural stiffness and resistance to these oscillations is mainly offered by the pair of inverted L-shaped plane frames, indicated in Fig.1. The semi-spherical bearings at the top of the two columns in the lower rear-portal mounted on trucks serve to attenuate the stresses induced by the dynamic force and make these columns to work as pinned-ends struts. The two legs of the mast, at which top the tie-rods are linked, sit on semi-rigid connections that allow small rotations caused by dynamic varying stretching of both tie-rods and rear-rods.

3 Interactive theoretical-experimental-numerical approach

An interactive approach was used to calibrate a FEM model of the previously described structural-mechanical system that constitute the ship unloader. The structure was discretized by 428 space frame elements - leading to a system of 2122 linear equations - and the numerical modelling allowed for all the distributed and concentrated masses due to mechanical accessories and equipment installed on the structure. The FEM model is illustrated in Fig. 2 together with the unloader's dominant mode of oscillation, i.e. surging motion.

Experimental dynamic responses of the structure were obtained for two distinct conditions:

- free vibrations under impulsive loads produced by instantly starting and stopping either the lifting operation of bucket or translation of the trolley.
- forced vibration caused by normal unloading operation.

Free vibration analysis

Fifteen micro-accelerometers (Kyowa, 1g) were installed on each unloader and used to record the dynamic responses in terms of longitudinal, transversal and vertical accelerations of various points of the structure. The filtered and amplified recorded analogical signals were then digitalized and used to identify the dominant vibration mode shapes and their associated natural frequencies, the latter through the frequency spectra obtained by applying the Fast Fourier

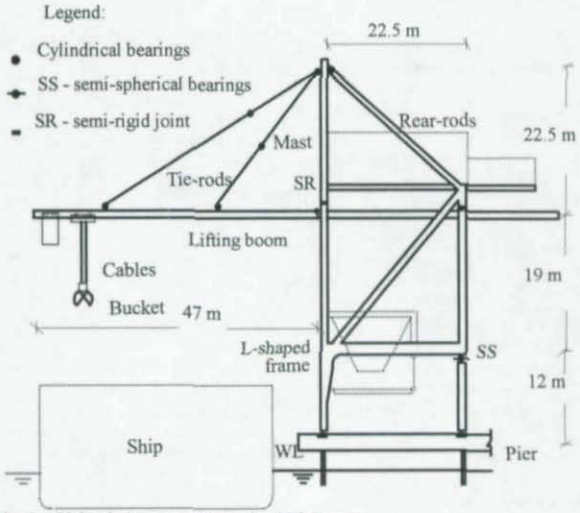

Fig. 1 - Unloader's structural-mechanical system

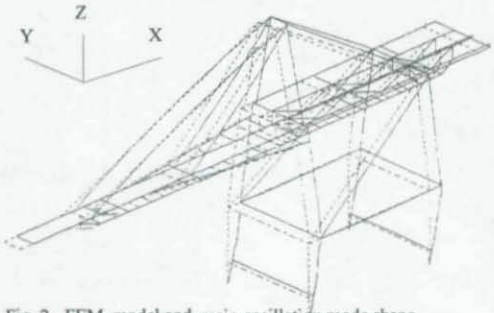

Fig. 2 - FEM model and main oscillation mode shape

Transform (FFT) algorithm to these signals. Damping factors for the lowest vibration modes could be easily evaluated through the logarithm decrement technique, resulting in: $\xi = 6\%$ for the lowest frequency global axial torsion mode, and $\xi = 5.5\%$ for the dominant longitudinal (surge) mode shape shown in Fig. 2.

Table 1 presents the correlation between experimental and theoretical results for natural vibration frequencies associated with some few mode shapes

Table 1 - Experimental x Theoretical Frequencies (Hz ± 0.04 Hz)

Mode Shape	Experimental	Theoretical
Axial Torsion mode	0.36	0.38
Surge mode (Fig. 2)	0.48	0.36
Sway mode	0.92	0.80
1st Bending of Boom	1.24	1.20
Transversal Bending	1.88	2.00
2nd Bending of Boom	3.24	3.00
Longitudinal Bending	4.56	4.50

It should be emphasized that calibration of the FEM model in terms of vibration frequencies was achieved simply by refining the mesh, considering all the articulated bearings and adjusting the location and overall distribution of concentrated masses due to accessories, machinery and equipment, according to the "as built" drawings of the unloaders.

Modelling of the dynamic load

A theoretical model for the dynamic load was formulated from experimental observation and measurements of the motion of the traveling bucket. This dynamic load can be described by the tension force in the suspension cables, according to the sketch shown in Fig. 3, as follows:

$$T = m_2 g(t/t_1) \quad ; 0 < t \le t_1. \tag{1.a}$$

$$T = m_2 \ddot{x}\sin\phi + m_2 L\dot{\phi}^2 + m_2 g\cos\phi \quad ; t_1 < t \le t_2. \tag{1.b}$$

being

$$T_x = T\sin\phi \quad (a) \quad ; \quad T_z = T\cos\phi \quad (b) \tag{2}$$

its components in the XZ plane, and

$$M = m_2 gl(t/t_1) \quad ; \quad 0 < t \le t_1. \tag{3.a}$$

$$M = (m_1 g + T_z)(l - x) \quad ; \quad t_1 < t \le t_2. \tag{3.b}$$

the force moment in relation to the $\bar{y}$ axis passing through the cylindrical bearings of the lifting boom, where

m_1 = mass of the trolley (20 t)

m_2 = mass of the bucket: full (40 t) or empty (20 t)
L = length of the suspension cables of the traveling bucket (~10 m)
l = distance between trolley's extreme positions on the boom (~30 m)
$\phi(t)$ = angular coordinate for the bucket pendular motion
$x(t)$, $\dot{x}(t)$, $\ddot{x}(t)$ = displacement, velocity and acceleration of the traveling trolley
g = acceleration of gravity
t = time (sec.)
t_1, t_2 = time instants corresponding respectively to the end of the lifting (t_1= 6 sec) and transporting (t_2= 16 sec) operation steps of the full bucket; being t = 0 the beginning of step D in Fig. 4.

Based on experimental observation the velocity of the traveling trolley was assumed to vary as a half-wave sine function of time,

$$\dot{x}(t) = \frac{l\pi}{\Delta t}\sin\frac{\pi t}{\Delta t} \qquad (4.a)$$

so that,

$$x = -l\cos\frac{\pi t}{\Delta t} \qquad (4.b)$$

$$\ddot{x}(t) = \dot{x}_{max}\frac{\pi}{\Delta t}\cos\frac{\pi t}{\Delta t} \qquad (4.c)$$

where
$\dot{x}_{max} = l\pi / \Delta t$ (~9.4 m/sec.) and $\Delta t = (t_2 - t_1)$ =10 sec. are respectively the maximum velocity reached by the traveling trolley and the traveling time of the full bucket to the hopper, according to the steps of unloading operation as clearly depicted in Fig. 4. This figure shows the variation with time of the experimentally measured axial strain at a section close to the semi-rigid joint located at the base of one of the two legs of the mast. The elapsed traveling time of the full bucket is clearly shown by this slow varying strain, measured at a specially selected spot to sense the applied dynamic loading.

Forced vibration analysis

With the previously described dynamic load the responses of the unloader were obtained in terms of nodal displacements and accelerations and also in terms of resultant forces and stresses in the elements of its space frame steel structure. A mass proportional damped modal analysis in the time domain, with 10 superposed vibration modes, was used to obtain the dynamic responses.

Straightforward correlation between numerical and experimental responses were made for accelerations and displacements at a few points in the structure; the most relevant being those related to the dominant longitudinal (surge) motion of the unloader. Superimposed in Fig. 5 are the experimental and numerical longitudinal acceleration responses at the joint (i.e. cylindrical bearing) of the lifting boom; and as it can be seen they correlate favorably. Table 2 shows a comparison between experimental and numerical averaged peak amplitudes of longitudinal and vertical accelerations and displacements at the tip of the lifting boom. These results together with

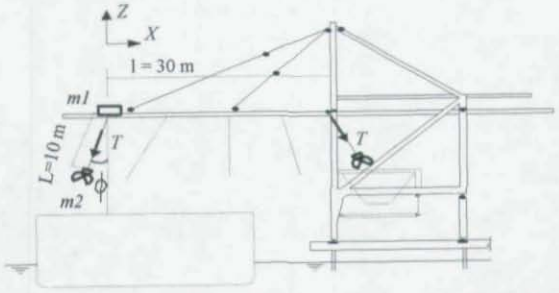

Fig. 3 - Theoretical model for dynamic load: Travelling trolley with pendulum

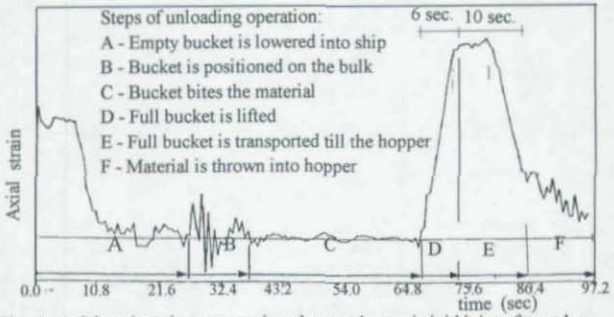

Fig. 4 - Axial strain x time at a section close to the semi-rigid joint of mast leg

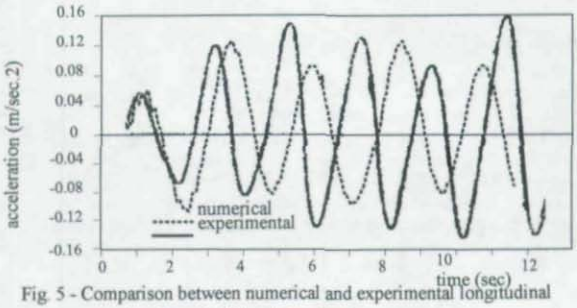

Fig. 5 - Comparison between numerical and experimental longitudinal accelerations at lifting boom level

Fig. 5 serve to demonstrate that the numerical results obtained with the calibrated FEM model correlate very favorably, both qualitatively and quantitatively, with their experimental counterparts.

Table 2 - Comparison between numerical and experimental averaged peak response amplitudes at the tip of lifting boom

Peak amplitudes	Experimental		Numerical	
	Displ. (cm)	Accel. (m/s²)	Displ. (cm)	Accel. (m/s²)
Longitudinal motion	±3.30	±0.13	±3.50	±0.10
Vertical motion	±9.90	±0.90	±11.00	±1.0

Under the cyclic action of the traveling trolley with the oscillating bucket the structure is put into a surging motion that is well depicted in Fig. 6 by the time response in terms of the surge displacement at the level of the semi-spherical joints. What can be readily noticed in this figure is the compound type of motion which results from the superposition of two modes: the natural surge mode of the structure with a period $T_S \approx 2.1$ sec.; and the pendular mode of the hanging bucket with a period close to $T_B \approx 6.5$ sec.

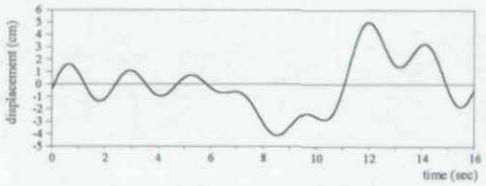

Fig. 6 - Longitudinal displacement x time response of the structure at level of the semi-spherical bearings. Time interval corresponding to steps D and E in Fig. 4.

Dynamic stresses

Structural stiffness and resistance to the dominant surging motion is mainly offered by the pair of inverted L-shaped plane frames. Thus, the round corners of these frames (see Fig. 7) had the most dynamically stressed and fatigue prone box-sections of the entire steel structure. Overall geometric proportions of these L-frames kept the round corners almost stress-free for the structure under static loads alone and, consequently, under dynamic loading the circumstances were such that high stresses were reversed repeatedly, in the same fashion as depicted in Fig. 6 for the longitudinal displacement at the same level of this focused section.

Stress analyses of this L-shaped welded box-section corner (delimited by the bolted sections as shown in Fig. 7) were carried out both numerically and experimentally. A 3-D finite element model as shown in Fig. 8 was used to perform the numerical stress analysis under prescribed distributed boundary forces derived from element end forces obtained with the dynamic responses of the space frame model of Fig. 2. To countercheck stress results from the 3-D FEM model, strain-gages were installed on the thin walls of the box-section corner and strain

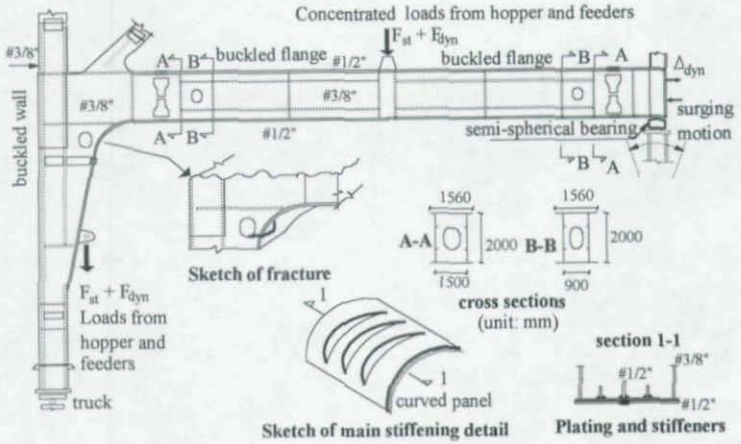

Fig. 7 - L-shaped plane frame: General characteristics and details of fatigue crack and stiffening

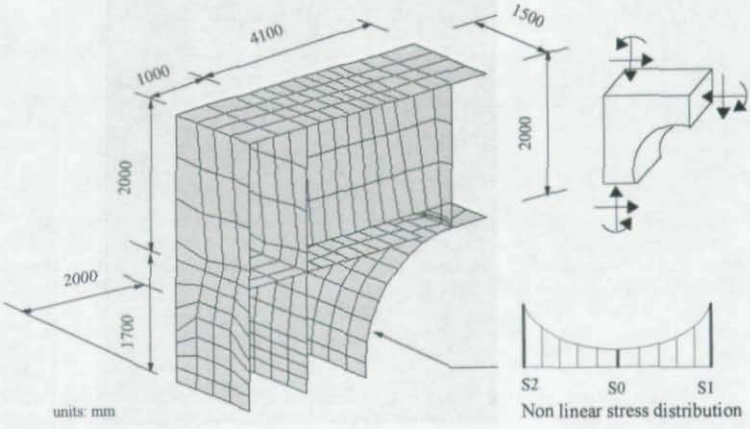

Fig. 8 - Section view of the 3-D finite element model of the inner-stiffened box-section corner of L-shaped frame

measurements were carried out during actual unloading operation. The unstiffened mild steel plates in these walls were only 3/8" thick (frontal and lateral plane walls) and 1/2" thick (curved wall). Because they were thin and wide, and of course geometrically imperfect, these unstiffened walls displayed a strong non-linear stress distribution across the box section. This was particularly so for the in-plane longitudinal stress distribution across the width of the curved wall in a section line indicated in Fig. 8. The dynamic peak values (e.g. maximum tension or compression) of these stresses at the center and edges of the curved wall are given in Table 3, while Table 4 shows their average values, effective (b_{eff}) to actual (b) widths ratios and the stress raiser factors (SRF) as defined ahead. It can be observed that in this case the shear-lag effect played the role of a stress raiser, leading to stresses at the edges of the curved wall that were over two times larger than the average stress. This was the source of the "stress raiser factor" with values indicated at the bottom line of Table 4. In relation to this matter it should be emphasized herein that the manhole in one of the lateral walls of the box-section corner, as shown in Fig. 7, did not constitute itself in any sort of strong stress raiser, as it could be thought at a first view. Strain measurements recorded from a line of rosettes installed on the web, in between the curved panel and the bottom of the manhole, showed that the principal stresses followed a longitudinal stress flow increasing towards the curved panel. The initiation of crack at this particular edge of the curved wall then resulted from a slightly higher local stress (S_1 as compared S_2 in Table 3) obviously influenced by the manhole.

Table 3 - Theoretical x Experimental dynamic longitudinal stresses at the curved wall of the box-section corner of the L-shaped plane frames

Local stresses	Theoretical stresses (MPa)		Experimental stresses (MPa)	
(see Fig. 8)	Tension	Compression	Tension	Compression
S_1	112.0	-79.8	71.7	-68.2
S_0	14.8	-12.5	11.2	-15.3
S_2	112.0	-79.8	62.0	-59.1

Table 4 - Comparison between theoretical and experimental characteristic values for stress distribution in the curved wall (see also Table 3)

Characteristic	Theoretical results		Experimental results	
values	Tensile	Compressive	Tensile	Compressive
$S_{average}$(MPa)	50.0	-37.0	30.8	-30.7
(b_{eff}/b)	0.447	0.463	0.439	0.461
SRF	2.24	2.16	2.17	2.07

4 Fatigue analysis

The calibrated models were used to estimate fatigue damages caused by the operational dynamic load at the most stressed sections of the structure [1]. Among these sections, those with high reversed stresses were termed the most fatigue prone sections. The results from the fatigue analysis of the box-section corner of the L-frame are brought herein to demonstrate the effectiveness of the used approach.

No considerable flaws, notches or minor cracks in any of the most fatigue prone sections were detected during thorough inspections of the entire structures of the two similar unloaders. Small initial defects associated with fabrication, installation and service use are nevertheless

altogether unavoidable and hard to be detected in such large steel structures. No matter how small, these imperfections can introduce non conservative errors into fatigue-life estimates, and this has been assessed by crack growth models derived from fracture mechanics. However these errors are generally minor compared to other uncertainties. Among these uncertainties those related to the modelling of the dynamic loading and structural system are the most relevant and frequent. Thus, what is always required to predict the fatigue-life of large field structures, is a refined and experimentally calibrated analytical or numerical model.

In the analysed case [2] the dynamic behavior of the structure was so simple that the most stressed and fatigue prone sections experienced only four different cyclic and well defined high stress levels at low frequencies. A deterministic approach to cumulative fatigue damage based on sound S-N curves could be then rationally applied to fatigue-life estimates of these unloaders structures. By having determined (numerically and experimentally) the hot spots for stresses at the edges of the curved wall, or more precisely at the welded junction between the curved wall and the webs of the box-section corner of the L-shaped frames, the aforementioned approach could be further used to forecast fatigue-cracks to be initiated at these spots.

The annual number of cycles of operation was estimated by the port authorities as $n = 2.1 \times 10^5$ cycles/year, and this was countercheked by monitoring one typical ship unloading operation.

Miner's rule together with the appropriate S-N curves [3,4] were used to estimate cumulative damage

$$D = \sum_{i=1}^{I} \frac{\bar{n}}{N_i} \geq 1.0 \qquad (5)$$

where,
$\bar{n} = n \times I$, is the total number of stress cycles that the section experiences per year, being I twice the number of cycles occurring for $\Delta t = 10$ sec., e.g. for both full and empty bucket travels.
N_i = the number of cycles for fatigue under each stress range ΔS_j; j = 1,...,J, being J the number of distinct stress ranges occurring for the to and fro traveling of the trolley on the boom.

The used S-N curve has the expression [3]

$$\text{Log}_{10} N_i = \text{Log}_{10} a + d.s + m.\text{Log}_{10} \Delta S_j \qquad (6)$$

where, for welds parallel to the direction of the applied stress like in the box-section corner of the L-frames, s = 0.1822; m = -4.0; $\text{Log}_{10} a = 15.3697$.

By applying a stress raiser factor (SRF) to the average stress ranges ΔS_j as taken from Table 4 the following fatigue life estimates T_F was obtained for the selected section:

T_F = 11.2 years, with SRF = 2.1, for the most stressed section in the curved wall of the box-section corner.

This result together with a service life T_S = 10 years led to an estimated ulterior service life $T_U = T_F - T_S$ = 1.2 years, that was soon corroborated by the occurrence, almost two years

later, of an extensive fracture in one of the two similar unloaders. Under repeated and reversed high stresses a crack, initiated at the predicted hot spot, grew quickly to dangerous length and almost led to the collapse of the whole structure of one of the unloaders: the one most on duty. Collapse only did not occur because the large crack could be seen by the people in charge of the maintenance of the machines. A sketch on Fig. 7 gives a glimpse of the extension of this fracture that reached around 980 mm (~ 39") of total length.

5 Repairing and upgrading

The structural failure corroborated initial predictions and compelled to designing the needed structural reinforcing and stiffening details which were carried out to repair and upgrade the steel structures of the two unloaders. The steel used in these structures and in the strengthening details is a mild carbon steel with yield stress fy≅250 MPa (similar to the ASTM A-36). The design of such details was based on stress calculations performed with calibrated numerical models, onto which structural changes (e.g. plate thickness, stiffeners, etc.) were introduced and analysed. One of the most relevant detail was the thickening and stiffening of the curved walls of the box-section corners of the L-shaped plane frames. Three equally spaced longitudinal stiffeners with rectangular cross-section 1/2" (~12 mm) thick and of smooth varying depth (maximum of 6"(150mm)) were welded to the inner surface, and two 1/2" (~12 mm) thick curved steel plates were welded side by side on the outer surface of the curved wall. As illustrated in one detail in Fig. 7 these curved plates were welded along the edges and the middle line of the curved wall, and also along their ends, close to the splices at the bolted sections. The thickening of the curved wall, together with the welded stringers, was done in order to arrest the shear-lag effect and even up the distribution of longitudinal stress across the wall width. Moreover extensive plating was carried out to obviate further structural failures in places where either fatigue cracks could grow inadvertently or localized buckling occurred because lack of necessary stiffness to resist the added dynamic in-plane stresses. At this stage a refined plane stress FEM model of one L-shaped frame was also of the great aid to sensivity analysis. Flat shell elements were used to discretize the two webs while the flanges were modelled by bar elements.

Another relevant reinforcing/stiffening work was carried out to repair the buckled top flange (see Fig. 7) of the box girders of the L-frames, and also the buckled vertical front wall (see Fig. 7) of these same frames. Buckling of these flanges were caused by the combined dynamic effects of the sudden loading induced by large mass of material being thrown into the hopper and the bending moments created when the rear support (semi-spherical bearing) of the L-frame moves backwards. Under the simultaneous occurence of these two dynamic effects -and this could be observed not to be a rare event- high longitudinal compressive stresses were induced to these flanges and added to the already installed static compressive stresses. For the unstiffened top flange of the horizontal box-girder this situation was further worsened by the shear-lag effect in the regions of the support to the concentrated (static and dynamic) vertical loads, indicated in Fig. 7. Thus, close to this point dynamic stresses lead to cumulative fatigue damage at the flange/web welded connexion, although in a much less extent than in the curved wall, as in the case of this top flange there were lower and not reversible strains. Buckling of the unstiffened top flange occurred to the right and left of this support in a classical wavy pattern as illustrated in Fig. 9.a. Plating in the region of the supports and longitudinal sttiffeners were then used to reinforce the top flange, and transversal stiffeners were also welded to the webs, as illustrated in Fig. 9.b.

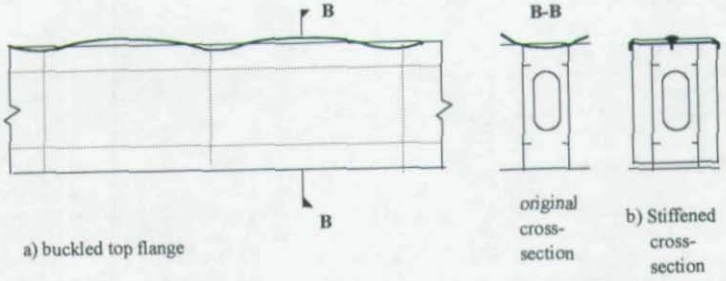

Fig. 9 - Buckled top flange of box-girder and reinforcing/stiffening details.

6 Concluding remarks

The reliability of an interactive theoretical-experimental-numerical approach to assess the dynamic behaviour of large steel structure is demonstrated by the application to a practical engineering problem involving fatigue-life estimates and buckling of box-section components. The calibrated numerical model resulting from this interactive approach is then shown to be a rational tool to evaluate the structural performance, to predict fatigue cracks and to point out and design the needed repairing to upgrade the steel structures of these ship unloaders. Details of the stiffening and plating carried out on the box-girders in order to arrest edge stresses due shear-lag and to prevent further buckling of top flange are also briefly described and serve to emphasize the need for further research on the role played by few and light longitudinal stiffeners, combined with thickening of flange, in the attenuation of shear-lag induced edge stresses.

References

1. Batista, R.C. & Roitman, N. *Structural Analysis of Ship Unloaders D1 and D2 of the Port of Sepetiba, Cia. Docas - RJ*, Contract Report COPPETEC ET-150543, Rio de Janeiro, May 1993.
2. Batista, R. C. *Structural Alterations of Ship Unloaders D1 and D2*, Cia. Docas RJ, Contract Report COPPETEC ET-150607, Parts I and II, Rio de Janeiro, December 1994.
3. New Fatigue Design Guidance for Steel Welded Joints (Issue 3), in *Offshore Installations: Guidance on Design and Construction*, Department of Energy, UK, May 1982.
4. Gurney, T. R., *Fatigue Design Rules for Welded Steel Joints*, The Welding Institute Research Bulletin, UK, May 1976.

NAME INDEX

NAME INDEX (Continued)

NAME INDEX (Continued)

NAME INDEX (Continued)

SUBJECT INDEX

SUBJECT INDEX (Continued)